Ultrasound and magnetic resonance techniques for the haemodynamic quantification of the peripheral vascular system

Amanda Jane Watson
BSc(Hons), MSc

Submitted in fulfilment of the requirements for the degree of Doctor of Philosophy

Department of Clinical Physics
College of Medical, Veterinary and Life Sciences
University of Glasgow

April 2013

Abstract

The aim of this thesis was to determine whether the blood flow velocities in the peripheral vascular system measured using phase contrast magnetic resonance imaging, PC-MRI, techniques could be used in the same way that blood flow velocities measured using spectral Doppler ultrasound are used to aid in the diagnosis of peripheral vascular disease. Specifically, we aimed to investigate the measurement of maximum velocities and the use of maximum velocity ratios; an area of investigation which has been neglected in studies of PC-MRI blood flow quantification to date.

A series of optimisation and comparison studies were carried out using in-house developed test phantoms. Key to the *in-vitro* work was the establishment of a dual modality flow test system which would allow comparison of identical flow conditions measured using ultrasound and MRI. The work was complemented by *in-vivo* studies in healthy volunteers. A 4D PC-MRI commercial work-in-progress protocol and software package became available during the study and was evaluated *in-vitro* and *in-vivo* using similar methods as for the 2D PC-MRI studies.

The main findings of the thesis were that 2D PC-MRI measurement of maximum velocities significantly underestimated those measured using spectral Doppler ultrasound. However, if corrections were applied to account for the overestimation of ultrasound maximum velocity due to spectral broadening, then the two methods were in agreement. In contrast, the use of maximum velocity ratios showed no difference between spectral Doppler ultrasound and 2D PC-MRI measurements.

It was noted that one of the potential problems with the use of 2D PC-MRI in the measurement of the maximum velocity at a stenosis is the accurate positioning of the 2D velocity encoded slice in the stenotic jet. 4D PC-MRI, with a time resolved velocity encoded volume dataset, offers a potential solution to this. However, our evaluation of 4D PC-MRI showed that it can significantly underestimate both maximum velocities and maximum velocity ratios in comparison with 2D PC-MRI and spectral Doppler ultrasound and requires further development before it can be used for peripheral vascular applications.

Table of Contents

List of Tables

List of Figures

Acknowledgements 1

From the beginning of this research project I was delighted to find that my colleagues in clinical physics, vascular surgery and radiology were encouraging, supportive and extremely helpful. I would, of course, like to thank all of them, but a few have had more involvement than others and merit mention by name.

Prof. Alex Elliott who, as my line manager, gave me permission and encouragement to undertake this project. Vascular surgeons Mr Alan McKay and Mr David Kingsmore who invited me to present and discuss my ideas at the vascular surgery research meeting and for assistance with the ethics committee application. Prof. John Moss and colleagues who invited me to present and discuss my ideas at their interventional radiology research meeting. Vascular technologist Gordon Burnside and the radiographers at Gartnavel General MRI who helped to collect the pilot data. The "new girls" at BHF MRI for their help with the tidying-up bits. Ramsey McIvor, John Pender and all the team in the mechanical engineering group who always seemed to understand what I meant regarding the latest phantom. My happy band of consenting, willing, healthy volunteers. Dr Dan Kusumadijiwada a fellow pioneer in the 4D MRI work. Prof. David Keating, who as my current line manager and postgraduate convenor has been ensuring that I finish what I started. My family and close friends, near and far, for supporting, encouraging and believing in me.

Particular thanks go to four individuals who have made my journey through the dauntingly thick forest of MRI so much easier. Without with their knowledge, enthusiasm, support and friendship I would have been lost: Dr. John Foster, Christie McComb, Kirsten Lanaghan and Tracey Steedman. In addition, John has done a fantastic job of keeping me in line in the final stages. For "stepping into the breach" and for his dedication to the role of supervisor I am truly grateful.

Finally, and most importantly, I would like to thank my dear husband Bob for his unending love and support, in sickness and in health.

Acknowledgements 2

This work was supported by a grant from the West Research Endowment Fund in Glasgow for the purchase of items associated with the development of the *in-vitro* test system.

Definitions / Abbreviations

ABPI	Ankle brachial pressure index
AAA	Abdominal aortic aneurysm
CCA	Common carotid artery
CE-MRA	Contrast enhanced magnetic resonance angiography
CTA	Computed tomography angiography
DSA	Digital subtraction angiography
ECA	External carotid artery
ECG	Electrocardiogram
EDV	End diastolic velocity
LDL	Low density lipoprotein
MRI	Magnetic resonance imaging
MRA	Magnetic resonance angiography
PC-MRI	Phase contrast magnetic resonance imaging
PI	Pulsatility index
PSV	Peak systolic velocity
roi	Region of interest
RI	Resistivity index
TE	Echo time
TOF	Time of flight
TR	Repetition time
venc	The PC-MRI velocity encoding parameter

Chapter 1 – Introduction: the quantification of blood flow in the peripheral vascular system

Peripheral vascular disease involves a narrowing (stenosis) and stiffening of the peripheral arteries due to the presence of atherosclerotic plaque. At sites of narrowing, there will be a local increase in the velocity or speed of blood flow compared with the velocity in the vessel before the area of narrowing. The narrower the vessel the higher the velocity will be. Two of the primary areas of concern are in the carotid artery system (which supplies blood to the head and brain), with the associated risk of stroke, and in the lower limb arterial system with associated pain, mobility and limb threat. However, atherosclerotic vascular disease can extend to the entire vascular system.

At the moment, the two main, non-invasive, diagnostic imaging methods of assessing arterial vascular disease to determine suitability for surgery or other intervention are Doppler ultrasound and a magnetic resonance imaging (MRI) technique known as magnetic resonance angiography (MRA).

In general, a carotid stenosis having a greater than 70% reduction in vessel lumen diameter will be considered suitable for surgery. In the lower limb a doubling of Doppler ultrasound velocity indicates a stenosed vessel but intervention is dependent on the distribution and severity of disease in the entire limb. It is therefore important to be able to provide an accurate assessment of both the location and the degree of any areas of arterial narrowing.

Doppler ultrasound techniques (Thrush & Hartshorne 2009) are used to quantify the percentage narrowing of any areas of disease by measuring changes in the blood velocity and calculating appropriate velocity ratios. Doppler ultrasound is a real-time imaging technique which can also use the ultrasound image of the vessels to help confirm the information indicated by the velocity measurements. Contrast enhanced subtraction imaging techniques used in MRA (Yucel 1995)

provide a good anatomic map of the distribution of flow (similar to that seen in digital subtraction angiography (DSA), an alternative technique which involves x-rays) and are sensitive enough to show areas of narrowing or occlusion. Although it is possible to make measurements of the diameter of vessels on MRA images, assessment of the degree of stenosis is usually a qualitative and subjective decision.

In summary, in current clinical practice, Doppler ultrasound provides quantitative measurement of arterial blood velocities to determine the degree of stenosis and MRA provides a qualitative map of the arterial distribution.

Ultrasound has the advantage of being less expensive and more patient acceptable than MRA. However, the nature of ultrasound means that it cannot be used to image areas where there are bone or gas (e.g. the bowel or lungs) this means that there are many regions of the body that are difficult or impossible to image with ultrasound. The increasingly obese population is a further limitation for ultrasound as the ultrasound is attenuated by tissue making it difficult to get good images from deep within the body. The anatomic map provided by MRA can provide good imaging in those areas inaccessible to ultrasound. However, there are many cases of uncertainty in the MRA assessment of the presence or degree of stenosis in such areas, which will not have complementary quantitative velocity information from ultrasound to inform the diagnosis. The exception to this is a technique known as phase contrast magnetic resonance angiography, PC-MRA, where the depiction of flow is due to the presence of phase changes which are directly related to blood velocity. This technique gives rise to the potential for blood velocity measurement; a technique which has indeed been used in cardiac applications but remains under-investigated in the peripheral vascular system.

This project aimed to address these issues by investigating the quantification of blood flow using velocity encoded PC-MRI techniques to determine whether methods used in spectral Doppler ultrasound, primarily maximum velocity measurement and maximum velocity ratios, might translate to MRI methods. This would raise the potential to provide additional diagnostic information for the assessment of peripheral vascular disease and would be of particular relevance to areas of the peripheral vasculature difficult to access by

ultrasound, such as the subclavian-brachial and aorto-iliac segments. Validation of the proposed methods required technical comparison between Doppler ultrasound and PC-MRI measurements of blood velocities using test phantoms prior to comparison studies on normal healthy volunteers.

Studies in the literature have shown that it is possible to gain quantitative information on both vessel diameters and blood velocity using PC-MRI data and that the quantification of blood flow is a recognised technique in cardiology (Lotz et al. 2002). However, only a limited number of authors have investigated the extension of the technique to the peripheral vasculature [e.g. (Caputo & Higgins 1992; Klein et al. 2003; Krug et al. 1995; Meyer et al. 1993; Pena et al. 1996)] and most have focused on the use of mean velocities and volume flow quantification. Although the feasibility of the basic technique has been established, there has been little work done to assess performance against Doppler ultrasound measurements or to develop it further with the aim of implementing usable clinical protocols to enhance vascular diagnosis.

In summary, the project is aiming to address the "gap" in the diagnostic information available to clinicians for the assessment of vascular disease by examining the feasibility of using maximum velocity measurement and maximum velocity ratios from PC-MRI measurements.

While the project is focused on peripheral vascular studies, as these represent the main application for both MRA and vascular ultrasound, the methods developed will have potential applications in other clinical areas such as renal medicine, cardiology and neurology.

1.1 Key aims of the thesis

The validation and comparison studies aimed to test the following hypotheses:

a) There is no difference in the velocity of arterial blood as measured using spectral Doppler ultrasound or PC-MRI techniques.

b) There is a difference in the velocity of arterial blood, as measured using spectral Doppler ultrasound or PC-MRI techniques, which takes the form of a quantifiable direct relationship between the two measurements.

c) There is no difference in the maximum velocity ratios for blood flow measured using spectral Doppler ultrasound or PC-MRI techniques

A positive outcome for any of the above would enable the technique to be developed further as a routine diagnostic tool.

1.2 Outline of the thesis

This thesis is concerned with the study of the measurement of arterial blood velocities in the human peripheral vascular system using MRI techniques and the feasibility of developing such techniques into an effective diagnostic tool for the assessment of atherosclerotic disease. The thesis consists of 10 chapters. Chapter 2 examines the anatomy, physiology and haemodynamics of peripheral vascular blood flow, the aetiology of atherosclerotic disease in the peripheral vascular system with an overview of the current methods of diagnosis. Chapter 3 looks in detail at the background and development of blood velocity measurements for the assessment of vascular disease which led to Doppler ultrasound as an established diagnostic tool. Chapter 3 also introduces the concept of velocity measurement using MRI; a technique developed for cardiology applications, but which remains under developed in other clinical areas. Chapter 4 summarises published work on the comparison between PC-MRI and spectral Doppler ultrasound, focussing on those studies most relevant to velocity measurement in non-cardiac vessels, in addition the development and

use of flow phantoms for ultrasound and MRI is summarised. This provides a background introduction to the practical work in chapter 5 which describes the flow test phantoms and other equipment used in the subsequent chapters as well as some preliminary work to calibrate the flow system and evaluate maximum velocity errors on the ultrasound scanner used. Practical examination of the PC-MRI velocity measurement technique in comparison with calibrated flow and with spectral Doppler ultrasound begins in earnest in chapter 6 with the use of steady state flow velocities to determine errors in PC-MRI velocity measurement and allow investigation of spatial variables. The comparative work is extended in chapter 7 with the use of pulsatile flow patterns to compare the temporal performance of the two techniques in terms of the ability to map temporal changes during the cardiac cycle. Chapter 8 describes the *in-vivo* studies with the use of an optimised PC-MRI protocol compared with standard spectral Doppler ultrasound techniques. In chapter 9 a new technique known as 4D flow PC-MRI is investigated and its potential as an alternative to 2D PC-MRI or Doppler ultrasound techniques is discussed. Finally, chapter 10 summarises the main findings of the work and examines the potential to extend the technique to other clinical areas as well as providing an overview of other further work which would help establish PC-MRI velocity measurement techniques for peripheral vascular applications.

Chapter 2 – Atherosclerotic disease in the peripheral arterial system

The peripheral vascular system, figure 2.1, is concerned with the arterial vessels distal to the heart and its greater cardiac vessels. While atherosclerotic disease may occur anywhere within the vascular tree, peripheral vascular medicine is dominated by the diagnosis and treatment of disease in the carotid arteries and in the lower limbs. Both anatomical regions may be investigated using ultrasound and magnetic resonance and are therefore ideal sites for the comparison of physiological measurements using the two imaging technologies; a facility required by this thesis.

For many authors, the term "peripheral" as used in association with vascular anatomy and pathology, refers to the lower limbs. However, in this thesis, the term "peripheral" will refer to the whole peripheral vascular system including the intra- and extra-cranial arteries. References to literature sources using the term "peripheral" will mention the anatomical regions of interest explicitly. However, for clarity some of the following sections in this and further chapters will be grouped under "carotid" and "lower limb" headings.

While atherosclerosis is the primary cause of arterial narrowing, this thesis is concerned with the quantification of the vascular system in general, and the diagnosis of haemodynamic disturbance regardless of cause. However, since the work is of relevance primarily in the diagnosis of atherosclerosis, a discussion of the disease provides appropriate contextual background for the research.

2.1 Incidence and prevalence of disease

The epidemiology of atherosclerosis can be difficult to isolate from the wide range of studies on associated cardiovascular disease and stroke. However it is widely acknowledged that cardiovascular diseases associated with atherosclerosis are a leading cause of death worldwide. The 2011 World Health Organisation report on non-communicable diseases (WHO 2011) reveals that, in the year 2008, more than 36 million people died from non-communicable diseases and 48% of those were from cardiovascular causes. Such high mortality

percentages and the clearly identified links between atherosclerosis and central and peripheral vascular diseases point to the importance of the early identification and treatment of atherosclerosis. In addition, stroke and peripheral vascular disease are leading causes of disability, particularly in the older population (SIGN 108 2008;SIGN 89 2006).

2.1.1 Carotid artery disease

Around 20 to 30% of all strokes may be accounted for by extracranial carotid artery stenosis (Fung & Saw 2007) approximately 90% of which are due to atherosclerosis. Carotid artery disease has been widely studied and there are recognised concomitant relationships with intracranial atherosclerosis, coronary artery disease and peripheral arterial disease. The association of extracranial carotid artery disease with the risk of stroke is also well recognised (Oates et al. 2009). Current recommendations are for all patients presenting with symptoms of a neural event, such as amaurosis fugax or TIA, to undergo carotid artery screening with Doppler ultrasound (SIGN 108 2008). Although Doppler ultrasound of the extracranial carotid arteries is a well established technique, the acoustic window is limited to a few centimetres distal to the carotid bifurcation. In addition, scans can be limited by the presence of calcified, shadowing plaque. Un-satisfactory scans are usually repeated by MRA and it is usual practice for carotid pathology identified by Doppler ultrasound to be confirmed either by a repeat Doppler ultrasound scan or an MRA scan.

2.1.2 Lower limb arterial disease

One of the most comprehensive studies investigating the prevalence and incidence of peripheral arterial disease, PAD, both symptomatic and asymptomatic, is the Edinburgh Artery Study (Fowkes et al. 1991) which undertook initial screening for PAD using ankle-brachial pressure index (ABPI) measurements, blood and ECG tests, physical data and questionnaires in a large random sample of the population. 4.5% of that population were symptomatic with some degree of claudication. However, 24.6% were asymptomatic but had abnormal ABPI results indicating the presence of moderate to severe PAD. The Trans-Atlantic Inter-Society Consensus Group for the Management of Peripheral

Arterial Disease (TASC II) 2007 in their most recent review (Norgren et al. 2007), examined several similar prevalence studies and summarised that, in developed countries, the total disease prevalence is in the range 3% to 10%, increasing to 15% to 20% in the over 70 age group. As for carotid artery stenosis, the majority of causes of narrowing will be atherosclerotic. Doppler ultrasound imaging is regarded and recommended as a first line imaging technique for the diagnosis of peripheral vascular disease (Bradbury & Adam 2007; Layden et al. 2012; SIGN 89 2006). However, although the lower limbs in their entirety may be assessed using Doppler ultrasound, proximal scans are often limited to the distal common femoral artery in the groin due to difficult imaging in the lower abdomen. Suspicion of aorto-iliac disease will usually require MRA or other angiographic imaging.

2.1.3 Other PVD

The upper limbs represent an easy target for spectral Doppler ultrasound, although, in practice, atherosclerotic disease of the upper limbs is relatively rare accounting for only 5% of all extremity disease (Thrush & Hartshorne 2009). In contrast, the proximal arteries of the upper limb, the bracho-cephalic and subclavian segments account for around 15% of symptomatic extracranial disease (Cho, Casserly, & Wholey 2005). The anatomic location of these vessels can make clear imaging and measurement using Doppler ultrasound difficult. Although ultrasound is frequently the first line imaging choice, any abnormal findings or unsatisfactory scans will indicate the need for alternative imaging such as an MRA.

Imaging of the abdominal aorta is usually performed in relation to the diagnosis of aneurysm, rather than stenosis. The acoustic window in the upper abdomen makes measurement of the size of the aorta sufficiently easy for the technique to be used in national AAA screening programmes (Cosford & Leng 2007). However, treatment decisions will usually require more extensive anatomical imaging such as MRA.

There are a variety of other regions such as the renal and mesenteric arteries and the intra cranial vessels for which, although it is possible to use Doppler ultrasound, visualisation is very much enhanced by the use of MRA. The following

texts will give an overview of disease in other arterial sites and the ultrasound and MRI methods used to image them:

J. D. Beard and P. A. Gaines. Vascular and endovascular surgery, Elsevier Health Sciences, 2009.

A. Thrush and T. Hartshorne. Peripheral vascular ultrasound: how, why and when., Edinburgh:Churchill Livingstone, 2009.

E. K. Yucel. Magnetic resonance angiography : a practical approach, McGraw-Hill Inc., 1995.

2.2 Anatomy and haemodynamics of the peripheral arterial vascular system

An holistic view of the vascular system would consider the heart, cardiac vessels and the venous return as well as the arterial system. For this thesis, however, which is concerned with improving the diagnosis of narrowing of the arteries in the peripheral vasculature, it is more useful to summarise the properties of the main peripheral arteries. It is also useful to consider the properties of blood in relation to imaging technologies and the structure of the arterial walls.

Figure 2.1, illustrates the anatomy of the arterial system in the human body with the most common sites for ultrasound imaging and the sites with poor acoustic windows highlighted.

2.2.1 Properties of arterial blood

Arterial blood leaves the heart in an oxygenated state to travel around the systemic vascular system. The red blood cells which are approximately 7.5 μm in diameter act as Rayleigh scatterers in the presence of ultrasound of frequencies in the MHz range (Oates 2001). The magnetic relaxation times, T1 and T2, of blood are higher than the surrounding tissue (Stanisz et al. 2005). These properties are important in the ultrasound and MRI imaging of blood. However, it is the movement of the blood that is the important, detectable, feature in Doppler ultrasound and PC-MRI techniques.

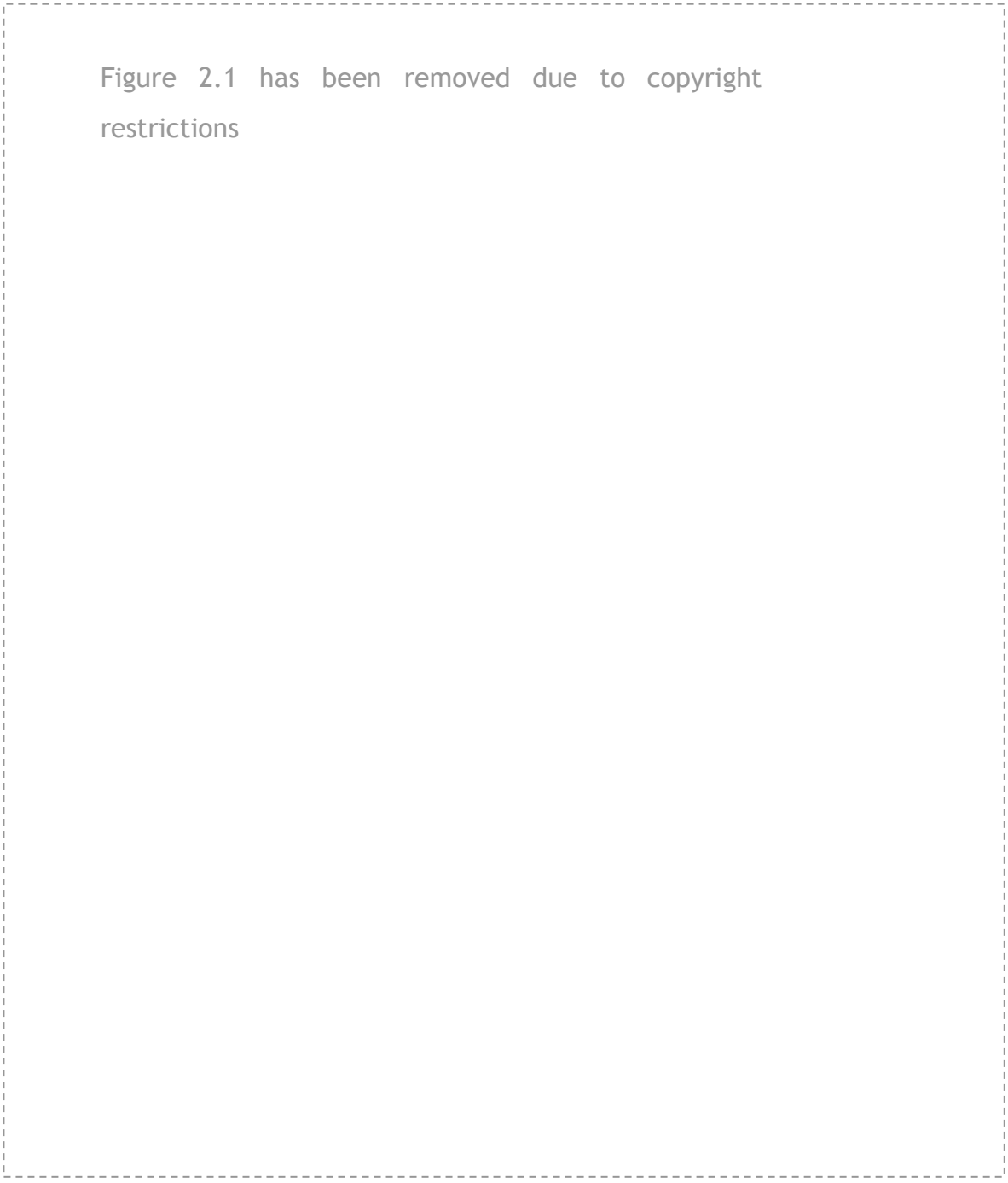

Figure 2.1: The arterial system of the human body. Areas shaded pink are those regions scanned most often using Doppler ultrasound. Areas shaded green are those regions for which an ultrasound scan will often be requested but are difficult to access using ultrasound. Adapted from Villareal (Villareal 2009).

2.2.2 Properties of arterial blood vessels

The physical properties of the arteries have a local influence on the haemodynamic pressure, velocity and flow volume and the associated temporal changes or pulsatility. Figure 2.2 is a schematic illustration of the layers of the arterial wall. Of the three layers of an artery, the inner layer or **intima** is the most important in relation to atherosclerotic disease. There is a single layer of vascular endothelial cells in contact with the blood. This endothelium responds to chemical changes and shear stresses from the blood to produce nitric oxide which diffuses into the underlying smooth muscle to produce relaxation and vasodilation.

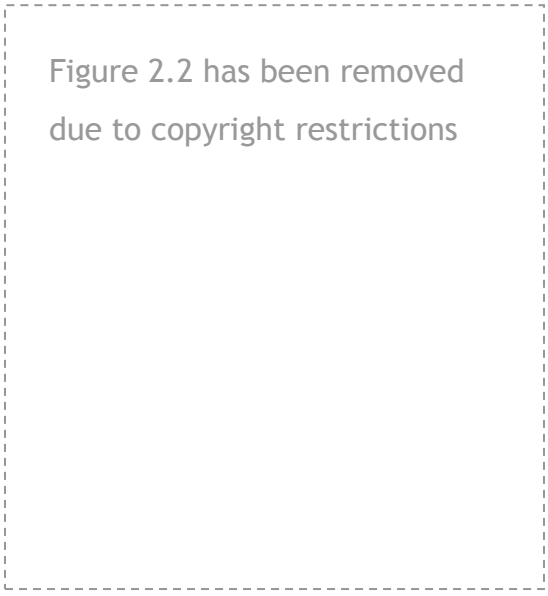

Figure 2.2: The three layer structure of an arterial vessel. (Slomianka 2009)

Chemical and physical stresses on the endothelial cells, the presence of low density lipoproteins, LDL, and the oxidisation of LDL deposits by free radicals can cause damage leading to atherosclerotic disease (Levick 2003).

The **media** consists of smooth-muscle cells arranged helically in a matrix of collagen and elastin fibres to provide mechanical strength and elastic contractile power, essential for pulsatile flow. The media layer is bounded by an inner and outer elastic layer which is fenestrated to allow communication between layers. The outer layer or **adventitia** consists mainly of a thick collagen layer with some

elastin which merges with the surrounding tissue while still allowing some movement. In larger arteries such as the aorta, proximal to the renal arteries, the adventitia will be thicker with its own blood supply or vasa vasorum.

2.2.3 Vascular haemodynamics

A full treatise on vascular haemodynamics is beyond the remit of this thesis and an excellent overview may be found in:

C. P. Oates. Cardiovascular haemodynamics and Doppler waveforms explained., London: Greenwich Medical Media Ltd, 2001.

There are, however, some key issues of relevance to the work of this thesis and which may be summarised as follows.

2.2.3.1 Laminar flow

In laminar, parabolic flow in a straight vessel with a circular diameter the flow of a fluid may be thought of as layers of concentric flow at different velocities; the slowest velocities at the vessel walls and the highest at the centre of the vessel. The shape of the velocity profile, v(r) as the radius, r, increases to its full diameter, R, with the centre velocity of v_{max}, may be described by equation 2.1.

Equation 2.1: the velocity profile for parabolic flow

$$v(r) = \left(1 - \frac{r^2}{R^2}\right) v_{\max}$$

For true parabolic velocity profiles, the mean velocity, $\bar{v}$, will be equal to half the maximum velocity, v_{max}, as in equation 2.2.

Equation 2.2: mean velocity of parabolic flow

$$\bar{v} = \frac{v_{\max}}{2}$$

Equation 2.2 can be a useful assumption when performing steady state flow validation studies. If the flow volume rate is known and laminar flow can be assumed then both the mean and maximum velocities can be calculated and used for comparison with a system making velocity measurements.

However, the flow will, in fact, cease to be parabolic as the velocity increases. Energy is lost in the form of a pressure drop, ΔP, which is dependent on the velocity, $\bar{v}$, the length of the vessel, l, the radius of the vessel, r and the viscosity, μ. The parameters are related in Poiseuilles's equation, equation 2.3.

Equation 2.3: Poiseuilles's equation

$$\Delta P = \frac{\bar{v} 8 l \mu}{r^2}$$

A consequence of these losses is that the velocity profile becomes flatter as the velocity increases and may be described as plug flow, before becoming turbulent at higher velocities. This transition has been found to occur at the point when the ratio of inertial forces to friction forces exceeds 2000. The ratio is usually referred to as the Reynolds number, Re, and can be described by equation 2.4 for a tube of diameter, D, fluid density, ρ, viscosity μ, and velocity, v.

Equation 2.4: Reynold's number

$$\mathrm{Re} = \frac{D \rho v}{\mu}$$

From the Reynolds number, it is possible to calculate a critical velocity for which turbulent flow will develop at Re = 2000. In a typical superficial femoral artery, the critical velocity may be calculated as 120 cms^{-1} and compared with a typical normal peak systolic velocity in the femoral of 80 cms^{-1} (Oates 2001).

If, in an experimental flow system, we wish to maintain laminar, parabolic flow for validation studies, then we need to be aware of the critical velocity for the vessel or tube diameter and of the inlet length, L, required to ensure that parabolic flow is established, which can be estimated using equation 2.5:

Equation 2.5: the inlet length for establishing laminar flow in a straight tube in metres (IEC 61685 2001;Oates 2001).

$$L = 0.003 D \,\mathrm{Re}$$

2.2.3.2 Pulsatile flow

Pulsatile flow is rather more complex to describe, as there are pressure changes and energy losses within each cardiac cycle as well as during the progression of the blood along the vessel. The equivalent of the Reynolds number for pulsatile flow is the Wormersley parameter, α, which is shown in equation 2.6, for a fluid of density, ρ, viscosity,μ, flowing through a vessel of diameter, r, with a pulsatile motion of angular frequency, ω (2πf).

Equation 2.6: the Wormersley parameter

$$\alpha = r\sqrt{\frac{\omega\rho}{\mu}}$$

For vessels with α <1 flow may be considered to be in a "quasi steady laminar flow" state. However, for higher values of α, the peak flow velocities will be slower than they would be for the same pressure gradient in the steady state as the acceleration of the flow is usually too short to bring the flow up to maximum before deceleration begins. This is easily observed with the application of voltages to drive steady state and pulsatile flow simulation systems.

2.2.3.3 Flow at a bifurcation

The peripheral vascular tree is composed of a multitude of bifurcations, or junctions, taking the blood into increasingly small vessels. At each bifurcation there is the likelihood of disturbed flow dependent on the geometry of the bifurcation. Turbulent flow can cause significant pressure fluctuations and shear stresses at the vessel endothelium which can accelerate the development of thrombus and plaque (Levick 2003). Atheroma is frequently found around bifurcation sites.

2.2.3.4 Flow in a stenosis

The determination of a degree of stenosis by the measurement of velocity ratios is common practice in clinical Doppler ultrasound. Such practice is reasonable as a result of the simple continuity equation for flow. If a tube of cross sectional area A_1, with mean velocity $\overline{v_1}$, narrows to an area of A_2, then to maintain the continuity of flow, the mean velocity must increase to $\overline{v_2}$, as in equation 2.7.

Equation 2.7: Continuity of flow rate $A_1\overline{v_1} = A_2\overline{v_2}$

In practice, in Doppler ultrasound studies, it is usual to use diameter reduction rather than area reduction and the velocity ratios that are used are peak maximum velocities, rather than mean velocities (Oates et al. 2009). Thus a peak velocity ratio of > 4 is equivalent to a diameter reduction of >70%.

2.3 The diagnosis of peripheral vascular disease

The effects of compromised arterial blood flow may be manifest in a variety of ways, depending on the location, severity and number of lesions. The symptoms of atherosclerosis may mimic symptoms found in other diseases. For example, many patients undergoing carotid artery imaging may have been referred via the ophthalmology departments, having initially presented with visual disturbances. Other "stroke-like" symptoms such as ataxia and paraesthesia may have a variety of causes such as brain tumour, multiple sclerosis or vitamin B12 deficiency. Critical lower limb ischaemia, where necrosis or gangrene have developed, is an obvious result of a compromised blood supply. However, the locations and severity of any occlusions or stenosis and the options for surgical or radiological intervention cannot be determined by clinical examination alone. Less severe lower limb PAD symptoms, such as intermittent claudication, may have other causes such as musculo-skeletal or neurological disorders.

The ability to measure and distinguish parameters relating to normal and abnormal blood flow has greatly influenced the differential diagnosis of vascular disease. Diagnosis and treatment planning has been significantly enhanced by the availability of a variety of methods of imaging the vascular system. In the following sections, an overview is given of the diagnostic techniques most commonly used in current vascular medicine practice.

2.3.1 Clinical diagnosis

For a diagnosis of peripheral vascular disease in the lower limb there are a number of key indicators the clinician will aim to determine when examining the patient (Beard & Gaines 2009):

- The presence and location of pain, whether it is rest pain or appears or associated with exercise. The site of pain is usually distal to any atherosclerotic lesion.

- The pallor and temperature of the foot. The capillary return in response to local pressure

- The presence or absence of pulses at the groin, knee and ankle

- History of any pre-disposition factors such as smoking, obesity, diabetes, cardiac disease or and family history of the same

Diagnosis for the upper limb will be similar but can be less definite as there is not the same claudication response to exercise as for the lower limbs. Diagnosis of carotid stenosis will also be less definite as the patient will usually present with neurological or ophthalmic symptoms which may have a variety of other causes. It would be rare for a patient with suspected arterial disease not to undergo some form of diagnostic test. However the test need not necessarily involve imaging and where imaging is required, clinical examination might direct the type of imaging. For example, thigh or buttock pain would indicate a possible aorto-iliac lesion so that the clinician might choose MRA as the first line imaging modality, rather than ultrasound.

2.3.2 Non-imaging diagnostic techniques

2.3.2.1 Ankle–brachial pressure index

Hand-held, continuous-wave Doppler ultrasound instruments in their simplest form provide an audible representation of the Doppler shifted frequency, as will be discussed in Chapter 3, from moving blood cells. They are a useful tool in the primary-care or vascular clinic setting, particularly when the presence or absence of regional pulses in the lower limbs cannot be detected by simple palpation. The devices often known as “pencil” or “pocket” Doppler may also be used in combination with a sphygmomanometer and cuff to determine the perfusion pressure at the ankle or foot. Measurements are generally done on the supine patient, at rest. To account for variations in the systemic pressure between patients, the ratio of the systolic posterior-tibial or anterior-tibial arterial pressure against the systolic brachial arterial pressure is determined; known as the ankle-brachial pressure index, ABPI. In the normal circulation, the pressures at the ankle would be the same or slightly higher than in the arm, giving an ABPI of 1.0 to 1.2. However, restricted flow in the legs will result in

reduced arterial pressure at the ankle giving ABPI values lower than 1.0. Evidence has shown that an APBI of less that 0.9 is up to 95% sensitive in detecting arterial disease and around 99% specific for the identification of normal vascular flow (SIGN 89 2006). Lower ABPI values are indicative of the increasing severity of vascular disease. In addition, the characteristic pulsation "sound" of the audible waveform can add to the diagnosis with triphasic waveforms generally indicating normal flow but dampened, monophasic Doppler signals indicating diminished flow and the likely presence of proximal disease. Some instruments may provide a linear, graphic representation of the flow waveform.

ABPI measurements are frequently used in the primary-care setting as well as the vascular lab as a quick, first-line indicator of the likely presence of arterial vascular disease. Current recommendations are that all patients suspected of having peripheral arterial disease should have ABPI measurements performed (SIGN 89 2006).

However, the ABPI test is limited in several circumstances: where the arteries are heavily calcified, as in many diabetic patients, and cannot be compressed; overlying oedema or gross obesity will reduce the sensitivity of the Doppler instruments; and care must be taken where there is overlying ulcerated or broken skin. A minority of patients will not tolerate compression of the legs by the cuff due to pain in which case imaging techniques are advised.

2.3.2.2 Toe pressures

In situations, as described above, when the arteries of the lower leg cannot be compressed or where arterial disease in the foot is suspected, a toe cuff with a photoplethysmeographic detector may be used to determine pressure ratios.

2.3.2.3 Exercise ABPI's

In patents with intermittent claudication, ABPIs may be normal when measured at rest. The working muscle requires a significantly larger volume of blood than resting muscle and a compromised vascular supply will represent a significant challenge leading to pain on exercise. It can be useful to test ABPI

measurements before and after an exercise challenge. In a vascular laboratory setting, a treadmill is the usual method and, when combined with a consistent testing protocol, can add to the diagnosis with a more reliable estimation of the distance to onset of claudication than the patients own estimation. Exercise testing must be performed with care in patients with a known history of cardiac disease and can be difficult in patients with concurrent respiratory or osteopathic disease.

2.3.3 Magnetic resonance techniques

Although the principles of nuclear magnetic resonance, NMR, and their application to the study of biological tissues, began in the 1940s, magnetic resonance imaging techniques have their origins in the 1970s with the work of Nobel prize winners Paul Lauterbur and Sir Peter Mansfield and major contributions from other researchers during the same era such as, Raymond Damadian and Richard Ernst (Geva 2006).

In general MRI imaging, the signals from moving blood and, in particular, pulsatile flow, give rise to artefacts that must be compensated for. However, the phenomena that give rise to these artefacts can be exploited to provide imaging and quantification of blood flow.

The imaging of the blood vessels using magnetic resonance techniques is generally referred to as magnetic resonance angiography, MRA, and provides a spatial, anatomical map of the vasculature within the scanned volume. There are three main methods of producing MRA images: time of flight, phase contrast and contrast enhanced imaging.

2.3.3.1 Time of flight imaging

Time of flight imaging is the oldest of the magnetic resonance techniques to image blood flow and has its roots in the late 1950s with the work of Singer (Yucel 1995). Time of flight is based on the inflow effects of spins moving into the imaging slice. Stationary spins within a slice will see all the applied

excitation pulses within a single pulse sequence or TR. However, spins moving through a slice may not see all the excitation pulses, depending on how fast they are moving through the slice.

2.3.3.2 Phase contrast imaging

The moving spins will also experience a change in phase which is dependent on their velocity and the gradient. Exploitation of these phase changes to create images of blood flow was begun in the 1980s with the work of Weeden and Dumoulin (Dumoulin 1995). The imaging methods used the application of a bipolar gradient to null out any change in phase due to the gradient with the resulting phase differences proportional to velocity. These mechanisms are described in more detail in chapter 3. Phase contrast imaging, PC-MRA, is of particular interest in this thesis as the application of further velocity encoding gradients allows direct measurement of velocities and quantification of flow.

2.3.3.3 Contrast enhanced vascular MRA

In contrast enhanced imaging, a bolus of a gadolinium based contrast agent is injected into the vascular system and its transit around the vascular system is imaged. The contrast agent lowers the T1 of blood and the resulting angiographic images are a result of the large enhancement of the blood signal compared to the tissue background. Careful timing is required to optimise the signal from the blood to ensue that arterial and venous phases are not shown in the same image. Optimisation depends on both the concentration of administered contrast agent and the circulation timings. This is an invasive technique for which some groups of patients, particularly those with renal impairment, are contraindicated. However it is a rapid imaging technique suited to large field of view imaging and has become the standard methods for MRA imaging of the vascular anatomy and has been shown to be the most accurate technique in the detection of stenosis (Collins et al. 2007a).

2.3.4 Measuring flow velocities using MRI

The phase contrast methods used for PC-MRI produce both magnitude and phase images for each slice of data collected. These images are velocity encoded with gradients whose strength is optimised to contain the maximum expected phase-shift due to moving blood on the region-of-interest. In the phase image generated by the velocity encoded sequence, the pixel intensity is directly proportional to velocity. If the image slice is gated to the cardiac cycle the velocities in a region of interest can be mapped in time, producing a waveform similar to the envelope of a spectral Doppler ultrasound waveform. The techniques involved will be discussed in more detail in chapter 3.

2.3.5 Ultrasound techniques

2.3.5.1 Ultrasound imaging

Ultrasound imaging in medicine has roots in sonar and non-destructive testing and the first demonstrations of the potential of ultrasound as a diagnostic imaging technique took place in the 1950s. A landmark publication by Professor Ian Donald in Glasgow (Donald, Macvicar, & Brown 1958) described the use of ultrasound in the diagnosis of abdominal masses. Professor Donald's group went on to develop the technique for obstetric imaging and, in parallel with other researchers across the world, developed one of the first ultrasound imaging systems in the early 1960s. At this early stage, the main advantage of ultrasound over the alternative of x-ray imaging was that ultrasound did not involve ionising radiation; a factor which continues to put ultrasound as the modality of choice for obstetric imaging. The next breakthrough was the development of real time scanning in the late 1960s and early 1970s which enabled the operator to perform rapid multi-plane assessments of volumes of tissue in real-time, rather than just selected scan planes, and to detect movement which saw the beginnings of echocardiology. A major improvement in image quality arrived with the development of electronic array scanning with the first commercial linear array scanner from Aloka in 1976 (Woo 2006). Ultrasound imaging was, for many years, perhaps regarded as the "poor-

relation" of imaging. Despite the advantages of being non-ionising, non-interventional and real-time the recorded still images gave poor anatomic clarity compared to the emerging heavily processed images of CT and MRI. However, the development of ultrasound scanners since the mid-1970s has closely followed developments in electronics and computing and as such has been able to take advantage of the rapid acceleration of both the processing power and the miniaturisation of integrated circuitry. Commercial ultrasound scanners sold today are smaller, less expensive, faster and with far superior imaging capabilities than their equivalents of only ten years ago. Enhanced processing capabilities mean that ultrasound can now use features available to other imaging techniques such as image compounding and adaptive smoothing but without compromising the real-time aspect of the technology. In addition, there continue to be developments in technologies unique to ultrasound such as harmonic imaging, acoustic radiation force imaging (ARFI) and other elastography techniques and, more recently, beamforming techniques which compensate for variations in the speed-of-sound in tissue.

While ultrasound imaging is an inexpensive and completely non-invasive modality its main limitation is that it cannot be used to image the entire anatomy. Large acoustic impedance differences causing total or near total reflection make it impossible to image beneath bony and air filled structures. In areas that are easily accessible to ultrasound, calcification in arteries can cause shadowing artefacts and the presence of bowel gas coupled with the depth of arterial vessels, makes imaging the ilio-femoral segment difficult. Imaging the obese patient can be a challenge to all technologies, particularly in ultrasound imaging where the ultrasound is exponentially attenuated with depth. However, more sensitive transducer technologies, processing techniques and facilities such as harmonic imaging are helping to overcome this problem.

2.3.5.2 Doppler ultrasound

Doppler ultrasound technologies for the assessment of blood flow developed almost in parallel with ultrasound imaging, but initially were separate diagnostic instruments. These continuous wave instruments provided an audible output representing the Doppler shift in the ultrasound frequency caused by the moving red blood cells. The audible signal was sometimes complemented by a graphic

trace of the Doppler frequency envelope. Such “listening” devices gave no positional, directional or equivalent velocity information but are useful for the simple detection of flow and subjective assessment of the quality of flow and are in routine use in contemporary vascular laboratories and other clinical settings.

2.3.5.3 Spectral Doppler

The introduction of pulsed Doppler and spectral analysers in the late 1960s and early 1970s enhanced the utility of Doppler instruments with signal depth estimation, directional information and the ability to assess the frequency content of the Doppler waveform. However, it was not until 1974, that real time pulsed Doppler was incorporated into ultrasound imaging scanners (Barber et al. 1974) creating what were known as the first duplex ultrasound scanners. This heralded the use of ultrasound imaging techniques for vascular imaging and saw the increasing establishment of vascular laboratory facilities as a dedicated service for vascular surgery and vascular medicine.

Duplex ultrasound involves a Doppler beam combined with the 2-D, B-Mode ultrasound image. If a vessel can be imaged then a small “sample volume” along the Doppler beam can be placed within the vessel and the Doppler shift frequencies within the sample volume may be analysed. Using the image of the vessel and an overlaid line representing the position of the Doppler beam, an estimation of the angle between the beam and the direction of flow can be made. The angle may then be used in the Doppler Equation (equation. 3.1 in chapter 3) to give an estimate of the velocity of flow as will be discussed in detail in chapter 3. A typical duplex scan will show the B-Mode image with a separate representation of the varying Doppler frequency or velocity with time. Modern scanners will generally use a velocity scale, rather than a frequency scale. Since the pulsed Doppler processing component of a duplex scanner uses spectral analysis of the echo signal from within the sample volume, the instrument is providing the frequency content of the Doppler shift as it varies in time. The spectral display at each sample point in time maps the different amplitudes of the spectral frequencies with different shades of grey along the vertical frequency or velocity scale. The spectral Doppler display therefore displays the frequency or velocity content of the flow varying in time allowing

haemodynamic characteristics to be examined in real time. Spectral Doppler has proved to be a valuable technique in examining haemodynamics and led to the development of a wide range of quantitative criteria to aid in the diagnosis of vascular disease. Spectral Doppler is a standard feature on all but the most basic of ultrasound scanners.

2.3.5.4 Colour Doppler

While spectral Doppler is able to provide a real-time frequency or velocity spectrum at a sample volume position selected by the user, researchers soon began to examine the feasibility of mapping flow. It soon became possible to create off-line colour maps of flow overlaid on the B-mode image. However, it was the development of phase autocorrelation techniques by researchers in Japan in 1983 which enabled rapid real-time colour flow imaging (Woo 2006). Autocorrelation involves analysis of the change in phase of the echoes from moving targets to estimate the velocity of the targets. The first commercial colour flow scanners appeared in the late 1980s and the autocorrelation technique is still in use on the majority of contemporary scanners; providing a map of mean velocity flow overlaid on the B-Mode image. The colour-map is generally user selectable but typically represents different directional flow as different colour hues e.g. red and blue, with a spectrum of shades or tones to represent the variation in velocities within a selected range.

With improvement in processing capabilities colour Doppler, formerly predominantly used on dedicated vascular ultrasound scanners, is now available on the majority of scanners and is routinely used in ultrasound imaging in general. Colour Doppler is used to identify the presence of flow in the normal and pathological tissues and prior to further analysis of the quality of flow using spectral Doppler.

2.3.5.5 Power Doppler

Power Doppler imaging developed in the 1990s as a simple re-mapping of the colour-flow information to display the amplitude of the Doppler signal as a shaded single hue rather than the direction and mean velocity of the conventional colour-flow map. This technique has the advantage of aiding the

visualisation of the continuity of flow and is particularly useful in assessing perfusion.

2.3.5.6 Tissue Doppler

The high amplitude signals of the moving tissues surrounding vessels are filtered out for the majority of colour Doppler imaging applications. However, in Tissue Doppler, the scan is optimised to display a colour map of the moving tissues rather than the blood pool. This technique is of most value in assessment of the myocardium rather than the peripheral vasculature.

2.3.6 Other imaging techniques

2.3.6.1 DSA

Digital subtraction angiography, DSA, has long been regarded as the "gold-standard" and was the first line imaging investigation for peripheral (and indeed central) vascular imaging for many years. The output from an X-ray image intensifier is digitised making it easy to produce subtraction images where a "mask" image is taken prior to the injection of an iodinated contrast agent into the vascular system. The "mask" image is then subtracted from subsequent contrast images to remove the image of bony structures and show only the contrast agent within vasculature. This provides a detailed two dimensional "map" of the vascular anatomy with areas of occlusion being obvious due to the absence of contrast agent on the image and stenosis usually fairly clearly delineated. Access is usually via the femoral artery in the groin regardless of the region of interest and skilled radiological practitioners can then inject the contrast agent into the relevant part of the arterial tree. DSA may be used with pressure catheters to assess the haemodynamic significance of lesions.

Although some examinations can be performed as a day surgery case many patients will require sedation and local analgesia or general anaesthesia. In addition the iodinated contrast agents are potentially nephrotoxic and there is a risk of technique related complications such as haematoma, arterial spasm, atrerio-venous fistula, subintimal dissection, embolisation and infection.

With the availability of alternative imaging modalities; ultrasound, MRI and CT, DSA is rarely used as a first line imaging technique. In current practice, DSA is more commonly used to guide vascular interventions such as angioplasty and stenting which are increasingly favoured alternatives to surgery (Beard & Gaines 2009; Olin & Sealove 2010; SIGN 89 2006).

2.3.6.2 CTA

Computed tomography, CT, was first developed in the early 1970's, concurrently but independently by Hounsfield and McLeod Cormack who later shared the Nobel Prize in Medicine. The first commercial scanners were produced in the mid 1970's and were first used for brain imaging. Computed tomography is an x-ray based technology which uses an array of moving source-detector positions from which an axial cross section through the body may be constructed. Early forms of the technology used series of consecutive axial slices. However, modern CT scanners employ multi-detector arrays and spiral (or helical) acquisition to enable good resolution in rapid whole-body volume scanning. The use of iodinated contrast agents enabled computed tomographic angiography (CTA) to provide volumetric imaging of the vasculature i.e. a large three dimensional anatomic map.

CTA has a number of advantages over MRA in that it has better spatial resolution, does not suffer from flow artefacts and can image calcification and metal implants. However, a significant disadvantage is the over representation of heavy calcification which can obscure stenosis. In addition, CTA is associated with the same risks, relating to ionising radiation and the use of iodinated contrast agents, as for DSA. CTA, where available, tends to be used as an alternative to MRA when the patient has metal implants or the MRA scan has been non-diagnostic.

2.4 Chapter summary

This chapter aimed to summarise peripheral vascular disease and the methods, particularly imaging methods, used to aid in its diagnosis. Only two of the imaging methods discussed have the capability of adding blood velocity measurements to the diagnostic tool-set: Doppler ultrasound and phase contrast MRI. While ultrasound techniques are well established in terms of both the imaging and the quantification of blood flow, they are often limited by poor acoustic windows. MRI techniques have the advantage of being able to image any part of the body. However, as will be outlined in chapter 4, the use of PC-MRI techniques to quantify the peripheral vascular system in the same way as for spectral Doppler ultrasound has not yet been fully investigated.

Chapter 3 – The use of ultrasound and MRI methods for imaging and quantifying blood flow.

This chapter aims to provide an explanation and discussion of the principles and technology under investigation in the thesis, namely spectral Doppler ultrasound and phase contrast magnetic resonance imaging, PC-MRI. For a comprehensive overview of the underlying technologies of ultrasound and MRI, readers are directed to other sources.

3.1 Ultrasound methods of quantifying blood flow

This section explores the background science and technology behind spectral Doppler ultrasound measurement of velocities and their use as an aid to the diagnosis of peripheral vascular disease. Although we are primarily concerned with measurements made from the spectral Doppler waveform, this technique is rarely used in isolation. On modern-day scanners, colour Doppler imaging is used to detect the presence of blood flow and aid in the positioning of the sample volume of the spectral Doppler beam and a brief overview of the technique will be given.

For an overview of the scientific principles and technologies involved in ultrasound imaging, readers are directed to the following source:

Hoskins, Peter R., Martin, Kevin, Thrush, Abigail. 2010. Diagnostic Ultrasound: Physics and Equipment. Cambridge University Press.

In addition, a comprehensive overview of the historical development, scientific principles, technological implementation and medical application of Doppler ultrasound is given in*:*

Evans, D. H. & McDicken, W. N. 2000. Doppler ultrasound: physics, instrumentation, and signal processing. New York, John Wiley & Sons.

3.1.1 The insonation of moving blood and the Doppler effect

Ultrasound techniques for the quantification of blood flow rely on the processing of signals from the moving red blood cells within vessels. Typically, red-blood cells are around 7.5μm in diameter and, consequently, act as Rayleigh scatterers with an echogenicty of around 43dB lower than surrounding tissue (Oates 2001). Such small scatterers produce a detectable echo signal, but the low amplitude relative to the echoes from surrounding tissue means that blood is represented as black on the grey-scale display of the B-Mode image suggesting that blood flow is not detectable, figure 3.1. However, frequency analysis of the returned echoes from the moving blood cells is the basis of well established techniques for the visualisation and quantification of blood flow.

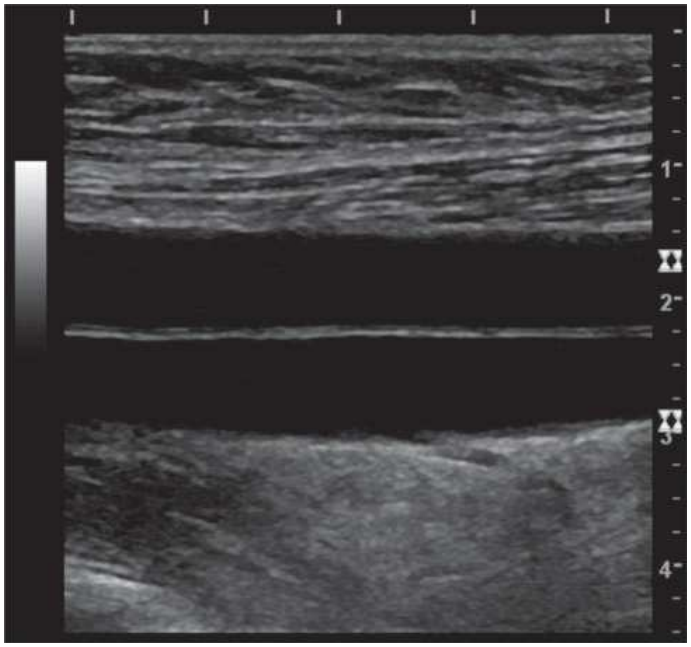

Figure 3.1: B-mode image showing two blood vessels with the blood shown as black due to the low signal intensity of echoes from the red blood cells compared to the surrounding tissue.

The Doppler effect was first identified by Christian Andreas Doppler, in 1842, who described the change in frequency of a wave for an observer in motion relative to the source of the wave. This was adapted for sound waves, with a moving source and a stationary observer, by Ballot in 1945. Its earliest use in medical applications was in the late 1950s, around the same time that ultrasound medical imaging devices were beginning to emerge. The first Doppler instruments were non-imaging, continuous-wave devices which operated on the principle that the echoes from moving red-blood cells would cause a shift in the

ultrasound frequency proportional to their velocity. This is illustrated in figure 3.2, and is the basis of the Doppler shift equation, equation 3.1.

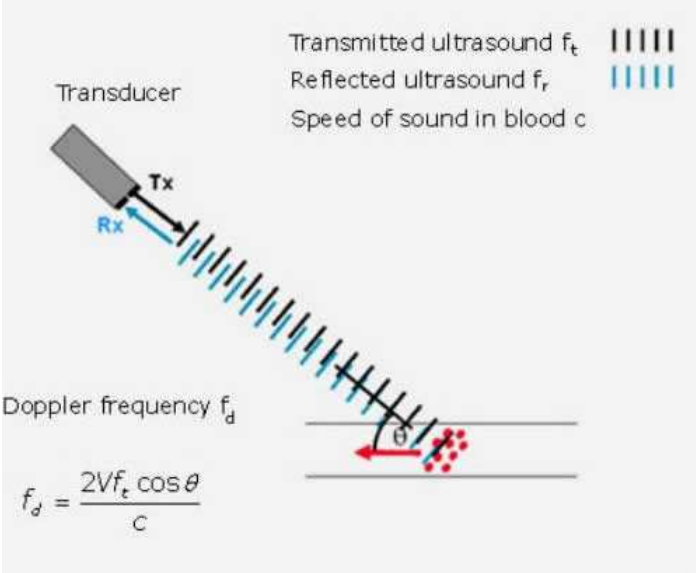

Figure 3.2: Calculation of the Doppler shift frequency, fd, for continuous wave ultrasound.

$$fd = fr - ft = \frac{2vft\cos\theta}{c}$$

Equation 3.1. The Doppler Equation

where *fd* is the Doppler shift frequency, *ft* is the transmitted ultrasound frequency, *fr* is the ultrasound frequency of the received echo signal, *v* is the velocity of the moving echo source, *θ* is the angle of insonation between the transmitted ultrasound beam and the direction of flow, *c* is the speed of sound value of 1540 ms^{-1} to which the ultrasound system has been calibrated.

If the Doppler frequency, f_d, can be measured, and the angle of insonation estimated, then it is possible to determine v, the velocity of the moving blood.

Evans (Evans & McDicken 2000), provides a derivation of the Doppler equation and further explanation of the phenomenon.

3.1.2 Visualisation of blood flow: colour Doppler imaging

Historically, non-imaging, spectral Doppler ultrasound techniques were developed before the visualisation of blood flow using ultrasound was considered. However, the use of colour Doppler ultrasound to image vasculature is now commonplace. Strictly speaking, colour Doppler is not a true Doppler technique, as for continuous wave Doppler, as it does not make use of Doppler shift frequencies; rather it determines the change in the round trip time for consecutive pulses from the transducer to a site of interest, or sample volume, by measuring changes in phase. The rate of change of phase can then be interpreted as a Doppler shift frequency allowing the Doppler equation, equation 3.1, to be used to estimate the velocity of the moving scatterers (Evans, Jensen, & Nielsen 2011).

Contemporary colour Doppler ultrasound scanners use phase autocorrelation techniques to estimate the velocity between consecutive pulses. Multiple echoes from the same moving reflector are collected using a series of transmitted pulses (Hedrick & Hykes 1995). Typically, between 8 and 18 pulses are used to give a good estimate of the mean velocity. Colour flow mapping involves representing the sample volume as a pixel of a colour and hue that relates to the magnitude and direction of the mean velocity. By having a grid of such sample volumes, a colour velocity map is created over the B-mode image, figure 3.3.

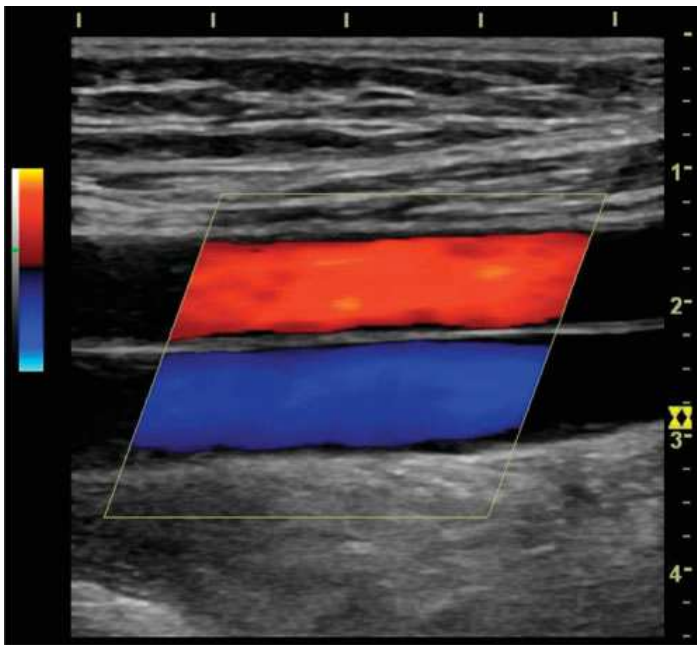

Figure 3.3: Colour Doppler image showing a colour Doppler map of mean velocity for the two blood vessels imaged in figure 3.1.

The processing involved in creating the colour Doppler map is restricted to the colour-box area so that frame-rates may be maintained to allow real-time imaging.

Although early attempts were made at using colour Doppler imaging for blood flow quantification (Picot et al. 1995), colour Doppler imaging is a visualisation technique and might be thought of as analogous to angiography in that it is indicating the presence and anatomic location of blood flow. However, colour Doppler techniques go further than angiography in that they are time resolved and indicate the velocity and direction of flow; features that the new 4D Flow MRI technologies are attempting to emulate (Markl et al. 2012a).

3.1.3 Spectral Doppler ultrasound measurement of blood flow

Where colour Doppler provides a visual map of flow over a region of interest, spectral Doppler ultrasound techniques perform more detailed analysis on a sample of echoes from a much smaller region.

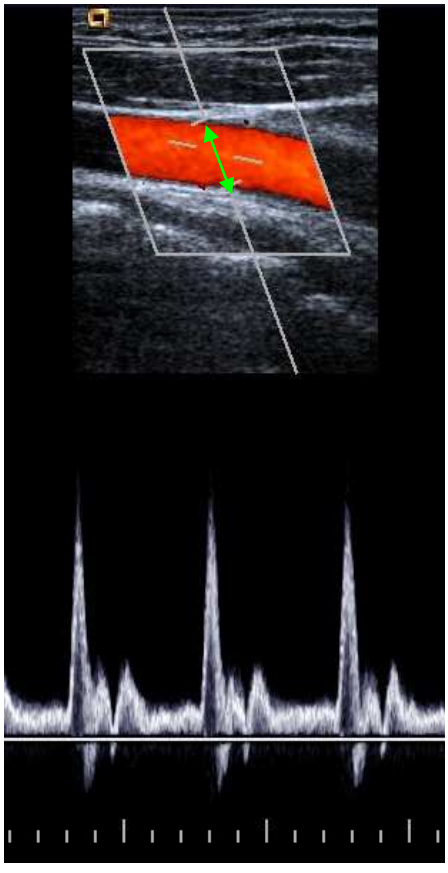

Figure 3.3: Spectral Doppler ultrasound. The spectral waveform at the bottom of the image is created by sampling the region highlighted by the green double arrow.

Figure 3.3 illustrates a colour Doppler image with the path of a spectral Doppler beam indicated in white. The region highlighted in green, known as the range gate or sample volume is the only part of the signal selected for analysis. However the analysis is repeated for consecutive time-segments allowing for a real time display of changes in velocity over time. Fast Fourier Transform, FFT, analysis of the extracted Doppler signal enables the range, or spectrum, of velocities within the sample

volume to be displayed for each time segment. Velocity measurements are made using manual placement of velocity cursors, or automated features which will detect the maximum and mean frequency envelopes over a section of the Doppler spectral display.

3.1.4 Physical limitations of Doppler velocity estimation

As will be discussed in section 3.1.6, spectral Doppler ultrasound has become the standard technique for the quantification of blood flow; in particular, the determination of blood velocities derived from the detection of Doppler shifted frequencies. Spectral Doppler methods of determining the degree of stenosis within a vessel focus on the accurate estimation of maximum peak systolic velocities and ratios with both technology and user protocols designed with this aim in mind. This can make direct comparison with technologies focussed around the quantification of mean flow or volume flow difficult. As discussed in chapter 2, the blood flow profile will vary both spatially and temporarily within vessels. Spectral Doppler ultrasound attempts to provide an accurate representation of the velocity profile as it changes in time. However, the following issues should be acknowledged as sources of error.

3.1.4.1 Beam flow angle effects

The angular term in the Doppler equation, equation 3.1, highlights the need to provide an accurate estimation of the beam-flow angle, avoiding angles greater than 60° to minimise calculation errors. For example: simple calculation using the Doppler equation reveals that at an angle of insonation of 80°, an angle estimation error of 1° will produce an error of 10%. It should also be noted that this cosine term means that the velocity of flow perpendicular to the ultrasound beam will be zero. Good angle estimation by the operator is easy in situations where there is good longitudinal imaging of straight sections of vessel. In reality, angle estimation can be difficult in situations where the vessel is curved, tortuous, stenosed or poorly imaged due to calcification shadowing or depth and resolution limitations. The use of multidimensional and vector Doppler ultrasound methods of velocity estimation to reduce angle related errors has been investigated (Steel et al. 2003). However, these methods involve off-line computation and have yet to be implemented on any commercial scanners.

3.1.4.2 Intrinsic spectral broadening

Spectral broadening of arterial waveforms is an acknowledged useful indicator of the presence of turbulence due to stenosis or of the "flattening" of the velocity profile due to post-stenotic flow dampening (Oates 2001; SVT 2001a; Thrush & Hartshorne 2009). It is, therefore, important that such changes are not masked out by the intrinsic spectral broadening of the ultrasound system itself. Intrinsic spectral broadening in spectral ultrasound exists due to the finite beam aperture size (Guidi, Licciardello, & Falteri 2000; Hoskins et al. 1999). The finite beam aperture size means that the direction of flow is subtended by a range of angles, rather than the assumed central beam angle. This is illustrated in figure 3.4.

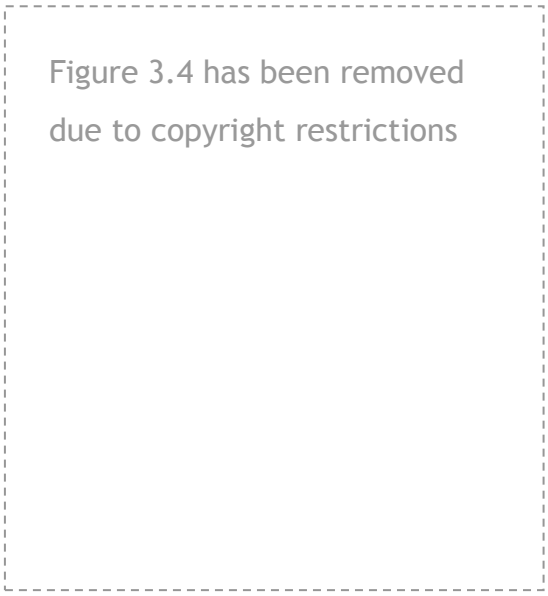

Figure 3.4: Illustration of the finite aperture reason for intrinsic spectral broadening. The on-screen image of the spectral Doppler beam is represented by the blue line with an angle correction for θ used in the calculation of velocities. However, the finite width of the Doppler beam results in a spread of Doppler frequencies and displayed velocities. Adapted from Hoskins (Hoskins 2011).

Flow signals are "seen" by all the elements forming the beam aperture with each element detecting flow at a different angle leading to a spreading of the range of Doppler shift frequencies. The angle correction in the calculation of velocities is only applied for the central, assumed beam angle, resulting in the angle estimation errors described in section 3.1.4.1 above, exacerbating the problem. Different manufacturers use different transducer element sizes and employ a variety of beam-aperture forming techniques which leads to variations in the velocity detection errors between manufacturers (Fillinger et al. 1996; Steinman et al. 2001; Ultrasound Equipment Evaluation Project 2004b). Spectral broadening generally leads to an overestimation of velocity and typically is of the order of 10% to 40%. The same multi-beam and vector Doppler methods

referenced in section 3.1.4.1 have been investigated as ways of overcoming the intrinsic spectral broadening effect as well as the errors due to angle estimation.

3.1.4.3 Beam geometry and sample volume issues

The problem of intrinsic spectral broadening due to the finite beam aperture, as described above, already hints that ultrasound beam geometry may be a source of error. The slice or elevational plane dimension can be a source of artefactual error in both B-Mode imaging and spectral Doppler measurement. In imaging, when the slice thickness is larger than the target being insonated, the summed display of echoes in the scan plane volume may mask out small objects. In a duplex Doppler image, when, for example, imaging a small vessel longitudinally, the vessel may not be clearly visible in the B-mode image if the diameter is smaller than the slice plane thickness. However, flow can still be detected and, indeed the volume will accommodate all the velocities contained within the vessel. Conversely, if the scan plane thickness is smaller than the vessel diameter, partial volume effects will occur. These effects are illustrated in figure 3.5.

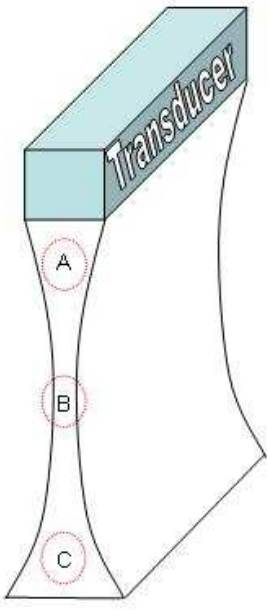

Figure 3.5: The effect of scan plane thickness. Vessels positioned at A and C will suffer in-fill effects and may not be imaged clearly. The same diameter vessel positioned at B will be imaged clearly and the full diameter shown but the full vessel, and therefore the full range of velocities, is not in the image plane.

Since the operator is generally focussed on maximising the displayed spectral velocities, it is likely that the Doppler volume captured for measurement will indeed contain the highest velocities but, as shown in figure 3.5, will

misrepresent the spectral content of the lower velocities close to the vessel wall. This will have the effect of overestimating the true mean velocity and therefore overestimating volume flow, something which has been confirmed by *in-vitro* studies (Ho et al. 2002) .

The use of inadequate sample volumes is a further source of partial volume error. The sample volume is the small region of interest used for the spectral Doppler sampling of flow, indicated by a pair of short parallel lines across the Doppler beam line indicator overlaid on the B-mode image, see figure 3.3. The user is in control of both the depth position and the width of the sample volume. Scanning protocols generally recommend a small sample volume e.g. 1/3 of the vessel diameter (SVT 2001a), placed in the centre of the vessel lumen or at the stenosis. Reducing the sample volume will further reduce the display of lower velocity components due to partial volume effects as described in the above paragraph and shown in figure 3.5. Since spectral Doppler ultrasound blood flow quantification is generally concerned with the measurement of peak velocities and their associated ratios, the use of a small sample volume is reasonable and, although it will not show the full range of velocities present, it will be able to show the increasing range of high velocity content due to turbulent stenotic flow. This technique will overestimate mean velocity values and a sample volume which encompasses the vessel diameter should be used if that quantity is required. It might be suggested that a wide sample volume should always be used since that technique gives less chance of missing the peak velocities as a more complete spectrum of frequency content of flow will be contained by the sample volume.

3.1.4.4 Temporal sampling rates (pulse repetition frequency)

A well recognised limitation in the estimation of velocities using the Doppler technique is the Nyquist limit which states that the minimum rate that a signal should be sampled, in order to determine the true frequency, is twice the true frequency. This is expressed in equation 3.2 where $f_d$max is the maximum detectable Doppler shift and PRF is the pulse repetition frequency, or sampling frequency.

Equation 3.2: The Nyquist limit

$$fd\max = \frac{PRF\max}{2}$$

Substituting Equation 3.2 into the Doppler Equation, Equation 3.1, we can rearrange to calculate the maximum detectable velocity, Vmax as shown in equation 3.3:

Equation 3.3: The maximum detectable velocity

$$V\max = \frac{cPRF\max}{4ft\cos\theta}$$

This places an upper limit on the velocities that may be determined using spectral Doppler ultrasound. Undersampling of the Doppler shift frequency when the Nyquist limit is reached will cause aliasing of the spectral display of velocities as illustrated in figure 3.6.

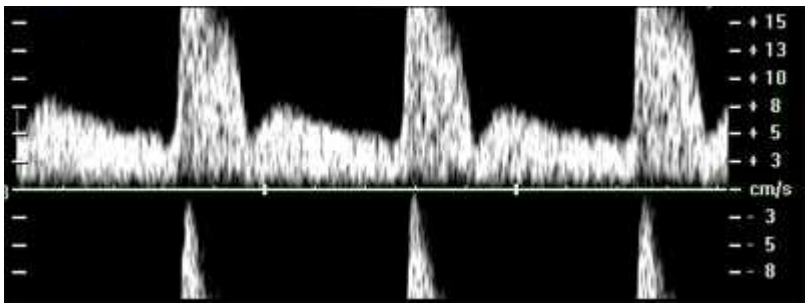

Figure 3.6: Spectral Doppler aliasing. When the Nyquist limit is reached the higher velocities within the spectrum are misinterpreted as low velocities.

Since the pulse repetition frequency is also inversely related to the depth, this will place a further upper limit on the velocities that can be measured in deeper vessels. Lower transmit frequencies will allow higher velocity flow to be sampled within the PRF limit and have the added advantage of less attenuation of the weak echo signals from the moving red blood cells. For these reasons the frequency for spectral Doppler used in duplex imaging is generally significantly lower than the transmit frequency used to produce the corresponding B-mode image. A consequence of the use of lower frequencies is, of course, the reduction in spatial resolution for the Doppler information.

Modern, high end scanners are generally able to cope with maximum velocities over a range of 3 to 5 ms^{-1} depending on the depth of the sample volume. From a practical, diagnostic, point-of-view the problem of velocity aliasing is

irrelevant when such velocity limits have been reached as velocities of such a high magnitude will in themselves indicate the presence of stenotic flow.

3.1.5 Other limitations of vascular ultrasound

A major disadvantage of the use of any ultrasound technique is when a poor acoustic window makes transmission and detection of ultrasound difficult or impossible rendering many anatomic regions unsuitable for ultrasound. Any interfaces which involve high impedance changes have the potential to cause acoustic shadowing or artefact, for example: the lungs, bowel gas, bone, calculi, atherosclerotic plaque. In addition, the increasingly obese population (World Health Organisation 2012) is challenging to a technology which is limited by depth dependent attenuation.

It is well known that there can be significant variability of spectral Doppler velocity measurements between operators and between different makes and models of scanners (Beach, Leotta, & Zierler 2012; Corriveau & Johnston 2004; Hadlock & Beach 2009). Some of these differences can be accounted for by sub-optimal scanning and measurement techniques (Lui et al. 2005) factors which, in theory, it should be possible to address via training and audit.

3.1.6 The development of velocity ratios and indices

This section will focus predominantly on spectral Doppler ultrasound as it is in this modality that the development and use of flow waveform indices for disease quantification have taken place and become established.

Velocity ratios have the potential to eliminate sources of systematic error in the measurement of the velocities. However, since, as discussed in section 3.1.4.1, the angle of insonation provides a major source of error, it is important that the spectral Doppler waveform for each artery is optimised separately before velocity measurement. Nevertheless, it may be speculated that the use of velocity ratios may translate between flow quantification modalities e.g. ultrasound and MRI, where there may be differences in the absolute measurement of flow velocity. This will, of course, rely on a linear response to true velocity in both modalities.

3.1.6.1 Carotid artery stenosis ratios

Doppler ultrasound techniques have been used in the determination of internal carotid artery stenosis since the 1980's when duplex Doppler became available on commercial ultrasound scanners. Several investigators (Blackshear et al. 1980; Lewis & Wardlaw 2002) developed and investigated the ratio of peak systolic velocity in the internal carotid artery, ICA_{PSV} versus peak systolic velocity in the common carotid artery, CCA_{PSV} as an indicator of the degree of lumen stenosis. However, other researchers explored a variety of alternative indices, all based on maximum velocity ratios (Bluth et al. 1988; Friedman et al. 1988; Knox, Breslau, & Strandness, Jr. 1982). Research in this area accelerated when, in 1991, the results of two large scale trials of surgical endarterectomy for the treatment of stenosis were reported. The North American Symptomatic Carotid Endarterectomy Trial (NASCET) (North American Symptomatic Carotid Endarterectomy Trial Collaborators 1991) and the European Carotid Surgery Trial (ECST) (European Carotid Surgery Trialists' Collaborative Group 1991) reported on the treatment of carotid artery stenoses with differing percentage reduction in diameter as determined by x-ray angiography. The NASCET trial showed a modest but significant benefit in patients with 50-69% stenosis with maximum benefit in patients with stenoses >70%. The ECST reported modest but

significant benefit in patients with 70-79% stenosis with maximum benefit in patients with stenoses >80%. These differences were due to the different methods of determining the percentage lumen reduction as shown in figure 3.7.

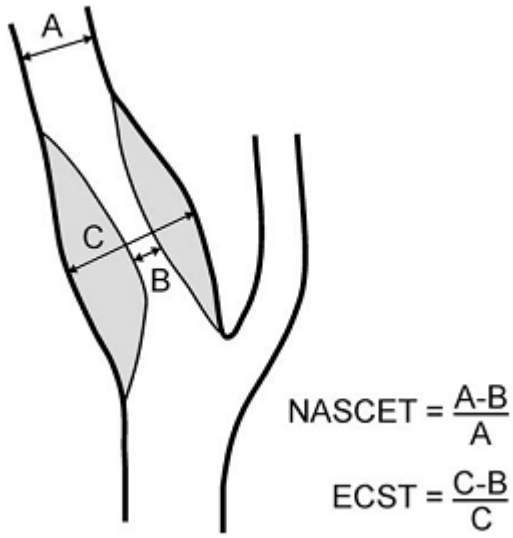

Figure 3.7: Schematic diagram of a stenosis of the internal carotid artery showing the NASCET and ECST methods of calculation of stenosis using diameter reduction.

Although the two trials were based on x-ray angiography, the availability of duplex and colour flow mapping on commercial ultrasound systems and the increasing work done on carotid artery investigation using those techniques meant that ultrasound represented a feasible, attractive, non-ionising and non-interventional alternative or adjunct to conventional angiography.

The different methods of stenosis quantification used in NASCET and ECST lead to some confusion translating Doppler velocity index measurements into relevant criteria for determining percentage stenosis, giving rise to a variety of consensus and guideline publications. This has resulted in international, regional and local variations in the combination of parameters used to determine stenosis.

Since the decision to treat has been based on these criteria since 1991, it has been essential that all methods of determining percentage of stenosis are consistent within a local site. In NHS Greater Glasgow and Clyde, the criteria for consideration for surgery has been a stenosis > 70% as defined by the NASCET criteria. The Current SIGN guidelines for the management of stroke (SIGN 108 2008) state that:

"Carotid endarterectomy (on the internal carotid artery ipsilateral to the cerebrovascular event**) should be considered in all:**

- Male patients with a carotid artery stenosis of 50-99% (by NASCET method)
- Female patients with a carotid artery stenosis of 70-99%"

A recent UK working group (Oates et al. 2009) has summarised the confusing issues and produced a set of recommendations on scanning methods and diagnostic criteria for the determination of internal carotid artery stenosis using spectral Doppler ultrasound. The diagnostic criteria are reproduced in table 3.1.

Table 3.1 has been removed due to copyright restrictions

Table 3.1: Consensus criteria for the determination of percentage stenosis of the internal carotid artery using spectral Doppler ultrasound measurement of maximum velocities and ratios (Oates et al. 2009).

Spectral Doppler ultrasound must therefore be capable of accurate measurement of:

- Maximum peak systolic velocity in the common carotid artery, CCA_{PSV}
- Maximum end diastolic velocity in the common carotid artery, CCA_{EDV}
- Maximum peak systolic velocity in the internal carotid artery, ICA_{PSV}

Such that the following ratios may be calculated:

- Peak Systolic Velocity (PSV) Ratio = ICA_{PSV} / CCA_{PSV}
- St. Mary's Ratio = = ICA_{PSV} / CCA_{EDV}

Commercial ultrasound systems have on-board facilities for the collection of velocity data and the calculation of velocity indices.

The methods and diagnostic criteria described in the recent recommendations have been endorsed by all relevant professional bodies in the UK and are likely to be adopted as standard thought the UK.

3.1.6.2 Common femoral pulsatility index

The pulsatility index (PI) in the form as used in current spectral Doppler assessment methods (SVT 2001c) is shown in figure 3.8.

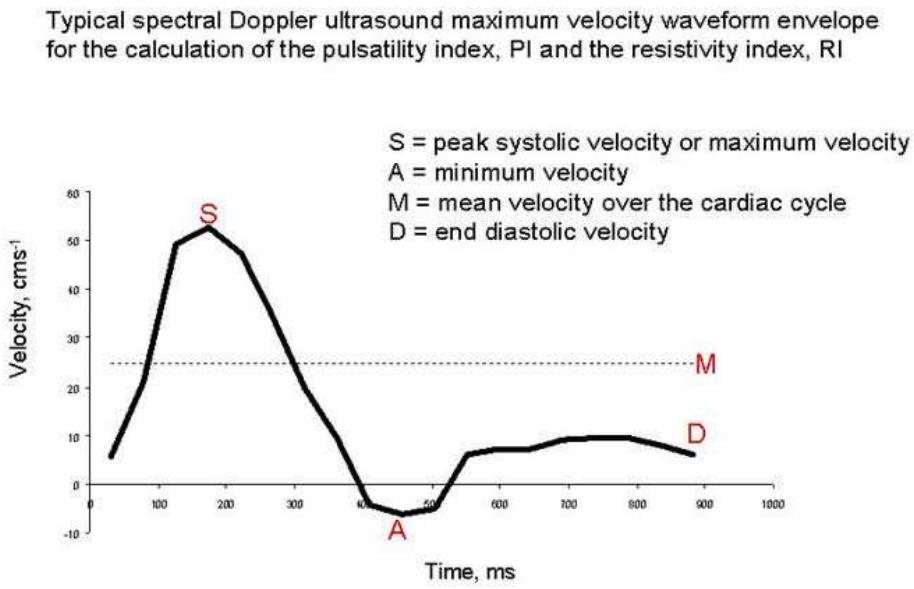

Figure 3.8: Parameters used in the calculation of the pulsatility index, PI.

The pulsatility index represents the maximum velocity excursion (systolic – diastolic) divided by the mean velocity over the cardiac cycle (Gosling & King 1974), i.e. PI = (S – A)/M. This index provides a numerical measure of the waveform shape and has been used in a variety of vascular imaging areas mainly to indicate proximal stenosis, or downstream resistance. The PI was first applied clinically in the late 1970s and is still in use today in many lower limb arterial scanning protocols. In peripheral vascular disease, PI measurement in the common femoral artery at the groin can indicate waveform dampening due to the presence of proximal stenoses in the aorto-iliac segment. A low (< 4) value of PI is regarded as indicating the presence of proximal disease. This was regarded as a useful technique since scanning of the aorto-iliac segment can be difficult due to body habitus and bowel gas. Lower limb arterial scanning protocols in vascular laboratories in Glasgow do not currently perform aorto-iliac scanning routinely; instead, the distal common femoral is scanned and the PI recorded, prior to scanning the rest of the limb. However, conflicting reports of the consistency and, indeed, usefulness of PI measurements have placed its role as a marker of aorto-iliac disease into doubt (Reddy et al. 1986). PI measurements can be complicated by the presence of outflow disease and by central cardiac disease. Most centres who record PI will regard a low value, in combination with visual assessment of the waveform and image, as an indicator for further investigation rather than as a confirmation of the presence of proximal disease.

For the pulsatility index, PI, to be used effectively requires accurate determination of:

- Maximum or peak systolic velocity of the waveform, S
- Minimum velocity of the waveform, A
- Mean velocity over the cardiac cycle, M

As for carotid imaging, commercial ultrasound systems have on-board facilities for the collection of velocity data and the calculation of velocity indices and usually provide auto-Doppler tracing for determination of the time average velocity and heart rate.

3.1.6.3 Resistivity index

A further, commonly used indicator of the waveform shape is Pourcelot's resistance index (Pourcelot 1976) which used the peak systolic and end diastolic maximum velocities. Using the diagram in figure 3.8, would give a resistivity index, RI = (S-D)/S. RI provides an indicator of waveform dampening due to distal resistance and is usually used in situations where low resistance forward flow is expected.

For the resistivity index, RI, to be used effectively requires accurate determination of:

- Maximum or peak systolic velocity of the waveform, S
- End diastolic velocity of the waveform, D

Although this index has been investigated for the assessment of carotid artery stenosis (Evans & McDicken 2000; Shakeri, Zarrintan, & Shakeri-Bavil 2008), it is more commonly used in renal applications (Valiente Engelhorn et al. 2012).

3.1.7 Other indices

The most commonly used spectral Doppler diagnostic indices have been described above. However, a number of other velocity ratios have been described such as the systolic to diastolic ratio, constant flow ratio and the early diastolic notch index. In addition, a number of indices using time parameters have been defined e.g. velocity acceleration, systolic decay time curve broadening index. Spectral broadening indices have also been investigated by a number of authors, particularly in relation to carotid artery stenosis. Description of the aforementioned indices and others is provided in a comprehensive review by Evans (Evans & McDicken 2000).

3.2 The use of phase-contrast magnetic resonance methods for imaging and quantifying blood flow.

This section explores the background science and technology behind PC-MRI imaging and blood flow quantification with a focus on velocity encoding and blood flow quantification.

For an overview of the fundamental principles underpinning MRI imaging and an overview of magnetic resonance angiography techniques, readers are directed to the following texts:

D. W. McRobbie, E. A. Moore, M. J Graves, and M. R. Prince. MRI From Picture to Proton, Cambridge University Press, 2003.

M. A. Bernstein, K. F. King, and X. J. Zhou. Handbook of MRI Pulse Sequences, Academic Press, 2004.

3.2.1 Phase contrast imaging techniques

All magnetic resonance imaging (MRI) is based on the physical principles of nuclear magnetic resonance (NMR). In medical imaging it is the magnetic resonance of the single proton within the hydrogen atom that is of interest; since hydrogen is abundant in biological tissues in the form of water and other molecules. In, particular, we are interested in what happens to the magnetic resonance of protons in the presence of an external magnetic field. Phase contrast imaging, PC-MRI utilises the phase shifts of protons moving through a magnetic field gradient.

When transverse magnetisation is created by an RF pulse and a magnetic field gradient is applied, the spins will precess at different frequencies and acquire phase shifts dependent on their position along the gradient. These position dependent phase shifts can be compensated for by applying an identical gradient of the opposite polarity. However, if a proton moves position in the time between the two gradient pulses, the phase shift will not be completely

cancelled out. The residual phase shift will depend on how far the proton moved during the time interval i.e. the velocity. This phenomenon, known as phase contrast MRI (PC-MRI), can be used to produce angiographic images where the contrast is due only to the motion of blood. PC-MRI is regarded as being sensitive to flow over a large range of velocities and can provide directional information.

PC-MRI is of particular interest to this thesis in allowing quantification of blood flow in terms of both volume flow and velocities over time.

The following sections will explore PC-MRI and its capabilities in more detail.

3.2.2 Phase contrast blood flow imaging

The phase contrast imaging technique uses gradient echo pulse sequences in preference to spin-echo as the rapid signal generation techniques involved in gradient switching lend themselves to a technique where spatio-temporal resolution is limited by gating to the cardiac cycle.

3.2.2.1 Gradient Echo

Gradient echo pulse sequences use matched gradients of opposite polarity to the encoding gradient to refocus spins and achieve coherence. Figure 3.9 shows a simple gradient echo sequence.

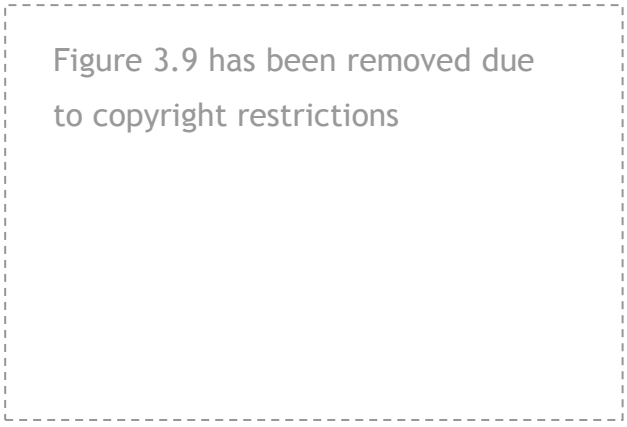

Figure 3.9: A Gradient-echo pulse sequence showing the application of gradients in all three axes. After the RF pulse has been applied the spins will dephase in the transverse plane. Application of a negative gradient in the frequency encoding direction, enhances dephasing. The readout gradient is applied with the opposite polarity so that at TE the signal has rephased and is at a maximum and can be read out. (Hornak 1996)

One of the advantages of gradient echo sequences is that they can use small flip angles which give magnetisation with components in both the longitudinal and transverse direction. There will be a loss of magnetisation due to the small angle

but this also means less time is required to recover the longitudinal component. The RF pulses are repeated rapidly such that, with careful selection of flip angles and TR, the signal will show a small decrease but, after a few pulses, will reach a "steady-state" where the increase in longitudinal relaxation is matched by the decrease in magnetisation due to the small angle. The effect is illustrated in figure 3.10. The steady-state situation may be referred to as saturation where each excitation and repetition will return the same level of signal.

Figure 3.10 has been removed due to copyright restrictions

Figure 3.10. Excitation and Relaxation magnetisation curves for flip angles of 20°, 30° and 45° with a repetition rate of 0.2. The signal decreases exponentially towards a level where the increase in longitudinal magnetisation at relaxation is matched by the loss of magnetisation due to the small flip angle. (Yucel 1995)

In the case of blood moving through the image slice, the spins flowing into the slice will not have reached the steady-state or saturation and will have a higher signal than the surrounding stationary tissue. This produces a flow related enhancement or bright-blood image where the intensity of the blood flow signal is related to the velocity of the blood (Yucel 1995).

Gradient echo methods are generally preferred for angiographic imaging as the enhanced blood flow signal is a more tangible phenomenon for further manipulation than the black-blood or signal voids generated by spin echo techniques. A major advantage of gradient echo techniques is that they are faster than spin echo with short TE and TRs making it easier to employ time-limited scanning techniques such as breath-hold and cardiac gating.

3.2.2.2 Velocity compensation

Phase contrast angiographic images are generally used with gradient echo acquisitions and make use of bipolar gradients to compensate for phase shifts. The bipolar gradients may be used to null out the phase-shifts in static tissue which may be non-zero due to static field inhomogenieties. Figure 3.11 illustrates the phase shifts from stationary and moving signals in the presence of a bipolar gradient. A phase contrast pulse sequence will generally have a pair of bipolar gradients within the sequence.

Figure 3.11: The phase shift ΔΦ due to velocity. The balanced bipolar gradient cancels out any phase shifts due to inhomogenieties in static tissue (McRobbie et al. 2003).

Considering the phase,Φ, of a spin precessing at the Larmor frequency, $\omega = \gamma B_o$ in a static magnetic field of magnitude B_o where γ is the gyromagnetic ratio.

Equation 3.4 $$\phi = \int \omega dt = \gamma \int B_0 dt$$

In the presence of a magnetic field gradient G_z, Equation 3.4 becomes

$\phi = \gamma \int (B_0 + G_z z) dt$ for "static" spins and

$\phi = \gamma \int [B_0 + G_z (z + vt)] dt$ for spins moving through the gradient in the z direction with a velocity v.

To calculate the phase change due to velocity we can calculate the difference between the two phases, static and moving, above, in the presence of a gradient of strength G and duration, T, i.e.

Equation 3.5: $\phi = \gamma \int_0^T Gvt \cdot dt = \left[\frac{1}{2} \gamma v G t^2 \right]_0^T = \frac{1}{2} \gamma v G T^2$ where GT^2 is known as the first moment of the gradient, M_1.

If the second gradient in the bipolar pair is of the same duration and amplitude but the opposite polarity then the negative of the result in Equation 3.5 may be derived so that subtracting the two gives a total phase shift of

Equation 3.6 $\phi = \gamma v M_1$ i.e. the phase shift due to the movement at velocity, v.

The phase contrast sequence will perform two acquisitions with the second bipolar gradient at the reverse polarity of the first, figure 3.12.

Figure 3.12 has been removed due to copyright restrictions

Figure 3.12: A cine phase contrast velocity mapping sequence showing a pair of velocity encoding bipolar gradients (red dotted circles) along the slice select axis. Adapted from McRobbie (McRobbie et al. 2003)

It is then possible to calculate a phase difference $\Delta\Phi$ which is dependent on the velocity and the difference between the two moments of the bipolar pulses, ΔM, equation 3.7.

Equation 3.7 $\Delta\phi = \gamma v \cdot \Delta M_1$

A phase image is calculated for each of the acquisitions and the two images subtracted. The phase will be constant for the static tissue but will vary for the moving blood so that the resulting phase image will be shown as a mid grey equivalent to zero flow with positive and negative directional flow shown as darker or lighter shades of grey. The PC sequence does of course also create a magnitude image from the acquisitions which may be combined with the phase-contrast image to further suppress random phase fluctuations from areas of low signal e.g. air. Figure 3.13 shows an example set of images collected during this study.

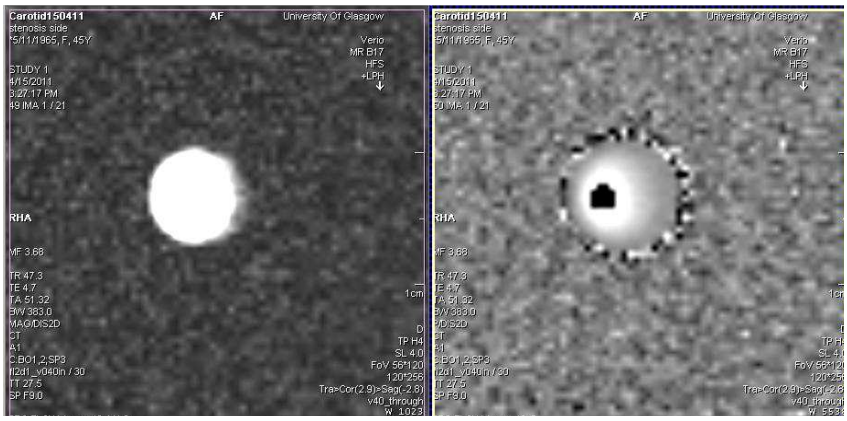

Figure 3.13: Example of a magnitude image (left) and a phase image (right) from a single time-point in a velocity encoded image acquisition slice. Note that the phase image on the right demonstrates velocity aliasing, or phase-wrap, due to the velocity encoding value being set at a level lower that the maximum velocity of flow at that point.

3.2.2.3 Velocity encoding and flow quantification

In the paired bipolar gradients described above, the second bipolar gradient is referred to as the velocity encoding gradient.

Velocities may be encoded using the venc, velocity encoding, parameter which is the velocity which will produce a phase shift of 180° or π radians, so that using equation 3.7,

$\pi = \gamma \cdot venc \cdot \Delta M_i$ and define venc as:

Equation 3.8 $$venc = \frac{\pi}{\gamma \Delta M_1}$$

Substituting for ΔM_1 in equation 3.7 gives

Equation 3.9
$$\Delta\phi = \frac{v}{venc}\pi$$

The usable phase difference is limited to ±π (±180°) so that it is possible to reliably determine velocities only when $|v| \leq venc$. For a high enough venc, it is possible to extract velocity from the measured phase difference (Bernstein, King, & Zhou 2004) by rearranging Equation 3.9:

Equation 3.10
$$v = \left(\frac{\Delta\phi}{\pi}\right) \cdot venc \qquad \text{-venc < v < +venc}$$

The ±π limitation on the measured phase difference can cause phase wrapping or velocity aliasing artefacts on the calculated images. This limitation will be discussed in more detail in section 3.2.6.4.

PC-MRI protocols require the user to set a venc value appropriate to the velocities likely to be encountered within the imaged volume. Setting the venc value will determine the amplitude and duration of the bipolar gradient pairs.

Velocity encoding may be applied in all three spatial encoding directions and it may be useful to do this when imaging volumes of tissue containing complex or tortuous vascular structures. Flow or velocity quantification methods, however, generally only use a single slice perpendicular to the direction of flow. Velocity sensitisation and therefore velocity encoding gradients are in the slice select direction. Pulse sequences such as that shown in figure 3.12, with flow encoding in the slice select direction are the focus of this thesis.

3.2.3 Time resolved quantification of flow velocities

So far we have considered the generation of velocity encoded images. However, when examining pulsatile flow, it is useful obtain a time-resolved depiction of the blood flow. A cine display of image will provide a qualitative, visual, assessment of flow patterns, minimising artefacts due to pulsatile movement. Using the same set of time-synchronised image slices, selection of a region of

known flow will allow the velocity and volume flow values to be graphed along a time axis providing quantitative information analogous to that provided by spectral Doppler ultrasound.

To achieve time-resolution in PC-MRI and collect data for a specified number of frames within the cardiac cycle, it is necessary to synchronise signal acquisition with the patient's heart rate. This may be done using cardiac or peripheral gating methods which give rise to additional technological challenges and limitations on the accuracy and quality of acquired data versus overall scan times.

3.2.4 Gated signal acquisition

Time-synchronisation of images for the assessment of pulsatile blood flow may be achieved using two methods of gating: Electrocardiogram (ECG) gating and peripheral pulse gating. ECG gating uses three or four lead MRI compatible electrodes to collect cardiac waveform data which is then used to enable triggered MRI sequence data collection and synchronisation. Peripheral gating is an alternative method which involves placing a photoplethysmography sensor on a finger or toe and using the graph of the arterial pulse for triggering and synchronous MRI data collection. The arterial pulse will be delayed compared to the R-wave of the ECG and there may be implications for either technique due to the position of MR data collection in the body relative to the site of trigger signal data collection. While peripheral gating may have practical and patient-acceptability advantages, one of its main disadvantages is that the arterial pulse is temporally much wider than the sharp R-wave of the ECG. The longer 'peak' duration for peripheral gating will limit the number of MRI slices that can be collected in the peak-to-peak (or R-R) interval and consequently limit the temporal resolution of flow velocity quantification.

ECG gating was used for data collection within this thesis and therefore merits further discussion. The ECG gating techniques described in the following sections could also be applied, with appropriate modifications, to other gating strategies.

3.2.4.1 ECG gating

The acquired ECG signal generally contains a sharp QRS component representing ventricular systole as shown in figure 3.14, with the sharp R-wave peak at the maximum point of systole. The R-wave peak represents an easily detectable trigger signal to initiate and synchronise MRI data collection. If the PC-MRI sequence has a sufficiently short TR, then a number of acquisitions can be collected within the R-R interval with the phase encoding steps repeated over the required number of cardiac cycles, as illustrated in figure 3.2.12. There are two methods of achieving synchronisation using triggering; prospective and retrospective gating.

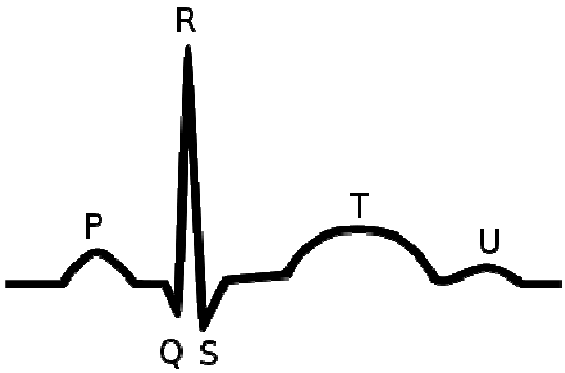

Figure 3.14: Typical form of an ECG waveform showing the sharp systolic QRS peak.

3.2.4.2 Prospective gating

In prospective gating or triggering, the system waits for a valid QRS wave to initiate the pulse sequence, figure 3.15.

Figure 3.15: Prospective ECG triggered data acquisition. After the R-wave is received. The first k-space line of the first cardiac phase is received, followed in sequence by the first k-space line of all the other cardiac phases. The second R-wave triggers the collection of the second line of k-space for each of the cardiac phases. (Finn et al. 2006)

The user selects the required number of image frames, known as cardiac phases, to be collected within the cardiac cycle. Once initiated, the pulse sequence is run for a single phase encoding step i.e. line of k-space, for each cardiac phase within the cycle. Subsequent k-space data lines are collected after initiation by the next detected QRS wave signal. Fast prospective gating techniques speed up acquisition time using segmented acquisition to collect multiple lines of k-space for each triggered acquisition. In order to maintain a consistent number of collected data frames or cardiac phases with a defined temporal separation, the user must define an acquisition window within the cardiac cycle where data will be collected. The acquisition window is followed by an arrhythmia rejection (AR) window where data is not collected. The AR widow allows for variations in heart rate but does mean that the data collected is not representative of the entire cardiac cycle i.e. there is "dead-time" during the AR period. Careful selection of the acquisition and AR windows is required to ensure that an appropriate data set is collected. Collecting data within the diastolic phase would minimise anatomical artefact due to movement whereas ensuring that the systolic component is included will allow assessment and quantification of temporal variation. Setting the acquisition window too long may result in missed heartbeats, thereby lengthening the overall scan time.

3.2.4.3 Retrospective gating

Retrospective triggering collects data continuously while noting the time period of the R to R interval for each collected data set, figure 3.16.

Figure 3.16 has been removed due to copyright restrictions

Figure 3.16. Retrospective ECG triggered data acquisition. The acquisition window is extended to the next R-wave. Acquisition of k-space data is in a similar sequence to that for prospective acquisition but with the R-wave acting as a time-marker rather than a trigger point . The time intervals between cardiac phases can thus differ if the time between R-waves varies. The resultant data is assigned an average cardiac phase timepoint, interpolated over the entire scan. (Finn et al. 2006)

In this case the QRS complex will initiate the phase encoding states but is used as a time marker, rather than a trigger. The user selects the required number of phases or frames within the cardiac cycle but the data is retrospectively fitted into each cardiac R-R interval regardless of its length. If the heart rate has varied during the scan then the retrospectively binned TR intervals will also vary. To achieve re-construction nearest neighbour data sets from the different encoding steps are matched for each cardiac phase. The interpolation of data has the potential to give errors, however an advantage of this technique is that the whole cardiac cycle is represented with no “dead-time”.

3.2.5 Time saving strategies: segmented data acquisition and view sharing

ECG gating and triggering techniques have, in general, been developed to address the needs of cardiac imaging and flow quantification. While contemporary gated pulse sequences compensate for velocity induced motion due to cardiac motion, artefact may still arise due to respiratory motion, so that sequences should ideally be performed within a single breath hold. However, temporal resolution for gated acquisition is poor, and is discussed as one of the limitations of the technique in section 3.2.6. One method of improving temporal resolution is the use of segmented data acquisition, figure 3.17, where a number of k-space lines are collected at each cardiac phase. This method increases the duration of each cardiac phase but reduces the number of heartbeats required to collect the complete data-set (Bernstein 2004; Finn 2006; McRobbie 2003)

Figure 3.17. Segmented gated acquisition. In this example five lines of k-space (i.e. 5 phase encoding steps) are acquired for each cardiac phase or timepoint. (Finn et al. 2006)

The temporal resolution can be improved with the use of view sharing or interleaved acquisition as illustrated in figure 3.18.

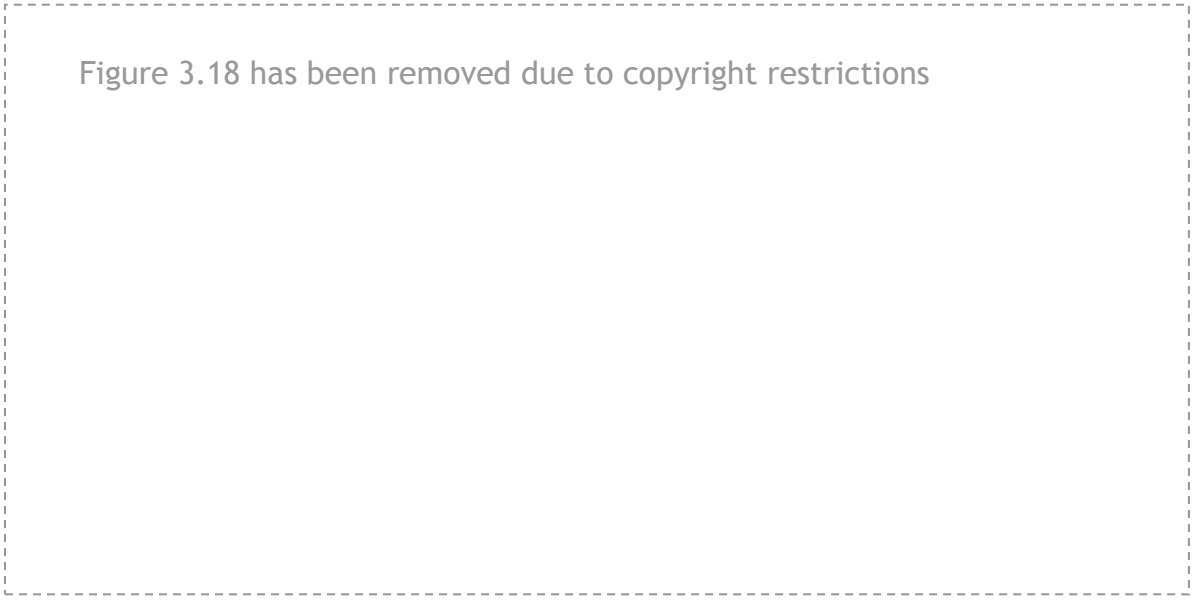

Figure 3.18: Interleaved or view-sharing acquisition. Data is acquired similarly to the segmentation described for image 3.17. However, the centre line of each cardiac phase is repeated between segments and the data shared around the central view, effectively generating twice the number of cardiac phases in this example. (Finn et al. 2006)

3.2.6 Physical limitations of MRI derived velocity estimation

The development of angiographic imaging using MRI has largely focussed on improving the visualisation of flow in vessels such that MRA has become an established imaging technique in the diagnosis of peripheral vascular disease. However, as was discussed in chapter 2, the quantification of flow, including velocity measurement has been developed for cardiac applications and the large, proximal cardiac vessels, where the trade off between image quality and temporal resolution may be less of an issue than for the smaller vessels of the peripheral vasculature. The factors influencing velocity accuracy need to be examined carefully. The following issues were explored in this thesis with particular reference to the peripheral arterial system.

3.2.6.1 Temporal resolution

The preceding part of this section has already mentioned temporal resolution and the need for the TR to be sufficiently small to give an adequate number of cardiac phases required to sample haemodynamic variation over the cardiac cycle (analogous to the ultrasound spectral Doppler waveform). The segmentation and view sharing techniques described in section 3.2.5 are aimed at reducing the overall scan time to within a single breath-hold and are implemented at the expense of temporal resolution. However, it is possible that such techniques are not essential when examining the peripheral arteries where respiratory motion is not such an issue. Velocity encoded 2-D acquisitions designed for flow quantification can typically provide between six and sixty cardiac phases i.e. between 166ms and 16ms per phase or time-point. The key question for this study is whether such parameters will be sufficient to distinguish haemodynamic events of a few ms long, such as sharp systolic peaks, sufficiently well to accurately determine the peak systolic velocity. Studies in the ascending aorta have suggested that there may be a threshold of around 11 frames per cardiac cycle above which there is very little variation in the detected values of peak velocity or flow rate (Lotz et al. 2002). Such a phenomenon remains to be explored in the smaller vessels.

3.2.6.2 Spatial resolution effects

The trade off when performing temporal acquisitions in MRI is that the required short TR values, as described above, will limit the available spatial resolution. Inadequate spatial resolution can result in partial volume effects where a pixel will contain a range of spins at different velocities, possibly including non-moving spins, giving an average pixel value in the resulting phase image which will underestimate the true peak velocity value (Bernstein, King, & Zhou 2004; Finn et al. 2006; Lotz et al. 2002). Poor spatial resolution can also limit the detection of small vessels during the diastolic phase, where the overall signal is low, and inhibit accurate ROI selection for flow quantification.

Slice thickness is a parameter often overlooked in the quantification of flow. Considering a voxel of spatial resolution, where slice thickness is generally larger than the in-plane (x,y) resolution by a factor > 2, there may be additional averaging in the through plane direction. Such averaging may mask out velocity changes along the direction of flow. Of particular relevance to this thesis is the ability to detect maximum velocities and the issue of whether inaccuracies due to the guesswork involved in positioning the 2-D PC-MRI slice will outweigh underestimations due to the use of large slice widths.

3.2.6.3 Angular dependence

Velocity encoding in the through plane direction, requires the image plane to be orthogonal to the direction of flow, figure 3.19a.

Figure 3.19 has been removed due to copyright restrictions

Figure 3.19: In (a) the image plane is perpendicular to the direction of flow. In (b) the scan plane deviates from the direction of flow by angle β. (Bernstein, King, & Zhou 2004)

When the scan plane deviates from the direction of flow by an angle, ß, the velocity, v, will reduce to vcosß. Velocities will be underestimated but, provided accurate regions of interest are selected, the calculated flow rate should remain relatively unaffected since the increase in ROI size will compensate for the reduction in velocity. The slice thickness will also contribute to inaccuracies due to non-orthogonal scan planes. It has been suggested that scan plane deviations of less than 15° will have little effect on flow quantification (Bernstein, King, & Zhou 2004; Lotz et al. 2002). However, since the measurement of maximum velocities is the focus of this thesis, the effect of non orthogonal PC-MRI planes should be considered.

3.2.6.4 Velocity encoding limitations

The velocity encoding parameter, or venc value, described in section 3.2.2.3 places further limitations on the accuracy of velocity detection. Inadequate venc values can cause signal loss due to phase wrapping as can be seen in the phase image in figure 3.13. This phenomenon is similar to velocity aliasing in ultrasound spectral Doppler due to inadequate pulse repetition frequency sampling. However, it is possible to set venc values of the order of 5 to 6 ms^{-1}, higher than the maximum detectable velocity on the majority of ultrasound scanners. MRI manufacturers will, typically, recommend a venc setting of 20% higher than the maximum expected velocity as higher venc settings will have a negative effect on the SNR of the phase image and consequently affect the accuracy of the maximum velocity values (Lotz et al. 2002; Bernstein, King, & Zhou 2004). This effect has been demonstrated *in-vitro* for steady-state flow (Lotz et al. 2002), but the true effect on pulsatile flow, which requires detection of high systolic peaks and low diastolic velocities, remains under-investigated. When exploring the possibility of the use of velocity ratios similar to those used for ultrasound spectral Doppler haemodynamic investigations, careful consideration needs to be given to the influence of venc settings.

3.3 PC-MRI and spectral Doppler ultrasound compared

While the focus of this thesis is to compare PC-MRI and spectral Doppler ultrasound in the quantification of blood flow velocities, it is useful to make a comparison, in this preliminary chapter, of the known advantages and disadvantages of the two techniques. Table 3.2 compares the two techniques in terms of the ability to quantify velocities. Table 3.3 highlights key differences in the practicalities of each method.

In this thesis, the aim is not to investigate the replacement of one technique by the other, rather, it is to investigate whether the velocity data based techniques used with spectral Doppler ultrasound to aid the diagnosis of peripheral vascular disease could be translated for use with PC-MRI velocity data. The mention, in table 3.2, of velocity underestimation with PC-MRI and velocity overestimation with spectral Doppler ultrasound might cause the reader to raise doubts, such that those two issues merited closer investigation during this study.

	PC-MRI	*Spectral Doppler ultrasound*
Advantages	Region of interest can encompass the entire vessel lumen. Possible to correct maximum velocity aliasing	Velocity data derived from signal analysis. Good temporal and spatial resolution
Disadvantages	Velocity data derived secondary to image formation. Potential underestimation of velocities due to spatio-temporal velocity averaging. Poor spatial and temporal resolution. Aliasing of maximum velocity due to incorrect selection of velocity encoding parameter.	Sample volume can cover the vessel diameter but coverage in the slice dimension is unknown. Overestimation of maximum velocity due to spectral broadening. Aliasing of maximum velocity due to incorrect selection of velocity scale but limited by Nyquist limit.

Table 3.2: summary of the main advantages and disadvantages of PC-MRI and spectral Doppler ultrasound velocity measurement.

	PC-MRI	*Spectral Doppler ultrasound*
Advantages	MRA imaging can be used to guide the region for further analysis. "Raw" data output for off-line analysis of a range of quantities.	Dynamic, responsive real-time imaging. Well established criteria for haemodynamic based diagnosis of peripheral vascular disease. Rarely unacceptable examination. Low cost
Disadvantages	Unusable if patient is not MRI compatible. Under investigated for haemodynamic based diagnosis of peripheral vascular disease. Operator dependent data collection. Examination often unacceptable to patients. High cost	Unusable if the acoustic window is poor. No "raw" data collection. Measurements must be made accurately during the scan. Operator dependent data collection.

Table 3.3: summary of the main practical advantages and disadvantages of PC-MRI and spectral Doppler ultrasound.

Chapter 4 – Comparative and complementary techniques; *in-vivo* and *in-vitro*

A survey of the published literature relevant to this thesis focussed on studies comparing MRA or PC-MRI with spectral Doppler ultrasound, in particular, those studies involving or making reference to peripheral vascular and carotid arterial territories. The following sections have separated the key publications to highlight *in-vivo* studies and *in-vitro* phantom work, although some studies will overlap both areas.

4.1 *In-vivo* comparisons between different diagnostic techniques

With the establishment of magnetic resonance angiography, MRA, techniques as valid and useful methods for the assessment of peripheral vascular disease (Yucel 1995), a number of studies have examined how it compares with other imaging methods. Comparison with the other anatomic visualisation techniques used in peripheral vascular diagnosis i.e. digital subtraction angiography and computed tomography can be made fairly directly , such studies generally have to acknowledge that MRA has the key advantage of not involving ionising radiation but can provide comparable diagnostic quality information in the majority of cases (Chan, Anderson, & Dolmatch 2010; Collins et.al 2007; Olin & Sealove 2010). Direct comparison with ultrasound assessment of peripheral vascular disease is not quite as straightforward. Ultrasound imaging and colour flow mapping can identify areas of stenosis and changes in flow patterns. However, the more established ultrasound method in peripheral vascular disease diagnosis is to use spectral Doppler, as an essential adjunct to real time B-Mode and colour Doppler imaging; to display blood flow velocity waveforms, measure velocities and to determine haemodynamically significant quantitative indices. A number of studies (Back et al. 2000; Hingorani et al. 2004b; Hingorani et al. 2004a; Leiner et al. 2005; Meissner et al. 2004; Soule et al. 2003; Visser & Hunink 2000) have compared assessment of stenosis from anatomic MRA images with similar assessment of ultrasound images, i.e. diameter reduction, and with percentage stenoses determined from the spectral Doppler ultrasound velocity

measurements described in chapter 4.1. However, these studies and currently accepted clinical practice would see the use of MRI and ultrasound techniques as complementary rather than competitive (Collins et al. 2007b).

The development of velocity measurement techniques for MRI gave rise to the potential for PC-MRI to provide quantitative information on blood flow similar to that provided by Doppler ultrasound. The technique was rapidly taken up and established for cardiology applications where it is now used routinely for flow volume assessment in the great arteries (Kilner, Gatehouse, & Firmin 2007) and there are a number of studies comparing MR flow assessment with Doppler echocardiography e.g. (Delfino et al. 2006; Marsan et al. 2009; Nogami et al. 2009; Stadlbauer et al. 2009). As discussed in section 3.2, quantitative blood flow measurements in the peripheral vasculature using MRI have been explored since the early 1990s, concurrent with development of the technique in cardiac applications. However, despite continuing work in this area, the technique has yet to become established for peripheral vascular applications, undoubtedly due to the ease with which Doppler ultrasound investigations can be performed in the peripheral anatomy. A consequence of this is that the peripheral vascular vessels, such as the carotid and femoral arteries, provide ideal sites for the *in-vivo* comparison, and potential validation, of techniques. Despite such "ease of access" there are only a limited number of validation studies in the literature which attempt to compare velocity measurements and velocity derived flow parameters in peripheral vascular vessel assessment using both MR and ultrasound techniques. One of the first authors to report on the technique was Caputo (Caputo et al. 1992; Caputo & Higgins 1992) who examined flow velocities in the popliteal, anterior tibial, posterior tibial and peroneal arteries of 10 healthy volunteers using velocity encoded cine MR in comparison with ultrasound spectral Doppler measurement. The results showed good correlation between techniques for the velocity waveforms of the popliteal and tibial-peroneal arteries. The authors also explored pulsatility and resistance indices and pre and post stenotic waveforms (Masui et al. 1995). Nesbitt (Nesbitt et al. 2000) used an MRI fast Fourier flow method to measure flow velocities in the femoral arteries of healthy volunteers and patients. The authors observed the MRI derived maximum flow velocities to be around 10 to 15 % lower than those detected using Doppler ultrasound. This study also reported on the validation of

the MRI measurements in a simple pipe phantom with known velocities verified by timed volume collection assessment. However, that validation was not repeated for Doppler ultrasound. More recent studies continue to use the approach of single modality phantom validation to complement modality comparison studies. In the work of O'Brien (O'Brien et al. 2008) which assessed flow in stenotic jets it was demonstrated that MR and Doppler peak velocities agreed well for velocities below 400cms^{-1}, with MR underestimating at higher velocities; the MR phantom work highlighted the decreased reliability of the MR phase estimates at higher velocities.

There is limited evidence in the literature of studies which attempted to complement comparative clinical studies with phantom validations for both MR and Doppler ultrasound. One exception is the work by Ho (Ho et al. 2002) which used MR phase contrast and spectral Doppler to measure blood flow volumes in the carotid and vertebral arteries of 40 patients. This study also looked at ultrasound colour M-mode for flow volume quantification. Unfortunately, the study is flawed by having two different phantoms so that an absolute comparison between techniques is not possible. However, the separate phantom validation tests showed that MRI and ultrasound M-Mode techniques gave good agreement with known flow volumes while the spectral Doppler measurements overestimated the true flow. This was reflected in the *in-vivo* studies which showed large variations ($p<0.05$) between techniques with spectral Doppler consistently giving higher values. The compared quantities in the study were flow volumes derived from mean velocities. In the spectral Doppler assessment of peripheral arterial vessels it is, generally, the maximum peak velocities that are used rather than the mean and the author acknowledges the potential for inaccuracies in estimations of both mean and maximum Doppler velocity as is discussed in this thesis in section 3.1. A study by Lee (Lee et al. 1997), did investigate comparative measurements of peak-systolic velocities in the aorta and pulmonary arteries of healthy volunteers finding reasonable agreement between techniques although Doppler measurements were generally higher and flow volume derived from Doppler was significantly higher. This work was complemented by a simple flow phantom study which, although limited details are provided, appears to use an identical flow phantom set-up for both MRI and ultrasound, albeit with simulated femoral rather than cardiac waveforms.

The established methods of blood flow quantification between MR and ultrasound differ in approach; with PC-MRI techniques developed predominantly for cardiac applications which focus on volume flow estimations derived from mean velocity measurements whereas the use of spectral Doppler in the assessment of peripheral arterial disease uses maximum velocities and associated velocity ratios. In this sense it may be said that neither technique may be regarded as a "gold standard". When developing and assessing comparable flow quantification techniques it is therefore essential that the "true" flow volume and velocity can be validated in a test phantom. The ideal situation will be to have an identical flow phantom set-up which can be tested using both MRI and ultrasound.

4.2 Comparative studies using test phantoms

The use of test objects or phantoms is well established in medical imaging in all areas. Test phantoms are used widely for calibration, optimisation, quality assurance and training. However, they have a useful, if not essential, role in the research and development of new imaging technologies and techniques. Test phantoms avoid the need to use human or animal test subjects with the associated ethical issues and problems associated with biological variability. For ionising imaging techniques, test phantoms become essential on safety grounds.

Test phantoms for imaging techniques may be broadly categorised into anthropomorphic and non-anthropomorphic. Anthropomorphic phantoms aim to mimic, as closely as possible, the image appearance of normal or pathological anatomy and can be a useful "substitute" for a human subject when optimising and developing imaging techniques. Non-anthropomorphic test phantoms will not attempt to mimic real anatomy; rather they will simplify key aspects of the anatomic image which the user wishes to investigate. Non-anthropomorphic test phantoms will often contain geometric structures or "targets" with calibrated properties e.g. levels of contrast, resolution separation distances, simplified 2-D or 3-D geometries. Both types of phantom are key to validation studies,

however, non-anthropomorphic test phantoms allow validation against simplified, calibrated quantities.

For the studies in this thesis, the use of test phantoms was complicated by the need to mimic both anatomy and physiology i.e. blood flow. Indeed, since the ability of MRI and ultrasound techniques to quantify flow was under investigation, it was the flow itself, rather than the surrounding tissue, that was considered the key feature for validation and comparison of velocity measurement. For the surrounding vessel and tissue structures, it was important that materials used could be used with standard MRI and ultrasound protocols without causing any significant artefacts. The implementation of these features is described in chapter 5, with the following sections in this chapter providing an overview of the use of flow, or flow simulating, phantoms by other authors.

4.2.1 MRI flow phantoms

Despite the prevalence of velocity encoded MRI as a technique for cardiac applications, investigators wishing to study the technique have done so with test phantoms based on a variety of clinical applications. The simplest phantom forms have used simple straight tube constructions. Early work by Stalberg and colleagues e.g. (Stahlberg et al. 1986) involved simple straight tube phantoms with a gravity fed flow system containing paramagnetically doped water. Although providing simple steady state flow, the phantoms allowed the authors to conduct a number of studies to develop flow imaging and flow measurement techniques for blood and CSF applications, including the assessment of stenosed flow (Stahlberg et al. 1992). Studies by Greil van der Weide and Bilecen (Bilecen et al. 2005; Greil et al. 2002; van der Weide, Viergever, & Bakker 2004) describe similar straight tube assemblies with pump driven steady state flow containing doped water, with van der Weide and Bilecen, in particular, focussing on peripheral vascular studies. A similar steady-state flow system which included a tight stenosis, has been used by O'Brien (O'Brien et al. 2008;O'Brien et al. 2009). The development of a commercially available (Shelley Medical Systems, London, Ontario, Canada) quality assurance test phantom set with an MR compatible pump system (Summers et al. 2005) has enabled a number of researchers to undertake flow phantom studies for MRI. The Shelly equipment

contains an MR QA set with a variety of tubes within rigid silicone, including simple stenosis models, and can provide a range of steady state and pulsatile flow patterns. Although the multi-site trial of the MR QA set (Summers et al. 2005) does not appear to have been reported on, the MR compatible system has been connected to a variety of anthropomorphic and simple flow phantoms. Although steady state velocities are useful for simplifying studies and providing absolute calibration of flow velocities, and are still used by authors for simple validation (Brandts et al. 2010), pulsatile waveforms provide more physiologic flow patterns and allow assessment of gating techniques and temporal resolution issues. This is reflected in more recent publications (Dambreville et al. 2010; van Amerom et al. 2009) which, although the test phantoms themselves are simple structures, employ pulsatile flow patterns to mimic renal and pulmonary blood flow. The development of anthropomorphic phantoms for MR flow applications (Chu & Rutt 1997; Frayne et al. 1993; Smith, Rutt, & Holdsworth 1999) can be a difficult process, however, the availability of commercially available "vascular" structures from Shelley has seen a number of recent publications describing their use in the development and evaluation of flow related MRI imaging and quantification techniques (George et al. 2010; Hollnagel et al. 2009; Marshall et al. 2004).

4.2.2 Ultrasound flow phantoms

Test objects and phantoms were first devised for non imaging Doppler techniques. However, with the incorporation in the 1980s of spectral Doppler on imaging ultrasound scanners, known as Duplex, and the further development of colour flow mapping techniques, the features required by Doppler ultrasound test phantoms became more complex. Hoskins (Hoskins 2008) has produced an excellent, comprehensive review of the historical development and current state-of-the-art of phantoms and test systems for the validation and investigation of ultrasound methods for imaging and quantifying arterial blood flow. Vibrating phantoms and electronic phantoms are generally regarded as being of limited utility other than for the testing of instrument sensitivity limitations. Despite this, some investigators continue to develop such methods

(Gittins & Martin 2010). Alternatively, inexpensive, simple string phantoms may be useful for velocimetry assessment as such are recommended for routine QA testing (IPEM 2010). The primary aim of Doppler ultrasound imaging and blood flow quantification is the assessment of the haemodynamic changes caused by the presence of vessel stenoses which none of the aforementioned phantom methods are capable of mimicking. Only fluid flow phantoms can begin to approximate the true haemodynamic situation and they have become regarded as the preeminent test system for Doppler ultrasound (Hoskins 2008). Much work has gone into the development of flow phantom systems and their associated tissue and blood mimic requirements, culminating in the publication of an international standard ultrasound flow phantom (IEC 61685 2001). This phantom had been used as a reference for further development, particularly in the development of anatomical vessel constructions (Poepping et al. 2002; Poepping et al. 2004) and the mimicking of the elastic properties of vessels (Hoskins 2008).

4.2.3 Dual or multi-modality phantoms

One of the first anthropomorphic phantoms described for multi modality peripheral vascular applications was a carotid phantom, using a lost-wax casting technique, developed by Frayne (Frayne et al. 1993) for x-ray, ultrasound and magnetic resonance vascular imaging. Although the phantom was mainly used for comparing imaging techniques, a limited flow assessment was conducted which demonstrated good agreement (within 4.4%) for volume flow measurements of steady-state flow using Doppler ultrasound and velocity encoded MRI. Hoppe (Hoppe et al. 1998) developed a pump driven system giving pulsatile flow in a simple stenosis model. The fluid used was a water/yoghurt mix which provided scattering for validation of flow using a Doppler guidewire. However, this phantom was not used to test non-invasive Doppler techniques. Recent studies (Hollnagel et al. 2007; Hollnagel et al. 2009), have compared MR and laser Doppler velocimetry measurements of flow in anthropomorphic cerebral artery phantoms. The work demonstrated good agreement between techniques for flow in straight arterial segments but, understandably poorer

agreement for more complex flow geometries. However, it is unlikely that this comparative study can be easily translated directly to the clinical situation as laser Doppler velocimetry cannot be used for that particular clinical application. It is often difficult to achieve true comparison between MR and ultrasound flow measurement techniques when using test phantoms mainly due to the need for phantoms to have MR compatibility, scattering within the blood mimicking media for Doppler ultrasound and appropriate paramagnetic and acoustic characteristics. These issues are discussed in more detail in chapter 5. Some authors have attempted comparison studies which involve phantom modifications between modalities such as extending inlet and outlet tube lengths and blood mimic (McCauley et al. 1995) or, indeed, using different phantoms (Ho et al. 2002). Both these authors also focussed on volume flow measurements rather than velocity measurement. An attempt to validate mean velocity measurements in an identical phantom for Doppler and MRI ran into similar problems when using different blood mimics and different flow rate ranges (van Oostayen et al.). The comparative study by Lee (Lee et al. 1997) which was discussed in section 4.1, did use the same phantom system for both imaging modes. This study compared simulated normal and stenosed femoral-like blood flow *in-vitro* and found that Doppler ultrasound based measurements consistently overestimated predicted flow. However, the clinical comparison in the same study was for the aorta and pulmonary artery, therefore not truly comparable to the *in-vivo* measurement situation. In addition, the use of a standoff pad to make Doppler measurements of flow within the Perspex tubes represents a far from ideal Doppler phantom as the high impedance of Perspex has the potential to cause signal distortions and losses (Hoskins 2008). Although both simple and anthropomorphic dual modality phantoms continue to be developed (Allard et al. 2009; Cloutier et al. 2004; Surry et al. 2004), their use in truly comparative studies of ultrasound and MRI flow quantification techniques remains limited.

4.3 Summary of main issues emerging from the review of literature

Limited research on the use of velocity encoded MRI to assess the peripheral vasculature.

Velocity encoded MRI studies tend to focus on the determination of flow volumes derived from mean velocities rather than maximum velocities and velocity spectra as used in Doppler ultrasound.

Comparative studies suggest that MRI techniques produce lower values for flow and velocity than those measurements derived from spectral Doppler; this warrants deeper investigation.

The use of MRI derived velocity ratios is under-investigated in the clinical studies and uninvestigated in phantom situations.

There are gaps in the evidence for true comparison between spectral Doppler ultrasound and PC-MRI methods of blood velocity quantification, particularly in relation to measurement in the peripheral arteries. This gap may be partially addressed by the establishment of an appropriate dual modality flow system capable of providing a true *in-vitro* comparison.

Chapter 5 – The development of *in-vitro* flow testing systems for ultrasound and MRI

The use of test phantoms to investigate and compare diagnostic techniques avoids the use of human subjects with their associated ethical, logistical and safety issues. Scanning test objects provides the opportunity to investigate a variety of scanning parameters methodically and thoroughly.

Test phantoms in both MRI and Ultrasound are fairly well established; albeit, the use of flow phantoms in both modalities less so, as discussed in the previous chapter. The challenges of this particular study required development of test phantoms which could be used with both MRI and ultrasound i.e. MRI compatible with appropriate acoustic properties. Such *in-vitro* systems were required to enable absolute comparison of the quantification of flow between the two techniques, something which cannot be done *in-vivo* due to temporal and spatial biological variations. The use of test phantoms enabled velocity measurement techniques to be compared and allowed optimisation of the MRI scanning protocols prior to use in *in-vivo* studies.

For this particular study, the key component of the flow phantom was the production of a moving target capable of producing frequency shifts measurable by ultrasound and phase shifts detectable by MRI. It was, therefore, considered important to attempt to match the haemodynamic, acoustic and magnetic properties of the blood mimic to that of real blood. However, although the properties of the materials enclosing the flow, “vessel” wall and “tissue”, were less important, consideration was given to constructions and materials that would enable imaging by minimising artefacts and any consequential signal loss in both modalities.

5.1 Flow test phantom development and construction

The main components of a flow phantom consist of a vessel or vessels, through which a blood mimic is pumped, surrounded by a block of tissue mimicking medium. A controllable pumping system is required to provide a range of steady state and pulsatile velocities. Key acoustic and magnetic features that would be required of a phantom and flow system are summarised in table 5.1.

Feature	*Ultrasound*	*MRI*
Blood mimic	Velocity 1570 ± 30 ms^{-1} Density 1050 ± 100 kgm^{-3} Viscosity 4 ± 0.4 mPas Non-aggregating scattering particles 5μm Newtonian fluid	T1 1932 ± 85 ms at 3T T1 1441 ± 120 ms at 1.5T T2 275 ± 50 ms at 3T T2 327 ± 40 ms at 1.5T Density 1050 ± 100 kgm^{-3} Viscosity 4 ± 0.4 mPas Newtonian fluid
Tubing/vessel wall	Velocity 1540 ± 15 ms^{-1} Diameter > 0.5mm Low acoustic distortion Inlet length to achieve laminar flow.	T1 1420 ± 38 ms at 3T T1 1060 ± 155 ms at 1.5T T2 32 to 50 ± 4 ms at 3T T2 35 to 44 ± 6 ms at 1.5T Inlet length to achieve laminar flow.
Surrounding media / tissue mimic	Velocity 1540 ± 15 ms^{-1} Attenuation 0.5 ± 0.05 $dBcm^{-1}MHz^{-1}$	T1 1420 to ± 38 ms at 3T T1 1060 ± 155 ms at 1.5T T2 32 to 50 ± 4 ms at 3T T2 35 to 44 ± 6 ms at 1.5T
Container and connecters	Non constricting connectors. Leak-proof assembly Access to an acoustic window	Non constricting connectors. Leak-proof assembly. Non-metallic scatterers
Flow pumping system	Good temporal resolution and flow stability	Good temporal resolution and flow stability. MRI compatible or through waveguide assembly.
Flow waveforms	Steady state and pulsatile	Steady state and pulsatile

Table 5.1: The main features required by a dual modality (MRI and Ultrasound) flow phantom (Hoskins 2008; IEC 61685 2001; Stanisz et al. 2005).

5.1.1 Phantom materials

There have been some excellent, recent reviews relating to the development and use of ultrasound test objects including the relevant acoustic properties (Browne et al. 2003; Culjat et al. 2010; Hoskins 2007; Hoskins 2008). Of

particular relevance to this thesis is the review by Hoskins (Hoskins 2008) which discusses the development and use of flow phantoms and the international standard for a flow test object (IEC 61685 2001). Chapter 4 discussed the phantom methods used for testing and validating MRI flow imaging and quantification. However, the majority of the phantoms used are unsuitable for use with ultrasound having: no surrounding tissue mimic, rigid construction, non-scattering blood-mimics.

5.1.1.1 Blood mimic

The blood mimicking fluid, BMF, used was that described in Terlinck (Terlinck 1998) and incorporated into the IEC flow phantom standard (IEC 61685 2001). While this was developed as a blood mimicking fluid for Doppler ultrasound studies and has been widely used as such, its use as a suitable fluid for MRI based flow studies has not been investigated. However, since the fluid was developed to mimic the density and viscous properties of blood and contains no ferromagnetic materials, it was used for the both the ultrasound and MRI based studies.

The BMF was made to the exact "recipe" contained in the IEC Flow Phantom document (IEC 61685 2001) such that the acoustic properties of the fluid were as in table 5.1.

The T1 and T2 magnetic relaxation times of the BMF were measured using the techniques described in 5.1.1.2.3 and are shown below in table 5.2

	T1 (ms)	*T2(ms)*
1.5T	831.61 (± 34.58)	254.45 (± 2.11)
3.0T	1336 (± 40.35)	122.92 (± 48.31)

Table 5.2: T1 and T2 for the blood mimicking fluid on the 1.5T and the 3.0T MRI scanners.

5.1.1.2 Tissue mimic

Water based gels have proved useful in the development of test phantoms for both ultrasound and MRI with the high water content providing an acoustic velocity and impedance close to the average tissue value and sufficient hydrogen protons to give tissue like magnetic properties. The most commonly used gels are based on gelatine, agar and poly vinyl alcohol (PVA) cryogels. The author had experience of the manufacture and use of all three gel types, particularly the latter two, for ultrasound phantom construction.

The tissue mimic selected was a poly vinyl alcohol (PVA) cryogel. The acoustic, magnetic, mechanical and temporal stability properties of this type of material have been investigated by a number of authors, as discussed in chapter 4, and the gel has previously been proposed as suitable for multimodality phantoms (Surrey 2004). Its popularity as a phantom material, as evidenced in the literature, appears to have grown in recent years undoubtedly due to the relatively low cost, ease of manufacture, structural and temporal stability and resistance to bacterial growth compared with agar and gelatine based gels. The gel is created by dissolving PVA powder in water and subjecting the resulting solution to a series of freeze thaw cycles. Each cycle will increase the cross-linking of molecules enabling different material properties to be achieved.

5.1.1.2.1 PVA gel preparation

PVA gels have the advantage that prior to undergoing thermocycling, they are in a liquid state such that they can be poured into any container to surround vessel structures.

The gels were fabricated using a 15% or 10% PVA (Sigma-Aldrich, Gillingham, UK) solution in sterile water with 0.5% of a 9.5 % concentration benzalkonium chloride (Sigma-Aldrich, Gillingham, UK) solution added to avoid bacterial growth. The PVA was dissolved in the liquid by heating in a microwave oven using frequent stirring to avoid aggregation of particles. Degassing of the prepared solution was assisted by the use of a vacuum chamber. Once cooled and degassed, the solution was poured into a prepared container and placed in a freezer which had been modified to incorporate a thermocycler, developed in-

house. The thermocycler allowed the number, duration and temperature of the freeze and thaw cycles to be selected. In this study the gels were held at -20°C and +20°C. For the initial straight tube phantom an in-house established "recipe" was used using 15% PVA with a 5 freeze-thaw 12 hour cycle program. However, prior to construction of subsequent phantoms the thermocycling was reduced to 10 hour holding periods to account for the time taken for the gels to equilibriate at each cycle switch, so reducing the overall time of fabrication. The finished gel was then kept in a sealed container and surrounded by sterile water with benzalkonium chloride solution, to prevent dehydration and bacterial contamination.

A study was carried out to investigate the properties of 10% and 15% PVA gels over one to six 10 hour, ± 20°C thermocycles, to investigate which would produce the most appropriate magnetic and acoustic properties.

5.1.1.2.2 Acoustic properties of the tissue mimicking gel

The acoustic property of primary interest was the speed of sound. This was determined using a GE Logiq e ultrasound scanner with a 12L-RS linear transducer operating at 10MHz in B-mode. The scanner distance callipers were used to measure the imaged thickness as displayed on screen, d_{us} and digital vernier callipers were used to measure the actual thickness d_{actual}, with all measurements repeated five times. The speed of sound of the PVA gel, c_{gel} is given by equation 5.1.

Equation 5.1. $$c_{gel} = 1540 * \left(\frac{d_{actual}}{d_{us}} \right)$$ in ms^{-1}.

The results of the measurements are displayed in figure 5.1, where the error bars represent ± one standard deviation as determined by repeat measurement. The results suggest that, for both concentrations, any thermocycling scheme with greater than one cycle should give a reasonable approximation to the speed of sound in soft tissue.

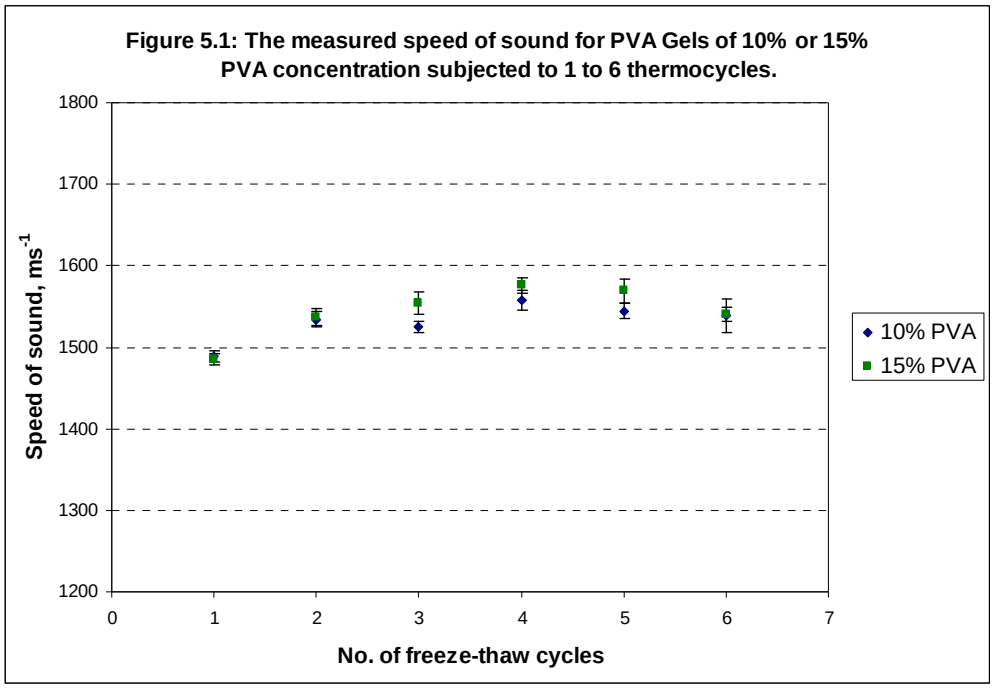

5.1.1.2.3 Magnetic properties of the tissue mimicking gel

The longitudinal relaxation time, T1 and transverse relaxation time, T2 for each of the tissue mimicking gels produced was measured using the MRI scanners described in section 5.2.1, by collecting image slices through a homogenous region in the centre of each gel. For T2 measurements a spin-echo sequence was used with the TR held at 2000ms while the TE was varied between 50ms and 350ms. For the T1 measurements an inversion sequence was used with the TR held at 4000ms, TE at 10ms and the TI varied between 100ms and 2400ms. A region of interest was drawn on a visibly homogenous region of the image of the gel and translated to the other slices and images within the sequence. The mean pixel intensity, *S*, was determined and plotted against the varied parameter, whether TE or TI. T1 and T2 were determined by fitting an exponential curve of the form:

$$Sa = So\left(1 - 2e^{\left(\frac{-TIa}{T1}\right)}\right)$$ to give T1 and

$$Sa = Soe^{\left(\frac{-TEa}{T2}\right)}$$ to give T2.

The results of the tests are illustrated in figures 5.2 and 5.3 for T1 and T2 respectively. The results for 15% PVA in the 1.5T scanner compare reasonably well with the work of Chu and Rutt (Chu & Rutt 1997).

Figure 5.2: T1 relaxation times for PVA Gels of 10% or 15% PVA concentration subjected to 1 to 6 thermocycles.

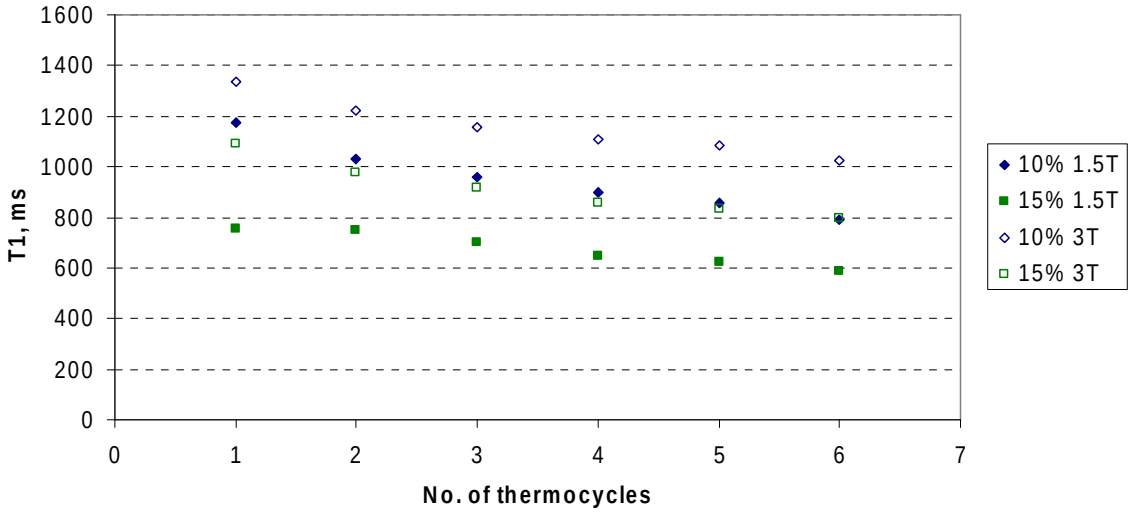

Figure 5.3: T2 relaxation times for PVA Gels of 10% or 15% PVA concentration subjected to 1 to 6 thermocycles.

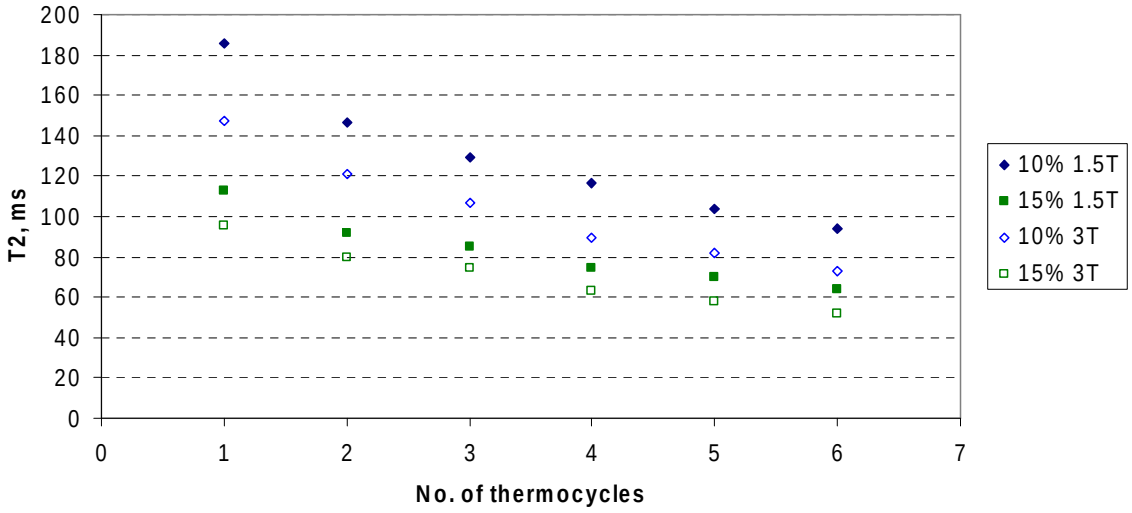

5.1.1.3 Vessel tubing

A variety of vessel wall materials have been used by other authors, such as silicone rubber, PVA, latex, polyethylene, Perspex and glass (Hoskins 2008). One of the commonly used materials is C-flex tubing (Cole-Parmer Ltd., Walden, UK), a thermoplastic elastomer which has a velocity of sound of 1556 cms^{-1} (Hoskins 2008), close to that of ultrasound. However, it is known that C-flex can cause Doppler spectral distortion but that these can be minimised by using thin walled tubing, straight sections of tubing, careful alignment of the beam and vessel axis and, ideally beam widths smaller than the diameter of the vessel (Hoskins & Ramnarine 2000). In recent years there has been a trend towards the use of wall-less flow phantoms for Doppler ultrasound. These have the advantage of avoiding the attenuating effects of vessel wall materials and allowing clearer visualisation of underlying structures. However, they have the disadvantage of being less robust with reduced temporal stability due to the ingress of fluid into the tissue mimicking material. For the purposes of this comparative study of the measurement of flow velocities, the key issue was to create a flow system capable of providing reproducible velocities. The issue of acoustic attenuation from the vessel walls was, therefore, of little consequence, provided minimal signal losses could be assumed and a detectable Doppler signal could be achieved.

For the simple phantom, C-flex tubing of dimensions inner diameter 3.2 mm, wall thickness 0.8 mm, was used. For the carotid artery phantoms a commercial structure, as described in section 5.1.3, was used.

5.1.2 Simple straight tube phantom

The simple straight tube phantom was designed to allow examination of undisturbed flow over a range of physiologically appropriate velocities. The phantom used 3.2 mm inner diameter C-flex tubing. The vessel was mounted in a 2L polythene container with dimensions 27.8 x 11.5 x 10.3 cm (Lock & Lock, Hana Cobi Plastic Co, Ltd., Seoul, Korea) with approx 25 cm of vessel extending beyond the container at either end. The vessel was surrounded by a tissue

mimicking PVA gel of a standard "recipe" developed in previous work prior to the optimisation work described in 5.1.1. The measured T1 and T2 relaxation times of the gel are given in table 5.3

	T1 (ms)	*T2(ms)*
1.5T	470.90 (± 9.02)	61.60 (± 13.42)
3.0T	663.94 (± 232.39)	49.34 (± 1.41)

Table 5.3: T1 and T2 for the PVA gel in the straight tube phantom on the 1.5T and the 3.0T MRI scanners.

5.1.3 Carotid bifurcation pair phantom

A pair of carotid bifurcation models was purchased from Shelley Medical Imaging Technologies, Ontario, Canada. The models were constructed from a thin-walled silicone elastomer based on the work of Poepping et al. (Poepping et al. 2004) and modelled on a typical carotid artery bifurcation segment as derived by Smith et al. (Smith, Rutt, & Holdsworth 1999). The vessel walls were 1mm thick with inner diameters of 8mm for the common carotid artery (CCA) segment, 5.52 mm for the internal carotid artery (ICA) segment and 4.62mm for the external carotid artery (ECA) segment. One of the models represented a normal bifurcation while the other had a symmetric narrowing at the origin of the ICA with an inner diameter of 1.68mm, representing a 70% stenosis using the NASCET method of diameter reduction (Oates 2009).

A perspex box was constructed in which the vessel was mounted using the recommended push-fit coupling components to allow non-constricting connection to the flow system, figure 5.4. Perspex marker rods on the side walls of the phantom aided reproducible positioning of 2D phase contrast flow quantification planes during MRI and provided marker points for comparative imaging sites when using ultrasound compared with MRI. Based on the work described in section 5.1.1 above, a 10% PVA mixture was selected with three 10 hour freeze-thaw cycles to surround the vessels. During the freeze thaw cycling, the vessels were filled with glycerol to minimise any shape deforming due to expansion of the surrounding gel during the freezing cycles. The finished

phantom was topped up with distilled water containing 0.05% Benzalkonium chloride solution and a lid fitted which could be removed for ultrasound imaging.

The measured T1 and T2 values in the completed phantom are shown in table 5.4

	T1 (ms)	*T2(ms)*
1.5T	793.42 (± 11.11)	201.92 (± 0.23)
3.0T	1331.79 (± 31.30)	139.50 (± 0.90)

Table 5.4: T1 and T2 for the PVA gel in the carotid phantom on the 1.5T and the 3.0T MRI scanners.

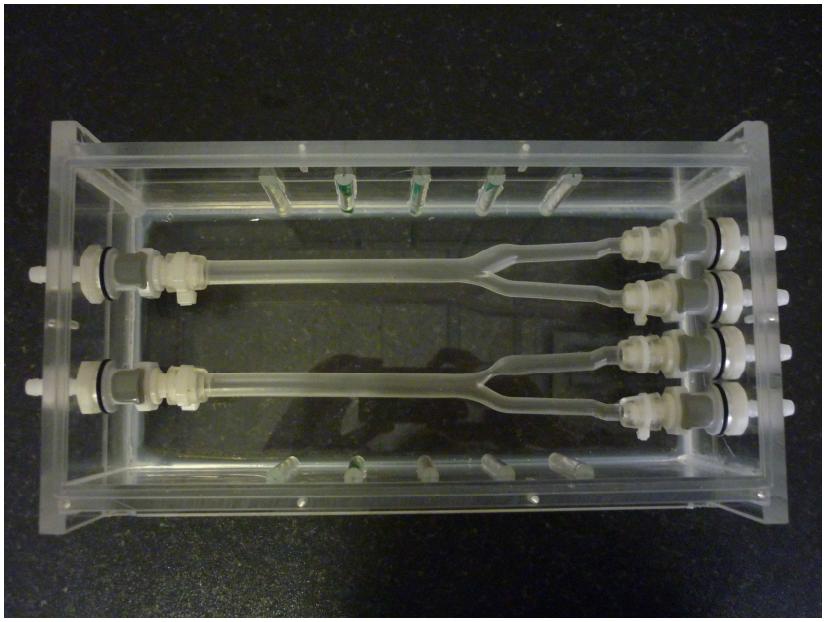

Figure 5.4: The carotid phantom construction prior to filling with PVA gel

5.1.4 Other phantoms

An additional test phantom resource available to the project was a QA phantom set from Shelley Medical imaging Technologies, Ontario, Canada. The set, figure 5.5, consisted of a pair of rigid silicone blocks.

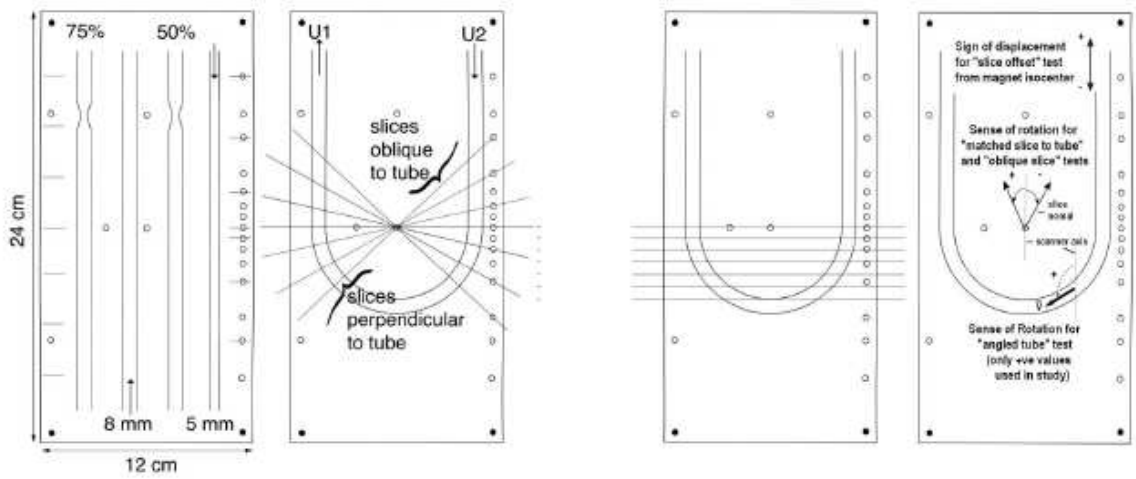

Figure 5.5: The MR QA phantom set (Shelley Medical imaging Technologies, Ontario, Canada).

The straight tube block had two straight tubes of 8 mm and 5 mm diameter and two 8mm diameter tubes one with a 50% stenosis and the other with a 75% stenosis. The u-bend block had a single 8mm diameter tube with a 180° bend. The "vessels" in these phantoms were wall-less. Although it was not possible to use ultrasound imaging with these phantoms due to large impedance changes between the solid silicone and the blood mimicking fluid, they did provide a useful tool for the evaluation of MRI flow visualisation and quantification within known geometries and avoided artefacts due to tissue or gel motion.

5.1.5 Flow pumping system

The flow was pumped through the system using an A-mount suction-shoe gear pump manufactured by Micropump (Micropump Inc., Vancouver, USA). The model no. L22094, which had a flow rate of 1.17 mL/rev, was selected to enable a range of physiologic flow velocities within tubing diameters typical of peripheral arterial vessels i.e 20 to 200 cms^{-1} in diameters 3 to 8 mm.

5.1.5.1 Establishing laminar flow

A key element in the establishment of steady flow in phantom systems is the avoidance of flow disturbance requiring estimation of the inlet length, L, which for steady flow may be approximated by $L \approx 0.03 D \mathrm{Re}$ (IEC 61685 2001; Oates

2001), where D is the diameter of the vessel and Re is the Reynolds number, which is the ratio between inertial force and friction force, as described in Chapter 2, that can be used to determine the onset of turbulence. For continuous, non-pulsatile flow in a straight tube, non-turbulent flow may be assumed when Re < 2000. For a 3.2mm diameter tube, the inlet length will thus be 19.2 cm. However, this relates to a critical velocity of 238 cms^{-1} in a tube of that diameter. Maintaining an inlet length of > 25 cm should be sufficient to ensure stable, parabolic flow for velocities up to 300 cms^{-1} in the 3.2 mm diameter tube. The carotid phantom had an inner diameter of 8.0 mm in the CCA section requiring an inlet length of > 48 cm. The long lengths of tubing required for the MRI studies made it easy to maintain long inlet lengths.

5.1.6 General experimental set-up

A schematic of the configuration used for test phantom studies of both MRI and Doppler ultrasound flow measurement is shown in figure 5.6.

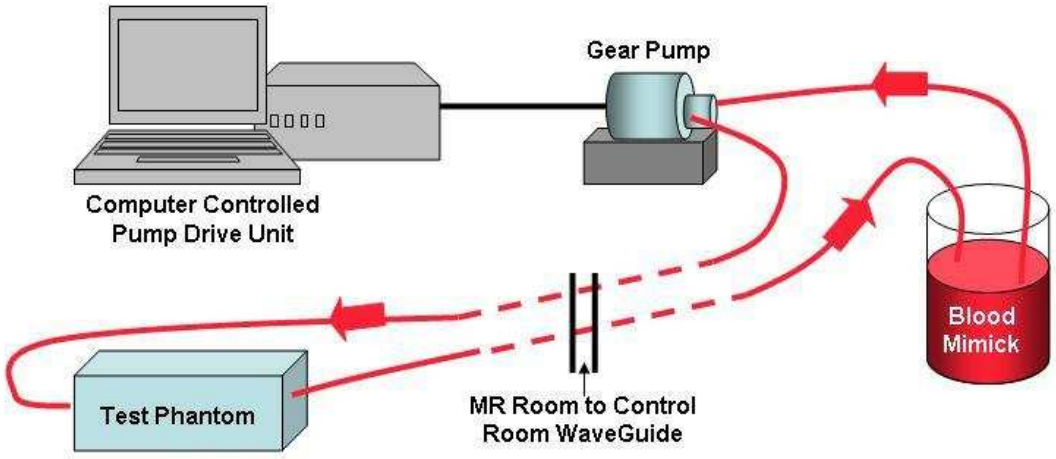

Figure 5.6: The general experimental set-up of the flow circuit for measurements using PC-MRI and spectral Doppler ultrasound.

5.1.6.1 PC-MRI measurements

The test phantom was placed such that the direction of flow was along the axis of the magnet bore, towards the back of the scanner. The inlet and outlet flow tubing was passed from the scanner room through the waveguide into the control room. The blood mimic reservoir, pump assembly and pump controller were located in the MRI control room.

A six channel body coil was positioned over the test phantom such that the long axis of the coil was approximately in the direction of flow. Foam wedges were used to position the inlet tubing along the scanner couch to ensure an adequate inlet length for maintaining stable laminar flow.

A rapid turbo-flash localiser scan was done at the start of each scanning session. The resulting images were used to minimise the region of interest to encompass the test phantom only and to locate the velocity encoded slice in a position orthogonal to the direction of flow. For the straight tube phantom, a slice approximately at the mid-point along the length of the test phantom was used, avoiding any areas where there were obvious TMM inhomogenieties such as air bubbles adjacent to the vessel. For the carotid phantom, PC-MRI slices were placed at the appropriate region of interest.

The parameters for the collection of velocity encoded slice data are described in each of the relevant sections and chapters.

5.1.6.2 Spectral Doppler ultrasound

For ultrasound scanning, the flow circuit was removed to a dedicated ultrasound laboratory. However, the lengths of inlet and outlet tubing required for MR scanning, although unnecessarily long in this case, were maintained for experimental consistency. The linear transducer was positioned and clamped in place in an approximately central position along the direction of flow to give a clear longitudinal image of the vessel. The B-Mode image was optimised to position the image of the vessel central to the field-of-view with the focal region at the axial mid-point of the vessel. The Doppler parameters used for the collection of velocity data are described in each of the relevant sections below.

5.2 Scanner details

5.2.1 MRI scanner details

Siemens Sonata 1.5T with a six channel array body coil was used for phantom studies. The standard through plane phase-contrast sequence for flow quantification was a 5mm slice, retrospectively gated, single average acquisition sequence.

Siemens Verio 3.0T with a six channel array body coil was used for both phantom studies and *in-vivo* studies. A head and neck coil configuration was used for *in-vivo* studies and the neck coil used for a subset of the phantom studies. The standard through plane phase-contrast sequence for flow quantification was a 5mm slice, prospectively gated, single average acquisition sequence.

Philips Intera 1.5T with either a standard body coil or neck coil was used for the *in-vivo* pilot studies only.

Velocity measurement on both Siemens systems was performed using the Siemens Argus flow analysis software. For the pilot study, the Philips data was analysed in-house IDL program (Exelis Visual Information Solutions, Boulder, CO, USA).

5.2.2 Ultrasound scanner details

GE Logiq-e, portable ultrasound scanner with a **12L-RS linear transducer** which had a nominal bandwidth of 5 to 13 MHz. A standard "carotid" preset was used for velocity measurement which used a Doppler frequency of 5MHz.

Siemens Sequoia 512 dedicated vascular ultrasound scanner with 8L5 and 6L3 transducers using standard carotid or femoral scanning preset protocols respectively. This was used for the *in-vivo* pilot studies only.

Velocity measurements performed on collected spectral Doppler waveforms, either manually using the velocity cursors or using the "auto-Doppler" measurement features on the scanner.

5.3 Data analysis methods

The two very different methods of velocity measurement generated different types of data output which required different approaches to analysis to allow them to be compared effectively.

5.3.1 Ultrasound data

Spectral Doppler ultrasound methods on modern ultrasound imaging systems generate an image of the spectrum of velocities plotted against time, usually displayed next to or below a B-Mode image, with or without a colour Doppler region, showing the position of the spectral Doppler sample volume in the vessel of interest. The spectrum is updated in real time, but can be frozen for measurement. Users may make measurements by manual placement of the system measurement cursors or by using automatic measurement features such as auto-Doppler. For ultrasound systems the data output is in image format only with no raw signal data or numeric analysis data.

For steady-state or constant flow ultrasound data analysis was done using the automatic waveform trace facility, auto-Doppler, provided by the ultrasound scanner to determine the average peak velocity (TAmax) and average mean velocity (TAmean). An example ultrasound image with Doppler spectra and system calculations is shown in Figure 5.7.

For pulsatile flow, measurements of peak velocities were made, either using the auto-Doppler feature as described above or using the system callipers to measure maximum velocities manually. A minimum of ten different peaks were used for any one measurement. The resulting mean and standard deviation would thus capture any variations in the flow system, variations in the Doppler system measurement and display and operator cursor placement accuracy.

Where mean velocity was required, the ultrasound system Auto Doppler function was used to provide a mean and maximum trace, as shown in figure 7.1a and a temporal averaged mean velocity, V_{TAM}.

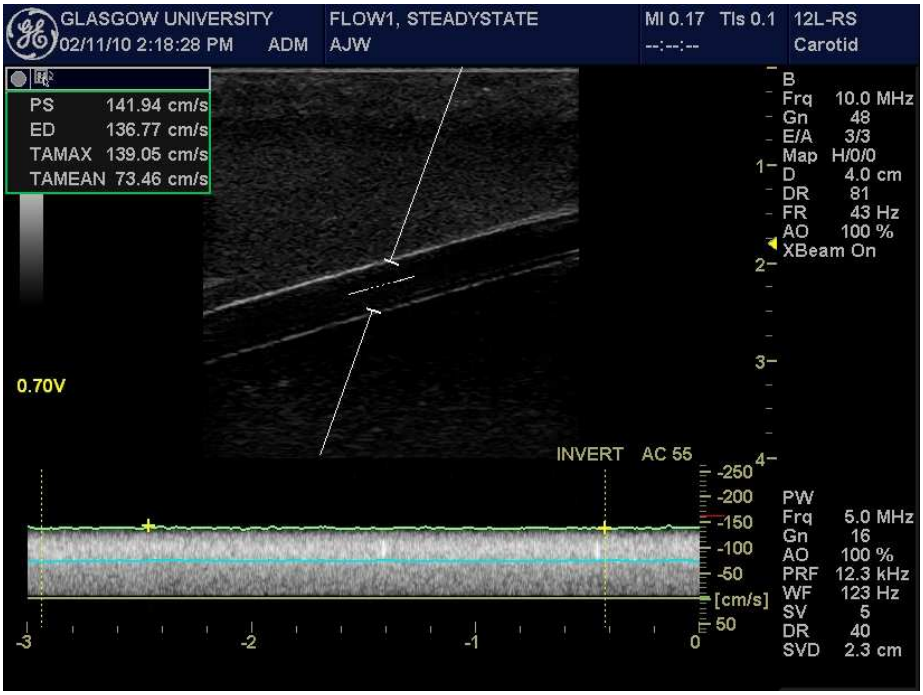

Figure 5.7. Example image of ultrasound data collected for the velocity of steady state flow in the 3.2 mm diameter straight tube phantom with the pump drive voltage at 0.7 volts.

5.3.2 PC-MRI data

The MRI data was analysed using the proprietary Siemens Argus analysis software which required display of the magnitude and phase images of the velocity encoded image data sequence to allow a region of interest (roi) to be drawn around the area of flow, as illustrated by example in Figure 5.8. For steady-state flow, the roi was then copied through the stack of images to give flow velocity information for each image pair corresponding to each timepoint.

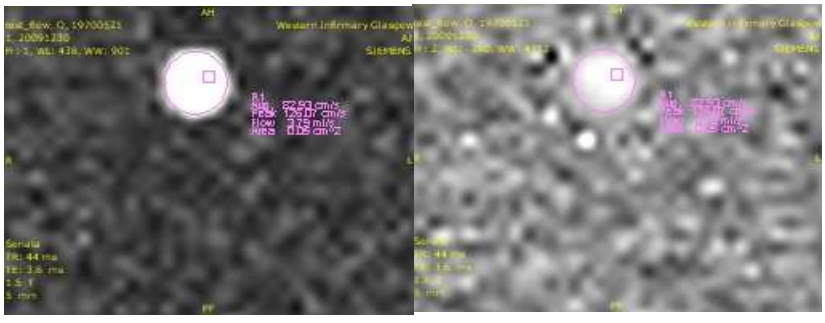

Figure 5.8 Example of the region of interest drawn on around an area of flow on the magnitude image (left) and the phase image (right) for analysis of flow quantification data.

The Argus program analysis yielded the average and peak velocity values over the range of data collection images (or timeframes within the pseudo-cardiac cycle). In theory, for constant flow, each timeframe should give identical phase-velocity information. However in practice, there were small differences between frames due to noise which enabled random errors to be determined. In addition to the velocity information the software also provided flow volume rates derived from the mean velocity and the area within the roi.

For pulsatile flow the region of interest, roi, areas, defined when using the Argus flow analysis program, had to be optimised to ensure that the roi was within the vessel walls as they appeared on the phase images. The low numbers of pixels within each roi meant that automatic segmentation of flow using Argus generally did not produce meaningful regions of interest and were more efficiently performed manually. This was a time consuming operation, particular for studies with high temporal resolution. However, for the determination of maximum velocity, rather than mean velocity or flow, it was sufficient to use a small roi, optimised to the phase image with the apparent smallest cross sectional area of flow, and copy that roi across the other images.

For comparative data where the number of cardiac phases was identical, it was possible to match the temporal positions of the highest peak values in the waveform to allow the waveform data points to be treated as matched pairs for Bland-Altman analysis as described below.

5.3.3 Bland-Altman analysis

When comparing the two methods of measurement of the same quantity, many authors will use correlation graphs and linear regression statistics to compare the two methods. However, it is highly likely that there will, indeed, be good correlation if they are measuring an identical quantity, without the measurements having to be identical. Of greater interest in comparative measurement studies is whether and how well the two methods agree. Bland-Altman graphs and statistics examine the difference in values between methods against the mean values of the two methods (Bland & Altman 1986; Gardner & Altman 1986). The mean of the difference values gives an indication of any bias between the measurements and the standard deviation provides the limits of

agreement. For the studies in this thesis, the 95% confidence limits of agreement were used i.e. ± 1.96sd. Statistical significance was tested using a paired, 2-tailed T-test such that high P values indicated low significance of any detected bias, suggesting that the null hypothesis of no significant difference between methods was held. In the cases where there was no significant difference between methods of measurement, the zero difference axis would be found well within the limits of agreement.

5.4 Preliminary studies: calibration of the flow pump system and assessment of ultrasound errors

The aim of the phantom studies of MRI velocity measurements was twofold; to validate against known flow velocities and to compare with the conventional method of spectral Doppler ultrasound velocity measurements. Consequently two key preliminary studies were required:

A timed volume collection calibration, using simple tubing of known diameters from which flow rates can be calculated and mean velocity values may be established.

An assessment of the errors in the estimation of maximum velocity as described in chapter 3.1.4. the intrinsic spectral broadening due to beam geometry and the consequent overestimation of maximum velocity.

5.4.1 Timed volume collection of steady state flow.

Flow rates were determined by collecting fluid from the phantom inlet tube over the range of steady state pump voltage settings. Fluid was collected using a calibrated Ohaus Ranger electronic balance (Ohaus Europe GmbH, Switzerland). Two sets of data were collected:

Set 1 using voltages relevant to the larger diameter flow phantoms, of 0.5V to 3.0V in 0.5 V steps for fixed time periods of 15s or 30s.

Set 2 using voltages relevant to the smaller 3.2 mm diameter flow phantom, of 0.1V to 1.0V in 0.1 V steps for fixed time periods of 30s or 60s.

A density value of 1,050 ± 40 kg m^{-3} for the BMF (IEC 61685 2001) was used to determine the volume from the collected weight. Each volume measurement was repeated ten times.

5.4.1.1 Results

Results for the two data sets are pooled in the correlation graph in figure 5.9 the dotted line is a fitted linear trendline with a zero intercept.

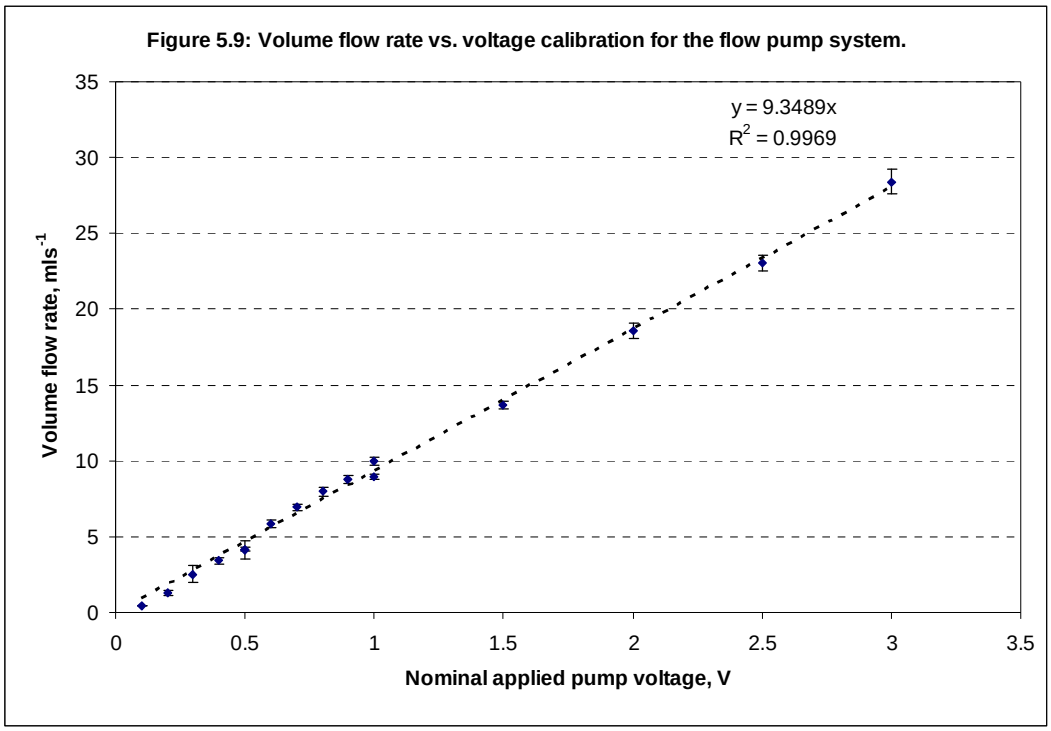

Figure 5.9: Volume flow rate vs. voltage calibration for the flow pump system.

The trendline in figure 5.9 suggests a good linear response of the pump to the applied voltage and provided a range of steady state flow volume per voltage rates which enabled calculation of mean flow volume, using Equation 5.2 The standard deviation values for the data in figure 5.9 were also fitted with a linear trendline giving an estimated error of ± 0.25 V (mls^{-1}) equivalent to a percentage error of ± 2.7%.

Equation 5.2: $$Flow\ (mls^{-1}) = 9.35 \cdot voltage\ (V) \pm 0.25 \cdot voltage\ (V)$$

In turn this enabled estimation of the mean flow velocity to be made in phantoms of known diameter, where laminar flow could be assumed using Equation 5.3.

Equation 5.3: $$MeanVelocity(cms^{-1}) = \frac{Flow(mls^{-1})}{\pi r^2}$$ where *r* is the radius of the tube in centimetres.

The two equations above, applied to a 3.2 mm diameter tube, yield the mean velocities, in table 5.5, for each voltage setting.

Pump Voltage, Volts	*Calculated Mean Velocity in 3.2 mm diameter tube, cms^{-1} ± 2.7%*
0.1	11.6
0.2	23.3
0.3	34.9
0.4	46.5
0.5	58.2
0.6	69.8
0.7	81.4
0.8	93.0
0.9	104
1	116
1.5	174
2	232
2.5	290
3	348

Table 5.5: Mean velocities in a 3.2 mm diameter tube, calculated from known flow volume calibration for a range of applied pump drive velocities.

5.5 Accuracy of ultrasound measurements of velocity

The use of spectral Doppler ultrasound for diagnosis of blood haemodynamics has, as discussed in Chapter 3, evolved such that the peak values of the velocity spectral waveform are recorded for use either as stand alone parameters or for further calculations. However, it has long been noted by several authors (Eicke et al. 1995; Gaynor et al. 2008a; Hoskins 1996; Steinman et al. 2001; Walker et al. 2004), and reiterated in a recent review (Hoskins 2011), that this method is flawed, primarily by intrinsic spectral broadening of the ultrasound instrumentation.

Intrinsic or geometric spectral broadening results from the finite aperture of the Doppler beam causing a range of beam-flow angles, rather than the assumed single angle which represents the central part of the beam.

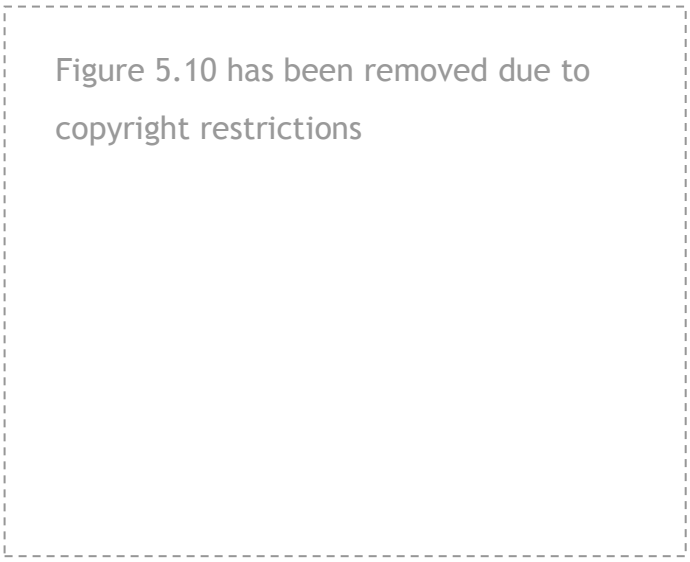

Figure 5.10: Illustration of the finite aperture reason for intrinsic spectral broadening. The on-screen image of the spectral Doppler beam is represented by the blue line with an angle correction for θ used in the calculation of velocities. However, the finite width of the Doppler beam results in a spread of Doppler frequencies and displayed velocities. Adapted from Hoskins (Hoskins 2011).

Hence, any single velocity estimated by the scanner will have an inherent error bounded by the velocity values generated by $f_{d,min}$ and $f_{d,max}$,as illustrated in figure 5.10, i.e. an intrinsic spectral broadening. If the aperture is symmetric it may be assumed that the mean frequency is a reasonable estimator of the true velocity.

We mentioned in chapter 4 how one of the key advantages that spectral Doppler ultrasound has over phase contrast MRI velocity measurements is that the fast Fourier analysis of the sampled Doppler signal provides a spectrum of velocities which, provided the sample volume encompasses the whole vessel, is representative of the range of velocities across the vessel at a point in time. The resulting spectrum of velocities mapped against time is representative of haemodynamic properties of the flowing blood e.g. plug flow, laminar flow, turbulent flow. An increase in the spectral broadening is seen as indicative of flow disturbance. However, the intrinsic spectral broadening can mask the true spectral broadening within fluid flow and consequently cause overestimation of any maximum velocities measured.

5.5.1 String phantom

An established method of assessing the intrinsic spectral broadening and consequent error on maximum velocity measurements is to use the ultrasound scanner system to interrogate a device capable of producing a single velocity signal. Such a requirement rules out the use of liquid flow phantoms which will have a varying velocity profile across the diameter of the flow lumen. String phantom devices (IPEM 2010) employ a thin, smooth "string" filament driven by a wheel of calibrated rotational velocity.

The string phantom used in this study was manufactured in-house. The phantom, shown in figure 5.11, used a water-tight motorised drive wheel to move an o-ring rubber "string" of diameter 1.6 mm, and was structured to ensure that all movement was below water so that air bubbles were not dragged into the liquid.

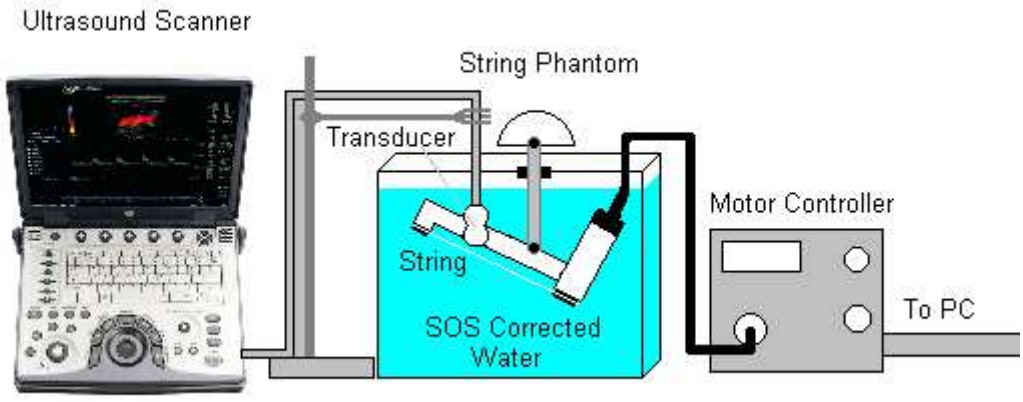

Figure 5.11: String phantom experimental set up.

The water within the phantom was degassed and 9% (volume) glycerol added to correct the speed of sound to 1540 m s^{-1}. The speed of sound was checked by measuring a known depth using the ultrasound scanner callipers. When the device is immersed in speed of sound corrected water, the top surface of the string provides an echo signal which is travelling at a single velocity. However, this is represented on the spectral Doppler display as a band of velocities rather than a single line. By measuring the upper and lower velocity limits of such bands, the estimated maximum velocity and estimated minimum velocity may be

used to provide an indication of the percentage intrinsic or geometric spectral broadening as in equation 5.4.

Equation 5.4: Percentage intrinsic spectral broadening, ISB(%)

$$ISB(\%) = 100 * \frac{EstimatedMaximumVelocity - EstimatedMinimumVelocity}{EstimatedMaximumVelocity + EstimatedMinimumVelocity}$$

It is also useful to compare the maximum velocity estimation and mean velocity estimation against the calibrated velocity of the string, equation 5.5.

Equation 5.5: Percentage maximum velocity error, Error(%)

$$Error(\%) = 100 * -\left(\left[\frac{EstimatedMaximumVelocity}{StringVelocity}\right] - 1\right)$$

However, before assessing the Doppler performance using the methods described above, the speed of the string phantom, particularly the rotation of the drive wheel, was calibrated.

5.5.1.1.1 String Phantom Calibration

The speed of the string was calibrated for each velocity setting using a calibrated Veeder Root Tachometer (Danaher Speciality Products, Elizabethtown, NC, USA) to measure the rotational speed of the drive wheel. This was done with the o-ring string attached to account for any tensioning effect from the stretched o-ring.

The results of the calibration are shown in figure 5.12. The following calibration, equation 5.6, can be determined for the string phantom:

Equation 5.6: String Velocity (cms^{-1}) = 320.45*Voltage (V) ± 0.07 cms^{-1}

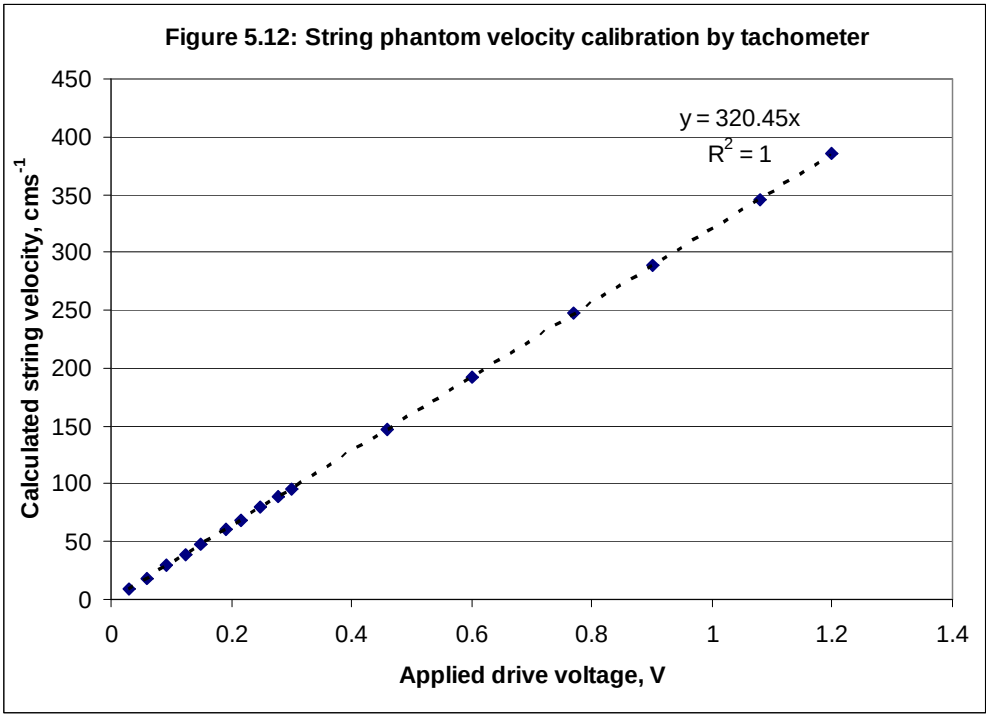

5.5.1.2 String phantom ultrasound experimental methods

The 12L-RS transducer in the GE Logiq e ultrasound scanner was positioned in the phantom such that the active face was fully in contact with the water and free from any air bubbles. Measurements were made using the same "CAROTID" preset used for the *in-vivo* studies with the exception of the acoustic output power which was reduced to 50% of maximum to minimise signal saturation from the strong unattenuated echo signal from the o-ring.

The Doppler beam sample volume, SV, cursor was positioned over the B-mode image of the string and angle correction applied. The indicated depth of the SV was 4.7 cm with a 5mm SV width at an angle of 51°. A range of voltage values was used to drive the string at a range of velocities reflective of those used in flow phantom experiments and that may be typically encountered in the normal and diseased physiology. The maximum and minimum velocities on the spectral display for each velocity setting were recorded using the ultrasound scanner velocity callipers with the set of eight callipers used to record eight values for each measurement so that an average could be generated. The recorded spectral Doppler ultrasound minimum, mean and maximum velocities are shown in figure 5.13.

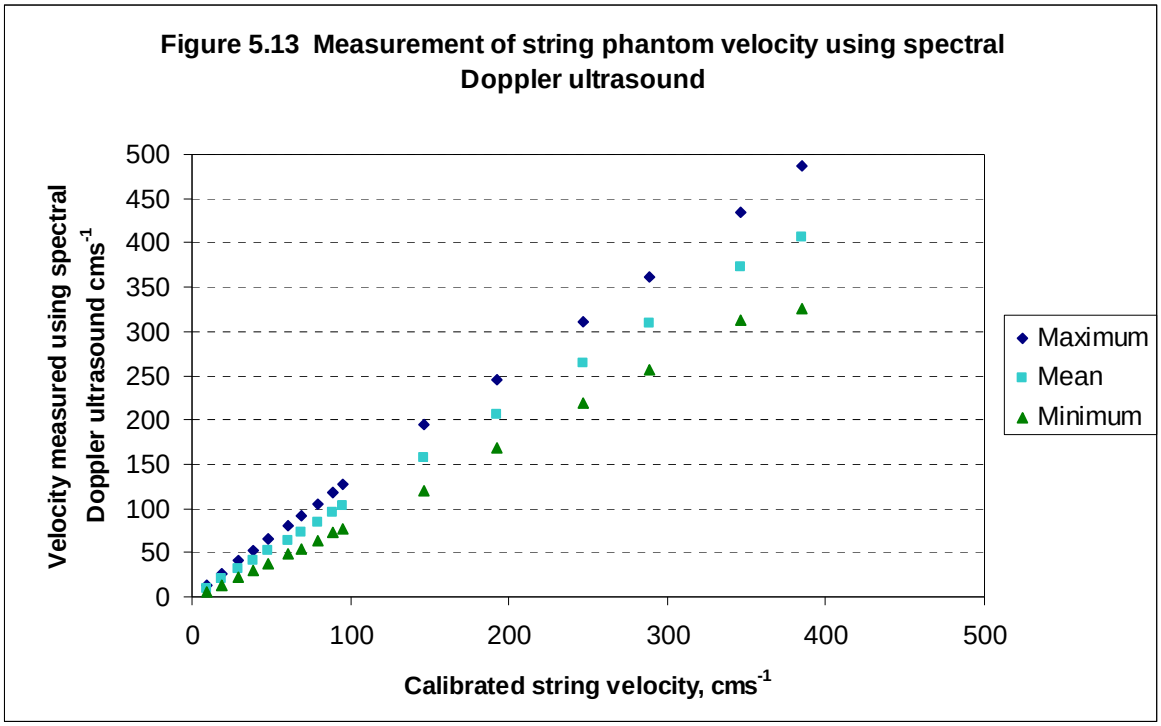

Equations 5.4 and 5.5 were used to calculate the percentage ISB and percentage error on the maximum velocity for each of the calibrated string velocity settings, results are shown in table 5.6.

Mean string velocity from calibration(cms^{-1})	*% error on string velocity calibration*	*% error on maximum velocity*	*%ISB*
9.09	0.77	48.34	40.91
18.45	0.16	39.60	29.99
29.40	0.07	38.83	30.88
38.77	0.07	36.52	28.08
48.12	0.04	36.68	27.37
60.71	0.05	33.55	25.61
68.60	0.06	33.66	25.25
79.64	0.04	32.72	24.59
88.67	0.04	32.32	23.77
94.91	0.04	33.81	24.38
146.95	0.03	32.31	23.44
192.10	0.05	27.72	18.69
247.35	0.05	25.89	17.59
288.34	0.04	25.57	17.12
346.00	0.04	25.38	16.34
385.24	0.05	26.28	19.70

Table 5.6: Percentage error on the maximum velocity and percentage intrinsic spectral broadening for a range of calibrated string velocities. The percentage error on the calibrated velocity is shown, for comparison, in column 2.

Comparing the results at string velocities of 190.32 cms^{-1} and 245.06 cms^{-1} with previously published work for string velocities of 200 cms^{-1} (Ultrasound Equipment Evaluation Project 2004a; Ultrasound Equipment Evaluation Project 2004b; Gaynor et al. 2008b) the % errors on the maximum velocity and the percentage intrinsic spectral broadening appear typical for linear transducers. From our own results, we may calculate a mean percentage error on the maximum velocity of 33% ± 6% over all velocities or 30.5% ± 3.5% for velocities over 50 cms^{-1} for comparison with Gaynor's results of 40% and 31% respectively.

For the determination of the maximum velocity using ultrasound, the correction factor of 33% could be applied to the Doppler ultrasound measurements for comparison with MRI derived velocity values.

From the Bland-Altman comparisons of string velocity with maximum spectral Doppler ultrasound velocity and with corrected maximum spectral Doppler ultrasound velocity, shown in graphs 5.14 and 5.15 respectively, it can be seen that spectral Doppler ultrasound maximum velocities have a mean bias of 28.3% higher than the true string velocity, but application of the correction percentages effectively removes that bias, taking it close to the zero line of no difference.

Figure 5.14: Bland-Altman comparison between calibrated string velocity and the maximum spectral Doppler ultrasound velocity (mean vs. %difference)

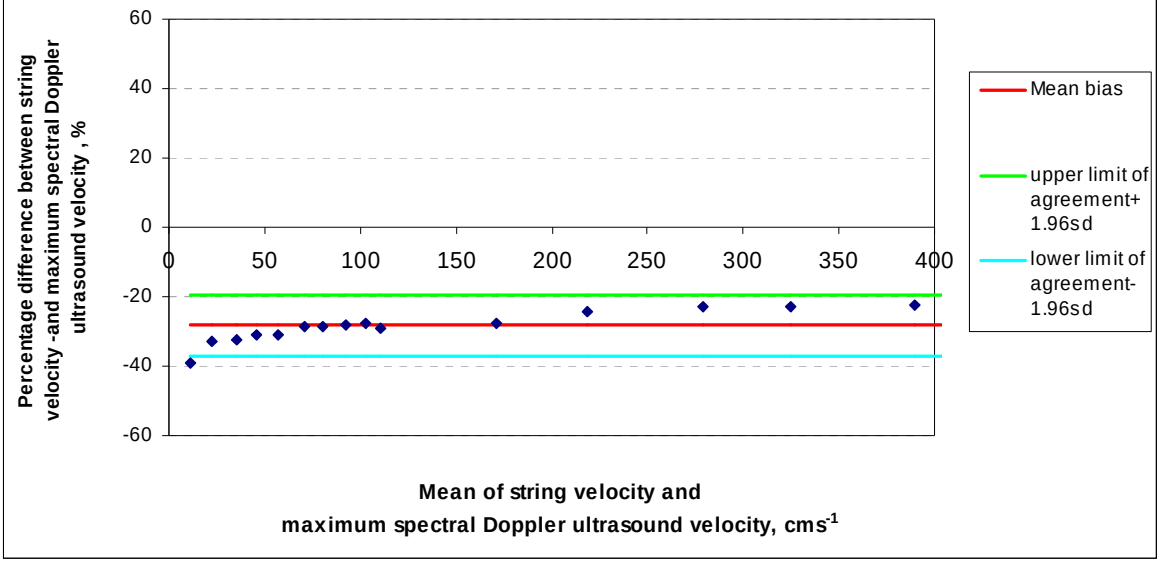

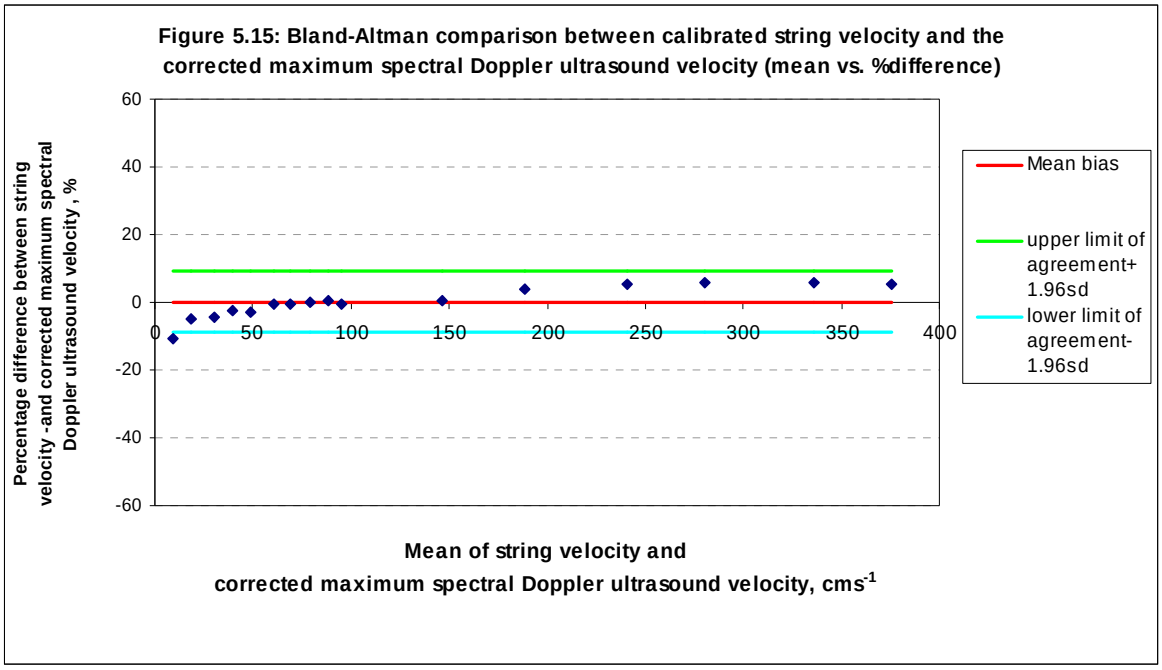

When comparing maximum velocities measured using spectral Doppler ultrasound with other methods of velocity measurement, the error on the maximum velocity for ultrasound should be considered.

5.6 Summary of chapter

In this chapter we established a set of flow phantoms and calibrated the flow pump system. This enabled comparison of spectral Doppler ultrasound and PC-MRI methods of velocity measurement against known flow volume rates and mean velocities.

A mean percentage error on the measurement of maximum velocity using spectral Doppler ultrasound has been estimated and may be applied to any such measurements in subsequent chapters.

Chapter 6 – Velocity and flow measurement: validation, optimisation and comparison under steady state flow conditions.

Prior to investigating any velocity measurement technique in vivo, it is useful to be able to validate it, *in-vitro*, against a "gold-standard" or established technique using a range of known values. The use of steady-state or constant flow velocities obviates temporal resolution issues and simplifies the investigation.

6.1 Introduction

In-vitro systems, which provide simple, steady state laminar flow in a straight tube, provide an efficient starting point for comparing the two methods of determining the velocity of flow. In the following investigations, although this thesis is primarily concerned with velocity measurements, some comparisons between the associated volume flow rate measurements are also made for ease of comparison with studies carried out by other authors.

It is difficult to regard ultrasound spectral Doppler measurement as the "gold-standard", despite its status as a more established technique, due to both the differences in the nature of the output data between techniques and the inherent errors in the spectral Doppler determination of maximum velocities, as described in chapter 3 and demonstrated in chapter 5. However, it is important to be able to make a direct comparison between methods if we are to be able to consider the use of key diagnostic haemodynamic parameters derived from PC-MRI velocity measurements. Both the straight tube phantom and the carotid phantom were designed such that ultrasound and MRI studies could assess identical flow patterns.

6.1.1 Validation of flow measurements

It has been common practice for authors to validate MRI phase contrast velocity measurement methods by establishing timed-volume collection flow rates, such

as were carried out in chapter 5, and to compare these values with 2D phase contrast derived MRI determination of flow rates in test phantoms. While this method would suggest that the associated velocities underlying the calculation of flow rate might compare similarly, it does not follow that velocity measurement can be described as having been validated using such methods, particularly when moving to the *in-vivo* scenario with pulsatile flow in compliant vessels. Nevertheless, the comparison of flow in its simplest form i.e. steady state, laminar flow in a straight vessel, against known flow values can give an indication of the potential for agreement between methods.

6.1.2 Optimisation of PC-MRI methods of velocity measurement

While we are aware that the temporal resolution requirements of the gated PC-MRI techniques will limit spatial resolution, it is useful to use steady state flow to take out the complication of temporal resolution enabling study of spatial parameters such as:

- Pixel dimension (spatial resolution)
- Slice thickness
- Scan-plane angle

6.1.3 Comparison between spectral Doppler ultrasound and PC-MRI methods of velocity measurement

As was noted in the literature survey in chapter 4, there have been only limited attempts to carry out truly comparative test-phantom studies of PC-MRI blood flow quantification compared with spectral Doppler ultrasound methods with published studies focussing on flow rates and mean velocities. However, although comparison of mean velocities is useful in that it can be related back to calibrated flow rates when steady state flow is considered, this thesis is concerned with the ability to use haemodynamic ratios and indices which use peak maximum velocity values.

6.2 Methods

6.2.1 Validation against calibrated flow rates

Using the flow system described in chapter 5, with the 3.2mm straight tube phantom attached and laminar flow inlet lengths maintained, a range of constant voltages were used to drive the blood mimicking fluid through the system. Using the pump voltage calibration for volume flow, the mean flow velocities used were estimated to be in the range 11.63 cms^{-1} (± 0.31 cms^{-1})to 116.3 cms^{-1} (± 3.14 cms^{-1}). With the flow system set up such that it should be reasonable to assume parabolic, laminar flow, the maximum velocity may be assumed to be twice the mean velocity (Oates 2001), i.e. in the range 23.26 cms^{-1} (± 0.63 cms^{-1}) to 232.6 cms^{-1} (± 6.27 cms^{-1}).

The same flow set up was used for both MRI and ultrasound measurements, the only exception being that the lid of the phantom was removed for ultrasound work. The scanning parameters used are described in table 6.1.

Use of the velocity encoded protocols on the MRI scanners required gating or triggering. For these constant flow conditions an internal trigger was selected with a nominal time of 1000ms, equivalent to a heart rate of 60 beats per minute.

For these preliminary measurements, the protocols used for PC-MRI measurements, and outlined in table 6.1, were the standard protocols for each scanner.

Ultrasound	*1.5 T MRI*	*3T MRI*
12LRS Linear Transducer	Body Coil	Body Coil
Carotid Pre-Set	Standard venc Single slice sequence	Standard venc Single slice sequence
Spectral Doppler frequency 5MHz	Slice Width, 5mm	Slice Width, 5mm
Sample Volume Width, 5mm at depth 2.3cm	Pixel Resolution 0.47mm X 0.47mm	Pixel Resolution 0.47mm X 0.47mm
Doppler Angle correction 55°	Slice Angle - orthogonal	Slice Angle - orthogonal
	TR = 44 ms, TE = 3.6 ms	TR = 47.3 ms, TE = 4.69 ms
	23 Cardiac Phases giving temporal resolution 43.4ms	19 Cardiac Phases giving temporal resolution 47.5ms
	Retrospective Gating with one average.	Prospective Gating with one average.
	venc setting varied 100, 120, 200 cms^{-1}	venc setting varied 100, 120, 200 cms^{-1}

Table 6.1. Scanning parameters for steady state velocity flow and comparison work using the 3.2 mm diameter straight tube phantom.

6.2.2 Optimisation of steady state velocity measurement using PC-MRI

The quantification of flow velocities using PC-MRI techniques is a gated or triggered technique which, as discussed in chapter 3, involves a trade off between temporal and spatial resolution. Several authors (Greil et al. 2002; Lotz et al. 2002) have looked at how various parameters affect the determination of velocities and flow measurements. The use of steady state flow of known velocity enables simplified optimisation of some of the PC-MRI parameter variables.

The following studies were carried out using the 3.2 mm diameter straight tube phantom in the 1.5T scanner. For each study, the same orthogonal slice plane was used for all measurements with the 23 cardiac phases used for statistical evaluation. The flow system was set to give a constant calibrated flow rate of

4.67 mls^{-1} (± 0.13 mls^{-1}). equivalent to a mean steady state velocity of 58.15 cms^{-1} (± 1.57 cms^{-1}).

6.2.2.1 Pixel resolution

To examine the effect of spatial resolution on the PC-MRI determination of velocity, the parameters in table 6.1 were used with a 384 x 512 matrix but a variable field of view, as shown in table 6.2, giving a 2-D pixel resolution from 0.18mm to 0.39mm. For the smallest field of view settings, only the "Fast" gradient modes were available and only "Normal" gradient modes for the larger field of view settings. Both gradient mode settings were used with an overlap for two of the field of view settings.

Gradient mode	FOV (mm)	Pixel dimensions (mm)	Pixels per tube area	Pixels per tube radius
FAST	69 x 92	0.18	249.07	8.90
	75 x 100	0.20	210.82	8.19
	82 x 110	0.21	175.29	7.49
	90 x 120	0.23	146.40	6.83
	97 x 130	0.25	125.39	6.33
NORMAL	90 x 120	0.23	146.40	6.83
	97 x 130	0.25	125.39	6.33
	105 x 140	0.27	107.56	5.85
	112 x 150	0.29	94.11	5.49
	120 x 160	0.31	82.35	5.12
	127 x 170	0.33	73.23	4.84
	135 x 180	0.35	65.07	4.55
	142 x 190	0.37	58.60	4.33
	150 x 200	0.39	52.70	4.10

Table 6.2. Variable Field of View (FOV) parameters for the study of spatial resolution effects. The pixels per tube area and pixels per tube diameter are calculated using the known tube inner diameter of 3.2 mm.

6.2.2.2 Slice thickness

The other voxel dimension, the thickness of the phase contrast slice, was investigated by using the parameters outlined in table 6.1, but with the slice thickness varied from 3mm (the minimum available on the 1.5T scanner) up to 10mm in steps of 1mm.

6.2.2.3 Scan plane angle

Using an orthogonal phase-contrast slice with the parameters outlined in table 6.1 as a starting point, geometric adjustment within the sequence adjustment function on the scanner was applied to tilt the slice by angles of ±10° and ±20°off the original orthogonal position.

6.2.3 Comparison of steady state velocity measurement.

Data collected using the study parameters listed in table 6.1. was used to compare both the mean and the maximum velocities measured over a range of phantom flow rates in the 3.2 mm straight tube phantom.

Use of the carotid bifurcation phantom with its simulated vessel anatomy, more compliant vessel wall material and softer surrounding gel allowed simulation of the *in-vivo* situation, while maintaining the artificial haemodynamic conditions of steady state flow. In addition, one of the bifurcation pairs in the carotid artery phantom had a stenosis at the proximal ICA branch with a diameter reduction equivalent to a 70% stenosis. The effect on the measured steady state haemodynamics of this known diameter reduction was investigated, giving the opportunity to examine large velocity increases due to the stenosis. The parameters for 3T imaging listed in table 6.1 were used to image the carotid phantom with venc values of 100, 200, 250, 300, 350, 400 cms^{-1} to account for the increase in velocities due to the stenosis.

6.2.4 Velocity indices

Further analysis was carried out in the carotid artery phantom to examine velocity ratios. In carotid artery Doppler ultrasound one of the key parameters in the diagnosis of internal carotid artery stenosis is the ratio of the peak systolic

velocity in the internal carotid artery, ICApsv, to the peak systolic velocity in the common carotid artery, CCApsv. ICApsv/CCApsv ratios of > 4 generally indicate a stenosis of > 70 %. (Oates et al. 2009). In other areas of the body, a doubling of velocities in usually regarded as being haemodynamically significant. Data from the carotid artery phantom was further analysed to compare the ICA/CCA steady state maximum velocities measured using PC-MRI and spectral Doppler ultrasound.

6.2.5 Data analysis

Data was analysed as described in chapter 5 with Bland-Altman comparisons where appropriate.

6.3 Results

6.3.1 Validation of steady-state PC-MRI flow measurements against calibrated flow rates

As we have discussed in previous chapters, it is difficult to regard either Doppler ultrasound or phase contrast MRI as a gold standard in the measurement of velocity. Doppler ultrasound is the more established of the two, but the potential errors are well known and have been discussed in the previous chapters.

However, in chapter 5, it was possible to obtain a calibrated volume flow rate for a range of constant flow pump drive voltages on the flow phantom system. It is therefore useful to first compare the MRI and ultrasound flow analysis against the calibrated flow, in line with the methods used by previous authors attempting to test MRI flow quantification. For the ultrasound measurements, the volume flow rate was estimated using the mean velocity and the known cross-sectional area of the tubing, which was confirmed by calliper measurements on the ultrasound image. In the PC-MRI Argus analysis, the volume flow rate was provided with the output data and had been derived from the user defined roi and the average velocity within that roi.

Bland-Altman Comparisons between the calibrated volume flow rate and ultrasound, 1.5T PC-MRI and 3.0T PC-MRI are illustrated in figures 6.1a, b and c.

At first glance, the flow volume rate calculated using ultrasound mean velocity measurements, figure 6.1.a, appears to give better agreement with the calibrated flow volume rate than either the 1.5T or the 3.0T PC-MRI determination of flow volume rate, figures 6.1 b and c. However, examination of the magnitude of the region of interest, roi, used in the MRI determination of flow revealed that these were significantly smaller than the true dimensions of the tubing cross sectional area of 0.08cm^2, leading to an underestimation of flow rate as revealed by the mean bias values of 2.52 ± 2.02 mls^{-1} for 1.5T PC-MRI and 2.20 ± 1.97 mls^{-1} for 3.0T PC-MRI.

Figure 6.1a: Bland-Altman comparison of the measurement of volume flow in a 3.2 mm diameter straight tube phantom - flow Volume calibration vs. flow derived from ultrasound temporal average mean velocity

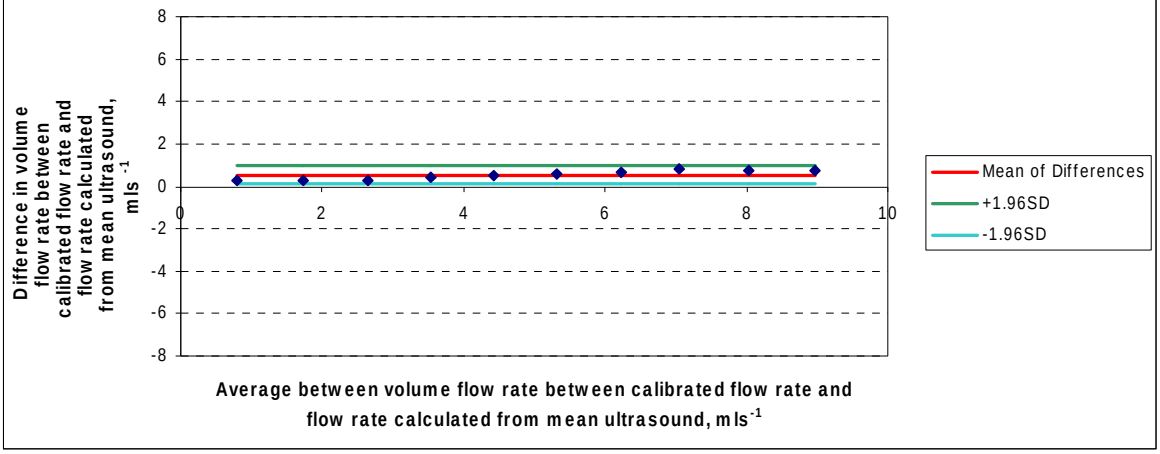

Figure 6.1b: Bland-Altman comparison of the measurement of volume flow in a 3.2 mm diameter straight tube phantom - flow volume calibration vs. flow from 1.5T PC-MRI calculated using Argus

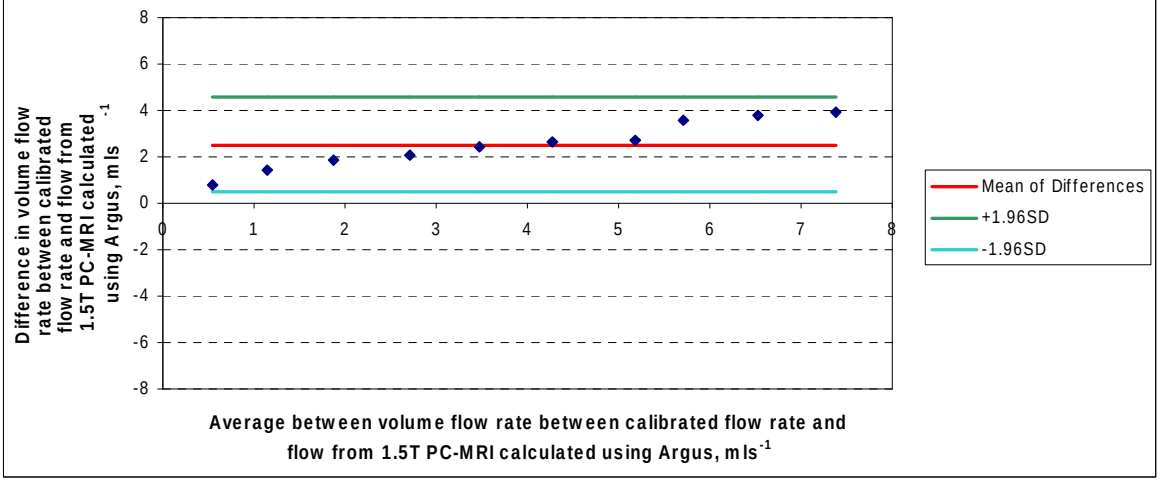

Figure 6.1c: Bland-Altman comparison of the measurement of volume flow in a 3.2 mm diameter straight tube phantom - flow volume calibration vs. flow from 3.0T PC-MRI calculated using Argus

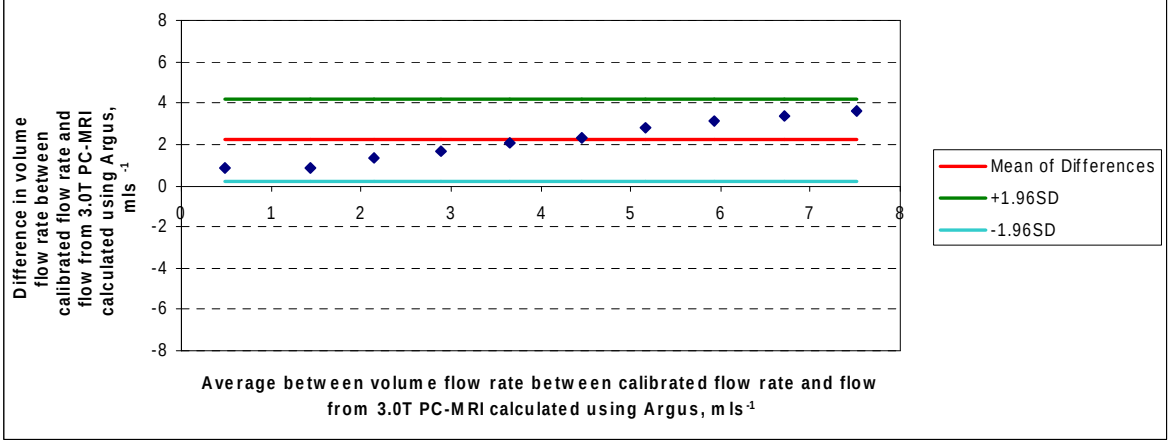

Using the mean flow velocities from the PC-MRI data and the true cross sectional area to calculate flow rates produces good agreement with the calibrated flow rates as shown in figures 6.1. d and e.

The Bland-Altman statistics and the p value for significance from a paired T-test for the comparisons made in figures 6.1.a to e are summarised in table 6.3.

In Figures 6.1 a to e and table 6.3, a positive value of bias represents a mean underestimation of calibrated flow by the imaging method. This appears to be the case for both the ultrasound and the PC-MRI methods. However, the statistical null hypothesis of no difference between measurement methods (the zero line in the Bland-Altman comparison graphs) is within the 95% confidence levels for 1.5T and 3.0T PC-MRI when the flow is calculated using the mean velocity and the known diameter of the vessel.

In clinical practice, however, using the known diameter of a vessel would not be an option and the analysis would be performed using methods such as those employed using the Argus flow analysis software in this study i.e. using the magnitude and phase images and drawing a region of interest encompassing the apparent cross section of flow. The results of this study highlight a potential flaw in the determination of volume flow rates when using PC MRI flow quantification: the apparent region of flow can appear to be smaller than the true lumen area. This effect was examined further by looking at steady state flow in the 5mm diameter and 8mm diameter straight vessels in the MR-QA phantom.

Method of flow rate measurement compared against the calibrated flow rate	*Mean bias (mls^{-1})*	*± Limits of agreement (mls^{-1}) (± 1.96σ)*	*P value*
Ultrasound Mean Velocity	0.53	0.43	< 0.01
1.5 T PC-MRI from drawn ROI	2.52	2.02	< 0.01
3.0 T PC-MRI from drawn ROI	2.20	1.97	< 0.01
1.5 T PC-MRI from mean velocity and true ROI	0.07	0.33	>0.05
3.0 T PC-MRI from mean velocity and true ROI	0.15	0.36	0.01<p<0.05

Table 6.3: Summary of main statistics from the comparison studies for flow rates in the 3.2 mm diameter straight tube phantom.

Figure 6.1d: Bland-Altman comparison of the measurement of volume flow in a 3.2 mm diameter straight tube phantom - flow volume calibration vs. flow from 1.5T PC-MRI calculated using mean velocity and true area

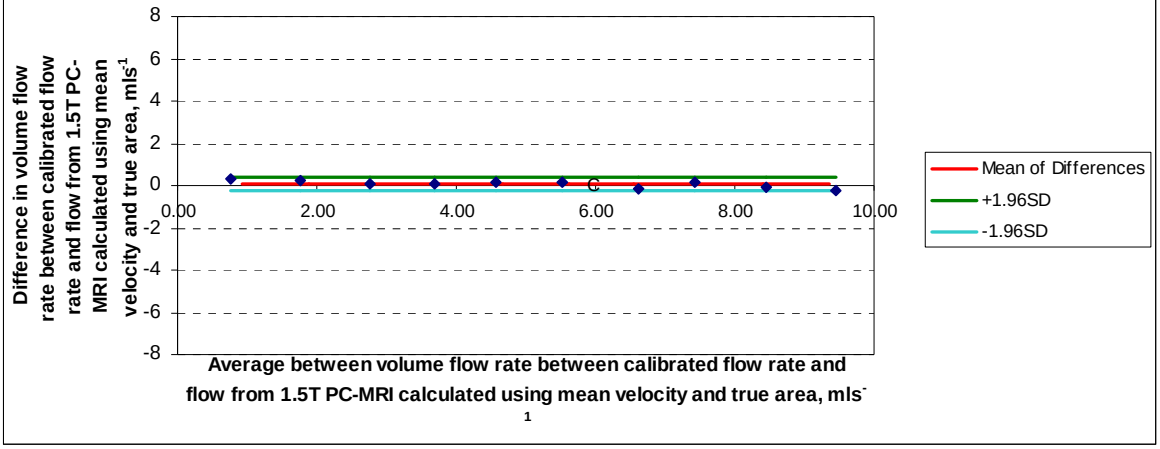

Figure 6.1e: Bland-Altman comparison of the measurement of volume flow in a 3.2 mm diameter straight tube phantom - flow volume calibration vs. flow from 3.0T PC-MRI calculated using mean velocity and true area

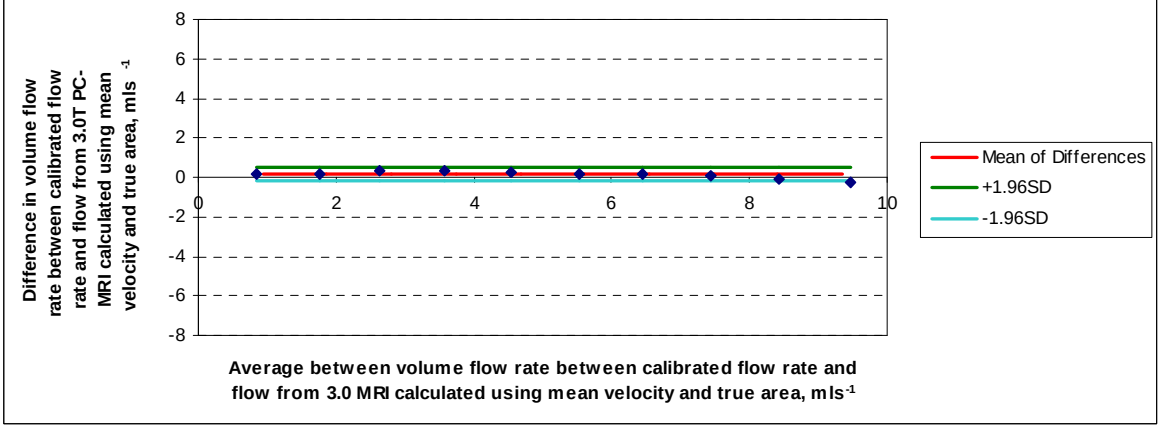

It is well known in the literature (Bernstein, King, & Zhou 2004; Greil et al. 2002; Lotz et al. 2002; Lotz et al. 2005; Tang, Blatter, & Parker 1993) that partial-volume effects can cause over estimation of flow, particularly for smaller vessels. However, the results in this study appear to contradict this with consistent underestimation. Figure 6.2 illustrates the magnitude of the underestimation for the different vessel diameters and magnetic field strengths with the error bars representative of the ±1.98σ limits of agreement.

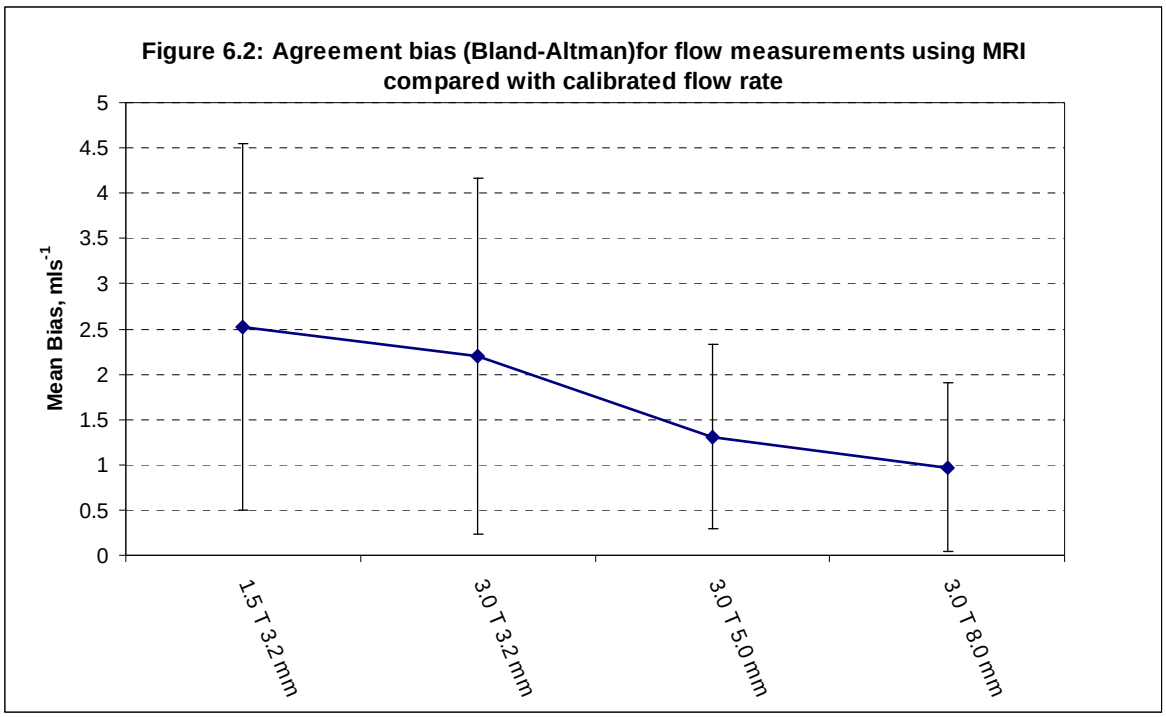

The results for the agreement between calibrated flow rates and MRI flow rates appear poor compared with agreements found by other authors (Lotz et al. 2005). However, those studies generally used larger diameter vessels with gadolinium doped blood mimics. Graph 6.2 does suggest that larger diameters will give better agreement. It is likely that variations in the phase contrast signal levels are affecting the appearance of the area of flow and hence the size of the ROI drawn for flow estimation. The effect of pixel dimensions in relation to the vessel size is examined and discussed further in section 6.3.2 where the results for spatial resolution effects are presented.

6.3.2 Results for the optimisation of parameters under steady state flow conditions

The optimisation parameters examined under steady state flow conditions were intended to allow examination of the spatial effects in the absence of temporal resolution considerations. In addition the absence of pulsatile flow ensured that no spatial changes were taking place (i.e. lumen contraction and expansion) which might further complicate parameters such as the pixels per radius.

6.3.2.1 Pixel resolution

Previous studies (Greil et al. 2002; Hofman et al. 1995; Lotz et al. 2005; Tang, Blatter, & Parker 1993) have tended to focus on flow measurements rather than velocity measurements in relation to spatial resolution, although Lotz (Lotz et al. 2002)* and Hofman (Hofman et al. 1995) suggested that partial volume effects associated with poor pixel resolution would cause over estimation of volume flow rates and underestimation of peak velocities.

*Lotz 2002 paper incorrectly states that partial volume effects underestimate flow rate but the illustrative graph contradicts this.

Figures 6.3 and 6.4 illustrate the effect on PC-MRI mean and maximum velocities respectively. For the mean velocity all measurements underestimated the calibrated mean velocity of 58.15 cms^{-1} but the highest resolution setting for both the Fast and Normal gradient modes came closest to the calibrated mean velocity value with underestimations of 4.5% for Fast mode and 4.4% for Normal mode. Above a threshold of 0.25mm for pixel size, the bias in measurements appears to settle down to a level between 23% and 28%. The maximum velocity measurements show no relationship with resolution and show a mean negative bias of 28% below the calculated value of 118.3 cms^{-1}.

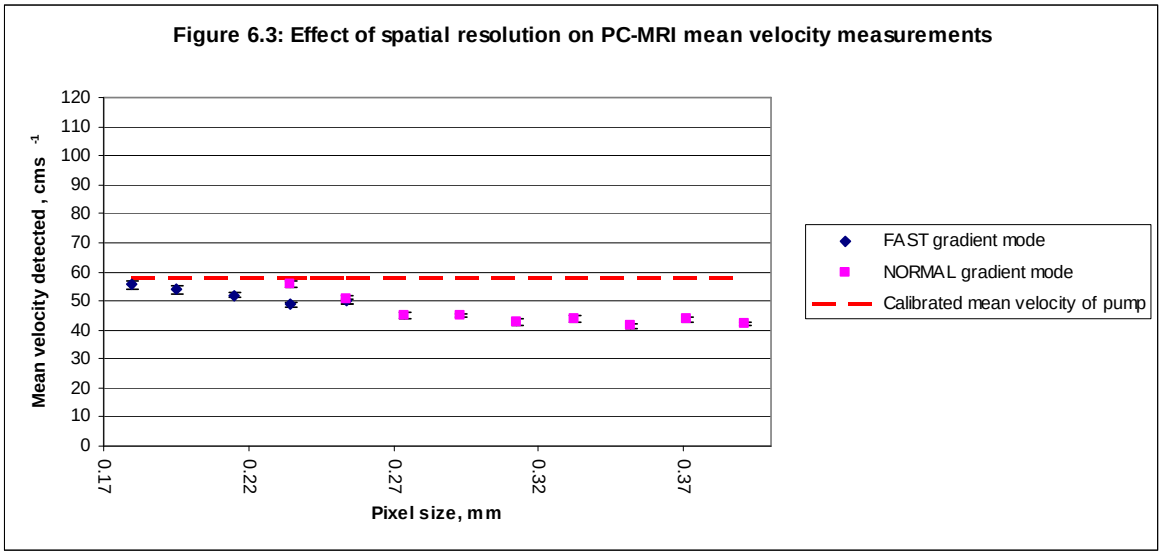

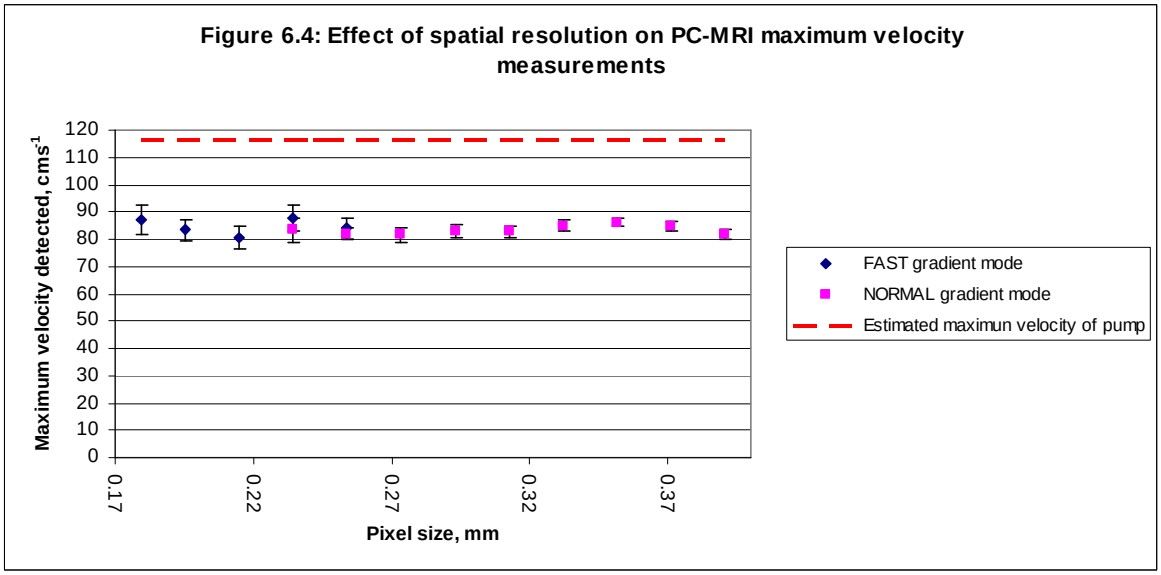

For comparison with the authors mentioned above, we can consider the equivalent flow rates. However, in the results for the comparison of measured flow rate with the calibrated flow rate, 6.4.1, it was noted that the dimensions of the roi used for flow analysis increased as the velocity increases and in all cases was much lower than the true cross section. The same was true for the pixel resolution study. The true values of the cross sectional area and the effect on the pixels-per-area are shown in table 6.4.

Gradient mode	FOV (mm)	Pixel dimensions (mm)	Measured area (mm^2)	Pixels per tube area	Pixels per measured tube area
FAST	69 x 92	0.18	**5.5**	249.07	**170.3**
	75 x 100	0.20	**5.6**	210.82	**146.8**
	82 x 110	0.21	**5.9**	175.29	**128.6**
	90 x 120	0.23	**6.6**	146.40	**120.2**
	97 x 130	0.25	**6**	125.39	**93.60**
NORMAL	90 x 120	0.23	**5.1**	146.40	**92.84**
	97 x 130	0.25	**6.1**	125.39	**95.11**
	105 x 140	0.27	**7.5**	107.56	**100.3**
	112 x 150	0.29	**7.5**	94.11	**87.77**
	120 x 160	0.31	**8**	82.35	**81.92**
	127 x 170	0.33	**7.9**	73.23	**71.94**
	135 x 180	0.35	**8.2**	65.07	**66.35**
	142 x 190	0.37	**7.7**	58.60	**56.11**
	150 x 200	0.39	**8.4**	52.70	**55.05**

Table 6.4. A modified version of Table 6.2 Variable Field of View (FOV) parameters for the study of spatial resolution effects, showing the area measured during the Argus analysis and the consequent effect on pixels per area. True lumen area was 8.04 mm^2.

6.3.2.2 Slice thickness

While acknowledging that partial volume errors should be considered for the entire voxel rather than just the pixel dimensions, few authors have specifically examined the effect of slice thickness. One exception was Greil (Greil et al. 2002) who examined the effect of slice thickness on flow rate measurements for thicknesses of 4, 6 and 8 mm, finding no significant difference between the three. For steady state flow in a straight tube, the slice thickness would not be expected to affect the measurement of velocity as confirmed by Figure 6.5.

6.3.2.3 Scan plane angle

The bipolar velocity encoding gradient required for phase-contrast flow quantification is applied in the slice selection axis and assumes that the direction of flow is along the same axis so that maximum velocity will be indicated by a maximum phase shift of 180°. In previous work, Greil suggested that inclinations of up to 40° produced acceptable errors for flow volume measurements (Greil et al. 2002)and Bernstein suggested up to 30° would be "tolerable" (Bernstein, King, & Zhou 2004). However, Lotz found that deviations of more than 15° gave errors of more than 10% for both peak velocity

measurement and flow rates (Lotz et al. 2002). Table 6.5 and Figure 6.6 illustrating the results for constant flow of 58.15 cms^{-1} suggest that deviations of between 10° and 20° have a significant effect on the mean velocity measurement but a smaller effect on the maximum velocity. Deviations greater than 20° affected all velocity measurements.

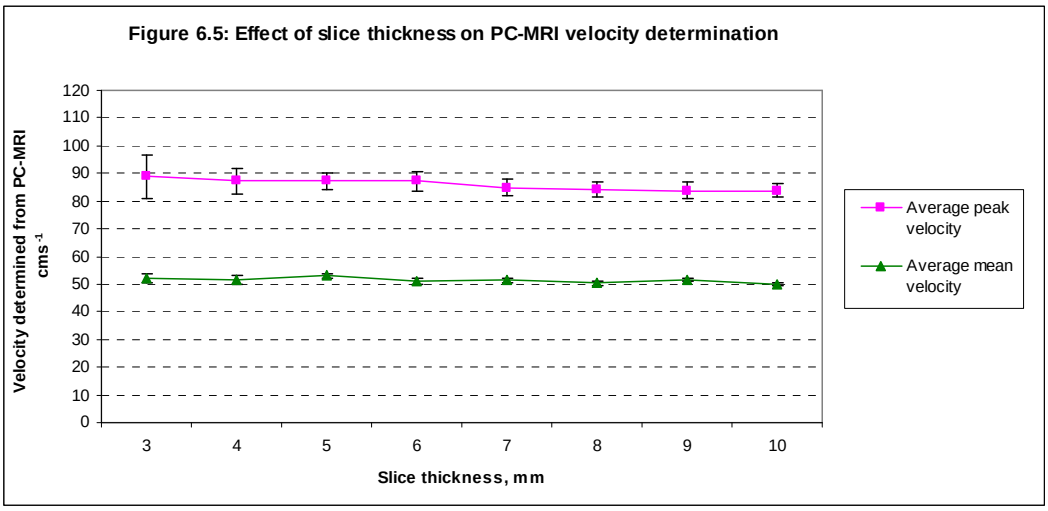

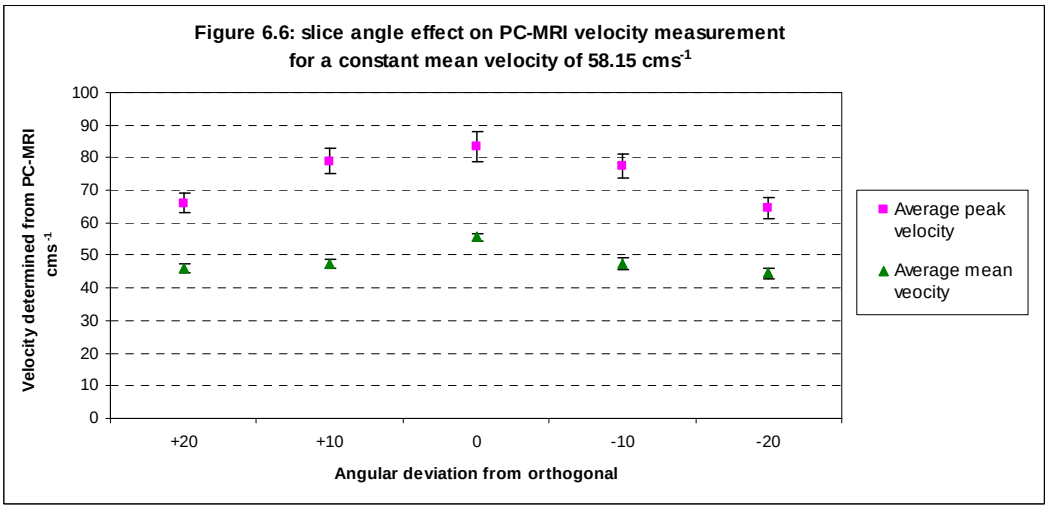

Scan plane deviation from orthogonal	+20°	+10°	-10°	-20°
Reduction in mean velocity	-17.3%	-14.5%	-14.6%	-19.8%
Reduction in maximum velocity	-20.7%	-5.2%	-7.2%	-22.5%

Table 6.5. Percentage reduction in measured velocity due to deviation of the scan plane from the orthogonal.

6.3.3 Inter method comparison of velocity measurements

In section 6.3.1, measurements of flow rates were compared against the calibrated range of flow rates. However, this thesis is primarily concerned with the use of velocities derived from PC-MRI data and how they compare with velocities derived from spectral Doppler ultrasound. A useful intermediate step is to consider the mean velocity of the flow produced by the flow pump circuit and compare with the mean velocity measured using ultrasound and MR methods. As discussed in chapter 5, if parabolic laminar flow is assumed, the mean velocity of a vessel of known diameter may be calculated from the known flow rate giving the range of velocities shown in table 5.2. Figures 6.7 a to c show the comparison of the spectral Doppler ultrasound, 1.5 T PC-MRI and 3.0T PC-MRI against the range of mean velocities from 11.63 cms^{-1} to 116.3 cms^{-1}.

The Bland Altman statistics are summarised in table 6.6. The results suggest that both the 1.5 T PC-MRI and the 3.0T PC-MRI measurements of mean velocity are in agreement with the range of mean velocities derived from calibrated volume flow rates within the 95% limits of agreement. For 1.5T PC-MRI the null hypothesis clearly holds. However, for 3.0T PC-MRI there is a small underestimation of 1.5 cms^{-1} which is of low statistical significance ($0.05<p<0.1$). For ultrasound, there is a significant ($p<0.001$) underestimation of 6.62 cms^{-1}. One explanation may be that the Doppler sample volume may not encompass the entire cross section of lumen, as discussed in section 3.1.4.3, unlike the roi used for PC-MRI velocity analysis.

Figure 6.7a: Bland-Altman comparison of the measurement of mean steady-state velocity values in a 3.2 mm diameter straight tube phantom - flow volume derived vs. spectral Doppler ultrasound temporal averaged mean

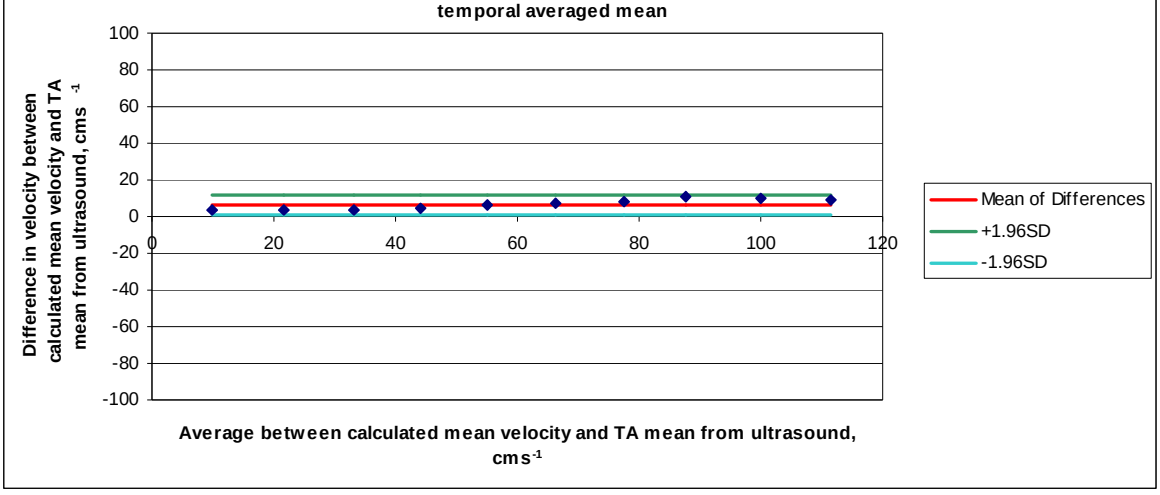

Figure 6.7b: Bland-Altman comparison of the measurement of mean velocity in a 3.2 mm diameter straight tube phantom- flow derived vs 1.5T PC-MRI

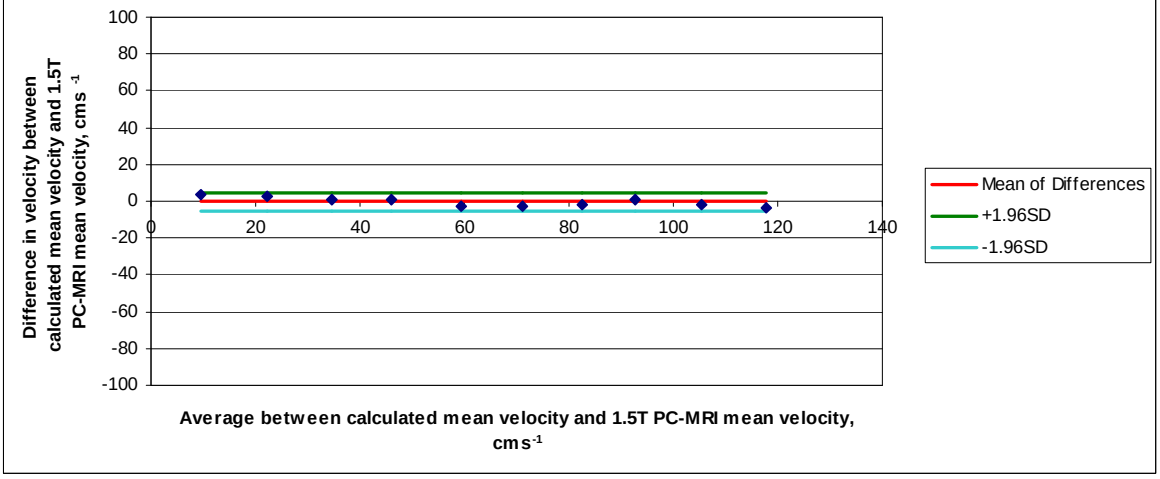

Figure 6.7c: Bland-Altman comparison of the measurement of mean velocity in a 3.2 mm diameter straight tube phantom - flow derived vs 3.0T PC-MRI

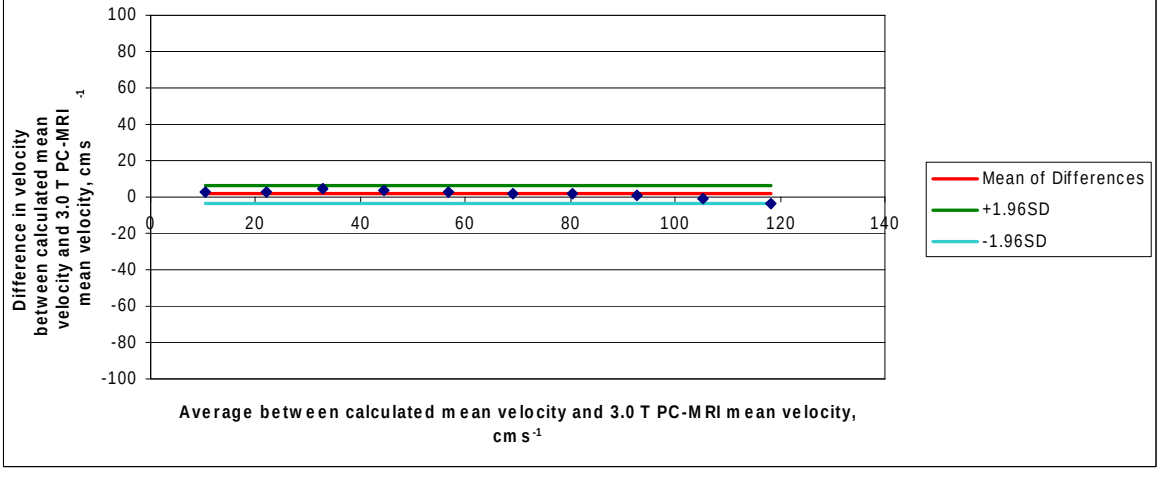

Method of velocity measurement compared against velocity derived from flow rate	*Mean bias (cms^{-1})*	*± Limits of agreement (cms^{-1}) (± 1.96σ)*	*P value*
Ultrasound Mean Velocity	6.62	5.30	<0.01
1.5 T PC-MRI Mean Velocity	-0.31	4.77	>0.1
3.0 T PC-MRI Mean Velocity	1.5	4.72	0.05<p<0.1

Table 6.6: Bland-Altmann analysis of mean velocities measured using ultrasound, 1.5T PC-MRI and 3.0T PC-MRI compared with the mean velocity derived from the volume flow calibration.

This intermediate analysis of ultrasound and MRI methods of velocity measurement against velocities derived from calibrated volume flow measurements may be extended to examine maximum or peak velocities of the same range of steady state velocities. For true parabolic flow, the maximum velocity can be estimated as twice the mean velocity (Oates 2001), giving the range of maximum velocities as 23.26 to 232.60 cms^{-1}. The Bland-Altman comparison plots for mean vs. difference and mean vs. percentage difference are shown in figures 6.8 and 6.9 respectively, with the summary statistics in table 6.7.

Method of velocity measurement compared against velocity derived from flow rate	*Mean bias*	*± Limits of agreement (± 1.96σ)*	*P value*
Ultrasound Maximum Velocity	19.56 cms^{-1}	22.66 cms^{-1}	<0.01
Ultrasound Maximum Velocity (percentage difference)	15.95%	9.13%	
1.5 T PC-MRI Maximum Velocity	30.86 cms^{-1}	23.62 cms^{-1}	<0.01
1.5 T PC-MRI Maximum Velocity (percentage difference)	27.99%	16.9%	
3.0 T PC-MRI Maximum Velocity	29.94 cms^{-1}	31.02 cms^{-1}	<0.01
3.0 T PC-MRI Maximum Velocity (percentage difference)	23.42%	4.6%	

Table 6.7: Bland-Altmann analysis of maximum velocities measured using ultrasound, 1.5T PC-MRI and 3.0T PC-MRI compared with the maximum velocity derived from the volume flow calibration.

Figure 6.8a: Bland-Altman comparison of the measurement of maximum steady-state velocity values in a 3.2 mm diameter straight tube phantom - flow volume derived vs. spectral Doppler ultrasound temporal averaged maximum

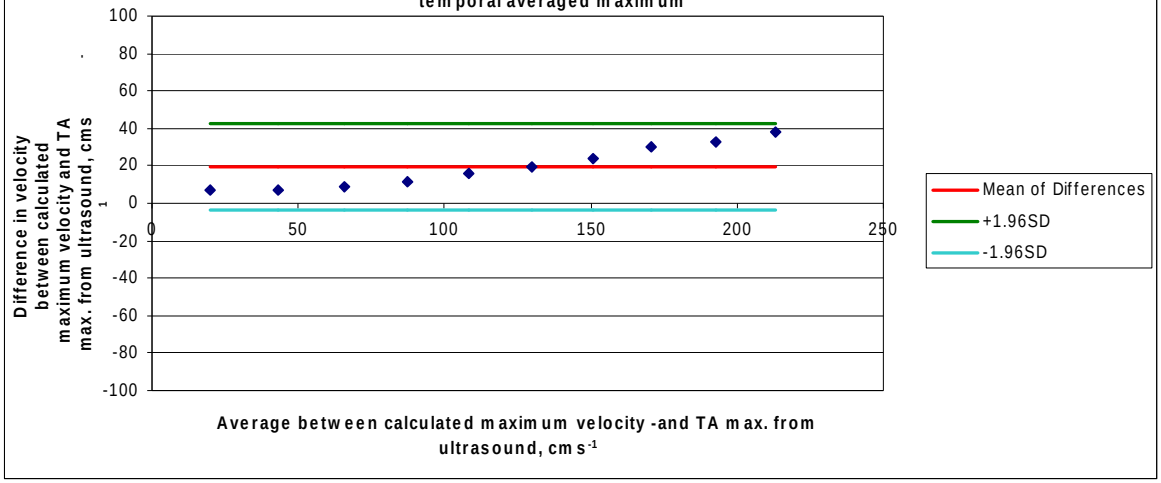

Figure 6.8b: Bland-Altman comparison of the measurement of maximum steady-state velocity values in a 3.2 mm diameter straight tube phantom - flow volume derived vs. 1.5T PC-MRI

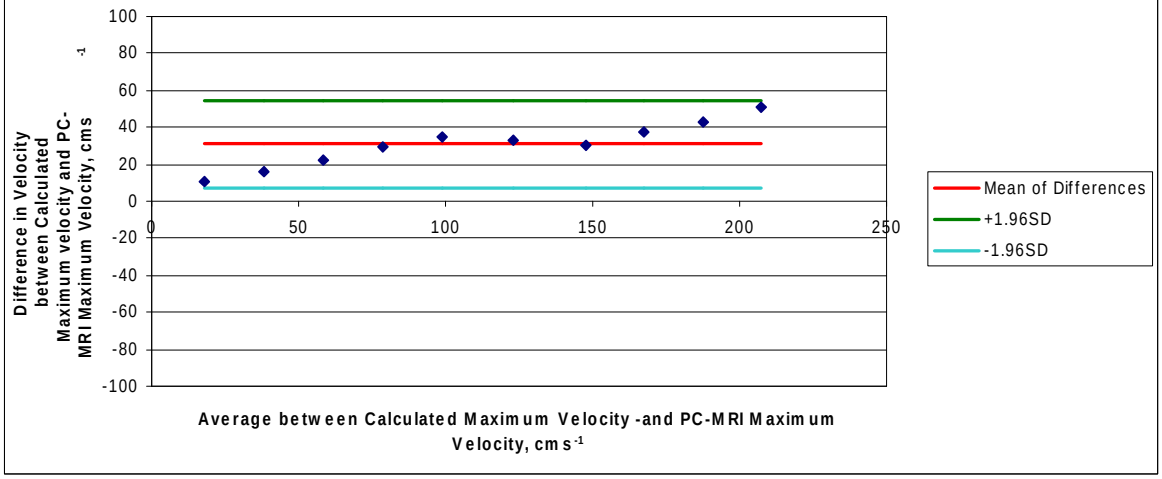

Figure 6.8c: Bland-Altman comparison of the measurement of maximum steady-state velocity values in a 3.2 mm diameter straight tube phantom - flow volume derived vs. 3.0T PC-MRI

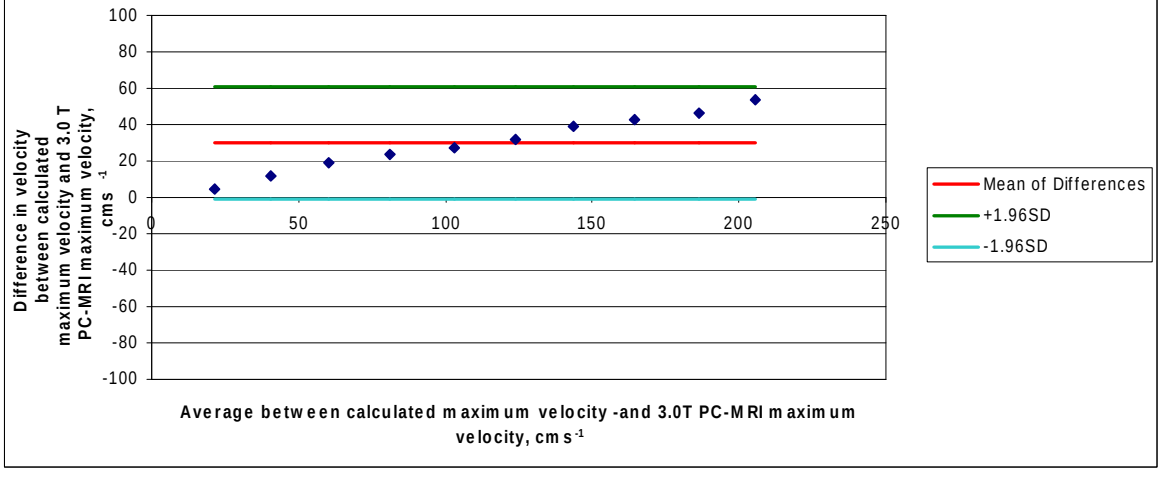

Figure 6.9a: Bland-Altman percentage difference comparison of the measurement of maximum steady-state Velocity Values in a 3.2 mm diameter straight tube phantom - flow volume derived vs. spectral Doppler ultrasound temporal averaged maximum

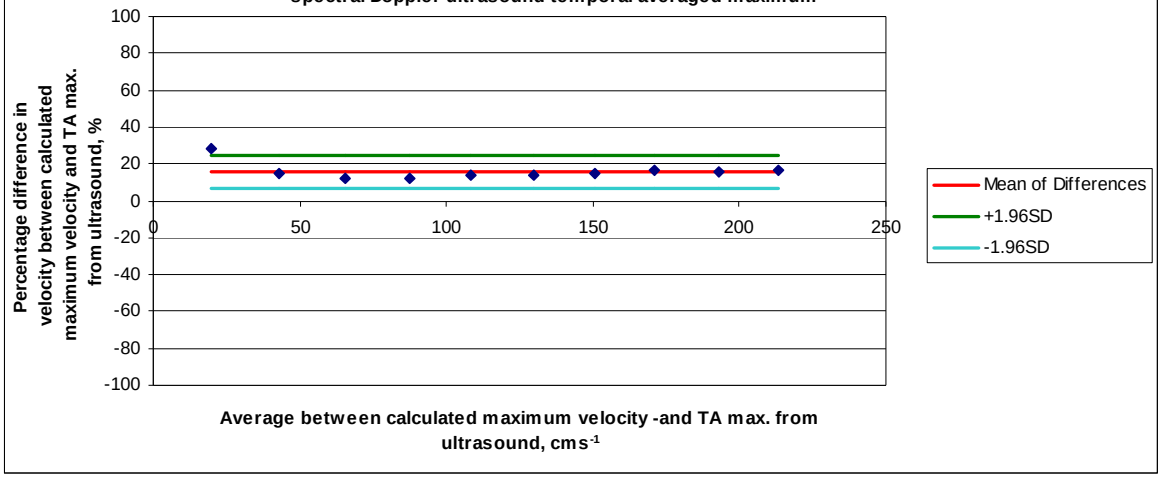

Figure 6.9b: Bland-Altman percentage difference comparison of the measurement of maximum steady-state Velocity Values in a 3.2 mm diameter straight tube phantom - flow volume derived vs. 1.5 T PC-MRI

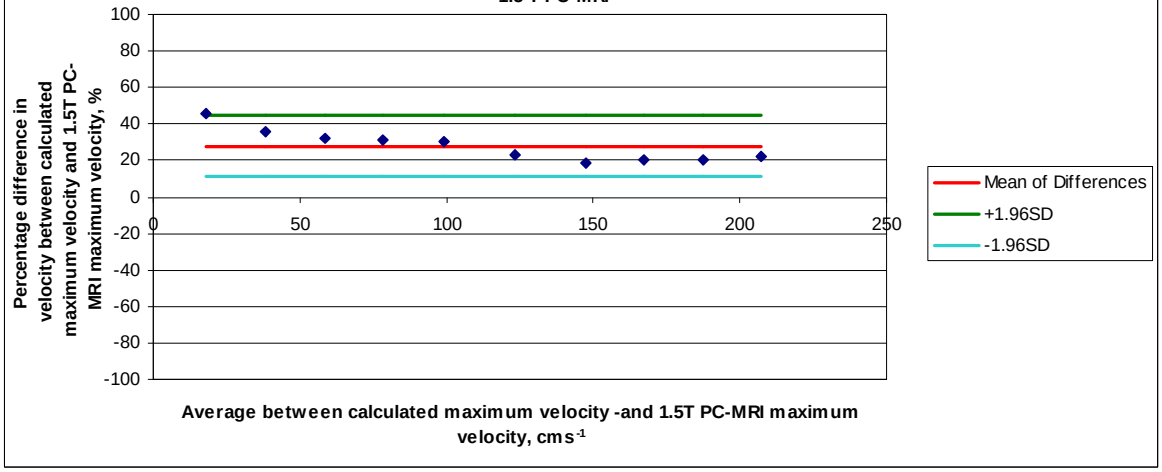

Figure 6.9c: Bland-Altman percentage difference comparison of the measurement of maximum steady-state Velocity Values in a 3.2 mm diameter straight tube phantom - flow volume derived vs. 3.0 T PC-MRI

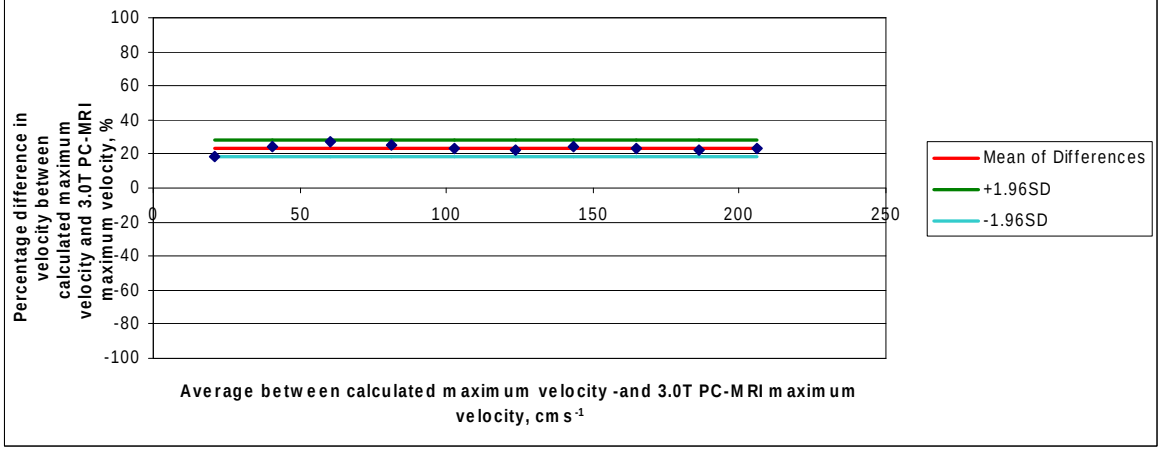

For the maximum velocity of steady state flow, all three measurement methods show a significant underestimation of maximum velocity which increases in magnitude as the velocities increase. Examining the percentage increase demonstrates that the percentage underestimation has a more linear response with the increase in velocity. It is interesting to note that the maximum velocity underestimation bias is lower for spectral Doppler ultrasound than it is for either of the PC-MRI methods. The inference from the analysis of the maximum velocity results would be that none of the three methods is capable of estimating the "true" maximum velocity (i.e. as estimated from the flow volume calibration). However, the apparent "overestimation" of ultrasound maximum velocities due to spectral broadening, as discussed in chapter 5, may be compensating for the overall underestimation, hence the magnitude of the percentage underestimation of maximum velocity for spectral Doppler ultrasound is significantly lower than for the PC-MRI methods.

The focus of this thesis was to examine how PC-MRI methods of velocity measurements compared with the more established spectral Doppler ultrasound methods. The key comparisons in this chapter are illustrated in figure 6.10 and 6.11 where the mean and maximum velocity values, over a range of steady state flow circuit settings, obtained using 1.5T and 3.0 T PC-MRI are compared against those measured using spectral Doppler ultrasound. The 1.5T and 3.0 T PC-MRI velocity values are also compared against each other. The summary statistics are shown in table 6.8.

Figure 6.10a: Bland-Altman comparison of the measurement of mean steady-state velocity values in a 3.2 mm diameter straight tube phantom - spectral Doppler ultrasound vs. 1.5T PC-MRI

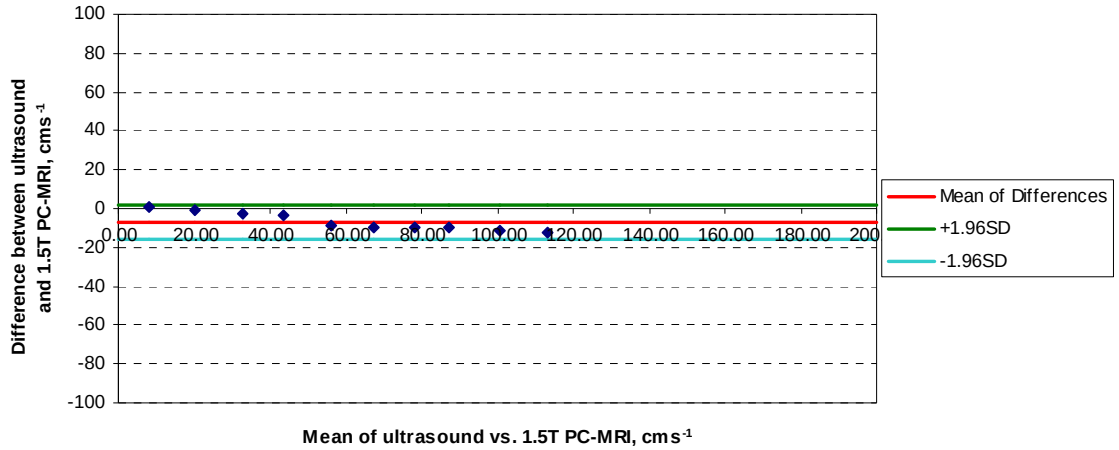

Figure 6.10b: Bland-Altman comparison of the measurement of mean steady-state velocity values in a 3.2 mm diameter straight tube phantom - spectral Doppler ultrasound vs. 3.0 T PC-MRI

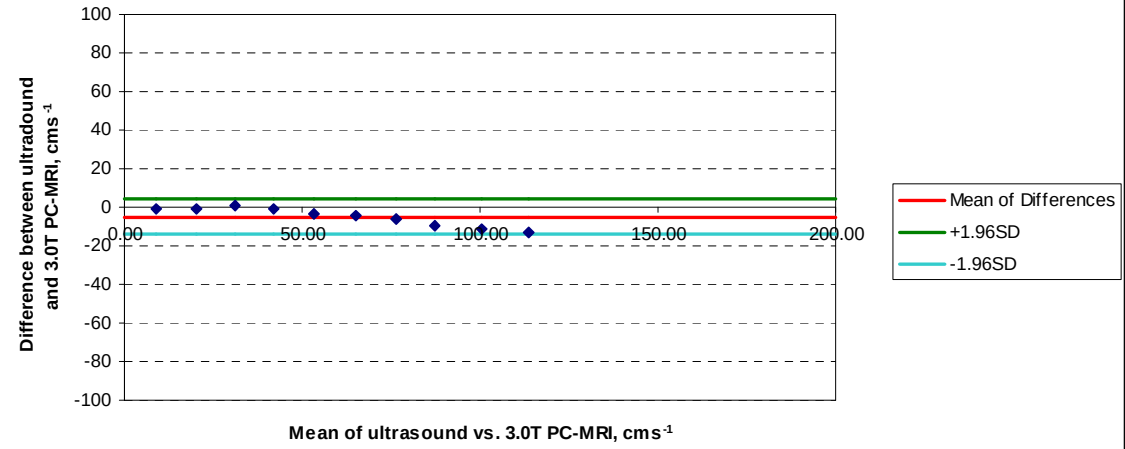

Figure 6.10c: Bland-Altman comparison of the measurement of mean steady-state velocity values in a 3.2 mm diameter straight tube phantom - 1.5T PC-MRI vs. 3.0 T PC-MRI

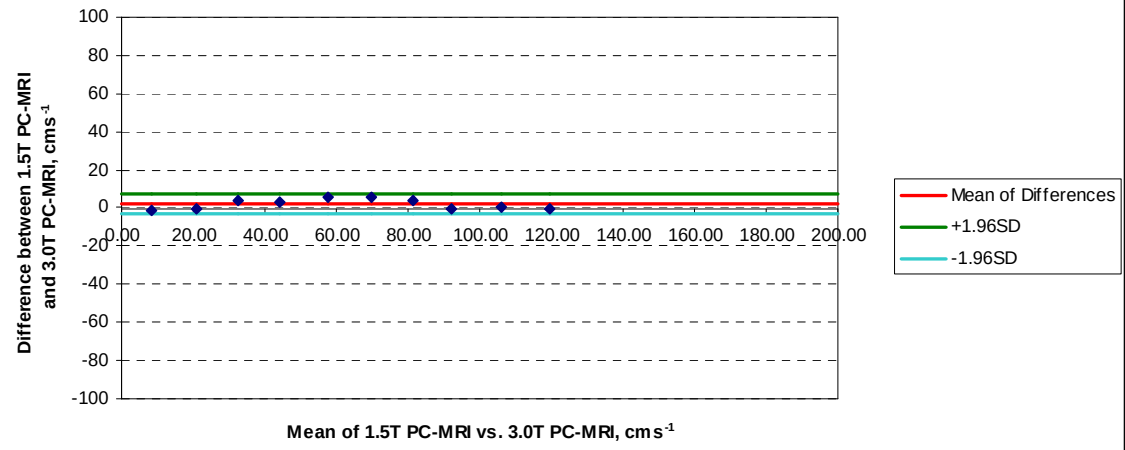

Figure 6.11a: Bland-Altman comparison of the measurement of maximum steady-state velocity values in a 3.2 mm diameter straight tube phantom - spectral Doppler ultrasound vs. 1.5T PC-MRI

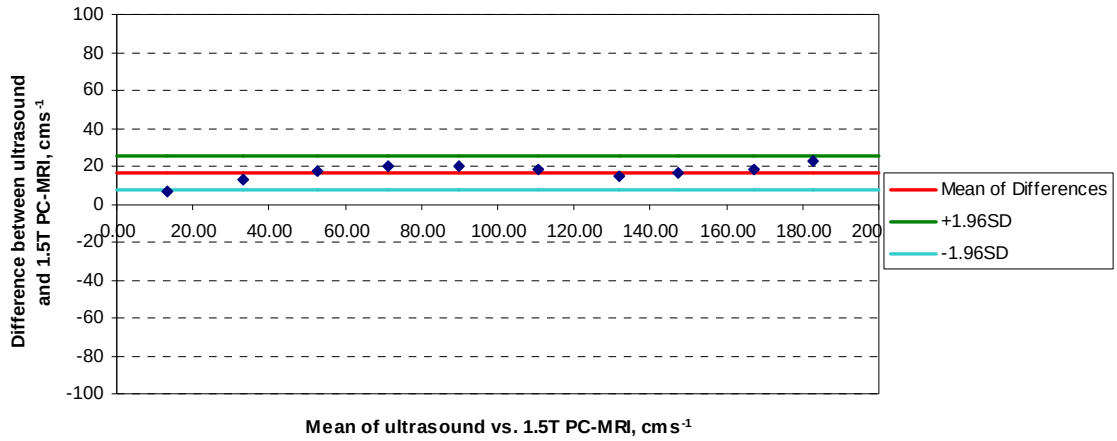

Figure 6.11b: Bland-Altman comparison of the measurement of maximum steady-state velocity values in a 3.2 mm diameter straight tube phantom - spectral Doppler ultrasound vs. 3.0 T PC-MRI

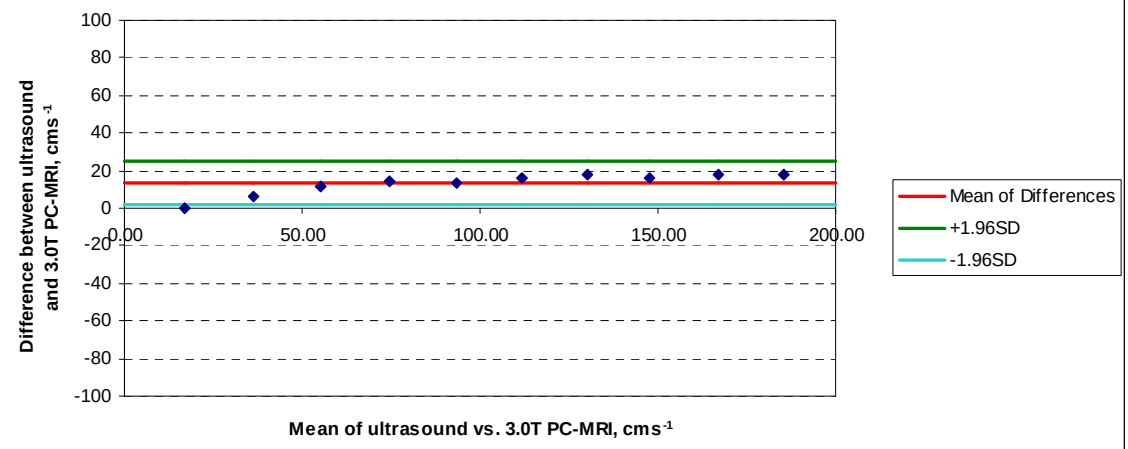

Figure 6.11c: Bland-Altman comparison of the measurement of maximum steady-state velocity values in a 3.2 mm diameter straight tube phantom - 1.5T PC-MRI vs. 3.0 T PC-MRI

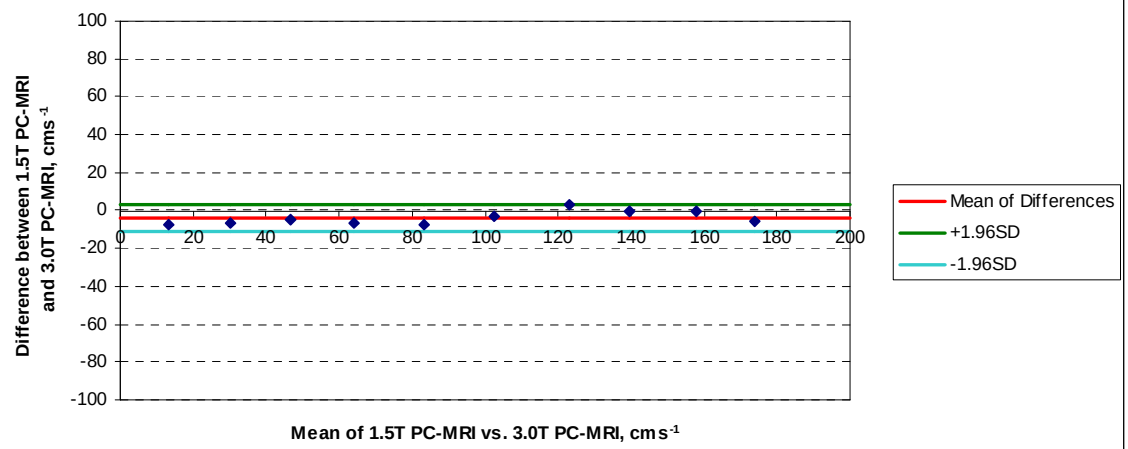

Comparison of velocity measurement methods	*Mean bias (cms^{-1})*	*± Limits of agreement (cms^{-1}) (± 1.96σ)*	*P value*
Mean Velocity: Ultrasound - 1.5T MRI	-6.9	9.1	0.001
Mean Velocity: Ultrasound - 3.0T MRI	-5.0	9.3	0.01
Mean Velocity: 1.5T MRI - 3.0T MRI	1.9	5.1	0.04
Maximum Velocity: Ultrasound - 1.5T MRI	16.8	8.9	<0.001
Maximum Velocity: Ultrasound - 3.0T MRI	13.0	11.6	<0.001
Maximum Velocity: 1.5T MRI - 3.0T MRI	-3.8	7.1	0.01

Table 6.8: Bland-Altmann analysis of intercomparison of velocity measurement methods between ultrasound, 1.5T PC-MRI and 3.0T PC-MRI. A positive bias represents an underestimation.

The comparisons made in figures 6.10 And 6.11 And in table 6.8 , suggest that PC-MRI velocity estimation techniques significantly overestimate mean velocities and underestimate maximum velocities when compared with spectral Doppler ultrasound measurements. Again this would be consistent with the errors due to spectral Doppler ultrasound spectral broadening.

6.3.4 Estimation of errors in relation to velocity scaling

The use of steady state velocities to investigate PC-MRI velocity measurement has the advantage of allowing an estimation of errors to be made from the velocity analysis data. The data for each flow pump voltage setting may be averaged over the number of cardiac phases in the pseudo-cardiac cycle. The velocity encoding was varied during the study with velocities less than 80 cms^{-1} having a venc setting of ±100 cms^{-1} and velocities greater than 80 cms^{-1} but less that 200 cms^{-1} having a venc of ±200 cms^{-1}. The smaller the measured value was in comparison with the venc value, the greater the calculated standard deviation.

For the ultrasound values, steady state measurement of maximum velocity was measured using the auto-Doppler feature which generated a temporal average peak maximum velocity value, TA_{MAX} between two points on a frozen segment of

the spectral Doppler display as shown in figure 5.7. Repeat analysis of different frozen spectral displays for the same pump voltage, generated no significant difference between the TA_{MAX} values. An estimated error was therefore generated which was based on the likely error of the operator placing the cursor at the maximum velocity point manually. The cursor precision in this case equated to the pixel resolution in the y or velocity dimension of the spectral display. The velocity scale in spectral Doppler ultrasound can be likened to the venc value for PC-MRI in that the difference between the maximum on the velocity scale and the measured value will affect the standard deviation of the measurement. The user generally maximises velocity scale such that the spectral display occupies no less that two thirds of the scale maximum display. The ultrasound pixel resolution was 0.67% of the full scale maximum of the spectral Doppler display. This was equivalent to a mean standard deviation of 1.75% over the range of steady-state measured values.

The estimated errors on maximum velocity measurements are summarised in table 6.9.

	1.5T PC-MRI	*3.0T PC-MRI*
Percentage error for values measured using venc ±100 cms^{-1}	± 3.85 %	± 1.52 %
Percentage error for values measured using venc ±200 cms^{-1}	± 3.58 %	± 1.51 %
Percentage error across all measured values regardless of venc.	**± 5.0 %**	**± 2.0 %**
Mean percentage error on ultrasound values	**± 1.75 %**	

Table 6.9. Estimated errors on measured maximum velocity values over the range 16.62 cms^{-1} to 194.11 cms^{-1} for PC-MRI and spectral Doppler ultrasound.

6.3.5 Results for the measurement of steady state velocities in the carotid phantom

Use of the carotid phantom provided the opportunity to investigate a higher range of velocities due to the presence of the tight stenosis in the ICA segment of the phantom.

Maximum velocities were investigated to give a direct comparison between the standard Doppler ultrasound method of measurement of peak velocity. At the highest pump setting of 3V, the velocities in the stenosed section of the phantom were shown to cause aliasing when using spectral Doppler ultrasound. This indicated that the Nyquist limit, as discussed in chapter 4, had been reached for the ultrasound system and suggests that the MRI method of velocity measurement may have an advantage over ultrasound in the measurement of higher velocity values. The maximum velocity values at the 3V steady state have been omitted from the comparison studies in this section.

The higher velocities in the stenosis required an increase in the PC-MRI venc value to 400 cms^{-1} which increases the overall error estimation for the 3.0T maximum velocity measurements from 2.0% (as in table 6.9) to ± 2.5%.

Figures 6.14 and 6.15 show Bland-Altman comparison of the maximum velocity values measured in the same section of the CCA and the stenosed ICA respectively. Figure 6.16 compares the ICApsv/CCApsv ratios for the different velocity settings. Table 6.10 summarises the Bland-Altman statistics.

Comparison of velocity measurement methods	*Mean bias*	*± Limits of agreement (± 1.96σ)*	*P value*
CCA max. velocity Ultrasound - 3.0T MRI	7.24 cms^{-1}	11.94 cms^{-1}	0.03
ICA max. velocity Ultrasound - 3.0T MRI	38.46 cms^{-1}	35.89 cms^{-1}	< 0.01
ICA/CCA Ratio Ultrasound - 3.0T MRI	0.40	0.92	0.13

Table 6.10: Bland-Altman analysis of intercomparison of velocity measurement methods between ultrasound and 3.0T PC-MRI in the carotid phantom. A positive bias represents an underestimation.

Figure 6.12: Bland-Altman comparison of the measurement of peak maximum velocity in a the CCA section of a carotid phantom - maximum steady state velocity measured using spectral Doppler ultrasound vs. 3T PC-MRI

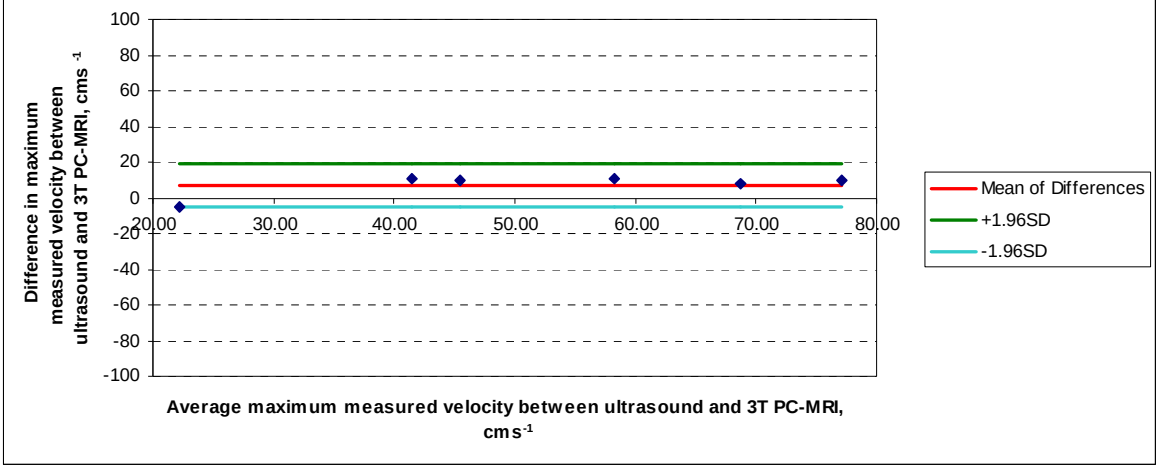

Figure 6.13: Bland-Altman comparison of the measurement of the mean maximum velocities in the ICA stenosis section of a carotid phantom - maximum steady state velocity measured using spectral Doppler ultrasound vs. 3T PC-MRI

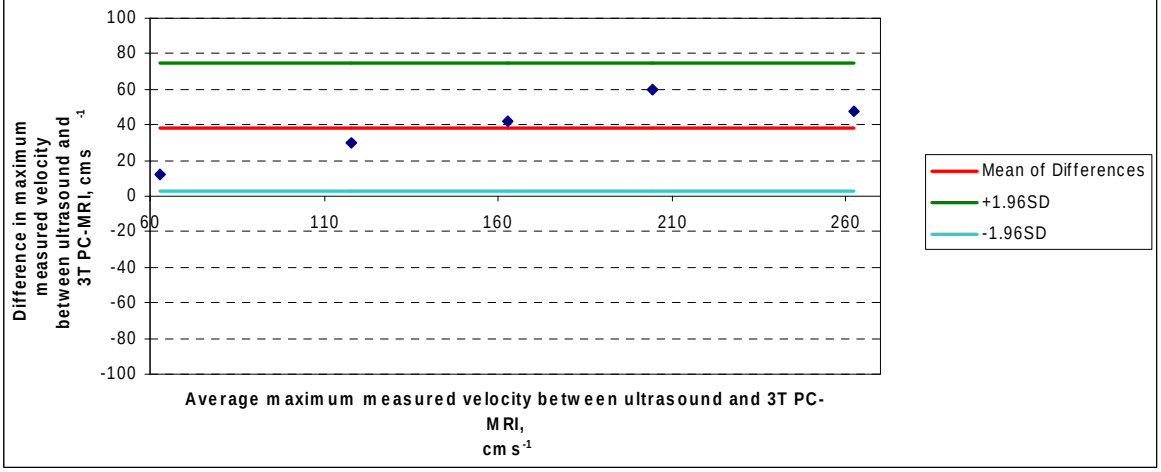

Figure 6.14: Bland-Altman comparison of the measurement of ICA/CCA maximum (steady state) velocity ratio in a carotid phantom - measured using spectral Doppler ultrasound vs. 3T PC-MRI

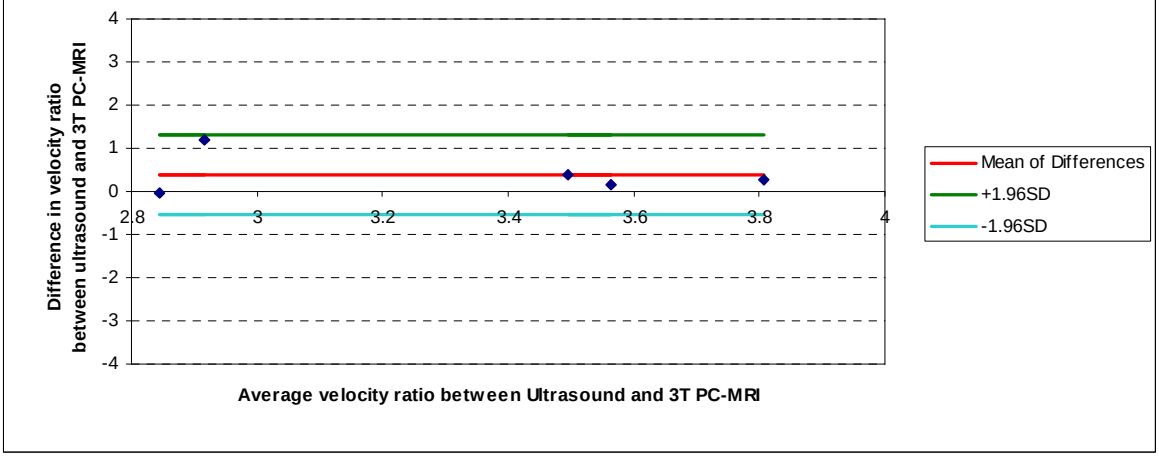

6.4 Summary of results and discussion on the measurement of steady state velocities

6.4.1 Volume flow rates

In the absence of comparable studies of velocity measurement in the literature evaluation of volume flow rate measurement was carried out. The results demonstrated a small but statistically significant underestimation bias of 0.53 mls^{-1} for ultrasound derived measurements. For the MRI measurement of flow it was expected that partial volume effects (Bernstein, King, & Zhou 2004; Greil et al. 2002; Lotz et al. 2002; Lotz et al. 2005;Tang, Blatter, & Parker 1993) might cause overestimation of the flow rates, particularly since this was a relatively small "vessel" compared with the majority of previous studies. However, there was a significant underestimation of volume flow rate for both MRI scanners. Closer examination of the data showed that the user-defined regions-of-interest, roi, had a much smaller cross sectional area than the true cross sectional area of the tube. This occurred despite careful selection of the roi areas using both magnitude and phase images. Recalculating flow rates using the true lumen cross-sectional area and the MRI derived mean velocities removed the bias for both scanners. However, this does not represent a scenario that could be replicated *in-vivo* where both the velocities and the vessel geometry are unknown. The roi area was also found to increase as the velocity increased suggesting that signal level effects were involved. The majority of flow measurement assessments *in-vivo* and *in-vitro* in the literature have been done on large vessels and with contrast agents. Heverhagen's (Heverhagen et al. 2002) *in-vitro* study showed that the addition of a gadolinium contrast agent had no significant effect on PC-MRI velocimetry but did improve the delineation of the vessel lumen, potentially affecting roi placement and volume flow rate calculations. A similar note of the improvement in vessel delineation was noted more recently by Lagerstrand (Lagerstrand et al. 2010).

Results suggest that in small vessels with no contrast agent, determination of volume flow rates may be unreliable, primarily due to poor delineation of the vessel diameter.

6.4.2 Optimisation of spatial parameters

The effect of pixel size on the maximum velocity was found to be minimal although all measurements were below that predicted from flow volume rate calibration. For mean velocity, there was also an underestimation which appeared to increase as spatial resolution decreased until a threshold of pixel size around 0.3 mm, after which it became fairly constant. The highest available resolution for the Fast and Normal gradient modes gave the best agreement with mean velocity from flow calibration measurements. It was noted that the cross sectional area of the user defined roi increased as the resolution decreased with the largest pixel dimensions giving roi areas close to the true area. Although partial volume effects will undoubtedly contribute in this case, it is likely that the underestimation of area due to low signal levels (in these small, non contrast enhanced vessels) will contribute to the overall underestimation of flow.

The slice thickness of the PC-MRI flow quantification slab was not expected to affect the measured velocity for this simple situation of constant flow in a straight tube. This was confirmed by experiment and, perhaps, the only point of note was that the standard deviation of the measurements increased for smaller slice values, reflecting poorer signal to noise in the thinner slices. Selection of larger slice thicknesses may help to address the signal strength / poor lumen delineation issues that have been identified so far. However, in practice, selection of a smaller slice thickness may help to retain the desired orthogonal orientation of flow in curved or tortuous sections as confirmed by the angular deviation measurements.

The results suggest that intuitive optimisation by minimising spatial voxel dimensions and attempting a scan plane as orthogonal to the direction of flow as possible should be used when making PC-MRI measurements of mean and maximum velocity. However, where signal levels are low due to the small size of vessel, lower velocities and lack of contrast agent, vessel delineation will be compromised and cause underestimation of volume flow measurements.

6.4.3 Mean velocities

Considering the measurement of mean velocities derived from the flow rate calibration performed in chapter 5 and the known geometry of the phantom, both MRI scanners demonstrate statistical agreement between measurements. The ultrasound scanner, however demonstrated a small (6.62 cms^{-1}) but statistically significant ($p<0.01$) underestimation in mean velocity. Although, the spectral Doppler sample volume was placed such that it encompassed the vessel lumen on the B-Mode image, areas of flow out-with the elevational scan plane geometry may not be captured, leading to a potential overestimation of the mean velocity (Evans 1985). However, mean velocities measured using spectral Doppler ultrasound are acknowledged to be subject to a variety of sources of error despite their use in clinical practice for measuring flow rates (Hoskins 2011). Inter-method comparison of mean velocities demonstrated that both MRI scanners appeared to overestimate mean velocity when compared with Doppler ultrasound. The 3.0T scanner demonstrated a small underestimation when compared with the 1.5T but the statistical significance of this was low ($p>0.01$).

The results suggest that mean velocity may be a reliable parameter for comparison and that potentially PC MRI gives a more accurate measurement than ultrasound of the true mean velocity.

6.4.4 Maximum velocities

Maximum velocities were calculated from the calibrated flow rates by assuming parabolic flow such that the maximum velocity may be assumed to be twice the mean velocity (Oates 2001). Both ultrasound and PC-MRI methods demonstrated significant underestimation of the maximum velocity with an increasing underestimation as velocity increased. The best performance in this case was ultrasound whereas the 1.5T PC-MRI had the highest absolute and percentage underestimation bias. The overestimation of peak or maximum velocity due to spectral broadening as described in the literature (Hoskins 2011) and demonstrated in chapter 5, would lead us to expect an overestimation compared with the calculated maximum velocity. However although the underestimation is

less for ultrasound than for MRI, the results might suggest that we cannot reliably predict maximum velocity from calibrated volume flow rates as we can for mean velocity. It is entirely possible that, despite careful set up of the flow system, there may be non parabolic flow across the lumen of the phantom tubing. Inter method comparison showed a highly significant underestimation bias for both MRI scanners compared with Doppler ultrasound. The 3.0T scanner demonstrated a small overestimation bias when compared with the 1.5 T scanner.

The results highlight the problem of using maximum velocity as a parameter for velocity comparison. It is difficult to know the "true" velocity profile and the magnitude of the differences between measurement methods increased with increasing velocity in all cases. Maximum velocity may be an unreliable parameter for comparison of methods.

In the carotid phantom, focussing on maximum velocity measurements, the different pump settings generated a range of velocities of approximately 20 cms^{-1} to 82 $cms^{-1,}$ in the mid CCA section, as measured using ultrasound. The range increased to approximately 69 cms^{-1} to 286 cms^{-1} due to the presence of the stenosis at the origin of the ICA branch. Comparison of maximum velocities measured using 3T PC-MRI revealed a small underestimation, of low significance, of maximum velocities compared to ultrasound. However, for the higher velocities in the stenosed region of the phantom, there is a large and significant overestimation bias for ultrasound compared with 3T PC-MRI. While this is likely to be due, in part, to ultrasound maximum velocity errors, it is more likely that the large discrepancy reflects the ease with which the rapid feedback involved in spectral Doppler ultrasound may be used to quickly search for a velocity maximum compared with the placement of a single PC-MRI slice with off-line analysis of data. What is encouraging, however, is that when examining the stenosis ratios, although ultrasound again shows a positive bias which is due to the bias in the ICA maximum velocities, the significance of the difference between ultrasound ratios and MRI ratios is low.

6.4.5 Estimation of errors

PC-MRI acquisition of velocity encoded data for steady state flow provided a useful means of investigating the system errors on velocity measurement in the absence of any temporal resolution considerations. The errors on the measurement of mean velocity of 2.52% for 1.5T and 1.60% for 3.0T were consistent with the level of percentage errors on flow rates determined by Greil (Greil et al. 2002) in a 1.T scanner. However, the larger percentage errors on the maximum velocity as shown in Table 6.9 are of more relevance in taking the work forward to determine maximum velocity for pulsatile flow in the straight tube phantom for velocities up to 200 cms^{-1}.

The error of 2.5% found when looking at steady state velocities in the carotid phantom is a reasonable estimation of measurement error to apply to the range of velocities when looking at a wider range of velocities such as those that would typically be involved in the determination of stenoses.

Examination of the steady state velocities also highlighted the influence of velocity scaling on measurement errors for both spectral Doppler ultrasound and PC-MRI.

Chapter 7 – Velocity measurement using ultrasound and MRI techniques under pulsatile flow conditions

The previous chapter considered the rather oversimplified situation of steady state flow in a straight vessel, allowing us to investigate spatial resolution and orientation issues when making velocity measurements. However, the sequences used for PC-MRI velocity measurements did require gating as described in chapter 5. The need for gating placed limitations on the optimum spatial resolution that could be achieved. In this chapter, we continue the in-*vitro* investigations, but come closer to the *in-vivo* situation with the creation of pulsatile waveforms within the flow system, enabling investigation of temporal resolution issues.

7.1 Introduction – temporal resolution considerations

When making comparisons between velocity quantification methods, authors generally refer to spectral Doppler ultrasound as having "good temporal resolution". However, the actual temporal resolution of spectral Doppler ultrasound is rarely defined or quantified and it remains an underdeveloped area in the field of Doppler performance testing (Hoskins & Ramnarine 2000). Temporal resolution in spectral Doppler is the time length of the data sample or segment used in the FFT analysis. As described in chapter 4, sequential consecutive time intervals are displayed along the horizontal time axis, to create the spectral display with the frequency or velocity content for each time segment displayed in grey-scale against the vertical axis. There is an inverse relationship between the length of the time segment used in the transform, T_a and the spectral resolution of the FFT, Δf_a as in equation 7.1.

Equation 7.1. $$\Delta f_a = \frac{1}{T_a}$$

Since arterial Doppler signals are not thought to be stationary for periods of greater than 10 to 20 ms (Evans & McDicken 2000), ideally less than 10 ms should

be used which would give a spectral resolution of 100Hz. Typical peak vascular velocities of 50 to 100 cms^{-1} equate to Doppler frequencies of 2 to 5 kHz for a 5 MHz transmit frequency, suggesting a potential further source of error on the peak velocity determined by spectral Doppler ultrasound which will be more significant for low e.g. diastolic velocities which produce frequencies in the tens to hundreds of Hz range.

It is well understood that the collection of MRI data which is gated or triggered to the cardiac cycle involves a trade-off between desired spatial resolution and desired temporal resolution. For the collection of single slice phase contrast data in small vessels, the ideal scan protocol would have sufficient voxels within the 2D slice to demonstrate the variation of velocities across the cross-section of vessel under study and sufficient temporal resolution to be able to map the changes in velocity across the cardiac cycle, in particular resolving any high velocity peaks within the cycle.

Despite the potential limitations of both ultrasound and MRI in determining the peak velocities of pulsatile flow, the approach taken for the comparison study was to treat spectral Doppler ultrasound as a "gold standard" and attempt to optimise both ultrasound and PC-MRI methods to obtain the highest measured peak systolic velocity for a given flow pattern, as would be done in the clinical situation when using spectral Doppler. In some cases, the mean velocities were also examined with a view to their potential as a reliable indicator of true velocity, as suggested by the results in chapter 6.

7.1.1 Optimisation of a protocol for the measurement of maximum velocities using PC-MRI

In the development of an optimised protocol for the measurement of blood velocities using PC-MRI which could potentially be used for comparative *in-vivo* studies, a number of parameters were investigated which might have the potential to compromise detection of maximum velocity values. The measurement of velocity in MRI studies has been influenced by the main application of cardiac studies with a desire to calculate volume flow and the need to measure mean velocities. Standard protocols for through plane velocity

measurement are thus focused on obtaining a good representation of the mean velocity for use in the flow estimation. However, to make a direct comparison with methods used in Doppler ultrasound, we need to measure maximum velocity. MRI protocol parameters that contribute to the averaging of the velocity values have the potential to reduce the true maximum detected velocity. In assessing this, the following parameters were tested:

- Temporal Resolution
- Gating Strategy
- Slice Thickness
- Velocity Encoding
- Coil Type

Examination of the parameters listed above contributed to an optimised protocol for the measurement of maximum velocity. A key component of the optimisation was to balance velocity measurement confidence with the desire to keep the PC-MRI quantification sequences as short as possible. Short sequences help to minimise movement artefact and the need for breath holding; important if the sequences were to be translated to applications in the more central vascular locations in the thorax and abdomen.

7.1.2 The determination of the degree of stenosis and haemodynamic indices

Analysis of results from the stenosed and non-stenosed sections of the carotid artery phantom was undertaken to compare maximum velocities and maximum velocity ratios using techniques developed for the classification of the degree of stenosis using spectral Doppler ultrasound data. It was also useful to examine other parameters such as the pulsatility index, PI and the resistivity index, RI. These dimensionless indices were designed to overcome the angle dependence errors associated with spectral Doppler ultrasound so, in theory, they have the potential to be valid for PC-MRI velocity measurements as any MR errors should cancel out.

7.2 Methods

7.2.1 Test phantoms and pulsed waveforms

Extension of the use of the steady state flow phantom, described in chapter 6, for the examination of pulsatile flow, required the creation of pulsatile drive voltage patterns capable of simulating physiological velocity waveforms when applied to the test phantoms. The first of these was designed for demonstrating pulsatile flow in the 3.2 mm straight tube phantom. It had a forward flow baseline voltage of 0.04V with two short (full width at half maximum, FWHM, 50ms) peaks of 2V and 0.5V, with a peak to peak separation of 235ms within a 1000ms repetition cycle. This was intended to mimic typical forward flow in a peripheral arterial vessel with a short systolic peak or R wave, followed by a smaller, short T wave with a long diastolic recovery. The repetition was 1000ms which was equivalent to a typical normal heart beat of 60 beats per minute. The voltage waveform is illustrated in Figure 7.1A with the corresponding ultrasound spectral Doppler velocity waveform shown in figure 7.1a.

In the steady state flow calibration work in chapter 5, we determined that a continuous drive voltage of 2V would give a mean velocity of approximately 233 cms^{-1} in a 3.2 mm diameter vessel. However, with pulsatile flow, there is energy lost during the rapid acceleration to a narrow peak with further losses in the semi-compliant vessel during expansion and contraction such that the expected peak velocity for a narrow voltage peak would be considerably lower than that for a continuous drive signal of the same voltage. The presence of a lower amplitude “third peak” prior to end-diastole was also noted and, as in physiological systems, is caused by reflections within the flow system.

Use of the carotid phantom required pulsatile drive voltage patterns with higher peak voltages, due to the larger inner diameter of the “vessel” i.e. 8.0 mm in the common carotid artery (CCA) section. A further two voltage waveforms were created, a simple single waveform peak of 3V with a base of 100ms and a simulated low resistance peak extending over 250ms with a plateau of 3V over 100ms. These were simplified to single peak waveforms as the more complex connecting system in the carotid phantom gave the potential to cause

reflections in the system. Both waveforms had an overall duration of 1000ms simulating a heart rate of 60 bpm. These waveforms and their corresponding ultrasound spectral Doppler velocity waveforms are shown in figure 7.1B, C, b and c.

As for the steady state velocity studies, the 3.2 mm straight tube phantom was regarded as a useful tool for examining parameter variation whereas use of the carotid bifurcation phantom with its simulated vessel anatomy, more compliant vessel wall material and softer surrounding gel allowed a closer approximation to the *in-vivo* situation, particularly when using simulated pulsatile velocity waveforms.

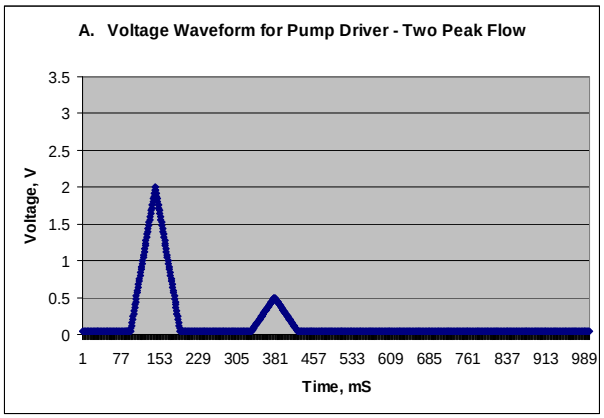

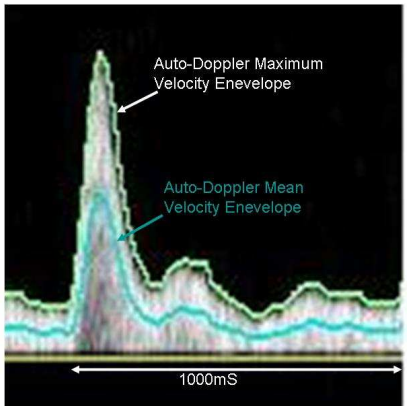

a. Spectral Doppler ultrasound waveform for the two peak, 2V drive voltage waveform. The the mean and maximum velocity auto-Doppler trace applied by the scanner are shown in blue and white respectively.

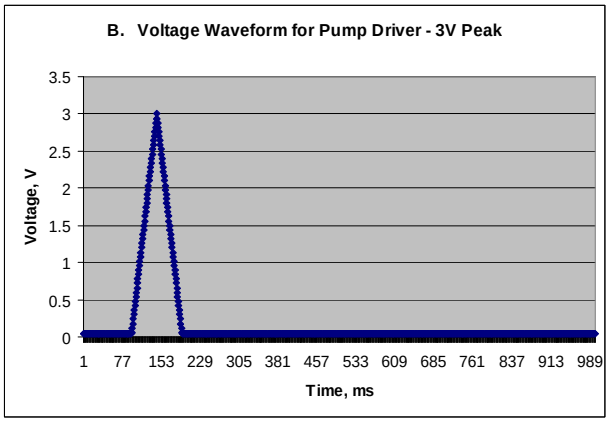

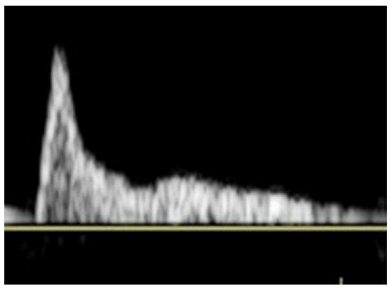

b. Spectral Doppler ultrasound waveform for the single peak, 3V drive voltage waveform.

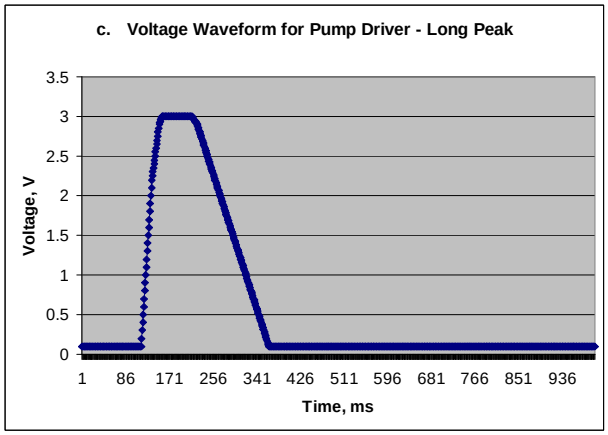

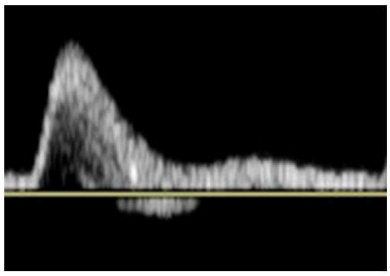

c. Spectral Doppler ultrasound waveform for the single long peak, 3V drive voltage waveform.

Figure 7.1: Pump input drive voltages used for flow phantom studies of pulsatile velocity detection. On the right are the input waveforms with the corresponding spectral Doppler ultrasound waveform on the right.

7.2.2 Ultrasound studies

The pulsatile waveforms were tested in the appropriate phantoms by optimising the spectral Doppler waveforms as would be done in the clinical situation i.e. optimised to give the maximum velocity with accurate angle correction. The sweep speed of the spectral Doppler display on the ultrasound scanner was set to give 4 to 5 peaks in any frozen display. Measurements of peak velocities were made using the system callipers to measure maximum velocities with a minimum of ten different peaks used for any one measurement. The resulting mean and standard deviation would thus capture any variations in the flow system, variations in the Doppler system measurement and display and operator cursor placement accuracy. Where mean velocity was required, the ultrasound system Auto Doppler function was used to provide a mean and maximum trace, as shown in figure 7.1a and a temporal averaged mean velocity, V_{TAM}.

7.2.3 Temporal resolution

Temporal resolution was investigated by varying the number of cardiac phases or signal sample intervals within the cardiac cycle; essentially, varying the TR. On the 1.5T scanner, where the standard protocol for PC-MRI velocity quantification used retrospective gating, variation of the number of phases was easy to select as the exact phasing is applied at the interpolative reconstruction phase based on the average cardiac cycle. However, it was anticipated that retrospective gating would potentially "average down" the maximum velocity values. Gating comparisons were made *in-vitro* and *in-vivo* to confirm this. For prospective gating the number of cardiac phases was more limited. The PC-MRI parameters and other key experimental condition used in this part of the study are summarised in table 7.1.

7.2.4 Gating strategies

It was highlighted in section 3.2.4 that the type of gating used, prospective or retrospective, has the potential to affect the maximum velocity detected due to averaging.

The PC-MRI parameters and other key experimental condition used in this part of the summary are summarised in table 7.1.

7.2.5 Effect of slice thickness

Slice thickness, when measuring the velocities of pulsatile flow was of particular interest in the scenario when the slice was placed at the position of the stenosis, in an attempt to determine the maximum velocity. It is well known (Oates 2001) that the maximum velocity caused by a stenosis is not located at the point of minimum lumen diameter. Rather, it is found just distal to the minimum diameter, within the stenotic jet. The real-time nature of Duplex Doppler ultrasound allows the operator to easily search for the maximum velocity. For PC-MRI measurements the velocity encoded slice must be positioned at a point where the stenosis appears on the corresponding anatomical imaging study. Studies were carried out to determine the effect on measured maximum velocity, in non-stenosed straight vessel sections, of the slice thickness and at the stenosis site to examine the trade off between using thick slices to cover all the velocities or thin slices with the risk of in-accurate slice placement. The PC-MRI parameters and other key experimental condition used in this part of the study are summarised in table 7.2.

7.2.6 Effect of velocity encoding

Knowledge of the peak velocity detected by ultrasound is a useful feature when carrying out phantom studies, enabling the investigator to set an appropriate, velocity encoding or venc value. However, in the clinical situation, the peak systolic velocity would be unknown and the user may be tempted to use a higher, venc value, particularly where a stenosis is suspected. A phantom study using the parameters listed in table 7.2 was carried out to examine the difference between velocities determined using velocity encoding settings of 120 cms^{-1} or 200 cms^{-1}.

Study:	Temporal Resolution	Temporal Resolution	Temporal Resolution	Gating	Gating
Scanner	1.5T	3T	3T	3T	3T
Coil	Body	Body	Body	Body	Body
Phantom	3.2 mm Straight	Carotid	Carotid	Carotid	Carotid
Flow Drive Waveform	Two peak, 2V	Short Peak, 3V	Long Peak, 3V	Short Peak, 3V	Short Peak, 3V
Gating Type	Retrospective	Prospective	Prospective	Prospective	Retrospective
Pixel Resolution, mm	0.23	0.47	0.47	0.47	0.23
Slice Thickness, mm	5	4	4	4	4
TE, ms	4	4.69	4.69	4.69	5.13
TR, ms	20, 26, 31, 37, 48, 59, 75	32, 47, 79	32, 47, 79	47.3	34.35
No. of Cardiac Phases	50, 46 ,36, 30, 23, 19, 15	62, 21, 12	62, 21, 12	19	30

Table 7.1: PC-MRI and other key experimental parameters used in the temporal resolution and gating studies.

Study:	Slice Thickness	Slice Thickness	Slice Thickness	Slice Thickness	Velocity Encoding
Scanner	1.5T	3T	3T	3T	3T
Coil	Body	Body	Body	Neck	Body
Phantom	3.2 mm Straight	Carotid	Carotid	Carotid	3.2 mm Straight
Flow Drive Waveform	Two peak, 2V	Long Peak, 3V	Long Peak, 3V	Short Peak, 3V	Two peak, 2V
Gating Type	Retrospective	Prospective	Prospective	Prospective	Retrospective
Pixel Resolution, mm	0.23	0.47	0.47	0.47	0.47
Slice Thickness, mm	3, 4, 5	2, 3, 4, 5, 6	4, 6, 8	4, 6, 8	5
TE, ms	4	4.69	4.69	4.69	4.69
TR, ms	20	47.3	94	94	47.3
No. of Cardiac Phases	50	19	58	58	19

Table 7.2: PC-MRI and other key experimental parameters used in the slice thickness and velocity encoding studies.

7.2.7 Body coil vs. neck coil

For the majority of the test phantom studies on the 3T scanner, a six channel array body coil (Siemens, Erlangen.) was used, placed on top of the test phantom in a reasonably central position with the flow tubing aligned in a foot-to-head direction through the bore of the main scanner. However, clinical MRI imaging of the carotid artery generally uses a neck coil. It was proposed to use the four channel array neck coil (Siemens, Erlangen.) for the *in-vivo* studies, therefore a comparison study was undertaken using the carotid artery phantom to determine whether there were any significant differences between the body coil and the neck coil which might influence the PC-MRI maximum velocity measurement protocol optimisation. The parameters in table 7.2 for the carotid phantom were used in the comparative studies.

7.2.8 Measurement of maximum velocity and the determination of the degree of stenosis.

Reminding ourselves of the primary aim of this thesis, which is to determine whether PC-MRI derived velocity waveforms can be used in a similar way to spectral Doppler ultrasound to aid in the diagnosis of peripheral vascular disease, it is useful to be able to test and compare methods using a phantom with a known degree of stenosis.

Table 7.2 summarises the PC-MRI parameters and other key experimental conditions used in a basic optimised protocol for the determination of maximum velocities. The velocity encoding parameter was adjusted as required and the maximum velocities at a number of sites along the carotid phantom were measured and compared with ultrasound data.

7.2.8.1 Indices and ratios

The key ratio of interest is the ratio of maximum peak systolic velocity in the internal carotid artery to the maximum peak systolic velocity in the common carotid artery, ICA_{PSV} / $CCA_{PSV.}$ However, it is important to assess other haemodynamic ratios and indices so that the technique may be translated to

other regions in the peripheral vascular system. The parameters tested using the optimised PC-MRI protocol were:

- Maximum PSV in a stenosis to pre-stenosis PSV, ICA_{PSV} / CCA_{PSV}
- St. Marys ratio, ICA_{PSV} / CCA_{EDV}
- Pulsatility index, maximum velocity excursion/mean of maximum velocity envelope
- Resistivity index, peak systolic velocity / end diastolic velocity

These parameters are defined in chapter 3.

7.3 Analysis of data

Ultrasound and PC-MRI datasets were analysed as described in chapter 5 and section 7.2.2 with Bland-Altman comparisons where appropriate.

Of key interest in this chapter where pulsatile flow is considered, aside from the determination of maximum velocity values, is the ability of PC-MRI techniques to map the characteristics of the velocity waveforms. For ease of comparative visualisation, peak velocity time points in the PC-MRI data output are matched so that the effect of varying sequence parameters may be compared. For comparison with ultrasound spectral Doppler waveforms, the time-points of key features were compared to allow the PC-MRI waveforms to be mapped over a single cycle from the spectral Doppler display.

7.4 Results

As for the steady state velocity studies in the preceding chapter, initial PC-MRI phantom studies to measure pulsatile velocities were carried out in the 3.2 mm diameter straight tube phantom using a 1.5T scanner, with later work using the carotid artery phantom in the 3T scanner as the work approached optimisation of a protocol for *in-vivo* studies.

7.4.1 Temporal resolution

The number of cardiac phases used and the equivalent TR for the 1.5T PC-MRI measurements of the pulsatile waveform in the 3.2 mm diameter straight tube phantom, with a two peak input voltage pattern as shown in figure 7.1, was as shown in table 7.3. The ultrasound values were found by analysis of the pixel data for the spectral waveform image where the pixel value was 10ms in the time axis direction giving 100 data points within the 1000ms simulated cardiac cycle.

Number of cardiac phases	50	46	36	30	23	19	15	100*
Temporal resolution (equivalent TR), ms	20	26	31	37	48	59	75	10*
Acquisition time, minutes.seconds	3.37	3.35	3.33	3.32	1.1	1.1	1.1	

Table 7.3: Varying temporal parameters used to study the temporal resolution of the 1.5T PC-MRI velocity quantification of pulsatile flow. The values in the last column highlighted by * are the equivalent values for the spectral Doppler ultrasound display.

The resulting mean and maximum, temporal velocity waveforms are shown in figures 7.2 and 7.3 where the temporal position of the peak systolic value has been matched for ease of comparison between studies.

Both figures suggest that all the temporal resolution values used are capable of demonstrating key features of the temporal waveform i.e. relative temporal

position of the two peaks and the end diastolic flow. However it is clear that at the highest velocities, equivalent to a peak systolic position, there is clear variation for both the mean and maximum peak velocities. These variations are illustrated graphically, and compared with the spectral Doppler ultrasound peak velocities for the same pulsatile flow, in figure 7.4. The peak spectral Doppler values were 114 ± 0.6 cms^{-1} for the maximum peak and 62 ± 1.5 cms^{-1} for the mean peak.

Figure 7.2: Mean velocity waveform for pulsatile flow in the straight tube phantom determined using 1.5T PC-MRI with varying temporal resolution

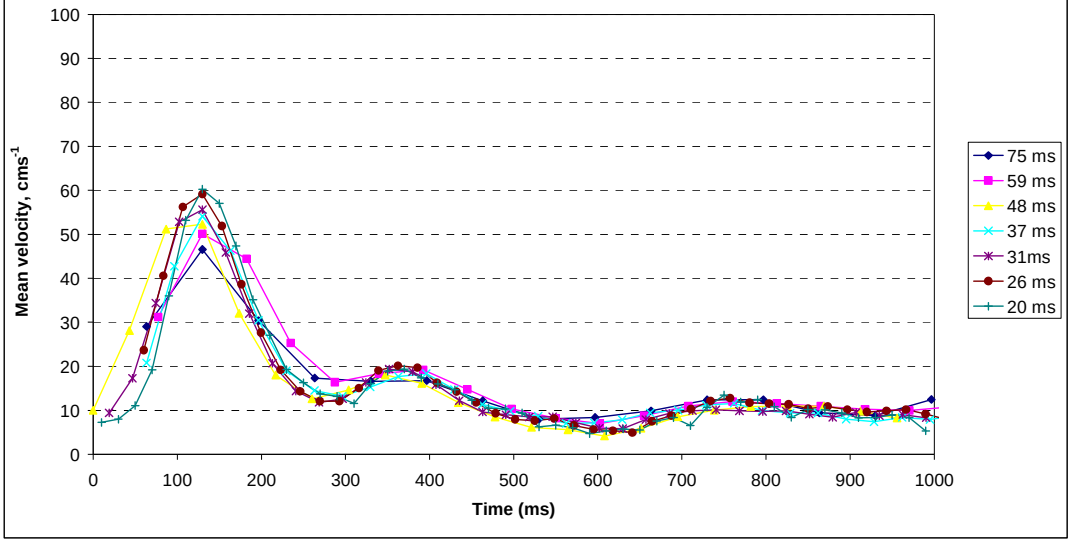

Figure 7.3: Maximum velocity waveform for pulsatile flow in the straight tube phantom determined using 1.5T PC-MRI with varying temporal resolution

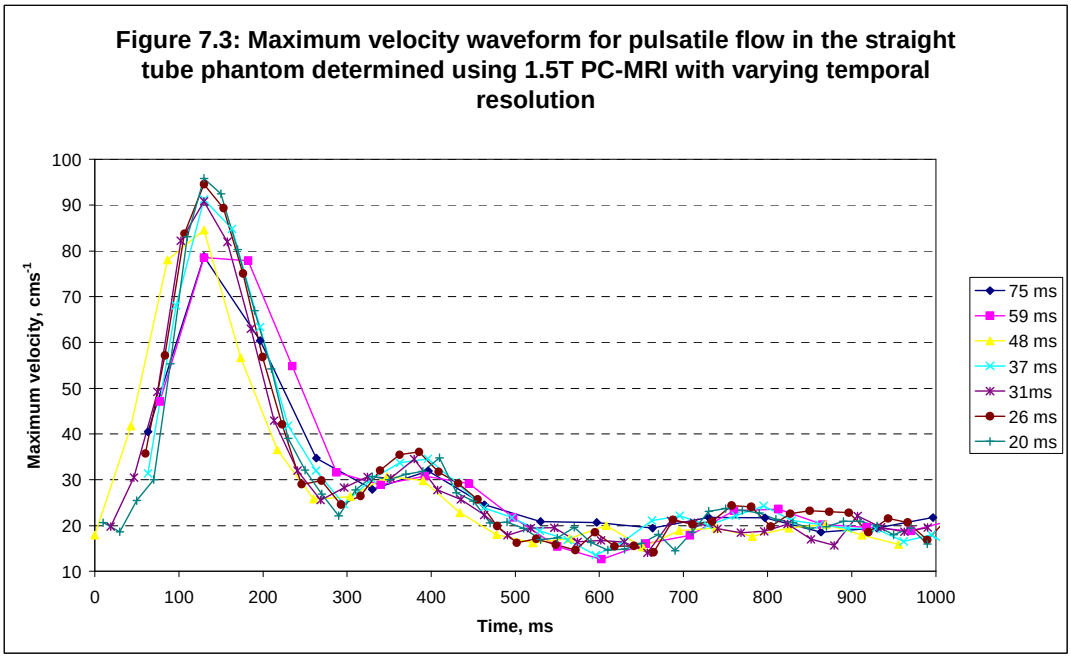

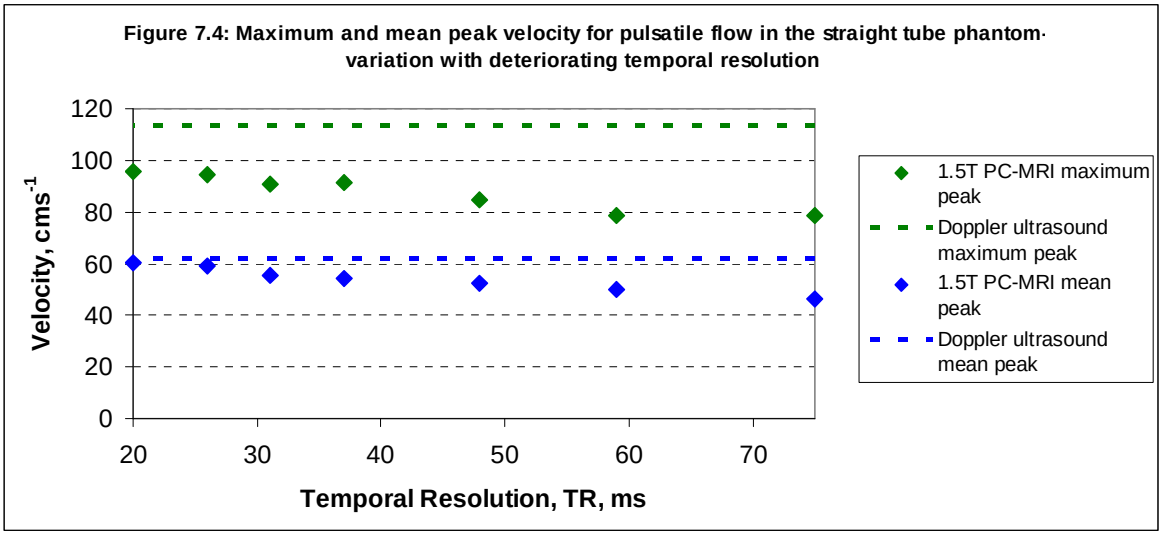

In the carotid artery phantom, a set of measurements were made in the mid-section of the common carotid artery. The phase encoded plane was held in that fixed position while the number of cardiac phases was varied as in table 7.4. This was repeated for both the short and the long 3V pump drive waveforms. Figures 7.5 and 7.6 show, for the short and long 3V peak respectively, the variation in maximum velocity waveform with temporal resolution.

Number of cardiac phases	62	21	12
Temporal resolution (equivalent TR), ms	15.0	47.3	78.7
Acquisition time, minutes.seconds	3.18	1.05	0.39

Table 7.4: Varying temporal parameters used to study the temporal resolution of the 3.0T PC-MRI velocity quantification of pulsatile flow.

Figure 7.5: Maximum velocity waveform for 3V short peak pulsatile flow in the mid-CCA section of the carotid phantom determined using 3.0T PC-MRI with varying temporal resolution

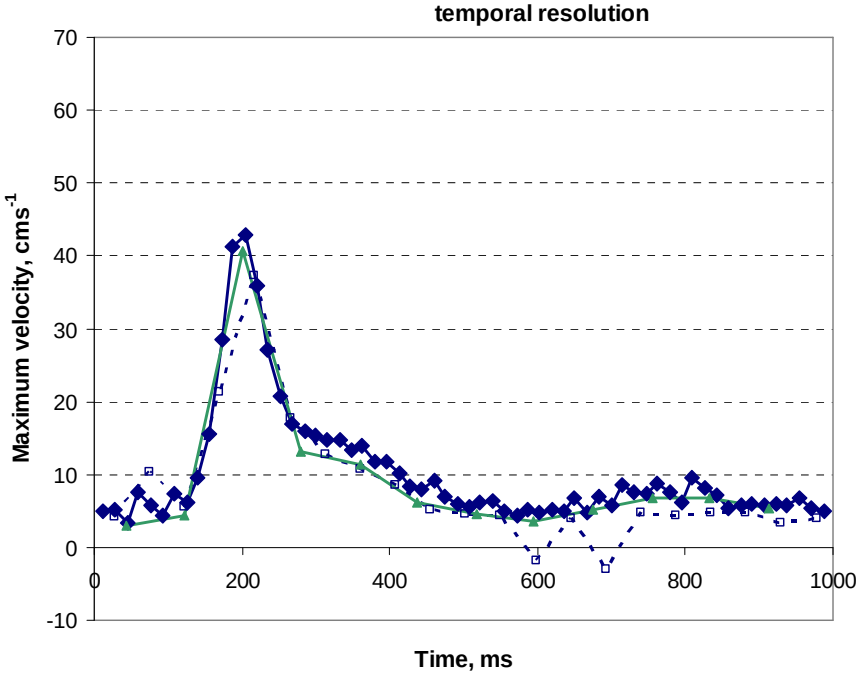

Figure 7.6: Maximum velocity waveform for 3V long peak pulsatile flow in the mid-CCA section of the carotid phantom determined using 3.0T PC-MRI with varying temporal resolution

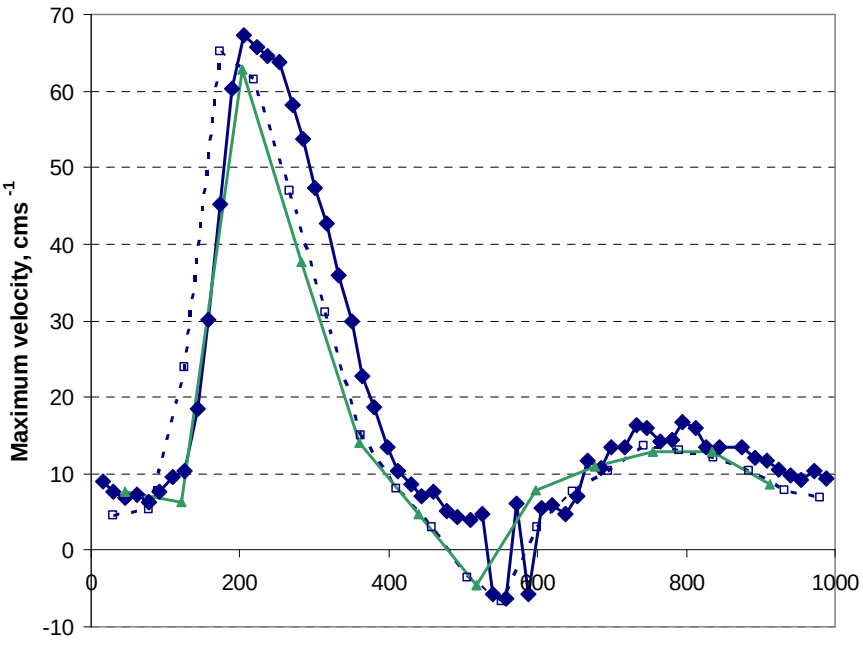

7.4.2 Effect of gating

The effect of prospective vs. retrospective gating on the velocity waveform profiles was examined in the mid-CCA section of the carotid artery phantom with the short 3V peak drive signal. Figures 7.7. and 7.8. show the comparative results for the mean and peak velocity profiles respectively.

Figure 7.7: Mean velocity waveform for 3V short peak pulsatile flow in the mid-CCA section of the carotid phantom determined using 3.0T PC-MRI with prospective and retrospective gating

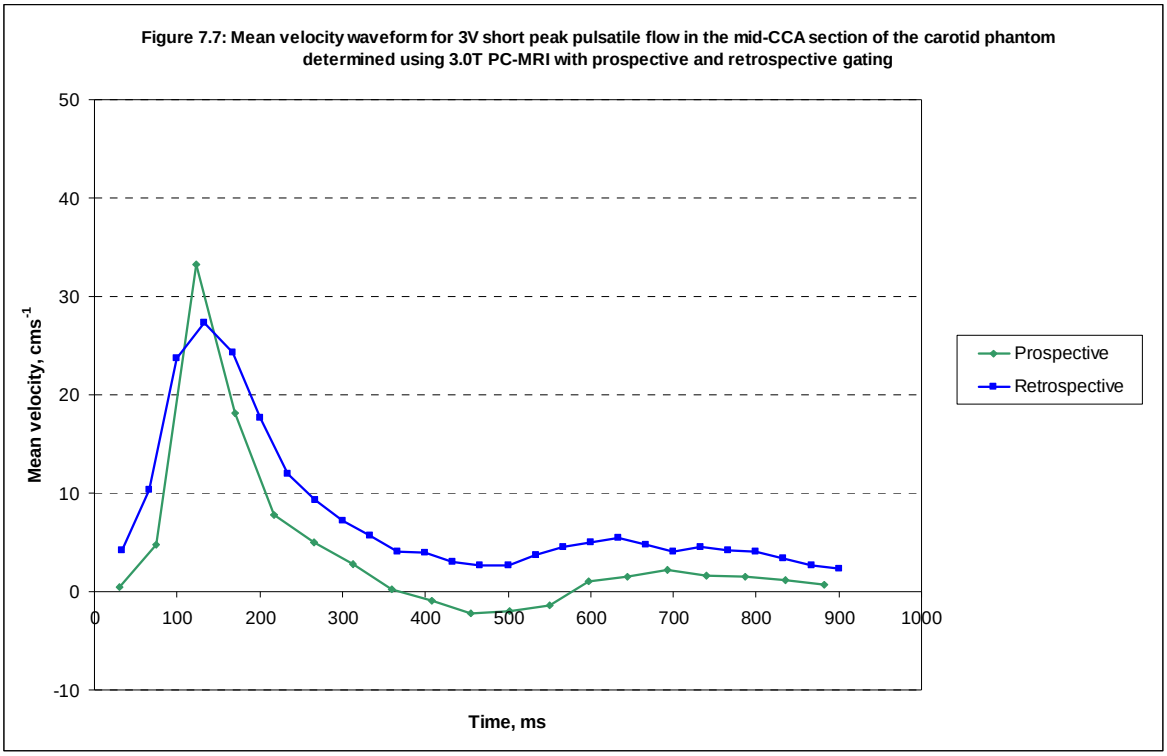

Figure 7.8: Maximum velocity waveform for 3V short peak pulsatile flow in the mid-CCA section of the carotid phantom determined using 3.0T PC-MRI with prospective and retrospective gating

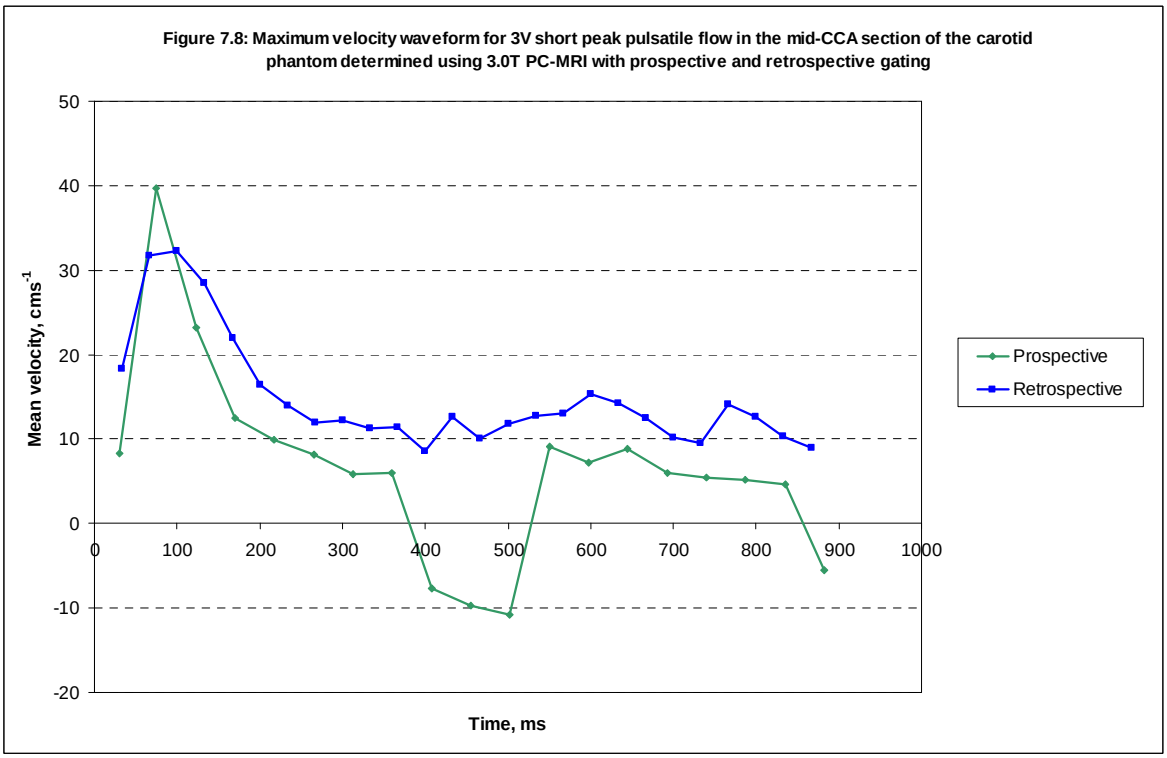

7.4.3 Effect of slice thickness

In the straight tube phantom with the 1.5T scanner, three different slice thickness widths were examined for the retrospectively gated sequence with 50 phases. The mean and maximum velocity waveforms are shown in figures 7.9 and 7.10 respectively. Statistical significance of the differences between the data, shown in table 7.5, was tested using a paired, 2-tailed T-test such that high P values indicated low significance of any detected bias, suggesting that the null hypothesis of no significant difference between methods was held. This was clearly the case for the mean velocities. However, there were significant differences between the maximum velocity waveforms for the differing slice thicknesses with an increasing level of underestimation of maximum velocity as the slice thickness width increased.

Comparison of PC-MRI Velocity determination under varying slice thickness	*Mean bias (cms^{-1})*	*± Limits of agreement (cms^{-1}) (± 1.96σ)*	*P value*
Mean Velocity: 3mm – 4mm	0.35	3.98	0.22
Mean Velocity: 4mm-5mm	-0.42	3.95	0.14
Mean Velocity: 3mm-5mm	-0.07	2.66	0.72
Maximum Velocity: 3mm-4mm	1.9	8.64	< 0.01
Maximum Velocity: 4mm-5mm	2.07	4.83	< 0.01
Maximum Velocity: 3mm-5mm	3.97	5.90	< 0.01

Table 7.5: Bland-Altman analysis of mean and maximum peak velocities in the straight tube phantom measured using 1.5T PC-MRI with three different slice thickness values.

Figure 7.9: Mean velocity waveform for pulsatile flow in the straight tube phantom determined using 1.5T PC-MRI, 50 cardiac phases, retrospectively gated - the effect of varying slice thickness

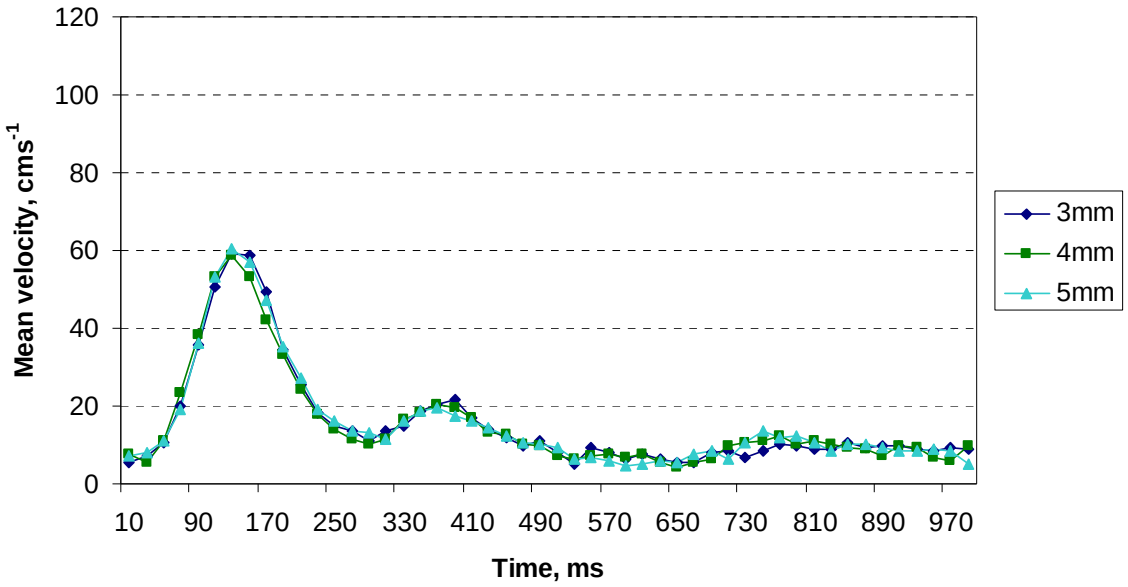

Figure 7.10: Maximum velocity waveform for pulsatile flow in the straight tube phantom determined using 1.5T PC-MRI, 50 cardiac phases, retrospectively gated - the effect of varying slice thickness

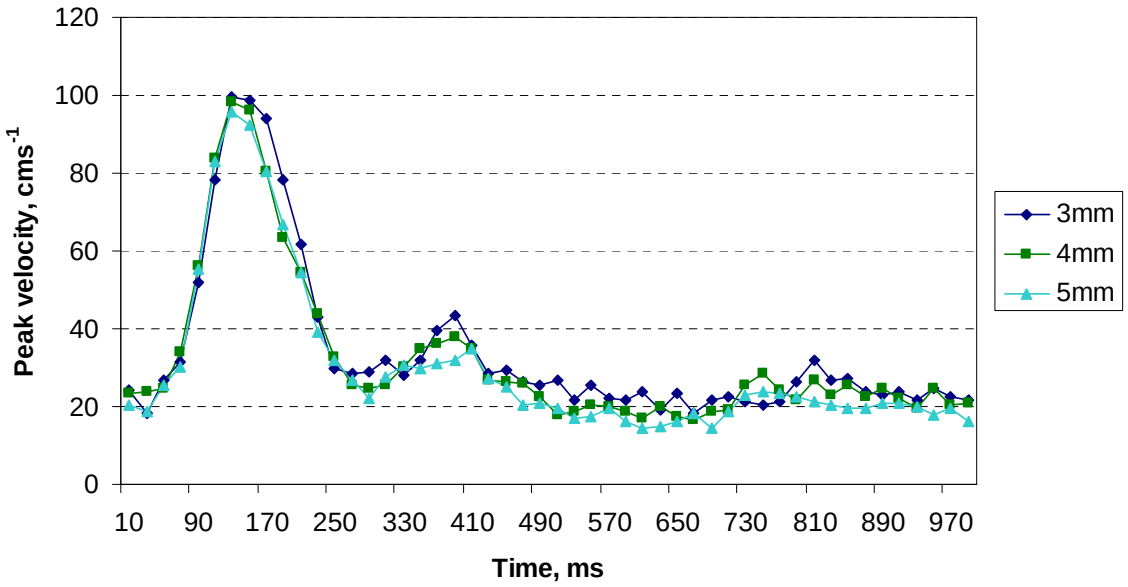

For the carotid phantom, using the 3.0T scanner, the effects of increasing the slice thickness from 2mm to 6mm were investigated using a prospectively gated PC-MRI protocol with 19 cardiac phases, focussing on the measurement of maximum velocities. The maximum velocity waveforms in the CCA section and the stenosed ICA section of the carotid phantom are shown in figures 7.11 and 7.12. The range of peak maximum velocities in the CCA was 52.69 cms^{-1} to 58.30 cms^{-1}, with the smallest slice widths giving the highest peak values. In the stenosed area of the ICA the peak maximum velocity range was 223.51 cms^{-1} to 192.71 cms^{-1}. However, in this case the 2mm gives the lowest peak value. It is possible that the 2mm slice is not detecting the area within the stenotic jet that gives the highest velocity.

It was noted that all slice thicknesses appeared to be able to detect the same main features of the waveform.

Further studies in the carotid phantom focussed on maximum velocity detection at the ICA stenosis site, comparing the larger slice thicknesses when using the body coil and the neck coil; as shown in figures 7.13 and 7.14 respectively. Table 7.6 shows that there was significant underestimation of the maximum velocities across the whole cardiac cycle as the slice thickness increased.

Comparison of PC-MRI velocity determination under varying slice thickness	*Mean bias (cms^{-1})*	*± Limits of agreement (cms^{-1}) (± 1.96σ)*	*P value*
Body Coil: 4mm – 6mm	15.3	13.3	< 0.001
Body Coil: 6mm-8mm	5.26	24.39	< 0.01
Body Coil: 4mm-8mm	20.56	25.09	< 0.001
Neck Coil: 4mm – 6mm	7.16	17.15	< 0.001
Neck Coil: 6mm-8mm	4.82	12.83	< 0.001
Neck Coil: 4mm-8mm	12.42	18.83	< 0.001

Table 7.6: Bland-Altman analysis of maximum peak velocities in the stenosed ICA section of the carotid phantom measured using 3.0T PC-MRI with three different slice thickness values and two coil types.

Figure 7.11: Maximum velocity waveform for long peak pulsatile flow in the mid-CCA section of the carotid phantom determined using 3.0T PC-MRI, 19 cardiac phases, prospectively gated - the effect of varying slice thickness

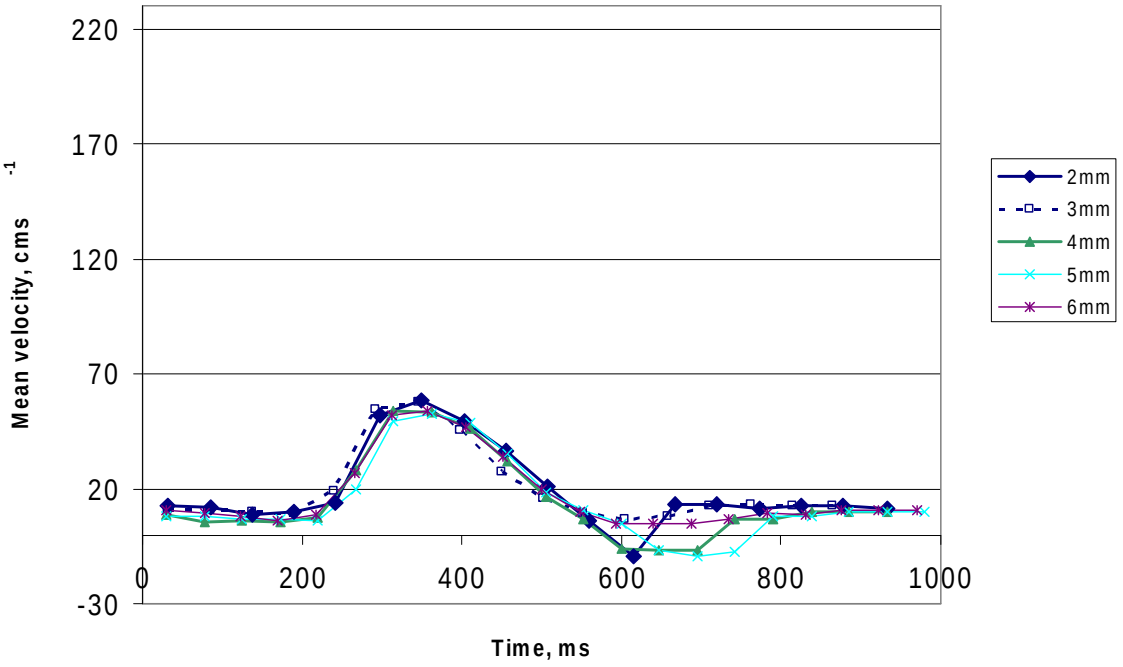

Figure 7.12: Maximum velocity waveform for long peak pulsatile flow in the mid-stenosis ICA section of the carotid phantom determined using 3.0T PC-MRI, 19 cardiac phases, prospectively gated - the effect of varying slice thickness.

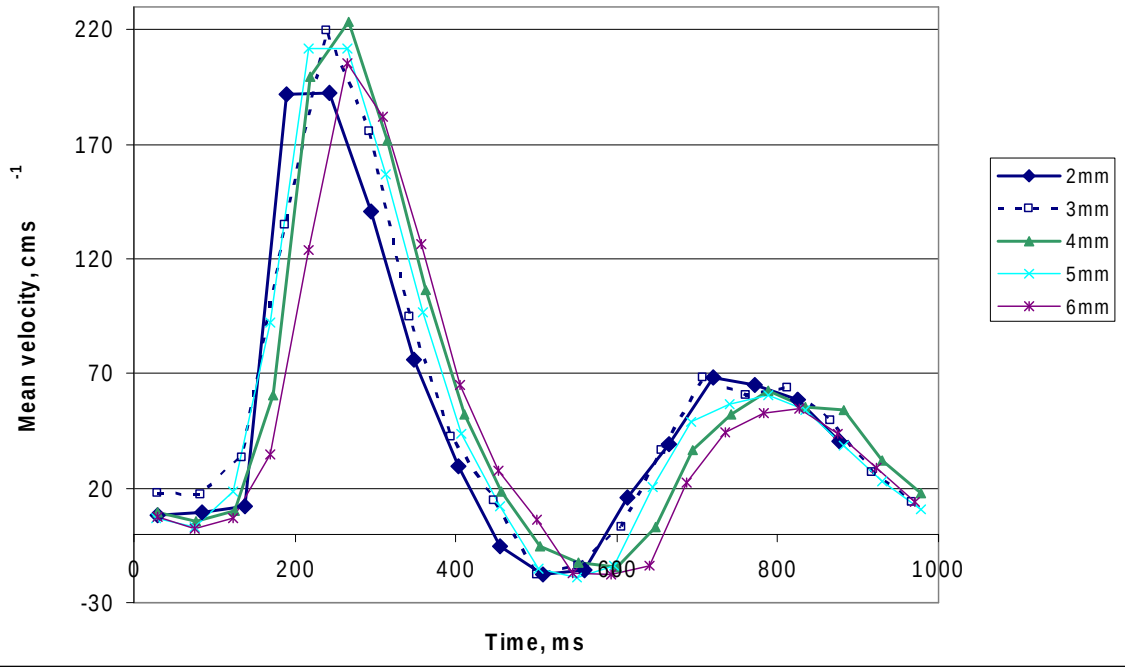

Figure 7.13: Effect of slice thickness on the measurement of maximum velocity using 3T PC MRI in the mid-stenosis section of the ICA segment of the carotid phantom using the body coil.

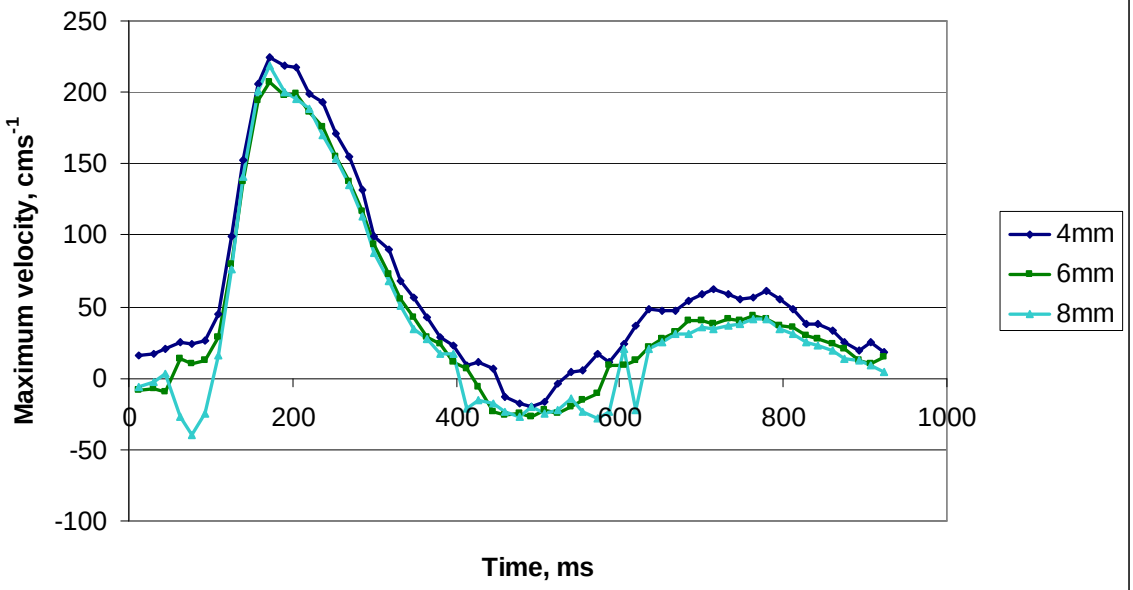

Figure 7.14: Effect of slice thickness on the measurement of maximum velocity using 3T PC MRI in the mid-stenosis section of the ICA segment of the carotid phantom using the neck coil.

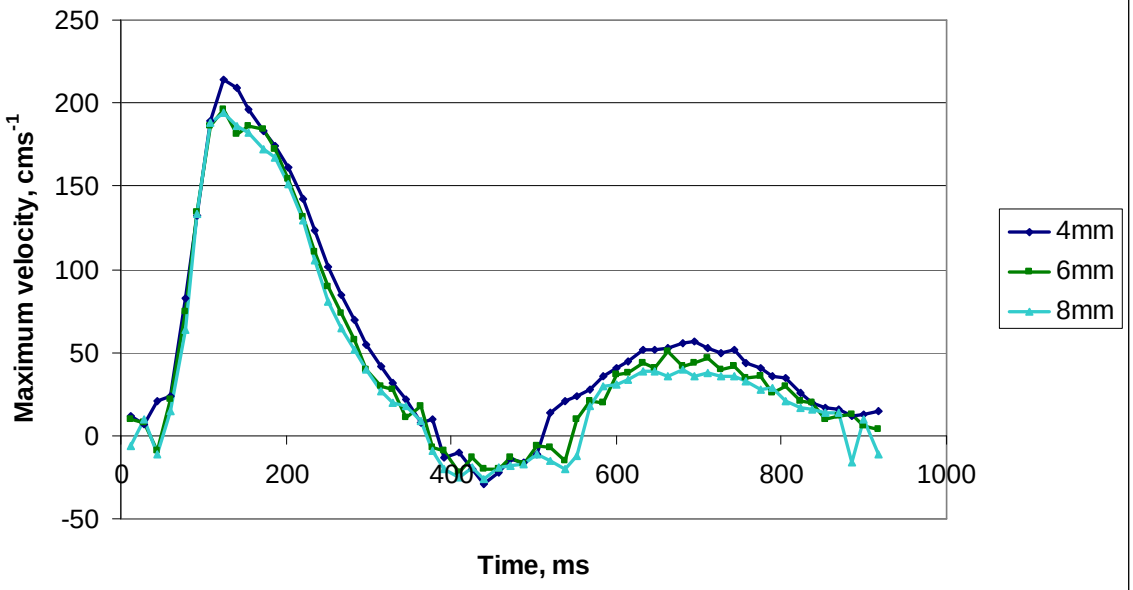

7.4.4 Effect of velocity encoding

Data from the 3.0T scanner measurements of the two peak flow pattern in the straight tube phantom was compared for two different values of velocity encoding. The maximum peak velocity was measured, using ultrasound, as 114 ± 0.6 cms^{-1} so that a venc value of 120 cms^{-1} would be a reasonable choice. This was compared with a venc of 200 cms^{-1}, which might be selected were the velocity unknown. The comparative waveforms for mean and maximum velocity are shown in figures 7.15 and 7.16 respectively. The Bland-Altman statistics in table 7.7 suggest that there is no significant difference between the two venc values.

Comparison of PC-MRI velocitydDetermination for different venc values	*Mean bias (cms^{-1})*	*± Limits of agreement (cms^{-1}) (± 1.96σ)*	*P value*
Mean Velocity: venc200- venc120	-0.95	21.08	0.7
Maximum Velocity: venc200- venc120	1.91	23.12	0.5

Table 7.7: Bland-Altman analysis of mean and maximum peak velocities in the straight tube phantom measured using 3.0T PC-MRI with two different velocity encoding values.

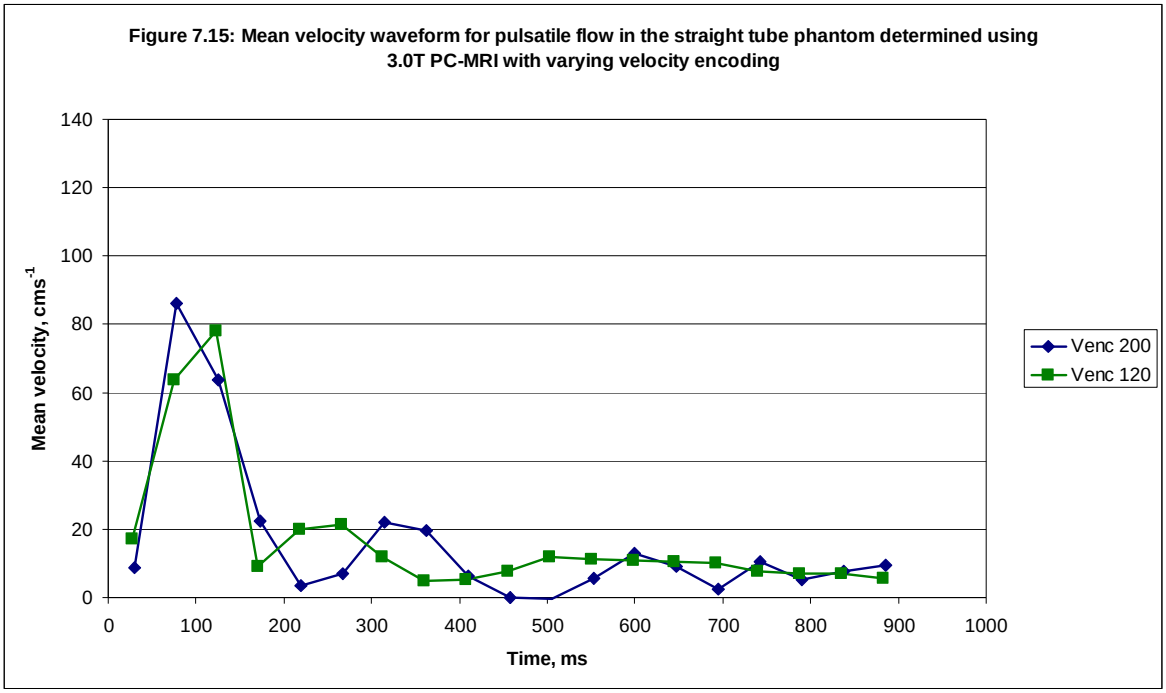

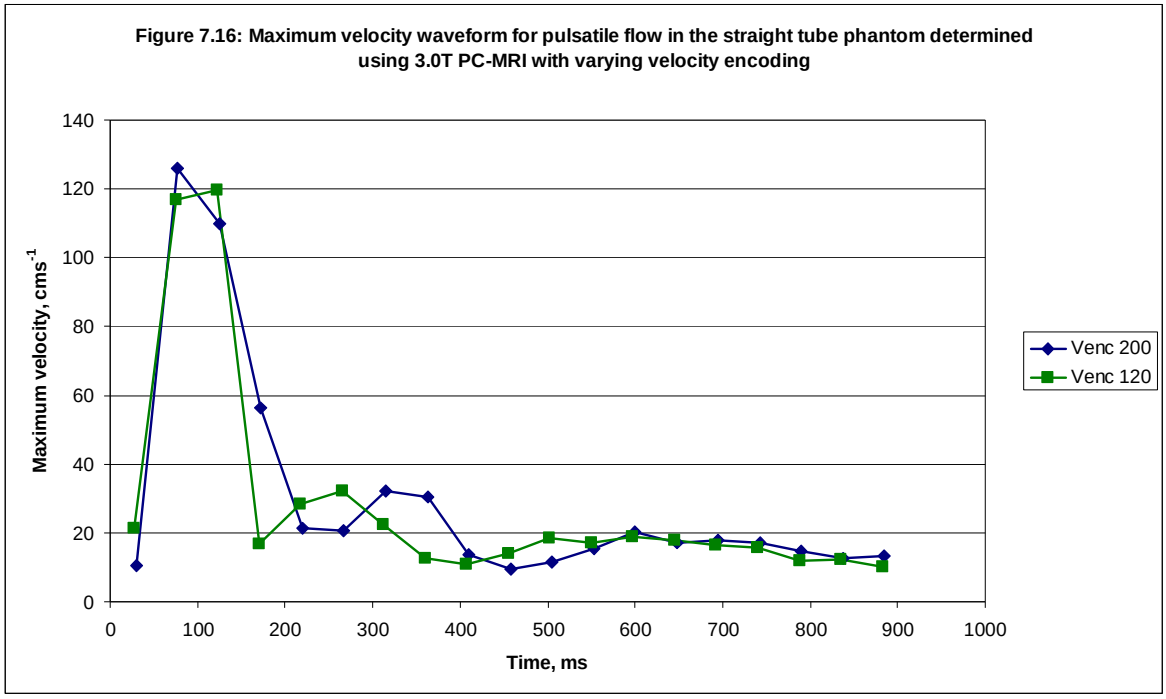

7.4.5 Body coil vs. neck coil

The emerging PC-MRI protocol for the measurement of maximum velocity was tested at various locations within the CCA and ICA stenosis sections of the carotid phantom using both the body coil and the neck coil compared with ultrasound measurements performed at approximately equivalent locations. The standard protocol used was a prospectively gated sequence with one average, short-term averaging, slice thickness of 4mm, TE = 4.69 ms and TR varied to give 19 cardiac phases or 58 cardiac phases over the 1000 ms cycle of the flow pattern. The higher temporal resolution was used for further investigation of the higher velocities at the stenosis site.

In figure 7.17 a and b show the maximum velocity waveform at two different sites in the CCA section of the carotid phantom; c and d show the maximum velocity at the ICA stenosis site. Table 7.8 shows the Bland –Altman statistics for the matched pairs of velocity profiles.

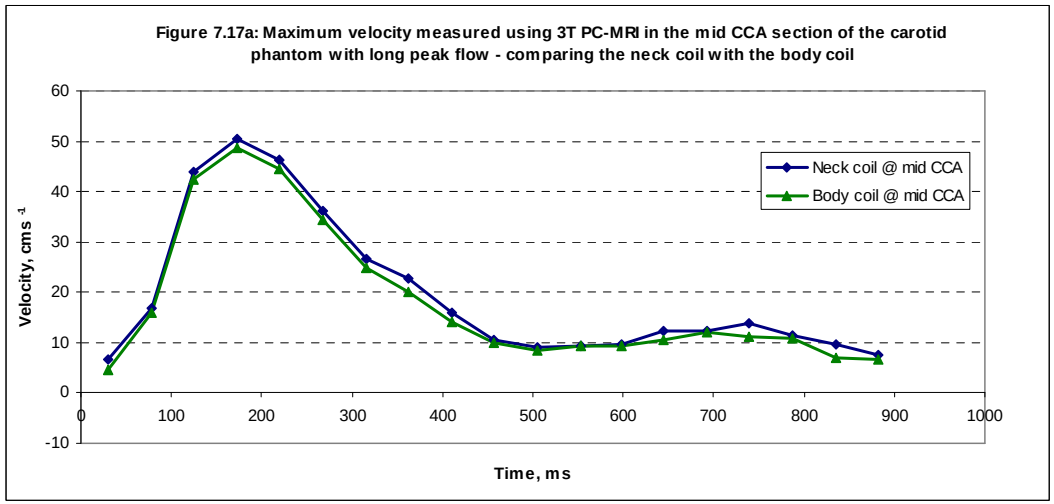

Figure 7.17a: Maximum velocity measured using 3T PC-MRI in the mid CCA section of the carotid phantom with long peak flow - comparing the neck coil with the body coil

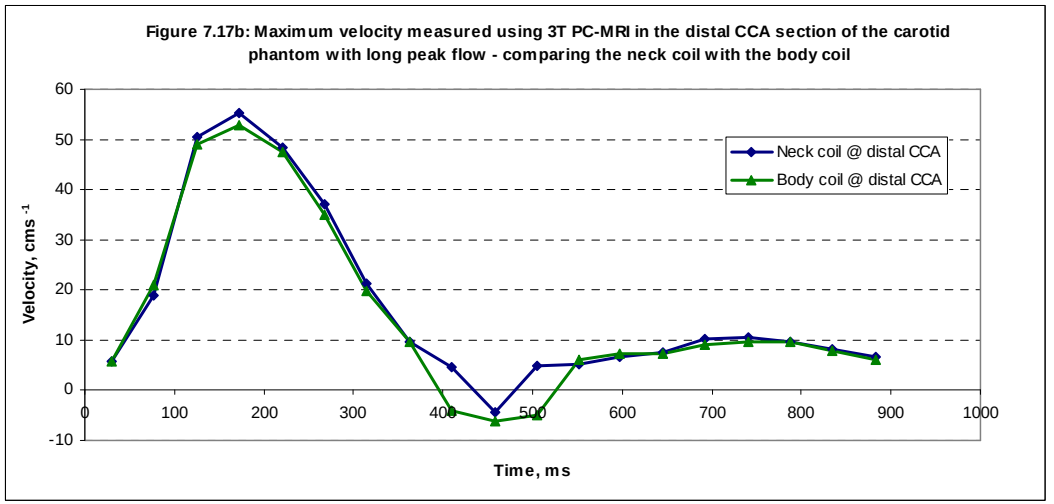

Figure 7.17b: Maximum velocity measured using 3T PC-MRI in the distal CCA section of the carotid phantom with long peak flow - comparing the neck coil with the body coil

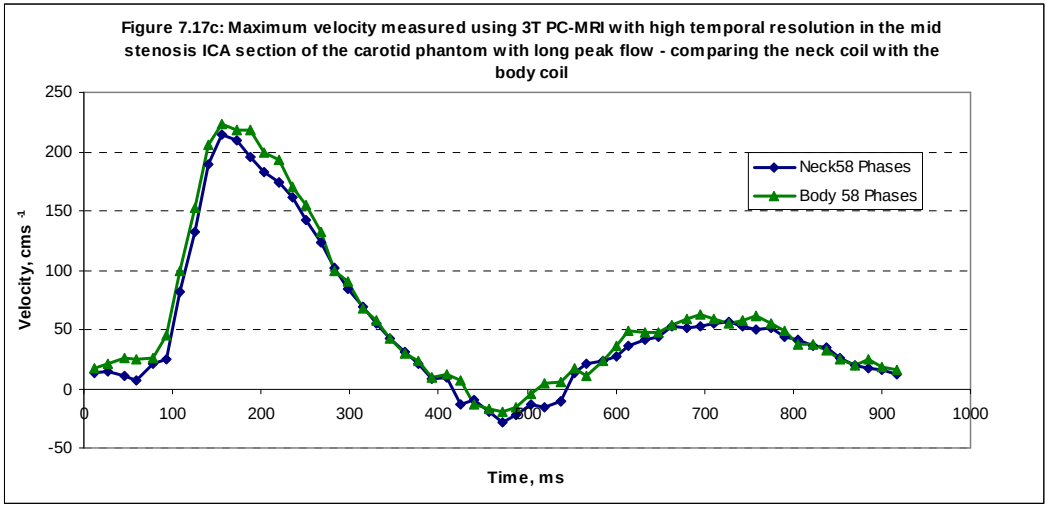

Figure 7.17c: Maximum velocity measured using 3T PC-MRI with high temporal resolution in the mid stenosis ICA section of the carotid phantom with long peak flow - comparing the neck coil with the body coil

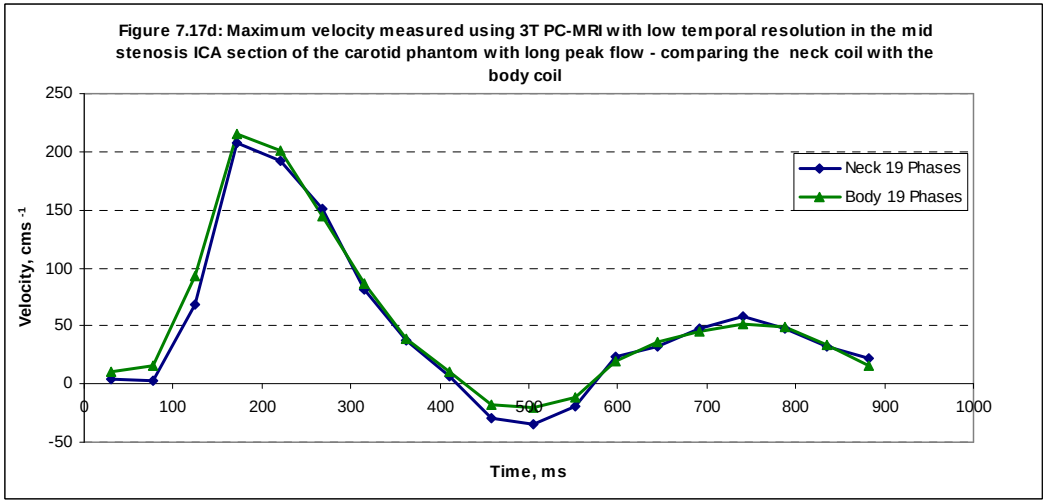

Figure 7.17d: Maximum velocity measured using 3T PC-MRI with low temporal resolution in the mid stenosis ICA section of the carotid phantom with long peak flow - comparing the neck coil with the body coil

Comparison of PC-MRI velocity determination for different MR coils	*Mean Bias (cms^{-1})*	*± Limits of Agreement (cms^{-1}) (± 1.96σ)*	*P value*
Mid CCA: Neck Coil – Body Coil	1.35	1.37	< 0.001
Distal CCA: Neck Coil – Body Coil	1.51	2.39	0.04
ICA stenosis 58 phases: Neck Coil – Body Coil	-6.84	14.38	< 0.0001
ICA stenosis 19 phases: Neck Coil – Body Coil	-4.42	15.67	0.03

Table 7.8: Bland-Altman analysis of maximum velocities in the carotid phantom measured using 3.0T PC-MRI comparing the neck coil with the body coil.

7.4.6 Comparison with ultrasound: measurement of maximum velocities and haemodynamic Indices

7.4.6.1 Ultrasound velocities

Ultrasound velocity waveforms were determined at key points along the carotid artery phantom using the perspex locators on the side of the container to give equivalent slice plane positioning for the PC-MRI studies. Maximum velocity values equivalent to peak systolic velocity, PSV, and end diastolic velocity, EDV, were recorded over a number of repetitions. Maximum velocities at other key features in the waveform e.g the second peak, were also recorded to enable registration of the graphed PC-MRI data with ultrasound spectral Doppler image excerpts. The PSV and EDV mean values from the ultrasound data are shown in table 7.9.

Figure 7.18 illustrates comparative maximum velocities for PC-MRI using the neck coil and the corresponding spectral Doppler ultrasound waveform at the same sites along the carotid artery test phantom, with the PSV values shown.

It is encouraging to note that the characteristic features or shape of the waveforms as displayed by spectral Doppler ultrasound, appear to be preserved by the shape of the PC-MRI waveforms.

Position in carotid phantom vessel	*Mean maximum PS velocity (± SD) cms-1*	*Mean maximum ED velocity (± SD) cms-1*
3V short peak Mid CCA	43.10 (± 0.87)	3.29 (± 0.56)
3V short peak Distal CCA	48.36 (± 0.93)	4.41 (± 0.29)
3V short peak Mid Stenosis	243.69 (±5.33)	13.5 (± 1.85)
3V short peak Stenosis Maximum	266.25 (±3.99)	18.8 (± 0.48)
3V long peak Mid CCA	55.98 (± 0.60)	7.61 (± 0.82)
3V long peak Distal CCA	69.39 (± 0.63)	10.85 (± 0.75)
3V long peak Mid Stenosis	240.02 (± 2.74)	21.86 (± 0.49)
3V long peak Stenosis maximum	277.95 (± 6.43)	23.22 (± 1.53)

Table 7.9: Mean maximum peak systolic and end diastolic velocities for two different waveforms, measured using spectral Doppler ultrasound at positions along the carotid artery phantom vessel.

Figure 7.19 Shows a Bland-Altman comparison graph comparing maximum peak systolic and end diastolic velocities for a pooled data set of 3.0T PC-MRI measurements compared against spectral Doppler ultrasound measurements at the same locations in the CCA and ICA segments of the carotid phantom.

Table 7.10 shows the Bland-Altman statistics for pooled data and for the PSV and EDV in each vessel, highlighting a large and significant underestimation of PSV in the ICA.

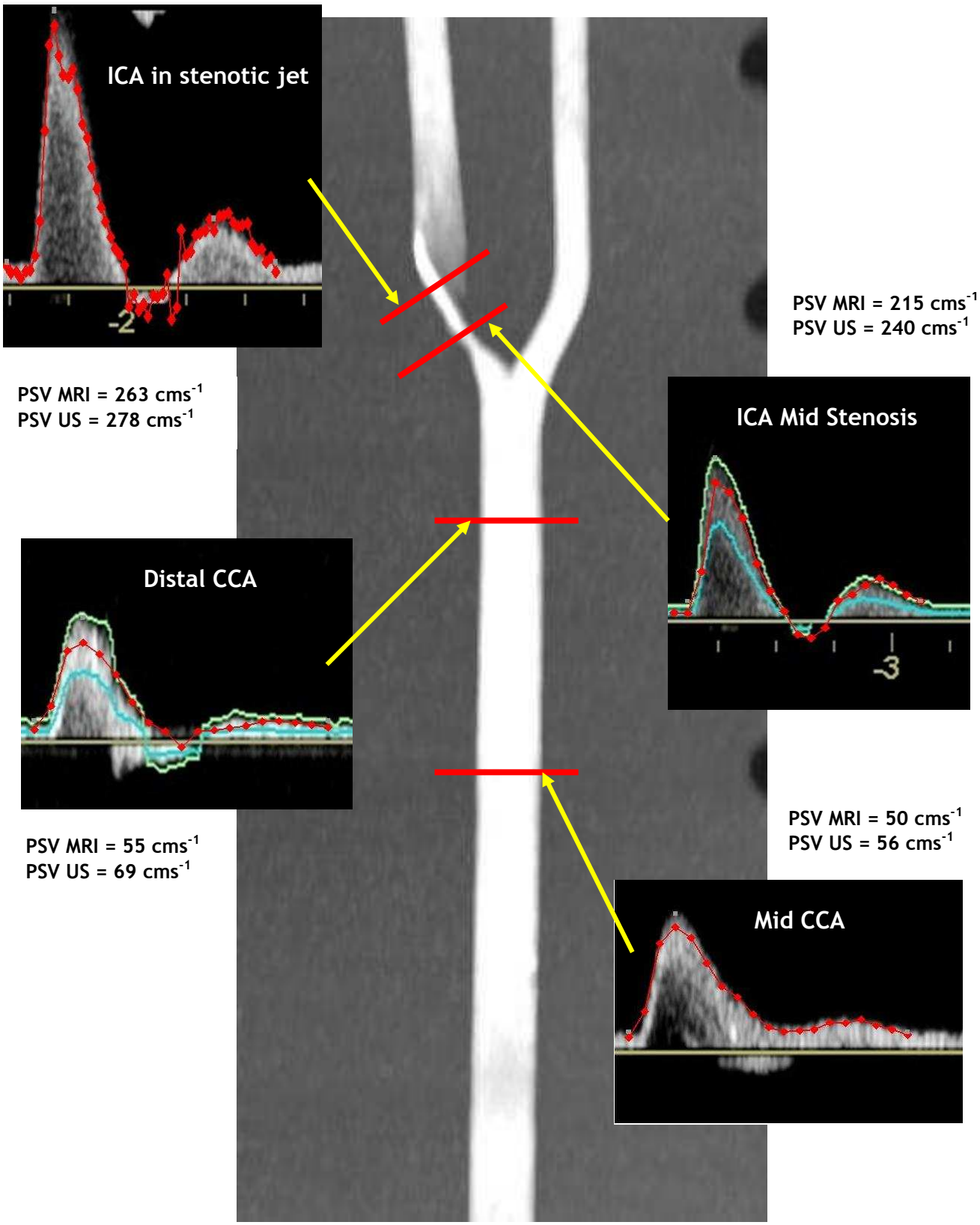

Figure 7.18: PC-MRI measurements of maximum velocity in the 3T scanner, compared with ultrasound measurements at the same location. PC-MRI shown in red mapped over the corresponding ultrasound spectral Doppler waveform.

Figure. 7.19: Bland Altman analysis of PC-MRI vs. spectral Doppler ultrasound measurement of maximum velocity (PSV and EDV) values in the carotid phantom - measurements recorded on different occasions using the optimised protocol

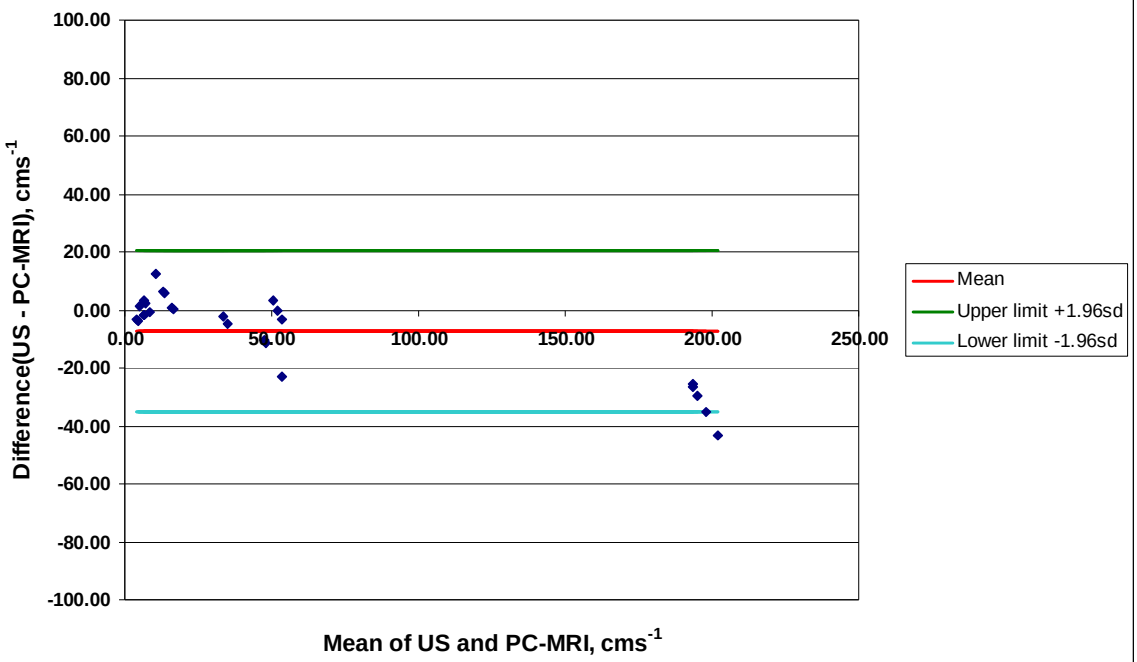

3.0T PC-MRI maximum velocity measurement compared with spectral Doppler ultrasound	*Mean Bias (cms^{-1})*	*± Limits of Agreement (cms^{-1}) (± 1.96σ)*	*P value*
All peak values	10.05	22.07	< 0.01
PSV in the CCA	7.8	18.51	0.05
EDV in the CCA	1.42	6.45	0.26
PSV in the ICA	27.52	14.13	< 0.01
EDV in the ICA	10.49	9.76	< 0.01

Table 7.10: Bland-Altman analysis of maximum velocities in the carotid phantom measured using 3.0T PC-MRI compared against spectral Doppler ultrasound measurements.

7.4.6.2 Ratios and indices

Considering the key ratios and indices, Figure 7.20 shows the Bland-Altman comparison for the ICA_{PSV} / CCA_{PSV} ratios derived from the ultrasound and PC-MRI velocities measured in the distal CCA and mid ICA stenosis locations in the carotid phantom.

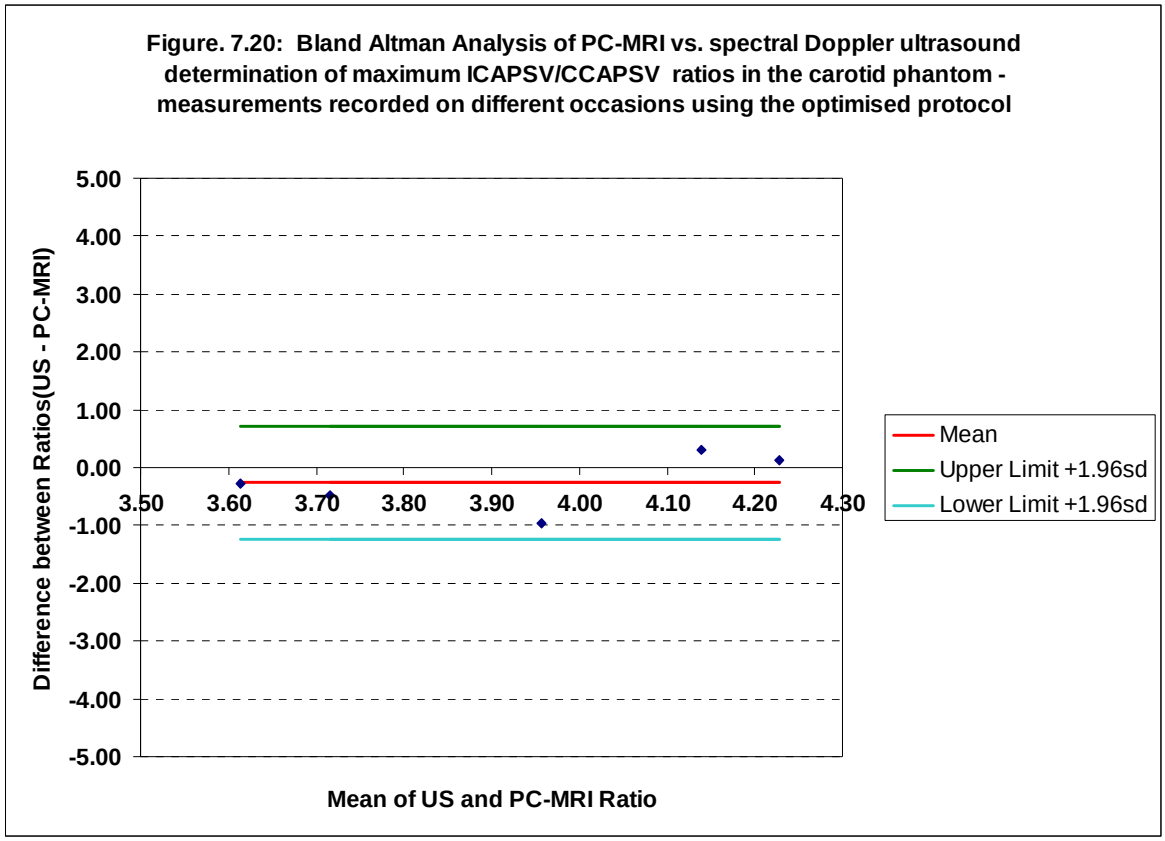

3.0T PC-MRI maximum velocity ratios compared with spectral Doppler ultrasound	*Mean Bias*	*± Limits of Agreement (± 1.96σ)*	*P value*
ICA_{PSV} / CCA_{PSV}	-0.26	0.98	0.30
St. Mary's Ratio	-6.85	22.99	0.26
Pulsatility Index, PI	-0.26	0.77	0.17
Resistivity Index, RI	-0.04	0.07	0.05

Table 7.11: Bland-Altman analysis of key haemodynamic ratios in the carotid phantom measured using 3.0T PC-MRI compared against spectral Doppler ultrasound measurements.

Table 7.11 summarises the statistics for the ICA_{PSV} / CCA_{PSV} ratios as well as other key haemodynamic ratios; St. Mary's ratio, pulsatility index and resistivity index. All ratios measured using PC-MRI were higher than those measured using spectral Doppler ultrasound, although the high p-value would suggest that none of these values are statistically significant. It should be noted that the limits of agreement are relatively large when compared with the range of measured values i.e. 3.47 to 4.44 for ICA_{PSV}/CCA_{PSV}, 22.12 to 45.81 for St. Mary's ratio, 3.57 to 4.93 for PI and 0.84 to 0.97 for RI.

7.5 Summary and discussion of results for *in-vitro* pulsatile flow.

The principle aim of this chapter was to finalise the development of a 2-D PC-MRI protocol for use in *in-vivo* studies which would be used to compare PC-MRI determination of maximum velocity parameters and ratios with those measured using the more conventional method of spectral Doppler ultrasound. Optimisation work, following on from that for steady state velocities, focussed on obtaining highest maximum or peak maximum velocity values while using PC-MRI, while acknowledging that these may not be as high as those found using spectral Doppler ultrasound with its inherent errors as discussed in previous chapters. The optimised protocol was then used to make a series of measurements of velocities and velocity ratios in the carotid artery phantom which were compared with ultrasound.

7.5.1 Optimisation studies

Having examined some spatial parameter issues in chapter 6, the focus of the pulsatile flow studies was to attempt to maintain high spatial resolution, since we are looking at relatively small vessels, while optimising temporal resolution. Although there is less need for breath hold or respiratory gating techniques when considering peripheral vessels rather than cardiac studies, there is still a need to minimise the scan time as the very nature of the PC-MRI technique, which collects image data over several cardiac cycles, makes it sensitive to motion artefact. In contrast, the real-time nature of ultrasound allows the user to compensate for movement and make instantaneous measurements.

7.5.1.1 Temporal resolution

Temporal resolution is acknowledged (Lotz et al. 2002; Thompson & McVeigh 2002) to be an issue in the MRI flow quantification. Many physiological waveforms have a short, 10 to 20 ms, post-systolic decrease in velocity, often becoming negative during that time (Oates 2001; Seitz et al. 2001). Poor temporal resolution can potentially miss this region leading to underestimation

of mean velocities and consequently flow when compared with ultrasound (Seitz et al. 2001).

Using the straight tube phantom with retrospectively gated flow, it was possible to create a range of cardiac phases from 15 to 50, with temporal resolution from 75 ms to 20 ms which revealed that the highest temporal resolution values of 20 ms and 26 ms gave the highest values of peak maximum and peak mean velocity. The converse was true for the poorest temporal resolutions, particularly for peak maximum velocities. However, the 20 ms resolution sequence had an acquisition time of 3.37 minutes compared with 1.10 minute for 75ms.

What was also of interest for pulsatile flow quantification was the ability of the PC-MRI sequence to accurately reflect the flow or velocity waveform. Figures 7.2 and 7.3 demonstrated that, although the varying temporal resolution affected the comparative velocity values, it had little effect on the depiction of the main temporal features of the waveform when compared with the equivalent ultrasound waveform in figure 7.1a. The detection of waveform features was further explored using the carotid phantom with the short and long pulsatile waveforms as depicted in figures 7.1b and c respectively. Both sets of waveform features were well depicted at all three resolutions used, although the velocity values increased with improving resolution, particularly for the more physiological, long peak flow pattern.

In selecting an appropriate temporal resolution, it was determined that a scan time of around one minute would involve minimal movement artefact and that the range of numbers of cardiac phases possible, 19 to 23, within that time frame would have only a small effect on the peak maximum velocity values.

7.5.1.2 Gating technique

For gated imaging studies, retrospective imaging techniques are preferred as they involve averaging and interpolation of data which can minimise artefacts found when using prospective gating (Sondergaard et al. 1993). However, for velocity quantification, such averaging will “average” down peak velocity values (Lotz et al. 2002), such that it may not be appropriate for flow quantification

where peak maximum velocities are required. In an *in-vivo* study, Seitz (Seitz et al. 2001) demonstrated that, although regression correlations between ultrasound and PC-MRI were poor, the mean peak systolic velocity for prospectively gated, non-breathold, PC-MRI, came closest to the mean peak systolic velocity measured in the same subjects using spectral Doppler ultrasound. Examining pulsatile flow in the carotid phantom, figures 7.7 and 7.8 demonstrate that for both mean and maximum velocities there is an obvious discrepancy between waveforms with lower peak maxima for retrospective gating despite the higher temporal resolution of the retrospective sequence. The retrospective waveforms appear "damped" when compared with the prospective data and the post-systolic prospective negative velocity features have been missed, an effect of retrospective gating noted by previous authors (Seitz et al. 2001; Sondergaard et al. 1993) which would contribute to lower mean velocity and flow calculations. The two gating types were also compared *in-vivo*, in chapter 8, giving similar results.

Since the quantification of velocity values is paramount in this thesis, prospective gating was used to minimise velocity averaging.

7.5.1.3 Slice thickness

In chapter 6 we looked at the effect of the slice thickness width on steady-state flow, concluding that it had little effect on velocity measurement, although there was a noticeable reduction in the error on the maximum velocity as slice thickness increased with the standard deviation reducing from ± 4.31 cms^{-1} for 3 mm to ± 1.53 cms^{-1} at 10 mm (figure 6.5). Averaging within the slice should, for steady-state velocities, produce a more robust average of all the velocity components within the slice. However, if there are spatial fluctuations in velocity, such as might take place with pulsatile flow in small vessels, particularly in the presence of disturbed flow, then there is the potential for large slices to "average-down" localised peak velocities. Non-cardiac studies of 2-D PC-MRI flow and velocity quantification have used a variety of slice thickness values ranging from 3 mm (Ho et al. 2002) to 8 mm (Seitz et al. 2001; Wetzel et al. 2001). However, there appears to be little evidence of any attempts to investigate the effects of slice thickness. Our own studies revealed that while there was little significant effect on the mean velocities, the maximum

velocities were significantly underestimated compared with ultrasound with greater underestimation as slice thickness increases. The results in the straight tube phantom and in the CCA section of the carotid phantom would suggest that a small slice thickness would maximise the peak velocity measurement. However, there are two reasons why the lowest 2 mm and 3 mm were not selected for the optimised protocol:

With undoped blood mimic in small vessels, such as the straight tube phantom, it was noticeable that there was minimal signal in both the phase and magnitude images for the diastolic flow time frames. Regions of interest had to be based on those where the higher systolic flow was visible, thus they could not be confidently optimised over the full cardiac cycle.

In the stenosed ICA section of the carotid phantom, the 2 mm slice appears to considerably underestimate peak maximum velocity, as illustrated in figure 7.12. At a region of stenosis, there will be considerable spatial variation of flow velocity along the vessel in the direction of flow, with maximum velocities in the stenotic jet just distal to the minimum vessel diameter (Oates 2001). It is probable that the 2 mm slice has detected the increase in velocity due to narrowing but has in fact missed the higher velocities in the proximal jet. The larger slice thickness planes, although centred at the same position, are spatially overlapping the higher velocity region. Accuracy of slice positioning is a more significant issue that slice thickness.

A slice thickness of 4 mm was selected for the optimised protocol as representing a reasonable compromise between obtaining good flow signal and minimising velocity averaging. The slice will require careful positioning in regions of known or suspected flow disturbance.

7.5.1.4 Velocity encoding

In the review paper by Lotz (Lotz et al. 2002), there is an excellent illustration of the effect on noise of increasing the velocity encoding, venc, parameter in relation to the actual velocity. In chapter 6, it was noted that the venc did

indeed influence the errors on the velocity measurement. However, in studies of pulsatile flow with two different venc values, 120 cms^{-1} and 200 cms^{-1}, comparing the mean velocity waveform and the maximum velocity waveform, there was no significant difference over the cardiac cycle.

Velocity encoding was optimised to expected flow velocities and set at no more than twice the expected peak maximum velocity.

7.5.1.5 MR coil selection

A series of measurements were repeated with the carotid phantom using the body coil and the neck coil, using identical study parameters at identical sites within the phantom. The waveform plots show that the waveform shape is maintained regardless of coil. Bland-Altman comparisons reveal a small underestimation of maximum velocities in the common carotid segment for the body coil compared with the neck coil. However, the neck coil measured slightly lower peak maximum velocities in the high velocity range within the ICA stenosis. The bias values of these studies are low (2 to 3 %) compared to the peak maximum velocities and of varying significance.

Selection of the body or neck coil may produce velocity differences of the same order as the measurement errors determined from steady state studies.

7.5.1.6 Comparison with ultrasound

It was noted during the survey of literature that there were few studies directly comparing flow quantification using spectral Doppler ultrasound with 2-D PC-MRI and of those in existence, the majority concentrate on flow measurements. The few that have looked at velocity measurements have made comparisons using regression analysis rather that Bland-Altman. Figure 7.18 shows the PC-MRI measurements, using the optimised protocol, mapped over the spectral Doppler waveform at sites along the carotid phantom. Although there are obvious differences in the maximum peak velocity. Bland-Altman analysis of all the data i.e. PSV and EDV at all sites, shows a significant mean underestimation bias of 10.05 cms^{-1} for PC-MRI. Applying regression analysis to the same data, for

comparison with other studies, shows a correlation of r = 0.99 as was found for phantom studies by Lee (Lee et al. 1997) when comparing PC-MRI with echocardiography. Separating out the data into peak systolic or end diastolic maximum velocities in the different vessels reveals low significance for the lower velocity range of values in the CCA segment of the carotid phantom.

7.5.1.7 Velocity ratios and the determination of stenosis

Further analysis of data from the stenosed carotid phantom generated the velocity ratios of ICA_{PSV}/CCA_{PSV}, St. Mary's ratio ICA_{PSV}/CCA_{EDV} , pulsatility index, PI and resistivity index, RI. All the ratios were higher for PC-MRI than for spectral Doppler ultrasound although the differences were not statistically significant. In a healthy volunteer study, Seitz (Seitz et al. 2001) looked at maximum velocity values along carotid arteries with the PI and RI ratios to compare PC-MRI with spectral Doppler ultrasound. Linear regression was used in that study giving 0.43 for PI and 0.29 for RI. The comparative regression statistics for the carotid phantom study were 0.81 for PI and 0.57 for RI, suggesting that optimisation of the PC-MRI protocol including the reduction of slice thickness may have improved the determination of velocity ratios.

7.5.2 An optimised PC-MRI protocol

The parameters in table 7.12 represent an optimised protocol based on the work carried out in this, and the preceding chapter. This was the basis for the 2-D PC-MRI data collection studies in human subjects in the following chapter.

Parameter	Value
Scanner	3T
Coil	Neck
Gating Type	Prospective
Pixel Resolution, mm	0.47
Slice Thickness, mm	4
TE, ms	4.69
TR, ms	47.3
No. of Cardiac Phases	19

Table 7.12: The parameters used in an optimised 2-D PC-MRI protocol for velocity measurement.

Chapter 8 – *In-vivo* validation of PC-MRI techniques vs. spectral Doppler ultrasound techniques for the quantification of arterial blood velocities and ratios.

As we investigate the potential of PC-MRI techniques for the investigation of peripheral arterial blood flow quantification, it is useful to compare against spectral Doppler ultrasound methods in sites such as the femoral and the extra-cranial carotid arterial systems which are easily accessed by both modalities. Validation in such regions would signal the potential of using PC-MRI to quantify blood flow in arterial regions where the available acoustic windows are poor, such as the subclavian-brachial segment and the aorto-iliac segment. It was noted in the survey of literature, in chapter 4, that there have been only a limited number of such comparative studies reported in the literature (Seitz et al. 2001). In addition to the comparison of maximum velocity measurement techniques, one of the aims of this part of the study was to investigate velocity ratios, in particular the ICA_{PSV}/CCA_{PSV} ratio used in spectral Doppler ultrasound of the carotid artery. This would give an indication of how well the use of such ratios might translate into other regions such as the subclavian or ilio-femoral segments.

The *in-vivo* validation and comparison of PC-MRI velocity measurement techniques against established spectral Doppler ultrasound methods was carried out using normal volunteer subjects. The *in-vivo* studies involved an initial pilot study to test the feasibility of using PC-MRI for measuring peripheral arterial velocities, testing and optimization of scan-protocols and comparison of PC-MRI measurements with spectral Doppler ultrasound. While much of the fundamental development and validation may be done using test phantoms, as in the chapters preceding this, there are many aspects that cannot be simulated in a test phantom, such as anatomical and physiological variations and patient movement problems. It was, therefore, necessary to recruit human subjects for the technique development and to establish the true feasibility of using the new technique as a potential diagnostic tool.

8.1 Ethical approval

Ethical permission was obtained from the local research ethics committee, LREC, prior to the commencement of the *in-vivo* studies, following advice and approval from on-site surgical and radiological staff. This approval applied to both the preliminary feasibility studies and the final, optimised protocol studies and allowed for repeat scanning of volunteers.

8.2 Preliminary volunteer studies

None of the MRI scanners on NHS and University sites in Glasgow routinely carried out velocity quantification of peripheral, i.e. non-cardiac, vessels. Consequently, the standard scanning protocols were largely untested for this application.

To investigate the feasibility of carrying out MRI velocity measurements in a clinical setting, an initial pilot study involving a number of healthy volunteer subjects was performed. This allowed preliminary investigation of scanning protocols, techniques and study logistics to be investigated.

8.3 Secondary volunteer studies – protocol optimisation and modality comparison

The majority of the optimisation studies were done using test phantoms as in the preceding chapters. However, it was useful to be able to check the results of some of those studies *in-vivo* such as the effect of gating (section 7.4.2) and the effect of velocity encoding (section 7.4.4); the parameters which were the most likely to be altered between subjects.

The optimised PC-MRI protocol developed in chapter 7 was used to study the carotid and vertebral arteries of a group of healthy volunteers for comparison against spectral Doppler ultrasound. A small group of four volunteers took part in both studies allowing comparison between non-optimised and optimised measurements, albeit on different scanners.

8.4 Methods

8.4.1 Pilot study

A pilot study was carried out at Gartnavel General Hospital Radiology Department and Vascular Laboratory. The purpose of this study was to investigate the feasibility of adding velocity encoded slice sampling on to standard MRA Peripheral Vascular protocols; to investigate methods of analysing the velocity encoded data; and to compare the MRI derived velocity measurements with Doppler ultrasound data from the same subjects.

8.4.1.1 Volunteer group

A total of 6 volunteers were recruited, 2 female and 4 male with ages ranging between 24 and 61. Volunteers underwent both MRI and ultrasound scanning of either the carotid or lower limb arteries. Some subjects underwent scanning of both anatomical regions. The resultant scan data comprised five lower limb studies and six carotid studies. 2D PC-MRI velocity encoded slices were collected at anatomical regions corresponding approximately to sites where the Doppler ultrasound velocity information was collected.

8.4.1.2 Scanning equipment and scan parameters

The scanners used in this pilot study were in routine clinical use at the hospital site. MRI scans were performed on a Philips Intera 1.5T scanner in the radiology department. Ultrasound studies were performed on a Siemens Sequoia 512 dedicated vascular Doppler ultrasound scanner.

For the MRI studies, standard MRA protocols as would normally be used in response to requests for MRA of the carotid or lower limb segments were used as a baseline. However, no contrast agent was used for the volunteer studies. The other departure from the normal protocol was the use of MRI compatible ECG leads on the subject's chest to allow cardiac gating of the flow signal sampling. Standard Philips "Q-Flow" sequences were used with variations depending on anatomical site and heart rate as in table 8.1.

Parameter	Value	Value
Region scanned	Carotid	Femoral
Coil	Syn-head/neck	Sense-body
Gating Type	Prospective	Prospective
Pixel Resolution, mm	0.7	1.2
Slice Thickness, mm	6	4
TE, ms	5.6	6.3 to 7.3
TR, ms	8.9	9.9 to 10.4
Views per segment	2	2
Temporal resolution	17 to 24	17 to 24
No. of Cardiac Phases	45	45

Table 8.1: The parameters used in a pilot study of 2-D PC-MRI for velocity measurement in healthy volunteers using the Philips Intera 1.5T scanner

Ultrasound studies were performed in the vascular laboratory at the same site, using modified standard protocols for carotid artery and lower limb arterial scanning based on those published by the Society of Vascular Technologists of Great Britian and Ireland (SVT 2001b; SVT 2001c). Scan parameters were optimised during the study as they would be for routine clinical scanning with the baseline parameters outlined in table 8.2.

Parameter	Value	Value
Region scanned	Carotid	Femoral
Preset	Carotid	PV-Artery
Transducer	8L5	6L3
Spectral Doppler frequency, MHz	4.0	3.5
Range gate size, mm	2.5	4

Table 8.2: The parameters used in a pilot study of spectral Doppler ultrasound velocity measurement in healthy volunteers.

8.4.2 Study protocol development

A selection of the *in-vitro* optimisation studies were repeated *in-vivo* prior to finalising the optimised protocol in chapter 7.

8.4.2.1 Scan parameters

The optimised protocol outlined in table 7.12 was used as a baseline for PC-MRI measurements *in-vivo* with the following variations:

- Averaging or number of acquisitions was 1 or 3.
- Gating was either prospective or retrospective
- Velocity encoding, venc was 120 cms^{-1} or 200 cms^{-1}.

These checks were carried out on the right side common carotid artery of a single healthy volunteer on the 3.0T Siemens Verio scanner using the neck coil. The subject was also scanned using the Logiq-e, portable ultrasound scanner with a 12L-RS linear transducer ultrasound for comparison with PC-MRI results.

8.4.3 Comparison studies

The optimised protocol, table 7.12, discussed in the previous chapter for 2D PC-MRI velocity measurement was tested by measuring the velocities in the extra-cranial carotid and vertebral arteries in a group of healthy volunteers. Peak velocity values and peak velocity ratios were compared with those obtained using standard protocol for spectral Doppler ultrasound carotid and vertebral artery imaging (SVT 2001b).

8.4.3.1 Volunteer group

A total of 13 volunteer subjects underwent bilateral scanning of the extra-cranial carotid and vertebral arteries using non-contrast PC-MRI and spectral Doppler ultrasound. There were 5 female and 8 male participants in the age range 21 to 65.

Four of the participants had also taken part in the pilot study of carotid artery scanning allowing for some comparison between optimised and non optimised PC-MRI protocols.

8.4.3.2 Scanning equipment and scan parameters

Ultrasound scanning was performed on volunteer subjects, using the GE Logiq e scanner with the 12L-RS linear transducer using the scan protocol and baseline conditions outlined in Table 6.2. Bilateral carotid and vertebral arteries were scanned on all subjects. The approach taken to data collection was to treat the scan as if it were a routine vascular lab assessment of carotid and vertebral arteries. The scan was done in the same timescale as it would take in a routine clinical setting. B-mode, colour Doppler and spectral Doppler were optimised throughout the scan, particularly angle correction and velocity scaling. Maximum PS and ED velocity data was collected by manual positioning of velocity callipers.

PC-MRI velocity data was collected on the same subjects, during the same imaging session, using the 3.0T Siemens Verio scanner with the baseline parameters outlined in table 7.12. The neck coil was used for velocity data collection, with a head coil in position over the patient during the scan to allow for additional data collection in the event of any adverse findings during the carotid and vertebral scan. The main departure from the parameters in table 7.12 was the venc parameter which was optimised after the first CCA 2-D PC-MRI slice had been acquired and analysed. The TR or effective spatial resolution was kept at a constant 47.5 ms so that the actual number of cardiac slices varied with the heart rate i.e. faster heart rates with a shorter R-R interval would have fewer slices.

8.4.4 Analysis of data

Ultrasound data was collected manually as described, with the image of the placed callipers on the spectral Doppler waveform along with the velocity values recorded for reference.

PC-MRI data from the Siemens Verio was analysed as described in chapters 6 and 7, using the Siemens Argus analysis package. However, the PC-MRI data from the Philips Intera was analysed using an in-house IDL program (Exelis Visual Information Solutions, Boulder, CO, USA) which generated velocity and flow output from the phase data images.

8.5 Results

As in the previous chapters, comparative data from ultrasound and PC-MRI was treated as a comparison of two methods of measurement of the same quantity and Bland-Altman methods were used to investigate agreement with paired T-testing used to examine the significance of any bias.

8.5.1 Pilot study results

Data from the pilot study generated 51 pairs of PC-MRI and spectral Doppler ultrasound velocity data sets, 33 in carotid artery sites and 18 in femoral artery sites. Figure 8.1 shows the Bland-Altman comparison for the pooled data set (carotid and femoral) maximum peak systolic velocity measurements. Figure 8.2 is the Bland-Altman comparison for the carotid data only. The statistics for the data-sets are shown in table 8.3. Neither the pooled data set nor the carotid data demonstrated good agreement with PC-MRI showing a large, statistically significant, underestimation bias relative to the range of velocities measured, when compared with ultrasound. Comparison of the femoral data set was better with an underestimation bias of 14.85 cms^{-1} for PC-MRI, but still relatively large (approximately 23%) compared with the range of measured velocities.

Comparing the carotid artery ratios, ICA_{PSV}/CCA_{PSV} , figure 8.3 and table 8.4, gave more encouraging results with PC-MRI underestimating the ratio with a mean bias of 0.1 compared with spectral Doppler ultrasound. The p value of 0.19 for the comparison would suggest is not significant i.e. there is no significant difference between the velocity ratio methods of measurement.

PC-MRI maximum velocity measurements compared with spectral Doppler ultrasound	Mean Bias (cms^{-1})	± Limits of Agreement (cms^{-1}) (± 1.96σ)	P value
All data (n= 51)	24.21	34.38	< 0.001
Carotid artery studies (n = 33)	29.32	33.72	< 0.001
Femoral artery studies (n = 18)	14.85	28.01	< 0.01

Table 8.3: Bland-Altman analysis of carotid and femoral artery peak maximum velocities: pilot study of velocities measured using non-optimised 1.5T PC-MRI compared against spectral Doppler ultrasound measurements.

PC-MRI maximum velocity ratios compared with spectral Doppler ultrasound	Mean Bias	± Limits of Agreement (± 1.96σ)	P value
ICA_{PSV}/CCA_{PSV}	0.10	0.44	0.19

Table 8.4: Bland-Altman analysis of carotid artery ICA_{PSV}/CCA_{PSV} ratios: pilot study of velocity ratios measured using non-optimised 1.5T PC-MRI compared against spectral Doppler ultrasound measurements.

Figure 8.1: Pilot in-vivo carotid and femoral artery study: Bland-Altman analysis of maximum peak systolic velocities, 1.5T PC-MRI vs. spectral Doppler ultrasound

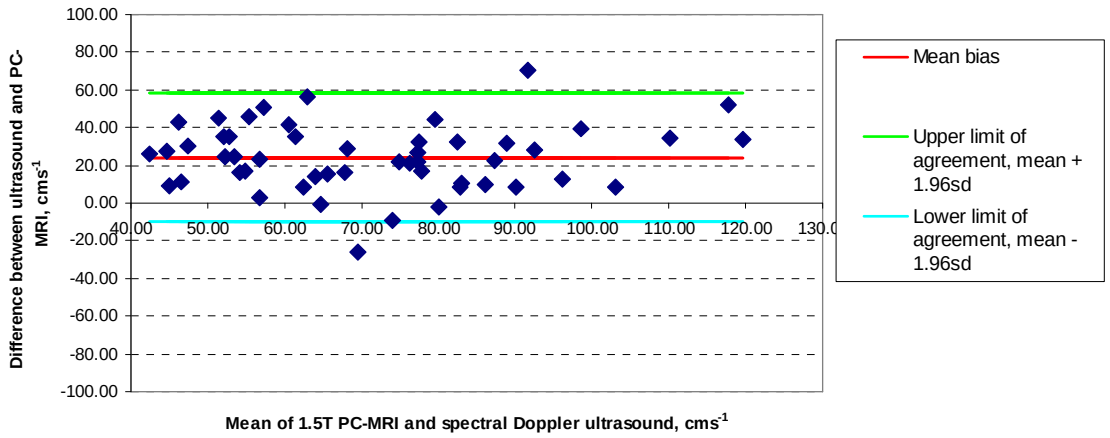

Figure 8.2: Pilot in-vivo carotid artery study: Bland-Altman analysis of maximum peak systolic velocities, 1.5T PC-MRI vs. spectral Doppler ultrasound

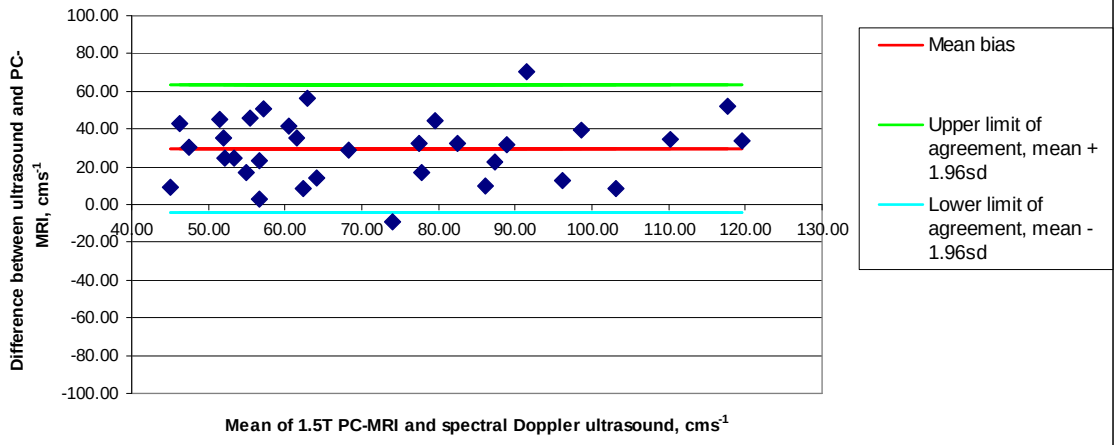

Figure 8.3: Pilot in-vivo carotid artery: Bland-Altman analysis of maximum peak systolic velocity ratio (ICA_{PSV}/CCA_{PSV}, 1.5T PC-MRI vs. spectral Doppler ultrasound

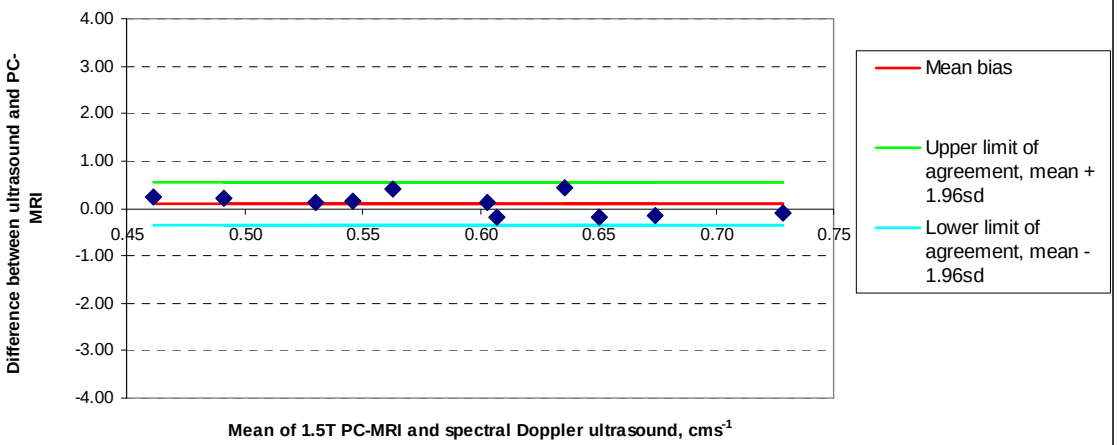

We may consider the findings of Gaynor (Gaynor et al. 2008b), which included the Sequoia ultrasound scanner and 6L3 and 8L5 linear transducers in their survey, that the ultrasound peak systolic velocities were overestimated by an average value of 31% for velocities > 50 cms^{-1}. Applying that figure to the ultrasound velocities in the pilot study generated comparisons with the Bland-Altman statistics shown in table 8.5

PC-MRI maximum velocity measurements compared with spectral Doppler ultrasound corrected by -31%	Mean Bias (cms^{-1})	± Limits of Agreement (cms^{-1}) (± 1.96σ)	P value
All data (n= 51)	4.45	31.15	0.05
Carotid artery studies (n = 33)	8.65	30.50	0.003
Femoral artery studies (n = 18)	-3.25	27.03	0.33

Table 8.5: Bland-Altman analysis of carotid and femoral artery peak maximum velocities: pilot study of velocities measured using non-optimised 1.5T PC-MRI compared against spectral Doppler ultrasound measurements corrected by -31%.

Comparing table 8.5 with table 8.3, it becomes apparent that use of the 31% correction on the spectral Doppler ultrasound certainly brings the two methods of measurement closer together, although the limits of agreement remain large.

8.5.2 Study protocol development

In the phantom studies of chapter 7, it was demonstrated that the type of gating used, prospective or retrospective, affected both the peak maximum velocity values and the maximum velocity waveform. When the test was repeated *in-vivo* similar results, figure 8.4, were found suggesting that prospective gating would produce higher values for the peak maximum velocity. It was also noted that applying averaging to the sequence, i.e. increasing the number of acquisitions per slice, gave a small but statistically significant ($p < 0.001$) reduction in measured maximum velocity.

Figure 8.4: The effect of gating and averaging strategies on the maximum velocity waveform in the common carotid artery, in-vivo, using 3.0 T PC-MRI

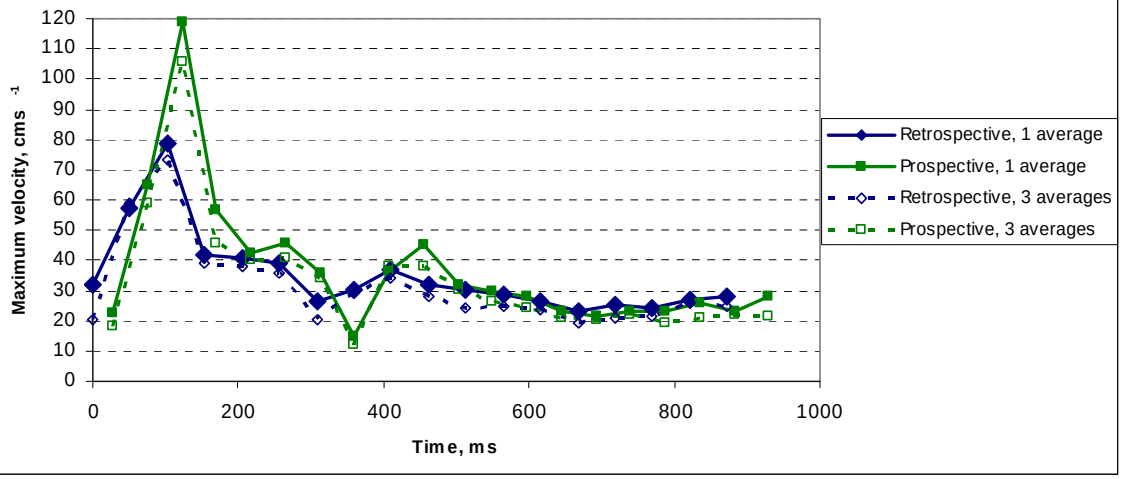

In the phantom studies in chapter 7, it was demonstrated that the choice of velocity encoding setting of 120cms^{-1} or 200 cms^{-1}, had no significant effect on the maximum velocities measured. However, *in-vivo*, the results, shown in figure 8.5, demonstrated a small, 3.68 cms^{-1}, underestimation for the venc 200 cms^{-1} maximum velocity results, of low significance (p =0.03). There was no significant difference between the mean velocities for the two venc settings.

Figure 8.5: The velocity encoding on the maximum velocity waveform in the common carotid artery, in-vivo, using 3.0 T PC-MRI

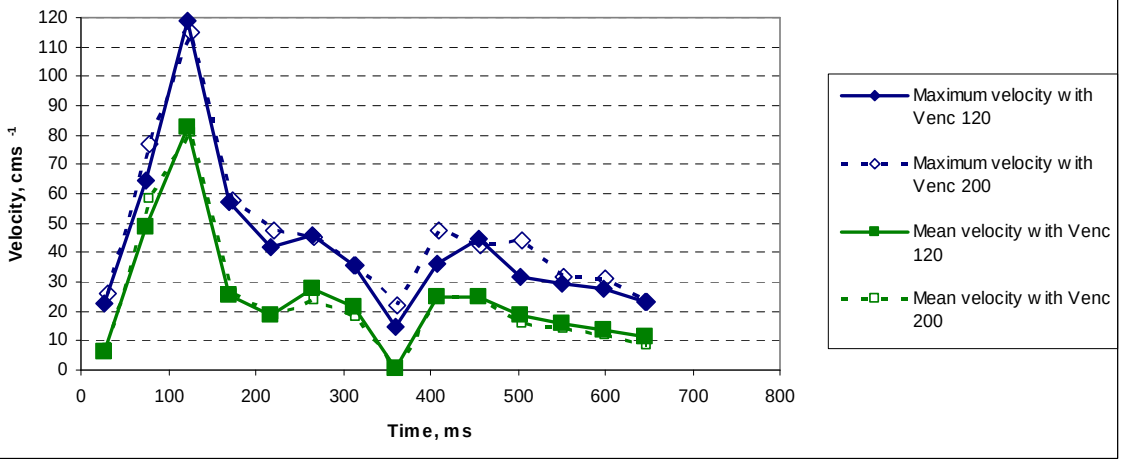

8.5.3 Comparison studies

The comparison study of optimised 3.0T 2D PC-MRI compared with spectral Doppler ultrasound generated 99 data pairs comprising maximum velocities in the common carotid, internal carotid, external carotid and vertebral arteries. Figures 8.6 and 8.7 show the Bland-Altman comparisons of maximum peak systolic velocity for all data and all carotid artery data respectively, with the statistics in table 8.6.

Figure 8.6: Comparison study in-vivo carotid and vertebral arteries: Bland-Altman analysis of maximum peak systolic velocities, 3.0T PC-MRI vs. spectral Doppler ultrasound

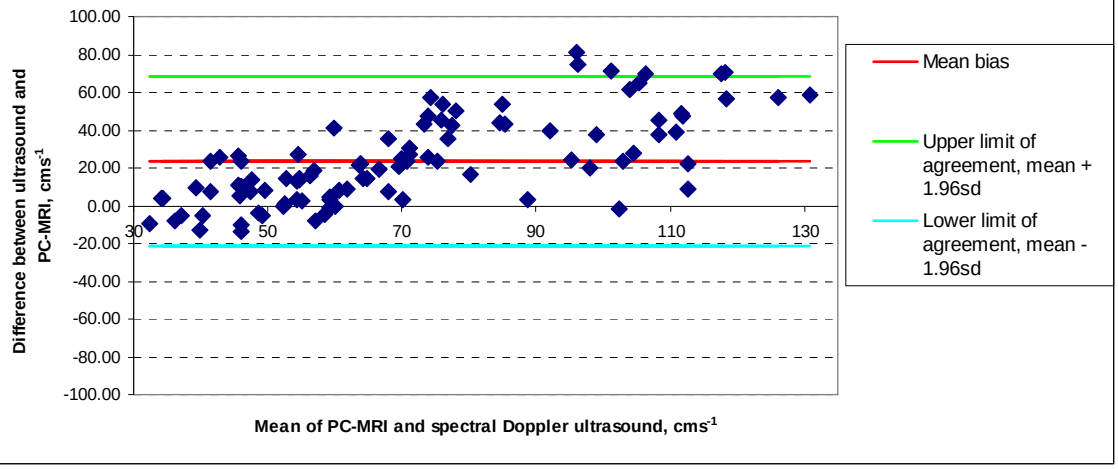

Figure 8.7: Comparison study in-vivo carotid arteries: Bland-Altman analysis of maximum peak systolic velocities, 3.0T PC-MRI vs. spectral Doppler ultrasound

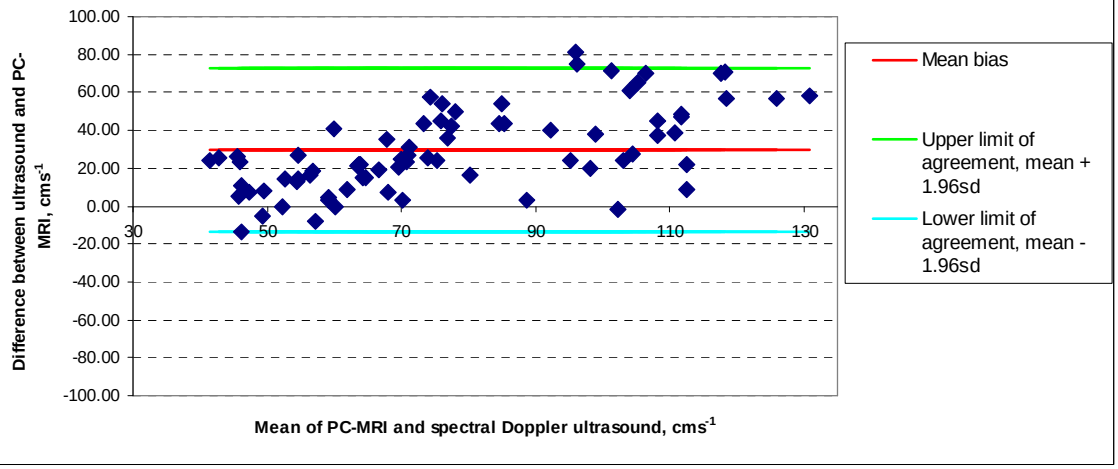

PC-MRI maximum velocity measurements compared with spectral Doppler ultrasound	Mean Bias (cms^{-1})	± Limits of Agreement (cms^{-1}) (± 1.96σ)	P value
All data (n = 99)	23.48	45.01	< 0.001
Carotid artery measurements (n = 76)	29.24	43.23	< 0.001
Vertebral artery measurements (n = 23)	3.66	24.47	0.17

Table 8.6: Bland-Altman analysis of carotid and vertebral artery peak maximum velocities: comparison study of velocities measured using optimised 3.0T PC-MRI compared against spectral Doppler ultrasound measurements.

Comparing table 8.6 with the pilot data results in table 8.3, it would appear that there is no improvement in the underestimation of PC-MRI measurements compared with spectral Doppler ultrasound, despite optimisation of the PC-MRI protocol.

However, as was found for the pilot data, the comparison of the results for carotid artery ratios, ICA_{PSV}/CCA_{PSV} , was rather more promising. As illustrated in figure 8.8 and table 8.7.

Figure 8.8: Comparison study in-vivo carotid artery: Bland-Altman analysis of maximum peak systolic velocity ratio (ICA_{PSV}/CCA_{PSV}) 3.0T PC-MRI vs. spectral Doppler ultrasound

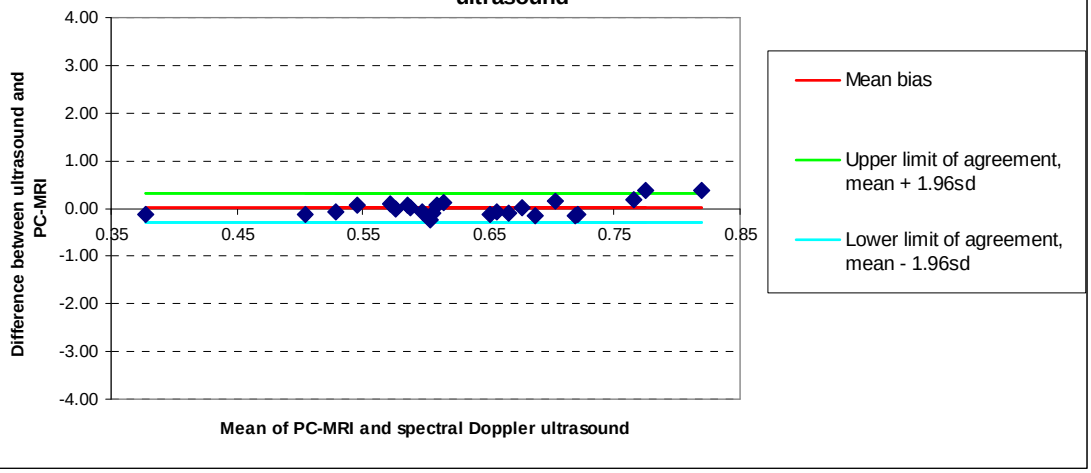

PC-MRI maximum velocity ratios compared with spectral Doppler ultrasound	*Mean Bias*	*± Limits of Agreement (± 1.96σ)*	*P value*
ICA_{PSV}/CCA_{PSV}	0.00	0.31	0.93

Table 8.7: Bland-Altman analysis of carotid artery ICA_{PSV}/CCA_{PSV} ratios: comparison study of velocity ratios measured using optimised 3.0 T PC-MRI compared against spectral Doppler ultrasound measurements.

The mean (± sd) ratio for PC-MRI was **0.63 ± 0.15**, and **0.63 ± 0.09** for spectral Doppler ultrasound giving a mean bias of 0.00 such that the null hypothesis holds and there is no significant difference between the two techniques.

As with the pilot data we can apply a correction to the maximum velocity data. However, we are able to base the correction on the string phantom data for the GE Logiq e scanner with the 12L-RS linear transducer presented in chapter 5. The percentage error on the maximum velocity was found to be 33.07 cms^{-1} for velocities greater than 50 cms^{-1}. Table 8.8 shows results for the maximum peak systolic velocity values measured using 3.0T PC-MRI compared against corrected spectral Doppler ultrasound measurements for all data and for carotid artery data.

PC-MRI maximum velocity measurements compared with spectral Doppler ultrasound corrected by -33.07%	*Mean Bias (cms^{-1})*	*± Limits of Agreement (cms^{-1}) (± 1.96σ)*	*P value*
All data (n= 99)	2.29	28.08	< 0.001
Carotid artery studies (n = 76)	6.69	31.77	< 0.001

Table 8.8: Bland-Altman analysis of peak maximum velocities: comparison study of velocities measured using optimised 3.0T PC-MRI compared against spectral Doppler ultrasound measurements corrected by -33.07%.

The results from this and the pilot data suggest that the perceived "underestimation" of PC-MRI maximum velocities is likely to be mainly due to the inherent "overestimation" of maximum velocities by spectral Doppler ultrasound.

8.5.3.1 Inter-study comparison

Four of the volunteers took part in carotid artery imaging in both the pilot study and the comparison study. This generated 24 measurement sites which had been tested using both MRI scanners and both ultrasound machines. While accepting that there may be differences between the two studies due to results being collected on different occasions, it is useful to compare our sets of results to investigate just how wide a variation might occur. The mean and standard deviation over all four volunteer measurements for each measurement type is shown in table 8.9. Tables 8.10 And 8.11 show the Bland Altman comparison statistics for maximum peak systolic velocity measurements and ICA_{PSV}/CCA_{PSV} ratios respectively.

	PSV mean (cms^{-1})	*PSV SD (cms^{-1})*	*Ratio mean*	*Ratio SD*
Pilot study Doppler	84.75	23.91	0.64	0.10
Comparative study Doppler	80.85	23.63	0.65	0.13
Pilot study PC-MRI	53.34	20.72	0.56	0.16
Comparative study PC-MRI	59.85	16.92	0.67	0.08

Table 8.9: Mean and standard deviations for the maximum peak systolic velocity and the ICA_{PSV}/CCA_{PSV} ratios in the carotid arteries of four healthy volunteers in the pilot study and the comparison study.

Maximum peak systolic velocity measurements	*Mean Bias (cms^{-1})*	*± Limits of Agreement (cms^{-1}) (± 1.96σ)*	*P value*
Comparison study: Doppler vs. 3.0T PC-MRI	21.00	29.51	< 0.001
Pilot study: Doppler vs. 1.5T PC-MRI	31.42	32.27	< 0.001
PC-MRI: 3.0 T vs. 1.5T	6.51	24.37	0.017
Spectral Doppler ultrasound: comparison study scanner vs. pilot study scanner	27.52	27.02	< 0.001

Table 8.10: Bland-Altman analysis of maximum peak systolic velocities in the carotid arteries of four healthy volunteers– pilot study data compared with comparative study data.

Maximum peak systolic velocity ratios	*Mean Bias*	*± Limits of Agreement (± 1.96σ)*	*P value*
Doppler vs. 3.0T	- 0.03	0.34	0.69
Doppler vs 1.5T	0.08	0.42	0.34
3.0 T vs. 1.5T	0.11	0.36	0.13
New Doppler vs. Old Doppler	0.01	0.34	0.86

Table 8.11: Bland-Altman analysis of carotid artery ($ICA_{PSV}/CCA_{PSV)}$ ratios for four healthy volunteers– pilot study data compared with comparative study data.

The peak systolic velocity results, in table 8.10 might suggest that differences between non-optimised PC-MRI and spectral Doppler ultrasound may only be slightly worse than differences between two different ultrasound scanners. However, applying the ultrasound maximum velocity corrections, we can re-draw table 8.10 to display the maximum velocity comparison data in table 8.12. The results show that the difference between the corrected velocities of the ultrasound scanners was not significant whereas more significance may be attributed to the higher values obtained when using the optimised 3.0T PC-MRI protocol compared with non-optimised 1.5T PC-MRI measurements.

Maximum peak systolic velocity measurements	*Mean Bias (cms^{-1})*	*± Limits of Agreement (cms^{-1}) (± 1.96σ)*	*P value*
Comparison study: Doppler vs. 3.0T PC-MRI	0.91	22.96	0.71
Pilot study: Doppler vs. 1.5T PC-MRI	11.36	28.08	< 0.001
PC-MRI: 3.0 T vs. 1.5T	6.51	24.37	0.017
Spectral Doppler ultrasound: comparison study scanner vs. pilot study scanner	-3.94	24.27	0.13

Table 8.12: Bland-Altman analysis of maximum peak systolic velocities in the carotid arteries of four healthy volunteers– pilot study data compared with comparative study data using corrected maximum spectral Doppler ultrasound velocity values.

8.6 Summary and discussion of results for the *in-vivo* studies.

Healthy volunteers were used in this study initially in a pilot study comparison of PC-MRI and spectral Doppler ultrasound. A single volunteer was used in the confirmation of some of the test-phantom studies during protocol optimisation. The main comparison study was to test how well an optimised 2D PC-MRI protocol might compare with spectral Doppler ultrasound. Our focus for this thesis was the comparison of peak maximum velocities and maximum velocity ratios.

8.6.1 Measurement of peak velocities

The pilot study provided a useful indication of whether standard 2D PC-MRI could be used to provide blood velocity data that could be used in the same way as spectral Doppler ultrasound is used, to aid the diagnosis of peripheral arterial disease. While being aware that the feasibility of PC-MRI in the peripheral arteries had been explored by authors such as (Caputo et al. 1992; Masui et al. 1995; Zananiri et al. 1993) any comparisons with ultrasound were generally focussed on mean velocities and flow volumes rather than on maximum velocities and maximum velocity ratios. The pilot study peak maximum velocity measurements revealed that spectral Doppler ultrasound was between 15 and 30 cms^{-1} higher than the PC-MRI maximum velocity values. However, the Philips Intera scanner used for the study was used for general imaging and MRA, hence the "Q-Flow" PC-MRI sequence was untested at the clinical site.

In the comparative study, with a larger study population, the results comparing the optimised PC-MRI measurements of maximum velocity were similar to those for the pilot study. However, for the four volunteers who took part in both parts of the study, the 3.0T optimised PC-MRI were approximately 10 cms^{-1} "better" or closer to the spectral Doppler ultrasound than was found for the un-optimised 1.5T PC-MRI in the pilot study, suggesting a potential improvement in the comparative study.

If we consider linear regression statistics, for ease of comparison with studies by other authors, correlation between spectral Doppler ultrasound and 1.5 T PC-MRI in the pilot study was r=0.66 for all carotid and femoral data and r=0.73 for the carotid data only. Correlation between spectral Doppler ultrasound and 3.0 T PC-MRI in the comparison study was r=0.78 for all carotid and vertebral data and r=0.74 for the carotid data only. We can compare with r=0.48 for maximum peak systolic velocities in the study by Seitz (Seitz et al. 2001) of carotid artery studies in 14 healthy volunteers using spectral Doppler ultrasound vs. 1.5 T prospective gated PC-MRI. In the animal studies by Jiang (Jiang et al. 2011) r=0.81 was found for the carotid PSV measurements of 4D (1.5T) PC-MRI, compared with spectral Doppler ultrasound; the mean bias for ultrasound PSV was 29.2 cms^{-1}, similar to our own findings.

8.6.2 Correction of maximum velocity errors

Errors on the maximum velocity of spectral Doppler ultrasound are well known and understood. However, despite the highlighting of such phenomenon to the ultrasound community in a recent review by Hoskins (Hoskins 2011) which reminded us that errors are typically around 30%, this remains largely ignored in the teaching and routine use of vascular Doppler ultrasound. Diagnostic criteria have developed, based around the measurement of maximum velocities. The most recent consensus guidelines (Oates et al. 2009) have several maximum velocity threshold values contributing to the diagnosis criteria for carotid artery stenosis.

A recent survey of 15 ultrasound scanners with 28 transducers in routine clinical use (Gaynor et al. 2008b) found a mean maximum velocity error of 31% for velocities greater than 50 cms^{-1}, consistent with those reported by others (Hoskins 2011). The scanner model and two transducers used in our pilot study were included in that study with both transducers having errors close to the group mean of 31%. Our own studies of velocity error for the scanner and transducer used in the comparison study, using the same string phantom technique, found a mean maximum velocity error of 33% for velocities greater than 50 cms^{-1}.

To date, the use of maximum spectral Doppler ultrasound velocity corrections when comparing with PC-MRI velocity measurement techniques has only been performed by one author. In the recent paper by Jiang (Jiang et al. 2011), corrected and non corrected velocity measurements were compared with results from a 4D PC-MRA technique. The technique used a method of velocity correction based on spectral broadening whereas our own study proposed a simplified method involving reducing the peak velocity by the mean percentage error on the maximum velocity. For the pilot study, the value determined by Gaynor (Gaynor et al. 2008b) of 31% and for the comparison study, the measured value of 33% was used. The corrections produced a dramatic reduction in the ultrasound mean bias, more so for the comparison study. However, although small compared with the range of velocities measured, the bias values were still statistically significant which may hint at small underestimation errors due to PC-MRI spatio-temporal averaging.

For the four volunteers who underwent carotid scanning in both parts of the study (table 8.12) applying the appropriate Doppler velocity correction reduced the bias of ultrasound measurements over 1.5T PC-MRI to a mean of 11.36 cms^{-1} ($p < 0.001$). For the comparison study of optimised 3.0T PC-MRI compared with corrected maximum velocity measured using spectral Doppler, there was no significant difference between the two methods.

In the consideration of maximum velocity measurements, we should not over look the comparison between different ultrasound systems. Comparing the carotid spectral Doppler measurements on the Siemens Sequoia 512 used in the pilot study with those from the GE Logiq e used in the comparison study, for the four volunteers who took part in both, shows a significant difference between the two with the GE system having a 27.52 cms^{-1} mean bias over the Siemens system measurements. Applying the appropriate maximum velocity correction factors reduces that bias to -3.94 but the p value of 0.13 suggests that there is no significant difference between the two ultrasound scanners. We may suggest from this that potentially, the differences between spectral Doppler ultrasound and PC-MRI maximum velocity measurements are no different than the difference between two different models of ultrasound scanners making measurements on the same subject on different occasions. The use of maximum

velocity corrections on different scanners may help to standardise spectral Doppler ultrasound measurements.

8.6.3 Maximum velocity ratios

A key parameter in the assessment and categorisation of stenosis is the use of peak velocity ratios. In particular, the ICA_{PSV}/CCA_{PSV} ratio is used to stratify the degree of carotid artery stenosis with >2 indicating 50% stenosis and >4 indicating a 70% stenosis and one of the criteria for recommending carotid endarterectomy surgery. Similar two-site ratios are used elsewhere in the body to quantify the degree of stenosis.

The values for the carotid artery ratios, ICA_{PSV}/CCA_{PSV}, in both the pilot study and the comparison study, were rather more encouraging than the maximum velocity results, showing no significant difference between PC-MRI and spectral Doppler ultrasound. The pilot study indicated a mean bias of 0.1 for ultrasound over PC-MRI although the p value of 0.19 suggested no significant difference between methods. For the comparison study the two methods of maximum velocity ratio measurement were in complete agreement with zero bias and p=0.93.

For the four volunteers who took part in both studies, none of the comparisons between different methods of measuring ICA_{PSV}/CCA_{PSV} ratios revealed any significant differences. The best agreement, ranked in order in terms of smallest mean bias and highest p value was found between the two ultrasound scanners, followed by Doppler vs. 3.0T PC-MRI, Doppler vs. 1.5T PC-MRI then 3.0T PC-MRI vs. 1.5T PC-MRI.

In summary, our findings suggest that the absolute measurement of maximum velocities using PC-MRI can only be compared with spectral Doppler ultrasound if a correction is applied to the ultrasound values to account for errors due to spectral broadening. It is possible to improve agreement with careful optimisation of the PC-MRI parameters.

In contrast, the use of maximum velocity ratios appears to translate well between and among modalities. Careful optimisation of PC-MRI parameters will optimise the agreement of ratio measurements in comparison with spectral Doppler ultrasound methods. This may allow the ratios to be used with PC-MRI data to grade a level of stenosis due to a lesion sited in a region inaccessible to ultrasound.

Chapter 9 – New and emerging methods of blood flow quantification and visualisation using MRI: 4D flow

During the lifetime of this thesis, a work in progress (WIP) sequence and analysis package for time resolved visualisation and quantification of three dimensional PC-MRI flow, known as 4D flow (Siemens, Erlangen), became available for use on the Siemens Verio 3T MRI scanner. This provided an opportunity to evaluate the potential of 4D Flow as a diagnostic tool in the quantification of vascular disease. Of particular interest with regard to the aims of this thesis was how the velocity quantification function of 4D PC-MRI would compare with 2D PC-MRI. In chapter 7, while examining the stenosis phantom, it was noted that incorrect positioning of the 2D flow encoded slice at the position of maximum velocity in a stenosed vessel had as much potential to underestimate the maximum velocity as for large slice thickness due to in-slice averaging. 4D PC-MRI offers an attractive solution to the problem of accurate slice positioning.

9.1 Introduction

The collection of a three dimensional volume of data is one of the main advantages of MR imaging techniques. The use of image subtraction methods for the visualisation of blood vessels were in use as far back as 1989 (Dumoulin et al. 1989) with volume data sets to create angiographic images of vessels. However, due to the short speed of image acquisition, contrast enhanced MRA is now the standard and routine method of obtaining a 3D volume image of the anatomy of the peripheral or non-cardiac vascular system. Use of phase contrast imaging methods have always offered the potential of adding functionality with time resolved velocity data volumes but these have been hindered by long acquisition times (Markl et al. 2012a). Recent interest in time resolved 3D PC-MRI methods, often referred to as 4D PC-MRI, has emerged as developments in acquisition and data processing have benefited from current improvements in computing power, with the potential to create time resolved volume data containing both functional and anatomical information.

A recent review by Markl (Markl et al. 2012a) provides an excellent overview of the development of the technique, the technology and the potential clinical applications.

While the majority of the development work testing 4D PC-MRI has been, as for 2D PC-MRI, in cardiac applications, a number of authors have tested techniques in peripheral areas such as hepatic vessels (Frydrychowicz et al. 2011; Roldan-Alzate et al. 2012; Stankovic et al. 2010), renal arteries (Bley et al. 2011; Francois et al. 2011), extra and inter cranial arteries (Chang et al. 2011; Harloff et al. 2009; Meckel et al. 2012) and the peripheral vascular system (Frydrychowicz et al. 2007). The focus of the majority of these studies has been on the visualisation technique with only a few examining velocity quantification and making comparisons with 2D PC-MRI methods. As for 2D PC-MRI, there has been a focus on the use of 4D-PC MRI for flow visualisation and flow volume quantification rather than measurement of velocities. The new 4D flow methods have also generated interest in the potential for quantifying pressures and wall shear stress with the ability to visualise temporal changes in flow patterns through the vessels, all features which are derived from velocity data.

There are few studies which have compared velocity measurement using 4D PC-MRI against 2D PC-MRI and/or spectral Doppler ultrasound. It has been found in the aorta, that 4D PC-MRI peak maximum velocities are close to that obtained by echocardiography and were significantly higher than maximum velocities from 2D PC-MRI (Nordmeyer et al. 2012). However in intra cranial applications (Meckel et al. 2012; Wetzel et al. 2007; Chang et al. 2011), carotid artery studies (Harloff et al. 2009) and portal venous measurements (Stankovic et al. 2010) it has generally been found that maximum velocities measured using 4D PC-MRI underestimate those measured using 2D PC-MRI and spectral Doppler ultrasound.

9.2 4D PC-MRI technology.

4D flow MRI requires acquisition of a volume of image data and velocity encoding of the volume data. The two methods of achieving this use conventional Cartesian three directional encoding or the more complex radial encoding.

9.2.1 Radial velocity encoding

Radial encoding involves data points in k-space being recorded in a radial trajectory so that the resulting data volume is a sphere (Gu et al. 2005). The isotropic resolution remains the same even for under-sampling giving the potential for scan time reduction while maintaining good resolution, although not without artefacts. It was noted from the literature that radial encoding techniques appear particularly successful in application with smaller vessels, complex anatomy and a wide range of flow velocities such as hepatic, renal and intracranial (Chang et al. 2011; Francois et al. 2011; Frydrychowicz et al. 2011).

9.2.2 Cartesian velocity encoding

The 4D flow WIP provided by Siemens used Cartesian three directional velocity encoding which has been used with some success in cardiac applications, particularly in the visualisation and quantification of flow in the aorta (Hope & Herfkens 2008). However, only a few authors have tackled the more peripheral vessels using this technique e.g. lower limb (Frydrychowicz et al. 2007), carotid (Harloff et al. 2009), intra cranial (Meckel et al. 2012).

Cartesian 4D flow encoded data acquisition as currently used collects, for each k-space line, four acquisitions; one reference scan and one for each of the three velocity encoding directions. Figure 9.1 illustrates the comparison between 2D PC-MRI acquisition and 4D PC-MRI data acquisition (Frydrychowicz, Francois, & Turski 2011). The resulting datasets produced for 4D analysis by the Siemens WIP comprise one volume of magnitude data and three sets of magnitude and phase 2D slices similar to those required by the Argus 2D flow evaluation software.

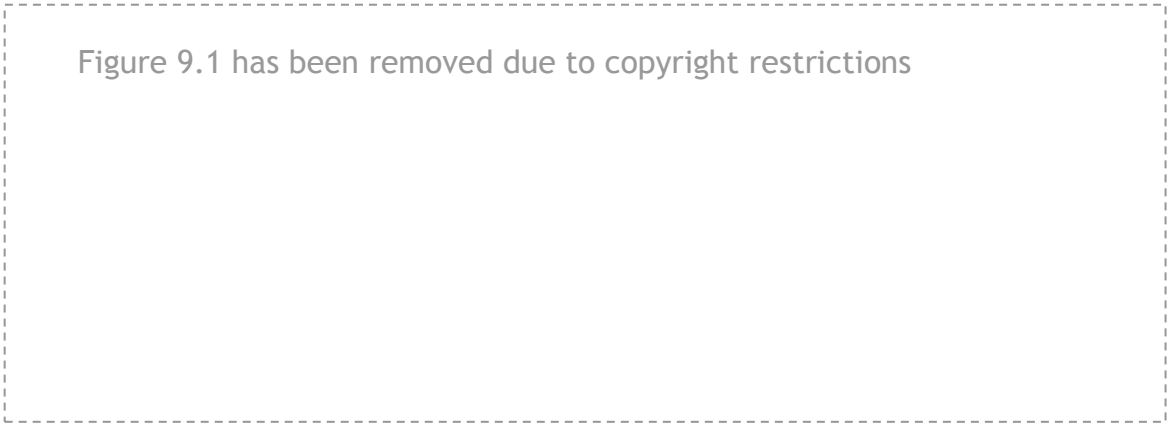

Figure 9.1: Velocity encoding for 2D and 4D PC-MRI. In A, the velocity encoding is in the through plane or z direction, creating a velocity encoded phase image for each sample point over the cardiac cycle. In B, velocity encoding is in all three directions, giving three sets of velocity encoded phase images. Adapted from Frydrychowicz et.al. (Frydrychowicz, Francois, & Turski 2011)

9.2.3 Scan time reduction techniques: GRAPPA

In 2D PC-MRI the need to collect two full sets of image data for each timepoint or phase in the cardiac cycle, places limitations on the spatial and temporal resolution and the overall acquisition time of the scan. In chapter 3, we described some time saving methods involving the segmentation or interleaving of k-space lines. The creation of time resolved volume datasets for 4D PC-MRI increases the temporal burden of acquisition and some of the more advanced methods of time saving data acquisition are required to avoid long acquisition times that might make a 4D scan clinically unfeasible or unacceptable. The Siemens Verio 3.0 T scanner used in this thesis employs a parallel imaging technique known as generalised autocalibrating partially parallel acquisitions, GRAPPA. Parallel MRI refers to any technique where multiple signal data points are acquired simultaneously, rather than one after the other (Sodickson 2005). The following is a short overview of the main principles behind GRAPPA, starting with the first step in the process known as simultaneous acquisition of spatial harmonics, SMASH.

9.2.3.1 SMASH imaging

In conventional MR imaging, the k-space steps in the spatial y-direction, referred to as the phase encoding direction, are produced by the application of different gradients. These create the phase encoded steps which, in k-space, can be thought of as spatial frequencies in the y-direction (McRobbie et al. 2003). The resolution, or pixel size, in the y-dimension of the final image is determined by the highest spatial frequency sampled, or the extent over which k-space is sampled, kmax. The field of view in the y-direction is determined by the frequency range we can sample and so is determined by the sampling rate Δk (Larkman & Nunes 2007). Figure 9.2, illustrates the idea of different lines in k-space being related to different spatial frequencies.

Figure 9.2 has been removed due to copyright restrictions

Figure 9.2: A schematic of k-space where the gradient steps applied on either side of the central, k = 0 line correspond to harmonics of spin modulation caused by those gradients. Adapted from Sodickson (Sodickson 2005).

The SMASH technique uses variations in the MR coil array sensitivity as a method of creating the spatial frequencies equivalent to those produced by the application of phase encoding gradient steps as described above. A regular array of coils will have a regular coil sensitivity pattern i.e. a spatial frequency pattern. The envelope of the pattern for the array may be thought of as a k = 0 line. It is then possible to generate harmonics of the fundamental coil spatial frequency to represent additional k-space lines as in figure 9.2. This technique can then be repeated for a reduced number of phase encoding gradient steps. The sets of k-space lines, real and simulated, generated using this technique are then interleaved to create the full image. In SMASH imaging, an additional set of reference k-space lines are added to the acquisition to create the auto calibration signal, ACS, or weighting signal for the coils. The datasets are fitted

to the ACS line and the process repeated several times to give an average weighting for image reconstruction (Griswold et al. 2002). Since the use of gradients is the most time consuming aspect of image acquisition, reducing the number of phase encoding gradient steps will significantly reduce the overall acquisition time.

9.2.3.2 GRAPPA

Generalised autocalibrating partially parallel acquisitions, GRAPPA, is a modified form of the SMASH technique. For GRAPPA, a number of lines for each of the coils are fitted to an ACS in just one of the coils, as illustrated in figure 9.3.

Figure 9.3 has been removed due to copyright restrictions

Figure 9.3: Coil array acquisition of data in GRAPPA. More than one k-space line acquired in each of the coils are fitted to an ACS line acquired in a single coil of the array. This is repeated for ACS lines in other coils and creates blocks of data which are combined during the image reconstruction. (Griswold et al. 2002)

This is repeated for ACS lines in the other coils and creates blocks of data which may be combined to construct the final image. Using this technique gives more data for the fitting of each "missing" k-space line resulting in a better fit, better signal to noise performance and better suppression of artefacts (Blaimer et al. 2004; Griswold et al. 2002).

9.2.4 Analysis of 4D datasets and velocity quantification

Although designed for the visualisation of flow dynamics, the velocity quantification part of the Siemens 4D flow package was of particular interest and relevance to this thesis. The collection of a volume of velocity encoded phase-contrast data raised the potential of a more satisfactory method of

"searching" for the peak velocity maxima and overcoming the uncertainty involved in the positioning of the 2-D phase contrast quantification slice, as discussed in chapter 7.

The aim of this chapter was to extend the methods used in the exploration of 2D-PC MRI to assess the potential of 4D PC MRI in the quantification of flow velocities and velocity ratios in the peripheral vascular system.

9.3 Methods

Three test phantom studies were used to investigate the velocity quantification capabilities of the 4D flow WIP and software package. Firstly, velocity validation in a simple straight tube phantom followed by a comparison of 2D and 4D PC-MRI for the determination of maximum velocities and maximum velocity ratios in the carotid phantom. Additional assessment of the determination of stenosis made use of a 50% stenosed straight tube in the MRQA set.

9.3.1 Velocity validation

In this study, the straight tube test object from the MRQA set described in chapter 5.1.6 was used with the simple 8.0 mm diameter, non-stenosed tube connected. A constant pump voltage was varied between 1 and 3 volts with the pump voltage-flow calibration from chapter 5 used to give a calibrated range of steady state mean velocities from 18.61 to 55.83 cms^{-1} (± 2.7%) and, assuming parabolic flow, maximum velocities of 37.22 to 111.65 cms^{-1} (± 2.7%). The 2D PC-MRI protocol was essentially the optimised protocol described in table 7.12. For 4D data collection the original WIP sequence, designed for imaging the aorta was optimised to compare with the 2D protocol. The small field of view enabled a reduction in the acquisition time so that a 16 slice volume of 3.0 mm slices collected a 48 mm slab in 5.36 minutes. The 2D and 4D study parameters are shown in table 9.1.

For the 2D PC-MRI acquisition the scan plane was placed at the centre of the vessel section within the phantom, perpendicular to the direction of flow. For 4D imaging the 16 slice slab was centred at the 2D slice position, again perpendicular to the direction of flow.

Parameter	2D PC-MRI	4D PC-MRI
Scanner	3T	3T
Coil	Body	Body
Gating Type	Prospective	Prospective
Pixel Resolution, mm	0.47 x 0.47	1.0 x 0.9
Slice Thickness, mm	4.0	3.0
Number of slices	1	16
TE, ms	4.69	3.7
TR, ms	47.3	60.7
No. of Cardiac Phases	19	15
Velocity encoding	100 to 150 cms^{-1}	100 to 150 cms^{-1}
Acquisition time	45 to 66 seconds	5.36 to 9.02 minutes

Table 9.1: The parameters used in an optimised 2-D PC-MRI protocol for velocity measurement.

9.3.2 Velocity and velocity ratio measurement using 2D and 4D PC-MRI

The carotid stenosis phantom was imaged using the 4D PC-MRI protocol outlined in table 9.1 but with 2 image slabs to cover the entire phantom length, taking the scan time up to 18 minutes. 2D PC-MRI scan planes were positioned in the distal CCA and at the ICA stenosis, with parameters as in table 9.1. Doppler ultrasound studies were also performed as described in chapters 6 and 7.

The 50% stenosis rigid silicone phantom from the MR QA set was also imaged using the same protocols as for the carotid phantom. This phantom had a wall-less 8 mm diameter lumen with a short symmetric stenosis narrowing to 4 mm diameter.

9.3.3 In-vivo example

One of the volunteers from the comparison study underwent 4D PC-MRI imaging of the carotid arteries, using a protocol based on that in table 9.1, using the neck coil and slice thicknesses of 3 mm and 4 mm. This allowed comparison with 2D PC MRI and spectral Doppler ultrasound for this subject.

9.3.4 Analysis of data

2D velocity data was analysed as described in the proceeding chapters using the Siemens Argus flow analysis package. 4D PC-MRI data sets, one volume of magnitude data and three sets of magnitude and phase 2D slices, were loaded in to the 4D Flow analysis package provided with the WIP. To obtain velocity data, a centreline for the vessel segment of interest is determined and the vessel lumen is modelled. In the "Flow Evaluation" feature, it is possible to select a number of planes along the vessel centreline, as illustrated in figures 9.4 and 9.5, equivalent to the roi selection in 2D analysis but with the planes based on the vessel model rather than the user having to draw an roi as is done in 2D flow analysis. Data from each plane is output in spreadsheet form containing flow rates, velocities and pressures. Of interest to this thesis is the ability to select to view "peak velocity" and then to navigate along the centreline to find the position giving the maximum velocity. Figures 9.4 and 9.5 show examples of the analysis screen for the validation and velocity comparison studies, respectively.

Data was compared using Bland-Altman methods as before.

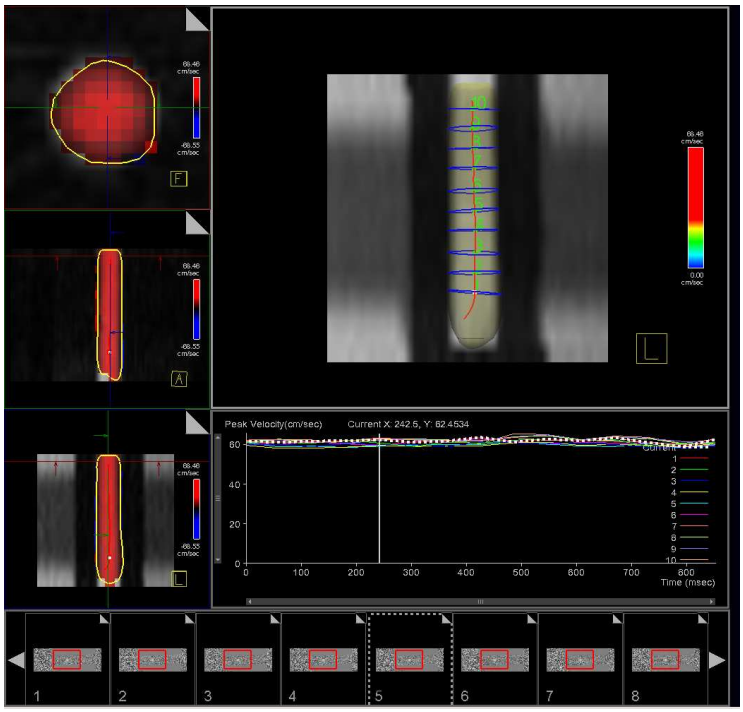

Figure 9.4: 4D flow analysis in the straight tube phantom with steady state flow. Left: colour velocity mapping in three directions. Top right: modelled vessel lumen with ten analysis planes. Lower right peak velocity waveform for each of the analysis planes.

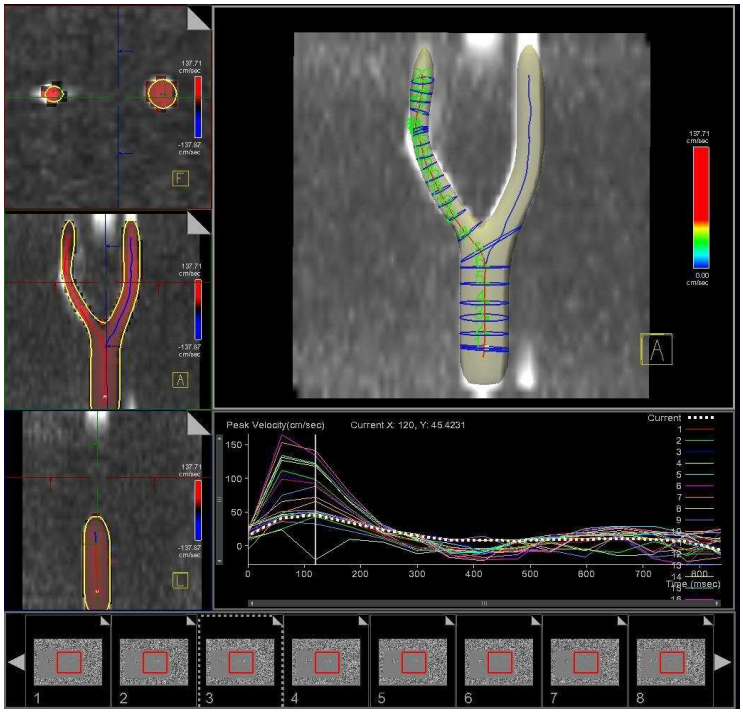

Figure 9.5: 4D flow analysis in the stenosed carotid phantom with pulsatile flow. Left: colour velocity mapping in three directions. Top right: modelled vessel lumen with twenty two analysis planes from the common carotid segment into the internal carotid segment. Lower right peak velocity waveform for each of the analysis planes.

9.4 Results

9.4.1 Validation with calibrated flow velocities

As in chapter 6, the use of steady state velocities enables calculation of an average value over all the time phases within the cardiac cycle, with the standard deviation giving an indication of the system errors for velocity measurement. Table 9.2 shows the average mean and maximum velocities for the range of flow pump settings used. Table 9.3 compares the mean percentage errors for each velocity measurement technique. For the 4D measurements the average values were calculated over all analysis planes as well as all time phases i.e. n = 15 for 2D PC-MRI but n = 150 for 4D PC-MRI.

	Calibrated mean velocity (cms^{-1})	*2D PC-MRI mean velocity (cms^{-1})*	*4D PC-MRI mean velocity (cms^{-1})*	*Calibrated maximum velocity (cms^{-1})*	*2D PC-MRI maximum velocity (cms^{-1})*	*4D PC-MRI maximum velocity (cms^{-1})*
1.0 V	18.61	19.78	16.51	37.22	32.53	33.68
1.5 V	27.91	26.93	24.35	55.83	46.56	46.95
2.0 V	37.22	39.49	31.92	74.43	58.89	61.16
2.5 V	46.52	47.23	38.24	93.04	70.32	71.99
3.0 V	55.83	56.80	45.03	111.65	79.29	80.30

Table 9.2: Average mean and maximum steady state velocity measurements using the flow pump calibration, 2D PC-MRI and 4D PC-MRI.

	Percentage error on the calibrated velocity measurements, %	*Percentage error on the 2D PC-MRI velocity measurements, %*	*Percentage error on the 4D PC-MRI velocity measurements, %*
Mean velocities	2.67	0.93	4.28
Maximum velocities	2.67	2.63	2.43

Table 9.3: Average percentage errors on mean and maximum velocity measurements for flow pump calibration, 2D PC-MRI and 4D PC-MRI.

The errors on the maximum velocity measurements are similar to the percentage error calculated for the calibrated flow pump maximum velocities. For maximum velocity measurement, the percentage error is smaller for 2D PC-MRI but larger

for 4D PC-MRI; possibly reflecting changes along the vessel lumen which would not be detected by the single 2D PC-MRI slice.

Table 9.4 shows the statistics for Bland-Altman comparisons between calibrated flow, 2D PC-MRI and 4D PC-MRI. As was found in chapter 6, there was no significant difference between the mean velocities from the flow pump calibration and the 2D PC-MRI measurements. However, there was a significant underestimation of mean velocity measured using 4D PC-MRI. In the measurement of maximum velocities, both 2D and 4D PC-MRI significantly underestimated the maximum velocity estimated from calibrated flow measurements.

Average steady state velocity measurements	*Mean Bias (cms^{-1})*	*± Limits of Agreement (cms^{-1}) (± 1.96σ)*	*P value*
Mean Velocity: Calibrated flow vs. 2D PC-MRI	-0.83	2.06	0.19
Mean Velocity: Calibrated flow vs. 4D PC-MRI	6.01	6.19	0.019
Mean Velocity: 2D PC-MRI vs. 4D PC-MRI	6.84	6.81	0.017
Maximum Velocity: Calibrated flow vs. 2D PC-MRI	16.92	19.25	0.026
Maximum Velocity: Calibrated flow vs. 4D PC-MRI	15.62	19.08	0.033
Maximum Velocity: 2D PC-MRI vs. 4D PC-MRI	-1.30	1.24	0.015

Table 9.4: Bland-Altman analysis of mean and maximum velocity measurement using 2D PC-MRI, 4D PC-MRI and compared with calibrated flow values.

Figures 9.6 and 9.7 show the Bland-Altman comparison graphs for 4D PC-MRI compared with 2D PC-MRI measurement of mean and maximum velocity respectively. 4D PC-MRI shows a significant underestimation of mean velocity compared with 2D PC-MRI, whereas there is a small but significant overestimation of maximum velocity for 4D PC-MRI compared with 2D PC-MRI measurement.

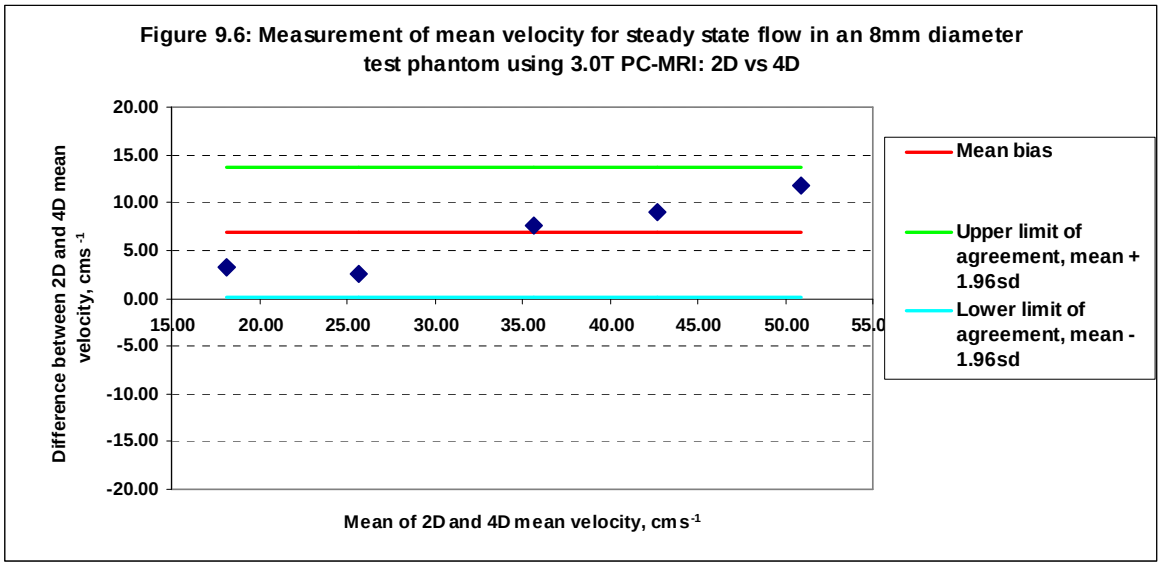

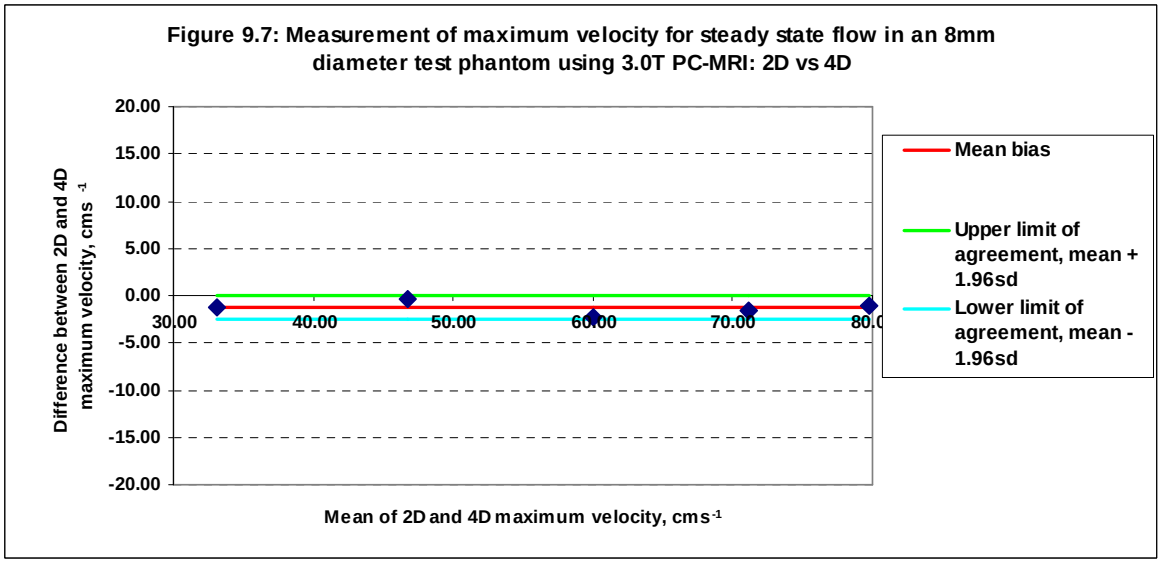

9.4.2 Comparison of velocity measurements and ratios

Testing the 4D WIP by imaging the carotid phantom allowed comparison with ultrasound as well as velocity measurements. Figures 9.8 and 9.9 show the comparative waveform or the 2D and 4D PC-MRI evaluated at the same positions in the CCA and ICA of the carotid phantom.

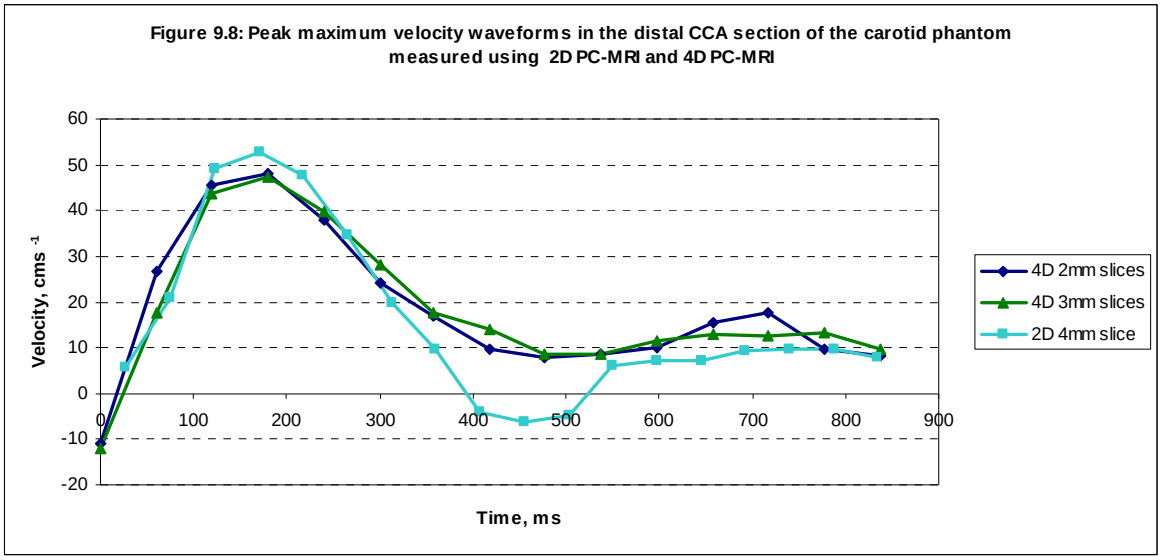

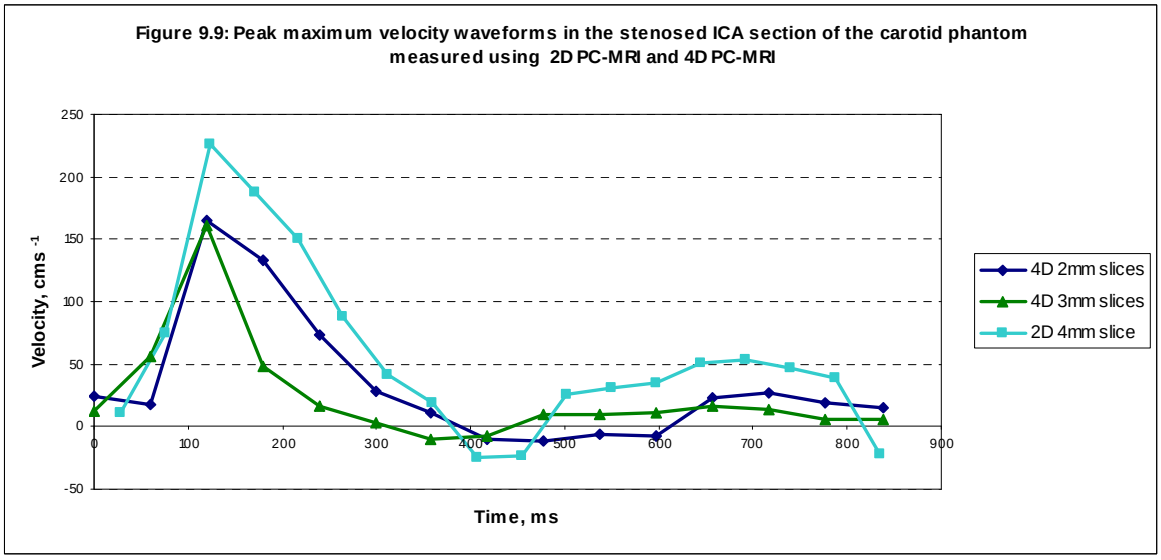

For the lower velocities in the CCA, figure 9.8 reveals an underestimation of the peak maximum velocity for 4D PC-MRI compared with 2D PC-MRI. There is little difference between the 2mm and 3mm slice width 4D PC-MRI datasets and neither appear to be able to detect the post-systolic negative velocities which were detected by both 2D PC-MRI and ultrasound (figure 7.1c).

Table 9.5 gives the Bland-Altman comparison statistics for 4D PC-MRI peak maximum velocity measurement in the CCA and ICA segments of the carotid phantom compared with 2D PC-MRI and spectral Doppler ultrasound. As in the preceding experimental chapters, comparison is also made with ultrasound corrected for maximum velocity errors.

Peak maximum velocity measurements	*Mean Bias (cms^{-1})*	*± Limits of Agreement (cms^{-1}) (± 1.96σ)*	*P value*
Spectral Doppler ultrasound vs. 2D PC-MRI	39.23	46.52	0.064
Corrected spectral Doppler ultrasound vs. 2D PC-MRI	-3.82	15.17	0.455
Spectral Doppler ultrasound vs. 4D PC-MRI	70.87	93.33	0.021
Corrected spectral Doppler ultrasound vs. 4D PC-MRI	42.17	80.25	0.070
2D PC-MRI vs. 4D PC-MRI	33.36	52.14	0.038

Table 9.5: Bland-Altman analysis of maximum velocity measurement using 2D PC-MRI, 4D PC-MRI, spectral Doppler ultrasound and corrected spectral Doppler ultrasound.

Although, the general lack of significance in table 9.5 can probably be attributed to the low number of paired data points, n = 6, in the comparison, it is clear that 4D PC-MRI considerably underestimates maximum velocities compared to both 2D PC-MRI and spectral Doppler ultrasound. Application of the ultrasound maximum velocity error correction reduces both the magnitude of the bias and the significance in comparison with 2D PC-MRI and 4D PC-MRI but there remains a large underestimation for 4D velocity measurements.

Considering the velocity ratios as we did in chapters 7 and 8, we can look at a typical data-set of ultrasound, 2D PC-MRI and 4D PC-MRI results for the carotid test phantom, collected during a single scanning session. Table 9.6 summarises the peak maximum velocity values and the ICA_{PSV} / CCA_{PSV} ratios for the three measurement methods, compared with the consensus guideline criteria for a greater than 70% stenosis (Oates et al. 2009).

	Peak maximum velocity in the CCA(cms^{-1})	*Peak maximum velocity in the ICA stenosis (cms^{-1})*	*ICA_{PSV} / CCA_{PSV} Ratio*
Spectral Doppler ultrasound	69.00	278.00	4.03
2D PC-MRI	52.82	226.03	4.28
4D PC-MRI (2mm)	47.90	165.24	3.45
4D PC-MRI (3mm)	47.32	161.35	3.41
Criteria for > 70 % stenosis		**>230**	**>4**

Table 9.6: Peak maximum velocities and ICA_{PSV} / CCA_{PSV} ratios measured in the carotid phantom using spectral Doppler ultrasound, 2D PC-MRI and 4D PC-MRI, compared with the criteria for a > 70% stenosis.

The stenosis in the phantom is known to be 70% in terms of diameter reduction, so it would be reasonable to expect "borderline" 70% results. However both the uncorrected spectral Doppler ultrasound values and the 2D PC-MRI results clearly indicate a > 70% stenosis but the 4D PC-MRI values suggest the stenosis is < 70% but > 50%.

For comparison the 50% stenosed vessel in the rigid silicone MRA QA Set was also imaged giving the resulting waveforms displayed in figure 9.10 and the data summarised in table 9.7.

Figure 9.10: Peak maximum velocity waveforms in the 50% stenosis phantom measured using 2D PC-MRI and 4D PC-MRIPeak max

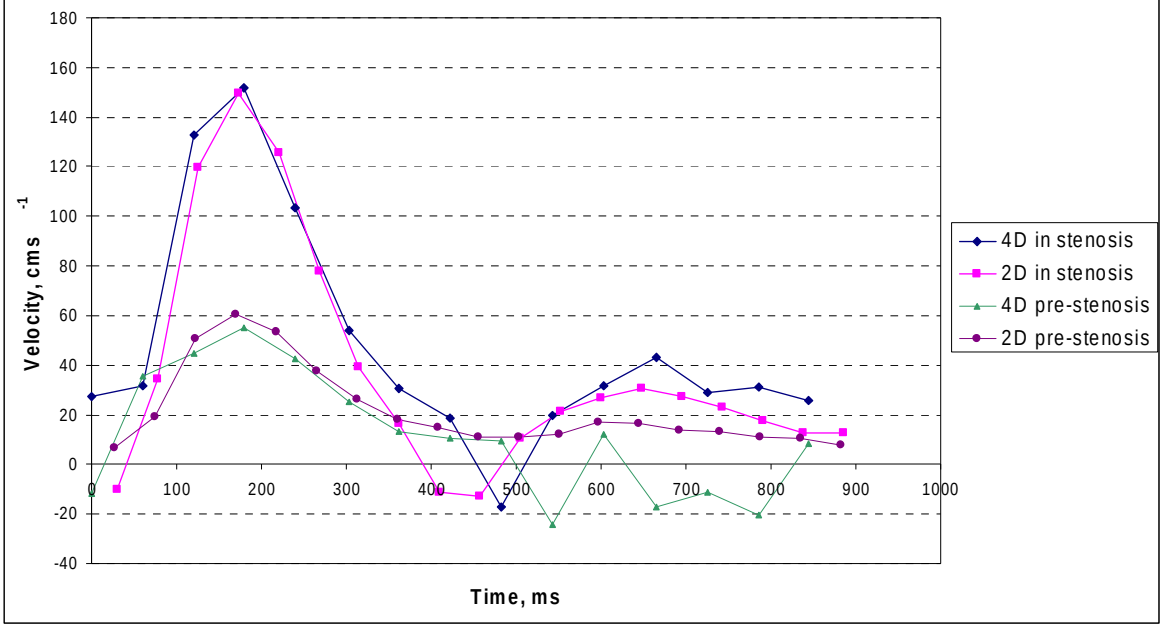

	Peak maximum velocity in the CCA(cms_{-1})	*Peak maximum velocity in the ICA stenosis (cms_{-1})*	*ICA_{PSV} / CCA_{PSV} Ratio*
2D PC-MRI	60.29	149.66	2.48
4D PC-MRI (2mm)	55.22	151.80	2.75
Criteria for 50 to 69 % stenosis		**>125**	**2 - 4**

Table 9.7: Peak maximum velocities and ICA_{PSV} / CCA_{PSV} ratios measured in the 50% stenosis phantom using 2D PC-MRI and 4D PC-MRI, compared with the criteria for a 50% to 69% stenosis.

The results for the 50% stenosis appear much closer than for the carotid phantom stenosis results. However, it is worth mentioning one key scan parameter that will affect the results. The in-plane pixel resolution of the 4D PC-MRI scans was 0.91 mm, this gives 19.3 pixels within the cross sectional area of the 4.0 mm diameter 50% stenosis but only 3.4 pixels within the cross sectional area of the 1.68 mm diameter carotid phantom stenosis. Such a small number of pixels will undoubtedly contribute to an averaging down of the velocities.

9.4.3 Results for the in-vivo example subject

A healthy 37 year old female volunteer, who was included in the comparative study cohort in chapter 8, also underwent 4D PC-MRI scanning. The maximum peak systolic velocity values were determined for the CCA, ICA, ECA and vertebral arteries bilaterally and the data set was pooled for comparison analysis. This subject has an unusually small right vertebral artery which was detected by Doppler and 2D PC-MRI but could not be resolved sufficiently for analysis by 4D PC-MRI. The right vertebral artery was, therefore, left out of the comparison. Bland-Altman comparison statistics and p-value for comparison of the 4D PC-MRI analysis of maximum peak systolic velocity compared against 2D PC-MRI and spectral Doppler ultrasound are shown in tables 9.8, 9.9 and 9.10.

Mean bias (cms^{-1})	Corrected Doppler	2D PC-MRI 4mm slice	4D PC-MRI 3mm slice	4D PC-MRI 4mm slice
Doppler		11.04	23.23	16.69
2D PC-MRI 4mm slice	**-5.57**		12.19	5.65
4D PC-MRI 3mm slice	**6.62**			-6.54
4D PC-MRI 4mm slice	**0.08**			

Table 9.8: Bland-Altman calculated mean bias for comparisons between 2D PC-MRI, 4D PC-MRI using 3mm and 4mm slice thickness widths and spectral Doppler ultrasound. Note: the second column is the comparison between the MRI measurements against spectral Doppler ultrasound corrected for maximum velocity error.

Limits of agreement, ±1.96SD (cms^{-1})	Corrected Doppler	2D PC-MRI 4mm slice	4D PC-MRI 3mm slice	4D PC-MRI 4mm slice
Doppler		18.87	22.47	26.61
2D PC-MRI 4mm slice	**12.16**		12.10	17.52
4D PC-MRI 3mm slice	**15.33**			8.37
4D PC-MRI 4mm slice	**20.13**			

Table 9.9: Bland-Altman calculated limits of agreement, ± 1.96*SD, for comparisons between 2D PC-MRI, 4D PC-MRI using 3mm and 4mm slice thickness widths and spectral Doppler ultrasound. Note: the second column is the comparison between the MRI measurements against spectral Doppler ultrasound corrected for maximum velocity error.

P value	Corrected Doppler	2D PC-MRI 4mm slice	4D PC-MRI 3mm slice	4D PC-MRI 4mm slice
Doppler		0.03	< 0.01	< 0.01
2D PC-MRI 4mm slice	**0.07**		< 0.01	0.17
4D PC-MRI 3mm slice	**0.08**			0.01
4D PC-MRI 4mm slice	**0.99**			

Table 9.10: P value for comparisons between 2D PC-MRI, 4D PC-MRI using 3mm and 4mm slice thickness widths and spectral Doppler ultrasound. Note: the second column is the comparison between the MRI measurements against spectral Doppler ultrasound corrected for maximum velocity error.

There was a significant ($p < 0.05$) difference between all PC-MRI measurements and spectral Doppler ultrasound. However, compared with ultrasound values corrected for the maximum velocity error, there was no significant difference for any of the PC-MRI techniques. For 4D PC-MRI compared against 2D PC-MRI, the 3 mm slice dataset consistently underestimated 2D values with a significant mean bias of 12.19 cms^{-1}. The 4 mm 4D slice dataset was not significantly

different from 2D measurements. There was a small but significant underestimation of the 3mm slice 4D PC-MRI compared with 4mm slice 4D PC-MRI.

The flow visualisation analysis software was also used with the *in-vivo* 4D data sets with a view to its potential in a larger study. Figure 9.11 showing the velocity vector patterns and figure 9.12 showing visualisation of flow streamlines give an indication of the potential of the software.

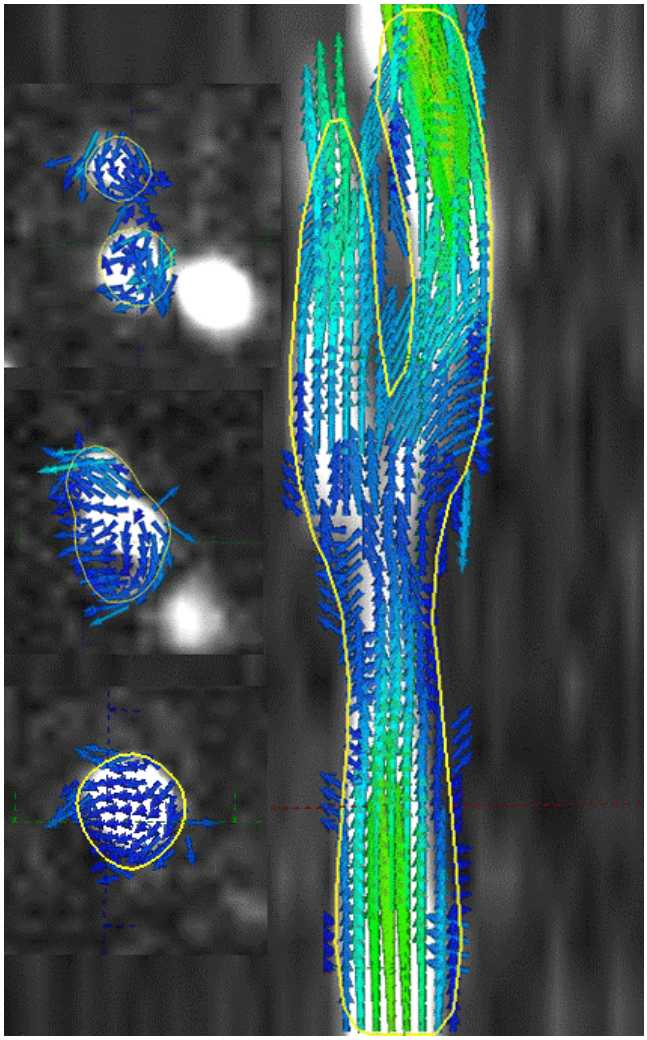

Figure 9.11: 4D PC-MRI flow vector mapping for the right side carotid bifurcation in a healthy volunteer subject. Insets on the right hand side show the flow in cross section with reasonably uniform flow in the common carotid, bottom, flow directions beginning to separate in the carotid bulb, middle, and separation of flow with an indication of spiral flow post-bifurcation, top.

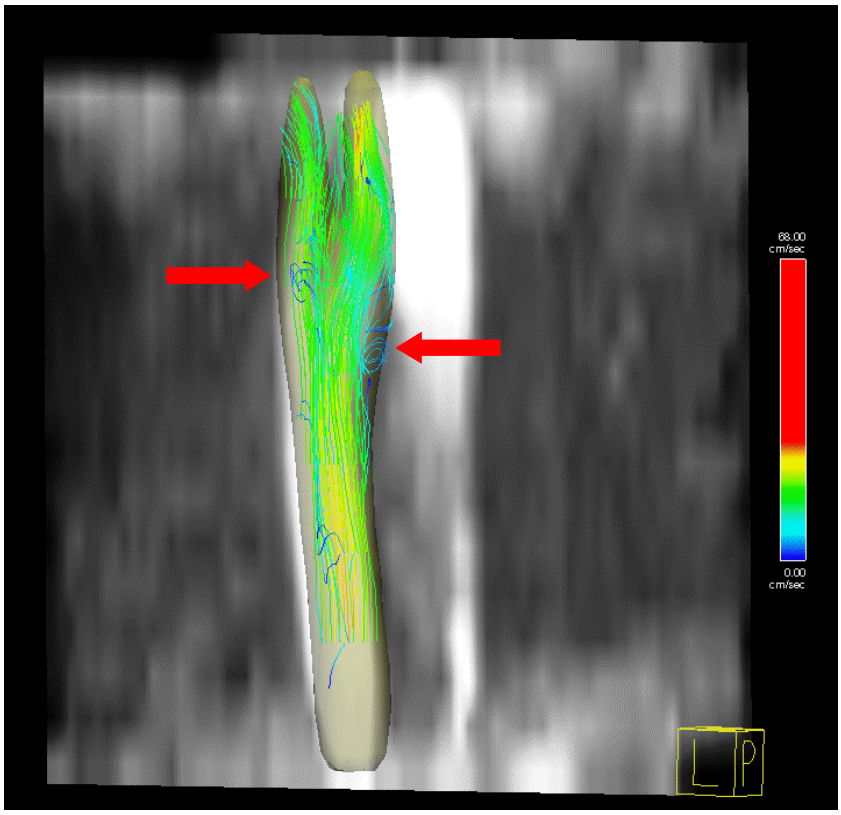

Figure 9.12: 4D PC-MRI stream line visualisation for the right side carotid bifurcation in a healthy volunteer subject. The red arrows highlight regions of possible disturbed flow due to the bifurcation.

9.5 Summary of results

4D PC-MRI flow represents a significant advance in the field of MRI blood flow imaging and quantification. Much of the focus of its use has been on the visualisation of flow patterns, while the possibilities of other quantification of parameters such as pressure differences (Bock et al. 2011), wall shear stress (Stalder et al. 2008) and pulse wave velocity (Markl et al. 2012b) offer potential enhancements in the assessment of atherosclerotic disease. Despite both the visualisation features and the quantification parameters being based on velocity measurement, there is little evidence in the literature of the consideration of velocity validation. Having carried out validation studies of 2D PC-MRI in this thesis, we had the opportunity to compare the 2D PC-MRI with 4D PC-MRI and to investigate the potential use of maximum velocity measurements and maximum velocity ratios from 4D data sets.

Validation of 2D PC-MRI and 4D PC-MRI steady state velocities against velocities from calibrated flow measurements revealed no significant difference for the mean velocities for 2D PC-MRI as was found in the steady state velocity studies in chapter 6. However, mean velocities for 4D PC-MRI and the maximum velocities for both PC-MRI methods significantly underestimated the calibrated values. Comparison of methods in the carotid phantom revealed the potential of 4D flow to underestimate the degree of stenosis based on maximum velocity and maximum velocity ratio measurement. Harloff et al. (Harloff et al. 2009) identified similar levels of velocity underestimation for 4D PC-MRI compared to spectral Doppler ultrasound in volunteer studies. Although they did not investigate the measurement of the high stenotic velocities and did not use the ICA_{PSV} / CCA_{PSV} ratios, it was found that, for the pulsatility and resistivity ratios, there was no significant difference between ultrasound and 4D PC-MRI. This supports our conclusion from chapters 7 and 8 that the use of spectral Doppler ultrasound ratios may be translated to 2D PC-MRI maximum velocity measurements with reasonable confidence. The same cannot yet be concluded for 4D PC-MRI maximum velocity measurement. The ability to navigate through the vessel to identify maximum velocity due to a stenosis was indeed easier than the guesswork involved in placing a single 2D velocity encoded slice. However,

the maximum velocity detected using 4D PC-MRI was significantly lower than for 2D PC-MRI.

Comparison with the results for the 50% stenosis phantom served to highlight the problem of pixel resolution when imaging small vessels. Agreement between 2D and 4D measurements appeared to be better in the 50% stenosis phantom than in the carotid phantom. However with far fewer pixels in the carotid stenosis cross section than in the 50% stenosis cross section, there would be considerable in-pixel averaging of velocities.

Results from our *in-vivo*, single volunteer example showed that, in terms of the measurement of maximum peak systolic velocities, correction of equivalent spectral Doppler ultrasound for maximum velocity errors removed the significance of any bias when compared with any 2D or 4D PC-MRI. Although results in this section should be viewed with caution as they represent only 7 data points in a single subject, they do agree with our findings for 3.0T 2D PC-MRI compared with corrected Doppler ultrasound in the comparative study in chapter 8. As in the phantom studies, 4D PC-MRI appeared to underestimate maximum peak velocities measured using 2D PC-MRI and the 3 mm slice measurements significantly underestimated those measured from 4 mm 4D PC-MRI slice data. The 3 mm slice 4D PC-MRI data also performed less well in the clear visualisation of flow vectors and streamline patterns and the promising images in the text are for the 4 mm slice data. One possible explanation may be that only the 4 mm slice thickness data has adequate signal level to produce the "correct" results from the vector calculations in the analysis software 4D reconstructions. However more work would be required to confirm this.

Temporal-spatial averaging has been acknowledged as a current limitation of 4D PC-MRI (Markl et al. 2012a) and more validation and optimisation studies are required to quantify and address this. 4D PC-MRI studies *in-vivo* tend to use a large field of view for multiple vessel visualisation, limiting the available spatio-temporal resolution. Potentially, the use of smaller 4D PC-MRI volumes, focused on an area of suspected stenosis or plaque, identified by anatomical imaging techniques, might help to address the underestimation of the quantification techniques.

4D PC-MRI offers an attractive flow quantification option with the ability to navigate along the time resolved velocity encoded 3D image of a vessel. However, the technique underestimates velocity measurement in smaller vessels and will require further optimisation before spectral Doppler ultrasound methods of haemodynamic quantification can be reliably translated to this new modality.

Chapter 10 – Summary of work and future directions

A key component, in achieving the aims of this thesis, was the establishment of a true dual-modality *in-vitro* system that could be used with confidence for the validation and comparison of velocity measurement techniques using PC-MRI and spectral Doppler ultrasound. A review of the literature revealed that, although dual modality phantoms had been proposed and developed (Allard et al. 2009; Cloutier et al. 2004; Frayne et al. 1993), there was no clear evidence of the use of a true dual-modality flow system for the comparison of velocity measurement using PC-MRI and ultrasound. There is no reason why commonly used configurations of ultrasound flow phantoms could not be adapted for use in an MRI scanner; something that was achieved easily by elimination of metallic components in the phantom housing and connection design. The flow system was adapted to use long lengths of connecting tubing for a flow circuit via the MR room waveguide. The MR scanner set-up was mimicked on a long lab bench for the ultrasound measurements to maintain the flow circuit and inlet lengths. Thus, an identical flow phantom configuration was constructed for validation and comparison studies.

The test phantom work provided a valuable body of evidence to inform and complement the *in-vivo* studies.

10.1 Summary of the main findings of the thesis

The study of PC-MRI for the measurement of flow velocities compared with spectral Doppler ultrasound in chapter 6, began, as for other authors, with validation against calibrated flow rates and steady state velocities. A significant finding here was the underestimation of flow rates by PC-MRI due to the lumen on the phase and magnitude images being smaller than the true lumen. While other authors (Bernstein, King, & Zhou 2004; Greil et al. 2002; Lotz et al. 2002; Lotz et al. 2005; Tang, Blatter, & Parker 1993) have described overestimation of flow rates due to partial volume effects; studies which have focussed on larger vessels such as the aorta. The underestimation of flow became worse at lower

velocities and for smaller vessels suggesting that low signal levels were contributing to the effect, particularly since we did not use contrast agents. However, with a relatively large pixel size compared with the vessel dimensions, it is likely that there is a degree of intra-voxel phase dispersion (McRobbie et al. 2003) where the pixels overlap with the vessel wall. Measurement of mean velocities derived from the flow volume calibrations showed agreement for both 3T and 1.5T PC-MRI measurements suggesting that the mean velocity measured using PC-MRI is a reliable measure of the true mean velocity.

The test phantom systems proved to be important vehicles for studies relating to the optimisation of PC-MRI study parameters in chapters 6 and 7. While the majority of the studies served to confirm findings by other authors in larger vessels, two parameters stood out as being of particular interest when applied to peripheral vessels and the potential to use maximum velocity measurements; temporal resolution and slice thickness.

The ideal protocol for time resolved PC-MRI measurement of flow velocities in small vessels would have high spatial and temporal resolution to map variations in velocity over the vessel cross section and to accurately identify key temporal features over the cardiac cycle. Minimising voxel dimensions and temporal sample point numbers (cardiac phases) is limited by the time required for the application of additional gradients for flow compensation and flow encoding and by the need to collect two full images for each timepoint within the cardiac cycle. Examination of different waveform patterns with different temporal resolutions revealed that, as might be expected, the highest resolution i.e. shortest TR values did indeed produce the highest peak maximum velocity values, due to less temporal averaging over the peak, but at the expense of longer scan times. However, even at high TR values PC-MRI appeared able to map the key temporal variations; important if spectral Doppler ultrasound waveform analysis techniques were to be adopted for PC-MRI. It was determined that having the number of cardiac phases at between 16 and 24 would give a reasonable compromise between maximising the peak maximum velocity and minimising scan times, accepting that the exact number in the *in-vivo* situation would depend on heart rate.

Having already minimised the possible pixel dimensions in the x,y image plane of the PC-MRI slice, the next voxel parameter of interest was the slice thickness. There appears to have been little attention paid to slice thickness optimisation in the literature, with some authors using relatively large slice thickness widths of up to 8mm (Seitz et al. 2001; Wetzel et al. 2001). Selection of an appropriate slice thickness is a balance between achieving adequate signal levels and the potential for averaging over the length of the voxel. This is particularly pertinent for smaller vessels where signal may be low and there may be short spatial variations within the slice. Our investigations in a straight tube phantom revealed that the smallest slice width gave the highest value for peak maximum velocity. However, introducing spatial variations such as the stenosis in the carotid phantom, showed that correct positioning of the slice within the stenotic jet was perhaps more important than the slice width itself. With a narrow slice it is easily possible to miss the position of peak velocity; a larger slice will mean more averaging but will have a higher chance of including the maximum velocity within the voxel. This is an area that appears to have been overlooked and which probably merits further investigation. A few authors have looked at stenotic jets in the aorta (O'Brien et al. 2008; Waters, Caruthers, & Wickline 2005) but have used large slice thicknesses (6 to 9 mm) and, although Waters did look at the effects of positioning, there do not appear to have been any studies attempting to optimise the slice thickness vs. position. Our investigations highlighted an issue that potentially may be resolved with the new 4D flow PC-MRI techniques which were discussed and investigated in chapter 9.

Comparison of maximum velocities and maximum velocity ratios, in the test phantom studies, even with an optimised scan protocol, was beginning to suggest that there was a significant underestimation of peak maximum velocities compared with spectral Doppler ultrasound, but that the maximum velocity ratios might be more reliably used between modalities. In our *in-vivo* studies in chapter 8, examination of data for the cohort of subjects who had taken part in both the un-optimised pilot study and the optimised comparison study, suggested that optimisation of the PC-MRI protocol did appear to improve the detection of maximum velocities using PC-MRI in comparison with spectral Doppler ultrasound. In this chapter we also used a very simple velocity correction factor for the peak maximum velocities determined using spectral

Doppler ultrasound. The mean percentage error on the maximum velocity discussed and determined in chapter 5, was applied and shown to effectively remove any significant difference between the optimised 3T PC-MRI measurements and the spectral Doppler measurements. Rather more encouraging were the results for the two-site velocity ratios which revealed no significant difference between measurement modalities. Results from the carotid phantom suggest that this may also be true for other commonly used velocity ratios. Although the potential for the direct translation of maximum velocity ratios from spectral Doppler ultrasound to PC-MRI is promising, it should be received with caution. Ideally the ratios should be tested on a range of waveforms and degrees of stenosis both *in-vitro* and *in-vivo* and further investigation is merited.

To summarise, we can return to the original hypotheses outlines in chapter 1:

a) There is no difference in the velocity of arterial blood as measured using spectral Doppler ultrasound or PC-MRI techniques. ***False: PC-MRI significantly underestimates measurements made using spectral Doppler ultrasound***.

b) There is a difference in the velocity of arterial blood, as measured using spectral Doppler ultrasound or PC-MRI techniques, which takes the form of a quantifiable direct relationship between the two measurements. ***True: however, the difference is due to the maximum velocity estimation error for spectral Doppler ultrasound. Determination of that error and correction of spectral Doppler ultrasound will remove the difference between modalities***.

c) There is no difference in the maximum velocity ratios for blood flow measured using spectral Doppler ultrasound or PC-MRI techniques. ***True: There is no significant difference between maximum velocity ratios, with no need for velocity correction to establish this***.

10.2 The practicalities of using PC-MRI to aid in the diagnosis of peripheral vascular disease.

Contrast enhanced MRI is the preferred MRI method of imaging for peripheral vascular disease due to its ability to produce rapid and detailed anatomical images of the entire vascular system without the need to use gating or breath-hold techniques. The imaging can usually be done without the presence of a radiologist, who would usually report on the scan volume off-line. The addition of 2D PC-MRI quantification slices would require assessment of the CE-MRA images to determine the presence of any stenosis and decisions regarding the positional placement of the velocity encoded slices. While this might be a feasible protocol for further research, it may not be appropriate for routine imaging and is unlikely to replace spectral Doppler ultrasound in those regions easily accessed by ultrasound. However for those lesions commonly found in the aorto-iliac segment and less commonly in the subclavian segment (Beard & Gaines 2009) it has the potential to assist in diagnosis by measuring blood flow velocities and ratios around stenosis sites. Potentially particularly useful where there is uncertainty in the degree of stenosis from the CE-MRI and where assessment of the quality of blood flow in potential graft anastomosis sites is required.

10.3 New technologies and other clinical applications

The emergence of 4D PC-MRI represents a major addition to the toolkit available for blood flow quantification in MRI. Although, not yet commercially available on the majority of scanners, interest in and enthusiasm for the technique is causing it to evolve rapidly (Markl et al. 2012a). The development of parallel imaging strategies to reduce timescales have made 4D PC-MRI a feasible tool for the visualisation and quantification of blood flow. It also represents a possible solution to one of the 2D PC-MRI flaws that was identified in this thesis i.e. correct positioning of the 2-D velocity encoded slice. The 4-D technique involves collecting a volume of data encompassing a section of the vessel of interest, with velocity encoding in all three directions. During off-line analysis, the user is able to simply navigate a plane through the vessel to measure velocities. As for 2D PC-MRI, most of the development work in what has become known as 4D

flow, has been focussed around the heart and the great vessels. However, this has not prevented exploration of the potential use in other vascular applications. The studies in this thesis have focussed on validation and comparison of peripheral velocities and velocity ratios with a view to the use of 2D PC-MRI velocities in peripheral vascular territories that are difficult to access using ultrasound. Having established that, although there are significant differences between the PC-MRI and spectral Doppler ultrasound measurements of maximum velocity, maximum velocity ratios might be translated reliably between modalities, and so we can identify some key areas where 2D and 4D PC-MRI may have a role.

10.3.1 Aorto-iliac vascular disease

CE-MRA is the imaging modality of choice for patients presenting with critical limb ischaemia or for thigh and buttock claudication where treatment may be indicated (Norgren et al. 2007; SIGN 89 2006). It is possible to image the aorto-iliac segment using ultrasound, however, this region is notoriously difficult to image, particularly in the larger patient and in the presence of bowel gas. Although PC-MRA techniques have been used in this segment (Steffens et al. 1997) the interest has remained anatomical with only one author (Wentland et al. 2006) attempting flow volume quantification in healthy volunteers. The vessels in the aorto-iliac segment are relatively large (around 1 cm) and easily imaged using CE-MRA so that there is no reason why 2D PC-MRI at selected sites could not be added to the scan protocol to quantify blood flow. In Doppler ultrasound scans of the lower limb, the pulsatility index, PI, in the distal common femoral artery in the groin is used as a measure of the dampening due to a proximal stenosis. However, there is some doubt as to the utility of this measure (Reddy et al. 1986). A comparative study of Doppler ultrasound and PC-MRI would enable the significance of the PI to be tested by measuring it using both techniques and using PC-MRI to examine the stenosis proximal to the groin. PC-MRI waveform and ratios would also enable quantification of flow at potential anastomosis sites prior to vascular graft surgery. Frydrychowicz et al. (Frydrychowicz et al. 2007) have extended the 4D flow techniques developed for visualisation of the aorta to image from the distal aorta down to the superficial femoral artery. Although focussing on visualisation of flow patterns, they did

demonstrate the facility of having velocity waveforms at selected sites along the arterial pathway.

10.3.2 Renal arteries

A recent review of imaging options for the diagnosis of renal artery stenosis (Zhang et al. 2009) stated that in comparison with other imaging modalities "Ultrasonography is the safest and least expensive but also the least accurate and most operator-dependent". Reasons for the negative part of that statement include difficult imaging due to bowel gas and body habitus as well as the technical challenges of imaging a small (5 to 6 mm diameter) artery at depth which requires lower frequencies with the consequent trade-off in poorer resolution. 2-D PC MRI has been used successfully to image the renal arteries and make measurements of renal blood flow, RBF, in the form of volume flow rates (Dambreville et al. 2010; Schoenberg et al. 2003; Zhang & Prince 2004). Although the satisfactory depiction of velocity waveforms has been noted (Schoenberg et al. 1997), investigators do not appear to have attempted to use key velocity indexes that would be used in spectral Doppler ultrasound studies: the ratio of peak systolic velocity in the renal artery to that in the aorta, known as the RAR, and the resistivity index, RI, as defined in chapter 3. The pulsatility index, PI also defined in chapter 3, would also give a useful indication of the dampening due to a proximal renal artery stenosis. For patients undergoing standard MRA of the abdomen for renal indications, the addition of a few carefully placed velocity encoded PC-MRI slices would not add significantly to the overall scan time and would allow RBF as well as velocity ratios to be determined. More recently, Bley et al. (Bley et al. 2011) have applied 4D VIPR (vastly undersampled isotropic projection reconstruction) techniques in animal studies to visualise and measure pressure changes across renal artery stenosis in comparison with invasive pressure transducer guide-wire techniques. Their results showed that pressures measured using 4D VIPR generally underestimated pressures measured using the invasive technique. It should also be noted that for stenosis ≥ 75%, 4D VIPR could not be used, highlighting the need for further optimisation before 4D PC-MRI techniques can realistically and reliably tackle smaller vessels.

10.3.3 Hepato-portal vessels

Doppler ultrasound imaging and quantification of the hepatic and portal veins is fairly well established (SVT 2004) and imaging of this segment rarely problematic except, perhaps, in the presence of very fatty livers. Imaging is usually accompanied by detailed B-mode imaging assessment with a qualitative assessment of spectral waveforms and noting of maximum velocity values rather than ratios. Only a few attempts have been made at flow and velocity quantification in the portal vein using 2D PC-MRI (Applegate et al. 1993; Sugano et al. 1999). Since velocity ratios are rarely used in association with this technique the use of 2D PC-MRI is unlikely to add anything to the diagnosis. However, 4D PC-MRI has been successfully tested in the hepato-portal regions using both radial (Roldan-Alzate et al. 2012) and Cartesian (Stankovic et al. 2010) geometries for visualisation and quantification. Images from the studies appear to suggest that radial techniques may be particularly effective at segmentation of complex vascularity in that region.

10.3.4 Subclavian arteries

The supra-aortic vessels in the upper thorax are easily imaged using MRA techniques but their anatomical position makes them difficult to image using ultrasound. The Doppler ultrasound diagnosis of a stenosis in the innonimate or subclavian arteries often has to be evaluated using indirect measures such as retrograde flow in the vertebral artery or damped waveforms in the brachial artery. There are only isolated case study reports in the literature relating to attempts to quantify subclavian stenosis and subclavian steal using 2D-PC MRI (Akin et al. 2011; Bauer et al. 2009). This is an area where there is unexplored potential to enhance the quantification of stenosis by using ratios based on pre, post and maximum velocity values. Quantitative evaluation by PC-MRA combined with qualitative evaluation using CE-MRA might be considered equivalent to the pre-operative accepted practice of having a stenosis diagnosed by Doppler ultrasound confirmed by MRA or vice versa. 72% of symptomatic subclavian artery lesions have concomitant vascular lesions in the carotid and vertebral arteries (Beard & Gaines 2009). MRA imaging for suspected subclavian lesions will generally image from the aortic arch to the circle-of-Willis, so that any

concomitant carotid lesions detected could be quantified haemodynamically during the same MRI session, avoiding the need for a carotid Doppler scan. Although 4D PC-MRA techniques have been demonstrated in the aorta, extra-cranial and intra-cranial arteries, the supra-aortic region appears to have been overlooked.

10.3.5 Extra- and intra-cranial arteries

Doppler ultrasound of the extra-cranial carotid and vertebral arteries is well established and it is unlikely that MRA will replace it as a first line diagnostic tool for suspected carotid disease or that PC-MRA would be incorporated into the those MRA scans. However, MRA has an important role as a secondary confirmation of carotid disease prior to any intervention, with imaging of a larger anatomic region able to detect any concomitant subclavian disease or intra-cranial problems. In such cases, PC-MRA could be used to quantify blood flow through stenosis. There has been considerable interest in the application of 4D PC-MRI in the extra-cranial carotid arteries (Harloff et al. 2009), although the majority of studies focus, not on the measurement of velocities, rather the visualisation of complex flow patterns and the potential to measure parameters derived from velocity data such as wall shear stress, WSS (Markl et al. 2012a).

Ultrasound scanning of the intracranial arteries can only be performed using limited acoustic windows, the most common being the temporal. The two Doppler ultrasound methods used to evaluate the intra-cranial arteries are both limited in the information they can provide. It is possible to image short segments of the cerebral arteries and detect spectral Doppler waveforms using transcranial colour Doppler, TCCD. Alternatively, transcranial Doppler, TCD is a non imaging technique that produces spectral Doppler waveforms and is often used to “listen” for emboli for periods of up to an hour. In contrast, MRA techniques give a full anatomic visualisation of the intracranial arteries. While there have been limited attempts to make measurements using 2D PC-MRI (Meckel et al. 2012), there has been considerable interest in using 4D-PC MRI for the visualisation of intracranial haemodynamics, particularly the complex flow within aneurysms (Hollnagel et al. 2009; Hope et al. 2010; Wetzel et al. 2007).

10.4 Suggested follow-on studies

The discussion above reviewed an array of potential clinical applications. However, there is undoubtedly further technical and clinical validation to be done before velocity quantification methods using PC-MRA are used routinely in peripheral vascular assessment. 2D PC-MRI quantification techniques to collect velocity data at selected positions will add very little time to a scan, the most significant difference from a routine CE-MRA scan will be the addition of cardiac gating. The work of this thesis suggests that the maximum velocity ratios used in vascular spectral Doppler examinations can be used with maximum velocities from PC-MRI data. More work is required to confirm that this remains the case for a variety of stenotic lesions *in-vitro* and *in-vivo*. The emergence of 4D PC-MRI techniques and the availability of WIP protocols and analysis software point towards inclusion and optimisation of 4D techniques in peripheral vascular studies. The following studies are suggested as appropriate follow-on work arising from this thesis.

10.4.1 In-vitro study of 2D and 4D PC-MRI in comparison with spectral Doppler ultrasound techniques for the quantification of haemodynamic parameters associated with stenosis.

This study would expand on the test phantom work of this thesis to develop a range of stenoses in a range of different diameter vessels with a wider range of pulsatile flow patterns, extending the 2D PC-MRI validation against Doppler. Our experience of the 4D PC-MRI WIP suggests that it requires further optimisation and a program of studies, similar to those performed for 2D PC-MRI, which should be planned before introducing it into the comparison studies. It may also be prudent to consider MRA methods of imaging and grading stenoses with a view to comparative clinical techniques.

10.4.2 In-vivo study of 2D and 4D PC-MRI in comparison with spectral Doppler ultrasound techniques for the quantification of haemodynamic parameters associated with stenosis.

A first stage in incorporating PC-MRA techniques into clinical diagnosis in the peripheral vascular system would be a study involving patients with known or suspected vascular stenosis. Patients would be selected at the vascular clinic stage and would comprise those patients who would be referred for imaging as part of the normal care pathway. In patients who would be expected to have routine CE-MRA, resulting images and diagnosis would be available for comparison with the velocity based techniques. All patients agreeing to take part in the study would undergo Doppler ultrasound imaging, 2D PC MRI and 4D PC MRI. The suggested anatomic territories would be the carotid and subclavian arteries and the aorto-iliac and femoral arteries, giving two regions easily accessed by ultrasound and two regions where ultrasound imaging and Doppler can be more difficult.

List of References

Akin, K., Kosehan, D., Kirbas, I., Yildirim, M., & Koktener, A. 2011, "Diagnosis and percutaneous treatment of partial subclavian steal: Doppler ultrasonography and phase contrast magnetic resonance angiography findings and a brief review of the literature", *Jpn.J.Radiol.*, vol. 29, no. 3, pp. 207-211.

Allard, L., Soulez, G., Chayer, B., Treyve, F., Qin, Z., & Cloutier, G. 2009, "Multimodality vascular imaging phantoms: a new material for the fabrication of realistic 3D vessel geometries", *Med.Phys.*, vol. 36, no. 8, pp. 3758-3763.

Applegate, G. R., Thaete, F. L., Meyers, S. P., Davis, P. L., Talagala, S. L., Recht, M., Wozney, P., & Kanal, E. 1993, "Blood flow in the portal vein: velocity quantitation with phase-contrast MR angiography", *Radiology*, vol. 187, no. 1, pp. 253-256.

Back, M. R., Wilson, J. S., Rushing, G., Stordahl, N., Linden, C., Johnson, B. L., & Bandyk, D. F. 2000, "Magnetic resonance angiography is an accurate imaging adjunct to duplex ultrasound scan in patient selection for carotid endarterectomy", *J.Vasc.Surg.*, vol. 32, no. 3, pp. 429-438.

Barber, F. E., Baker, D. W., Nation, A. W., Strandness, D. E., Jr., & Reid, J. M. 1974, "Ultrasonic duplex echo-Doppler scanner", *IEEE Trans.Biomed.Eng*, vol. 21, no. 2, pp. 109-113.

Bauer, A. M., Amin-Hanjani, S., Alaraj, A., & Charbel, F. T. 2009, "Quantitative magnetic resonance angiography in the evaluation of the subclavian steal syndrome: report of 5 patients", *J.Neuroimaging*, vol. 19, no. 3, pp. 250-252.

Beach, K. W., Leotta, D. F., & Zierler, R. E. 2012, "Carotid Doppler velocity measurements and anatomic stenosis: correlation is futile", *Vasc.Endovascular.Surg.*, vol. 46, no. 6, pp. 466-474.

Beard, J. D. & Gaines, P. A. 2009, *Vascular and endovascular surgery* Elsevier Health Sciences.

Bernstein, M. A., King, K. F., & Zhou, X. J. 2004, *Handbook of MRI Pulse Sequences* Academic Press.

Bilecen, D., Schulte, A. C., Heidecker, H. G., Aschwanden, M., Huegli, R., Jaeger, K. A., Ostheim-Dzerowycz, W., & Bongartz, G. 2005, "Lower extremity: low-dose contrast agent intraarterial MR angiography in patients--initial results", *Radiology*, vol. 234, no. 1, pp. 250-255.

Blackshear, W. M., Phillips, D. J., Chikos, P. M., Harley, J. D., Thiele, B. L., & Strandness, D. E., Jr. 1980, "Carotid artery velocity patterns in normal and stenotic vessels", *Stroke*, vol. 11, no. 1, pp. 67-71.

Blaimer, M., Breuer, F., Mueller, M., Heidemann, R. M., Griswold, M. A., & Jakob, P. M. 2004, "SMASH, SENSE, PILS, GRAPPA: how to choose the optimal method", *Top.Magn Reson.Imaging*, vol. 15, no. 4, pp. 223-236.

Bland, J. M. & Altman, D. G. 1986, "Statistical methods for assessing agreement between two methods of clinical measurement", *Lancet*, vol. 1, no. 8476, pp. 307-310.

Bley, T. A., Johnson, K. M., Francois, C. J., Reeder, S. B., Schiebler, M. L., Landgraf, R., Consigny, D., Grist, T. M., & Wieben, O. 2011, "Noninvasive assessment of transstenotic pressure gradients in porcine renal artery stenoses by using vastly undersampled phase-contrast MR angiography", *Radiology*, vol. 261, no. 1, pp. 266-273.

Bluth, E. I., Stavros, A. T., Marich, K. W., Wetzner, S. M., Aufrichtig, D., & Baker, J. D. 1988, "Carotid duplex sonography: a multicenter recommendation for standardized imaging and Doppler criteria", *Radiographics*, vol. 8, no. 3, pp. 487-506.

Bock, J., Frydrychowicz, A., Lorenz, R., Hirtler, D., Barker, A. J., Johnson, K. M., Arnold, R., Burkhardt, H., Hennig, J., & Markl, M. 2011, "In vivo noninvasive 4D pressure difference mapping

in the human aorta: phantom comparison and application in healthy volunteers and patients", *Magn Reson.Med.*, vol. 66, no. 4, pp. 1079-1088.

Bradbury, A. W. & Adam, D. J. 2007, "Diagnosis of peripheral arterial disease of the lower limb", *BMJ*, vol. 334, no. 7606, pp. 1229-1230.

Brandts, A., Roes, S. D., Doornbos, J., Weiss, R. G., de Roos, A., Stuber, M., & Westenberg, J. J. 2010, "Right coronary artery flow velocity and volume assessment with spiral K-space sampled breathhold velocity-encoded MRI at 3 tesla: accuracy and reproducibility", *J.Magn Reson.Imaging*, vol. 31, no. 5, pp. 1215-1223.

Browne, J. E., Ramnarine, K. V., Watson, A. J., & Hoskins, P. R. 2003, "Assessment of the acoustic properties of common tissue-mimicking test phantoms", *Ultrasound Med.Biol.*, vol. 29, no. 7, pp. 1053-1060.

Caputo, G. R. & Higgins, C. B. 1992, "Magnetic resonance angiography and measurement of blood flow in the peripheral vessels", *Invest Radiol.*, vol. 27 Suppl 2, pp. S97-102.

Caputo, G. R., Masui, T., Gooding, G. A., Chang, J. M., & Higgins, C. B. 1992, "Popliteal and tibioperoneal arteries: feasibility of two-dimensional time-of-flight MR angiography and phase velocity mapping", *Radiology*, vol. 182, no. 2, pp. 387-392.

Chan, D., Anderson, M. E., & Dolmatch, B. L. 2010, "Imaging evaluation of lower extremity infrainguinal disease: role of the noninvasive vascular laboratory, computed tomography angiography, and magnetic resonance angiography", *Tech.Vasc.Interv.Radiol.*, vol. 13, no. 1, pp. 11-22.

Chang, W., Landgraf, B., Johnson, K. M., Kecskemeti, S., Wu, Y., Velikina, J., Rowley, H., Wieben, O., Mistretta, C., & Turski, P. 2011, "Velocity measurements in the middle cerebral arteries of healthy volunteers using 3D radial phase-contrast HYPRFlow: comparison with transcranial Doppler sonography and 2D phase-contrast MR imaging", *AJNR Am.J.Neuroradiol.*, vol. 32, no. 1, pp. 54-59.

Cho, L., Casserly, I. P., & Wholey, M. H. 2005, "Subclavian, Brachocephalic and Upper Extremity," in *Manual of peripheral vascular intervention*, I. P. Casserly, R. Sachar, & J. S. Yadav, eds., Lippincott Williams & Wilkins, Philadelphia, USA, p. 120139.

Chu, K. C. & Rutt, B. K. 1997, "Polyvinyl alcohol cryogel: an ideal phantom material for MR studies of arterial flow and elasticity", *Magn Reson.Med.*, vol. 37, no. 2, pp. 314-319.

Cloutier, G., Soulez, G., Qanadli, S. D., Teppaz, P., Allard, L., Qin, Z., Cloutier, F., & Durand, L. G. 2004, "A multimodality vascular imaging phantom with fiducial markers visible in DSA, CTA, MRA, and ultrasound", *Med.Phys.*, vol. 31, no. 6, pp. 1424-1433.

Collins, R., Burch, J., Cranny, G., Aguiar-Ibanez, R., Craig, D., Wright, K., Berry, E., Gough, M., Kleijnen, J., & Westwood, M. 2007a, "Duplex ultrasonography, magnetic resonance angiography, and computed tomography angiography for diagnosis and assessment of symptomatic, lower limb peripheral arterial disease: systematic review", *BMJ*, vol. 334, no. 7606, p. 1257.

Collins, R., Cranny, G., Burch, J., Aguiar-Ibanez, R., Craig, D., Wright, K., Berry, E., Gough, M., Kleijnen, J., & Westwood, M. 2007b, "A systematic review of duplex ultrasound, magnetic resonance angiography and computed tomography angiography for the diagnosis and assessment of symptomatic, lower limb peripheral arterial disease", *Health Technol.Assess.*, vol. 11, no. 20, pp. iii-xiii, 1.

Corriveau, M. M. & Johnston, K. W. 2004, "Interobserver variability of carotid Doppler peak velocity measurements among technologists in an ICAVL-accredited vascular laboratory", *J.Vasc.Surg.*, vol. 39, no. 4, pp. 735-741.

Cosford, P. A. & Leng, G. C. 2007, "Screening for abdominal aortic aneurysm", *Cochrane.Database.Syst.Rev.* no. 2, p. CD002945.

Culjat, M. O., Goldenberg, D., Tewari, P., & Singh, R. S. 2010, "A review of tissue substitutes for ultrasound imaging", *Ultrasound Med.Biol.*, vol. 36, no. 6, pp. 861-873.

Dambreville, S., Chapman, A. B., Torres, V. E., King, B. F., Wallin, A. K., Frakes, D. H., Yoganathan, A. P., Wijayawardana, S. R., Easley, K., Bae, K. T., & Brummer, M. E. 2010, "Renal arterial blood flow measurement by breath-held MRI: Accuracy in phantom scans and reproducibility in healthy subjects", *Magn Reson.Med.*, vol. 63, no. 4, pp. 940-950.

Delfino, J. G., Bhasin, M., Cole, R., Eisner, R. L., Merlino, J., Leon, A. R., & Oshinski, J. N. 2006, "Comparison of myocardial velocities obtained with magnetic resonance phase velocity mapping and tissue Doppler imaging in normal subjects and patients with left ventricular dyssynchrony", *J.Magn Reson.Imaging*, vol. 24, no. 2, pp. 304-311.

DONALD, I., MACVICAR, J., & BROWN, T. G. 1958, "Investigation of abdominal masses by pulsed ultrasound", *Lancet*, vol. 1, no. 7032, pp. 1188-1195.

Dumoulin, C. L. 1995, "Phase-Contrast Magnetic Resonance Angiography," in *Magnetic resonance angiography : a practical approach*, E. K. Yucel, ed., McGraw-Hill Inc., pp. 19-33.

Dumoulin, C. L., Souza, S. P., Walker, M. F., & Wagle, W. 1989, "Three-dimensional phase contrast angiography", *Magn Reson.Med.*, vol. 9, no. 1, pp. 139-149.

Eicke, B. M., Kremkau, F. W., Hinson, H., & Tegeler, C. H. 1995, "Peak velocity overestimation and linear-array spectral Doppler", *J Neuroimaging*, vol. 5, no. 2, pp. 115-121.

European Carotid Surgery Trialists' Collaborative Group 1991, "MRC European Carotid Surgery Trial: interim results for symptomatic patients with severe (70-99%) or with mild (0-29%) carotid stenosis", *The Lancet*, vol. 337, no. 8752, pp. 1235-1243.

Evans, D. H. 1985, "On the measurement of the mean velocity of blood flow over the cardiac cycle using Doppler ultrasound", *Ultrasound Med Biol.*, vol. 11, no. 5, pp. 735-741.

Evans, D. H., Jensen, J. A., & Nielsen, M. B. 2011, "Ultrasonic colour Doppler imaging", *Interface Focus.*, vol. 1, no. 4, pp. 490-502.

Evans, D. H. & McDicken, W. N. 2000, *Doppler Ultrasound: Physics Instrumentation and Signal Processing* Wiley, Chichester.

Fillinger, M. F., Baker, R. J., Jr., Zwolak, R. M., Musson, A., Lenz, J. E., Mott, J., Bech, F. R., Walsh, D. B., & Cronenwett, J. L. 1996, "Carotid duplex criteria for a 60% or greater angiographic stenosis: variation according to equipment", *J.Vasc.Surg.*, vol. 24, no. 5, pp. 856-864.

Finn, J. P., Nael, K., Deshpande, V., Ratib, O., & Laub, G. 2006, "Cardiac MR imaging: state of the technology", *Radiology.*, vol. 241, no. 2, pp. 338-354.

Fowkes, F. G., Housley, E., Cawood, E. H., Macintyre, C. C., Ruckley, C. V., & Prescott, R. J. 1991, "Edinburgh Artery Study: prevalence of asymptomatic and symptomatic peripheral arterial disease in the general population", *Int.J Epidemiol.*, vol. 20, no. 2, pp. 384-392.

Francois, C. J., Lum, D. P., Johnson, K. M., Landgraf, B. R., Bley, T. A., Reeder, S. B., Schiebler, M. L., Grist, T. M., & Wieben, O. 2011, "Renal arteries: isotropic, high-spatial-resolution, unenhanced MR angiography with three-dimensional radial phase contrast", *Radiology*, vol. 258, no. 1, pp. 254-260.

Frayne, R., Gowman, L. M., Rickey, D. W., Holdsworth, D. W., Picot, P. A., Drangova, M., Chu, K. C., Caldwell, C. B., Fenster, A., & Rutt, B. K. 1993, "A geometrically accurate vascular phantom for comparative studies of x-ray, ultrasound, and magnetic resonance vascular imaging: construction and geometrical verification", *Med.Phys.*, vol. 20, no. 2 Pt 1, pp. 415-425.

Friedman, S. G., Hainline, B., Feinberg, A. W., Lesser, M. L., & Napolitano, B. A. 1988, "Use of diastolic velocity ratios to predict significant carotid artery stenosis", *Stroke*, vol. 19, no. 7, pp. 910-912.

Frydrychowicz, A., Francois, C. J., & Turski, P. A. 2011, "Four-dimensional phase contrast magnetic resonance angiography: potential clinical applications", *Eur.J.Radiol.*, vol. 80, no. 1, pp. 24-35.

Frydrychowicz, A., Landgraf, B. R., Niespodzany, E., Verma, R. W., Roldan-Alzate, A., Johnson, K. M., Wieben, O., & Reeder, S. B. 2011, "Four-dimensional velocity mapping of the hepatic and splanchnic vasculature with radial sampling at 3 tesla: a feasibility study in portal hypertension", *J.Magn Reson.Imaging*, vol. 34, no. 3, pp. 577-584.

Frydrychowicz, A., Winterer, J. T., Zaitsev, M., Jung, B., Hennig, J., Langer, M., & Markl, M. 2007, "Visualization of iliac and proximal femoral artery hemodynamics using time-resolved 3D phase contrast MRI at 3T", *J.Magn Reson.Imaging*, vol. 25, no. 5, pp. 1085-1092.

Fung, A. Y. & Saw, J. 2007, "Epidemiology and Significance of Carotid Artery Stenosis," in *Comtemporary Cardiology: Handbook of Complex Percutaneous Carotid Intervention*, J. Saw et al., eds., Humana Press Inc., Totowa, NJ, USA, pp. 3-10.

Gardner, M. J. & Altman, D. G. 1986, "Confidence intervals rather than P values: estimation rather than hypothesis testing", *Br.Med.J.(Clin.Res.Ed)*, vol. 292, no. 6522, pp. 746-750.

Gaynor, L., Byrne, B., Costello, D., Rowan, M., King, D., Browne, J., & Kenny, P. 2008a, "Accuracy of Peak Velocity Measurements in Doppler Ultrasound", *Irish Journal of Medical Science*, vol. 177, no. 8.

Gaynor, L., Byrne, B., Costello, D., Rowan, M., King, D., Browne, J., & Kenny, P. 2008b, "Accuracy of Peak Velocity Measurements in Doppler Ultrasound", Conference presentation The Irish Cardiac Society Meeting October 2008, web presentation accesses December 2012 http://www.isct.ie/presentations/AccuracyofPeakVelocityMeasurementsinDopplerUltrasound.pdf

George, A. K., Derbyshire, J. A., Saybasili, H., Saikus, C. E., Kocaturk, O., Guttman, M. A., McVeigh, E. R., Lederman, R. J., & Faranesh, A. Z. 2010, "Visualization of active devices and automatic slice repositioning for MRI-guided interventions", *Magnetic Resonance in Medicine*, vol. 63, no. 4, pp. 1070-1079.

Geva, T. 2006, "Magnetic resonance imaging: historical perspective", *J Cardiovasc.Magn Reson.*, vol. 8, no. 4, pp. 573-580.

Gittins, J. & Martin, K. 2010, "The leicester Doppler phantom--a digital electronic phantom for ultrasound pulsed Doppler system testing", *Ultrasound Med.Biol.*, vol. 36, no. 4, pp. 647-655.

Gosling, R. G. & King, D. H. 1974 "Arterial assessment by Doppler shift ultrasound", *Proc. R. Soc. Med.*, vol. 67, no.6, pp. 447-449.

Greil, G., Geva, T., Maier, S. E., & Powell, A. J. 2002, "Effect of acquisition parameters on the accuracy of velocity encoded cine magnetic resonance imaging blood flow measurements", *J.Magn Reson.Imaging*, vol. 15, no. 1, pp. 47-54.

Griswold, M. A., Jakob, P. M., Heidemann, R. M., Nittka, M., Jellus, V., Wang, J., Kiefer, B., & Haase, A. 2002, "Generalized autocalibrating partially parallel acquisitions (GRAPPA)", *Magn Reson.Med*, vol. 47, no. 6, pp. 1202-1210.

Gu, T., Korosec, F. R., Block, W. F., Fain, S. B., Turk, Q., Lum, D., Zhou, Y., Grist, T. M., Haughton, V., & Mistretta, C. A. 2005, "PC VIPR: a high-speed 3D phase-contrast method for flow quantification and high-resolution angiography", *AJNR Am.J.Neuroradiol.*, vol. 26, no. 4, pp. 743-749.

Guidi, G., Licciardello, C., & Falteri, S. 2000, "Intrinsic spectral broadening (ISB) in ultrasound Doppler as a combination of transit time and local geometrical broadening", *Ultrasound Med.Biol.*, vol. 26, no. 5, pp. 853-862.

Hadlock, J. & Beach, K. W. 2009, "Velocity variability in ultrasonic Doppler examinations", *Ultrasound Med Biol.*, vol. 35, no. 6, pp. 949-954.

Harloff, A., Albrecht, F., Spreer, J., Stalder, A. F., Bock, J., Frydrychowicz, A., Schollhorn, J., Hetzel, A., Schumacher, M., Hennig, J., & Markl, M. 2009, "3D blood flow characteristics in the carotid artery bifurcation assessed by flow-sensitive 4D MRI at 3T", *Magn Reson.Med.*, vol. 61, no. 1, pp. 65-74.

Hedrick, W. R. & Hykes, D. L. 1995, "Autocorrelation Detection in Color Doppler Imaging: A Review", *Journal of Diagnostic Medical Sonography*, vol. 11, no. 1, pp. 16-22.

Heverhagen, J. T., Hoppe, M., Klose, K. J., & Wagner, H. J. 2002, "Does the application of gadolinium-DTPA have an impact on magnetic resonance phase contrast velocity measurements? Results from an in vitro study", *Eur.J.Radiol.*, vol. 44, no. 1, pp. 65-69.

Hingorani, A., Ascher, E., Markevich, N., Kallakuri, S., Hou, A., Schutzer, R., & Yorkovich, W. 2004a, "Magnetic resonance angiography versus duplex arteriography in patients undergoing lower extremity revascularization: which is the best replacement for contrast arteriography?", *J.Vasc.Surg.*, vol. 39, no. 4, pp. 717-722.

Hingorani, A., Ascher, E., Markevich, N., Kallakuri, S., Schutzer, R., Yorkovich, W., & Jacob, T. 2004b, "A comparison of magnetic resonance angiography, contrast arteriography, and duplex arteriography for patients undergoing lower extremity revascularization", *Ann.Vasc.Surg.*, vol. 18, no. 3, pp. 294-301.

Ho, S. S., Chan, Y. L., Yeung, D. K., & Metreweli, C. 2002, "Blood flow volume quantification of cerebral ischemia: comparison of three noninvasive imaging techniques of carotid and vertebral arteries", *AJR Am.J.Roentgenol.*, vol. 178, no. 3, pp. 551-556.

Hofman, M. B., Visser, F. C., van Rossum, A. C., Vink, Q. M., Sprenger, M., & Westerhof, N. 1995, "In vivo validation of magnetic resonance blood volume flow measurements with limited spatial resolution in small vessels", *Magn Reson.Med.*, vol. 33, no. 6, pp. 778-784.

Hollnagel, D. I., Summers, P. E., Kollias, S. S., & Poulikakos, D. 2007, "Laser Doppler velocimetry (LDV) and 3D phase-contrast magnetic resonance angiography (PC-MRA) velocity measurements: validation in an anatomically accurate cerebral artery aneurysm model with steady flow", *J.Magn Reson.Imaging*, vol. 26, no. 6, pp. 1493-1505.

Hollnagel, D. I., Summers, P. E., Poulikakos, D., & Kollias, S. S. 2009, "Comparative velocity investigations in cerebral arteries and aneurysms: 3D phase-contrast MR angiography, laser Doppler velocimetry and computational fluid dynamics", *NMR Biomed.*, vol. 22, no. 8, pp. 795-808.

Hope, T. A. & Herfkens, R. J. 2008, "Imaging of the thoracic aorta with time-resolved three-dimensional phase-contrast MRI: a review", *Semin.Thorac.Cardiovasc.Surg.*, vol. 20, no. 4, pp. 358-364.

Hope, T. A., Hope, M. D., Purcell, D. D., von Morze, C., Vigneron, D. B., Alley, M. T., & Dillon, W. P. 2010, "Evaluation of intracranial stenoses and aneurysms with accelerated 4D flow", *Magn Reson.Imaging*, vol. 28, no. 1, pp. 41-46.

Hoppe, M., Heverhagen, J. T., Froelich, J. J., Kunisch-Hoppe, M., Klose, K. J., & Wagner, H. J. 1998, "Correlation of flow velocity measurements by magnetic resonance phase contrast imaging and intravascular Doppler ultrasound", *Invest Radiol.*, vol. 33, no. 8, pp. 427-432.

Hornak, J. P. 1996, *The Basics of MRI (Web Book)* Rochester Institute of Technology.

Hoskins, P. R. 1996, "Accuracy of maximum velocity estimates made using Doppler ultrasound systems", *Br.J Radiol.*, vol. 69, no. 818, pp. 172-177.

Hoskins, P. R. 2007, "Physical properties of tissues relevant to arterial ultrasound imaging and blood velocity measurement", *Ultrasound Med.Biol.*, vol. 33, no. 10, pp. 1527-1539.

Hoskins, P. R. 2008, "Simulation and validation of arterial ultrasound imaging and blood flow", *Ultrasound Med.Biol.*, vol. 34, no. 5, pp. 693-717.

Hoskins, P. R., Fish, P. J., Pye, S. D., & Anderson, T. 1999, "Finite beam-width ray model for geometric spectral broadening", *Ultrasound Med.Biol.*, vol. 25, no. 3, pp. 391-404.

Hoskins, P. R. & Ramnarine, K. V. 2000, "Doppler Ultrasound: Physics Instrumentation and Signal Processing," D. H. Evans & W. N. McDicken, eds., Wiley, Chichester.

Hoskins, P. 2011, "Estimation of blood velocity, volumetric flow and wall shear rate using Doppler ultrasound", *Ultrasound*, vol. 19, no. 3, pp. 120-129.

IEC 61685 2001, *Ultrasonics - Flow measurement systems: Flow Test Object.*, International Electrotechnichal Commission, Geneva, Switzerland.

IPEM 2010, *Report No. 102: Quality Control of Ultrasound Imaging Systems*, Institute of Physics and Engineering in Medicine, York

Jiang, J., Strother, C., Johnson, K., Baker, S., Consigny, D., Wieben, O., & Zagzebski, J. 2011, "Comparison of blood velocity measurements between ultrasound Doppler and accelerated phase-contrast MR angiography in small arteries with disturbed flow", *Phys.Med.Biol.*, vol. 56, no. 6, pp. 1755-1773.

Kilner, P. J., Gatehouse, P. D., & Firmin, D. N. 2007, "Flow measurement by magnetic resonance: a unique asset worth optimising", *J.Cardiovasc.Magn Reson.*, vol. 9, no. 4, pp. 723-728.

Klein, W. M., Bartels, L. W., Bax, L., van der, G. Y., & Mali, W. P. 2003, "Magnetic resonance imaging measurement of blood volume flow in peripheral arteries in healthy subjects", *J.Vasc.Surg.*, vol. 38, no. 5, pp. 1060-1066.

Knox, R. A., Breslau, P. J., & Strandness, D. E., Jr. 1982, "A simple parameter for accurate detection of severe carotid disease", *Br.J Surg.*, vol. 69, no. 4, pp. 230-233.

Krug, B., Kugel, H., Harnischmacher, U., Heindel, W., Schmidt, R., & Krings, F. 1995, "MR pulsatility measurements in peripheral arteries: preliminary results", *Magn Reson.Med.*, vol. 34, no. 5, pp. 698-705.

Lagerstrand, K. M., Vikhoff-Baaz, B., Starck, G., & Forssell-Aronsson, E. 2010, "Contrast agent influences MRI phase-contrast flow measurements in small vessels", *Magn Reson.Med.*, vol. 64, no. 1, pp. 42-46.

Larkman, D. J. & Nunes, R. G. 2007, "Parallel magnetic resonance imaging", *Phys.Med.Biol.*, vol. 52, no. 7, p. R15-R55.

Layden, J., Michaels, J., Bermingham, S., & Higgins, B. 2012, "Diagnosis and management of lower limb peripheral arterial disease: summary of NICE guidance", *BMJ*, vol. 345, p. e4947.

Lee, V. S., Spritzer, C. E., Carroll, B. A., Pool, L. G., Bernstein, M. A., Heinle, S. K., & MacFall, J. R. 1997, "Flow quantification using fast cine phase-contrast MR imaging, conventional cine phase-contrast MR imaging, and Doppler sonography: in vitro and in vivo validation", *AJR Am.J.Roentgenol.*, vol. 169, no. 4, pp. 1125-1131.

Leiner, T., Kessels, A. G., Nelemans, P. J., Vasbinder, G. B., de Haan, M. W., Kitslaar, P. E., Ho, K. Y., Tordoir, J. H., & van Engelshoven, J. M. 2005, "Peripheral arterial disease: comparison of color duplex US and contrast-enhanced MR angiography for diagnosis", *Radiology*, vol. 235, no. 2, pp. 699-708.

Levick, J. R. 2003, *An Introduction to Cardiovascular Physiology*, 4th edn, Arnold, London.

Lewis, S. C. & Wardlaw, J. M. 2002, "Which Doppler velocity is best for assessing suitability for carotid endarterectomy?", *Eur.J Ultrasound*, vol. 15, no. 1-2, pp. 9-20.

Lotz, J., Doker, R., Noeske, R., Schuttert, M., Felix, R., Galanski, M., Gutberlet, M., & Meyer, G. P. 2005, "In vitro validation of phase-contrast flow measurements at 3 T in comparison to 1.5 T: precision, accuracy, and signal-to-noise ratios", *J.Magn Reson.Imaging*, vol. 21, no. 5, pp. 604-610.

Lotz, J., Meier, C., Leppert, A., & Galanski, M. 2002, "Cardiovascular flow measurement with phase-contrast MR imaging: basic facts and implementation", *Radiographics*, vol. 22, no. 3, pp. 651-671.

Lui, E. Y., Steinman, A. H., Cobbold, R. S., & Johnston, K. W. 2005, "Human factors as a source of error in peak Doppler velocity measurement", *J Vasc.Surg.*, vol. 42, no. 5, pp. 972-979.

Markl, M., Frydrychowicz, A., Kozerke, S., Hope, M., & Wieben, O. 2012a, "4D flow MRI", *J.Magn Reson.Imaging*, vol. 36, no. 5, pp. 1015-1036.

Markl, M., Wallis, W., Strecker, C., Gladstone, B. P., Vach, W., & Harloff, A. 2012b, "Analysis of pulse wave velocity in the thoracic aorta by flow-sensitive four-dimensional MRI: reproducibility and correlation with characteristics in patients with aortic atherosclerosis", *J.Magn Reson.Imaging*, vol. 35, no. 5, pp. 1162-1168.

Marsan, N. A., Westenberg, J. J., Ypenburg, C., Delgado, V., van Bommel, R. J., Roes, S. D., Nucifora, G., van der Geest, R. J., de Roos, A., Reiber, J. C., Schalij, M. J., & Bax, J. J. 2009, "Quantification of functional mitral regurgitation by real-time 3D echocardiography: comparison with 3D velocity-encoded cardiac magnetic resonance", *JACC.Cardiovasc.Imaging*, vol. 2, no. 11, pp. 1245-1252.

Marshall, I., Zhao, S., Papathanasopoulou, P., Hoskins, P., & Xu, Y. 2004, "MRI and CFD studies of pulsatile flow in healthy and stenosed carotid bifurcation models", *J Biomech.*, vol. 37, no. 5, pp. 679-687.

Masui, T., Caputo, G. R., Bowersox, J. C., & Higgins, C. B. 1995, "Assessment of popliteal arterial occlusive disease with 2D time-of-flight MRA", *J.Comput.Assist.Tomogr.*, vol. 19, no. 3, pp. 449-454.

McCauley, T. R., Pena, C. S., Holland, C. K., Price, T. B., & Gore, J. C. 1995, "Validation of volume flow measurements with cine phase-contrast MR imaging for peripheral arterial waveforms", *J.Magn Reson.Imaging*, vol. 5, no. 6, pp. 663-668.

McRobbie, D. W., Moore, E. A., Graves, M. J., & Prince, M. R. 2003, *MRI From Picture to Proton* Cambridge University Press.

Meckel, S., Leitner, L., Bonati, L. H., Santini, F., Schubert, T., Stalder, A. F., Lyrer, P., Markl, M., & Wetzel, S. G. 2012, "Intracranial artery velocity measurement using 4D PC MRI at 3 T: comparison with transcranial ultrasound techniques and 2D PC MRI", *Neuroradiology*.

Meissner, O. A., Verrel, F., Tato, F., Siebert, U., Ramirez, H., Ruppert, V., Schoenberg, S. O., & Reiser, M. 2004, "Magnetic resonance angiography in the follow-up of distal lower-extremity bypass surgery: comparison with duplex ultrasound and digital subtraction angiography", *J.Vasc.Interv.Radiol.*, vol. 15, no. 11, pp. 1269-1277.

Meyer, R. A., Foley, J. M., Harkema, S. J., Sierra, A., & Potchen, E. J. 1993, "Magnetic resonance measurement of blood flow in peripheral vessels after acute exercise", *Magn Reson.Imaging*, vol. 11, no. 8, pp. 1085-1092.

Nesbitt, E., Schmidt-Trucksass, A., Il'yasov, K. A., Weber, H., Huonker, M., Laubenberger, J., Keul, J., Hennig, J., & Langer, M. 2000, "Assessment of arterial blood flow characteristics in normal and atherosclerotic vessels with the fast Fourier flow method", *MAGMA.*, vol. 10, no. 1, pp. 27-34.

Nogami, M., Ohno, Y., Koyama, H., Kono, A., Takenaka, D., Kataoka, T., Kawai, H., Kawamitsu, H., Onishi, Y., Matsumoto, K., Matsumoto, S., & Sugimura, K. 2009, "Utility of phase contrast MR imaging for assessment of pulmonary flow and pressure estimation in patients with pulmonary hypertension: comparison with right heart catheterization and echocardiography", *J.Magn Reson.Imaging*, vol. 30, no. 5, pp. 973-980.

Nordmeyer, S., Riesenkampff, E., Messroghli, D., Kropf, S., Nordmeyer, J., Berger, F., & Kuehne, T. 2012, "Four-dimensional velocity-encoded magnetic resonance imaging improves blood flow quantification in patients with complex accelerated flow", *J.Magn Reson.Imaging*.

Norgren, L., Hiatt, W. R., Dormandy, J. A., Nehler, M. R., Harris, K. A., & Fowkes, F. G. 2007, "Inter-Society Consensus for the Management of Peripheral Arterial Disease (TASC II)", *J Vasc.Surg.*, vol. 45 Suppl S, pp. S5-67.

North American Symptomatic Carotid Endarterectomy Trial Collaborators. Beneficial effect of carotid endarterectomy in symptomatic patients with high-grade carotid stenosis. N Engl J Med 325[7], 445-453. 15-8-1991.
Ref Type: Abstract

O'Brien, K. R., Cowan, B. R., Jain, M., Stewart, R. A., Kerr, A. J., & Young, A. A. 2008, "MRI phase contrast velocity and flow errors in turbulent stenotic jets", *J.Magn Reson.Imaging*, vol. 28, no. 1, pp. 210-218.

O'Brien, K. R., Myerson, S. G., Cowan, B. R., Young, A. A., & Robson, M. D. 2009, "Phase contrast ultrashort TE: A more reliable technique for measurement of high-velocity turbulent stenotic jets", *Magn Reson.Med.*, vol. 62, no. 3, pp. 626-636.

Oates, C. P. 2001, *Cardiovascular haemodynamics and Doppler waveforms explained*. Greenwich Medical Media Ltd, London.

Oates, C. P., Naylor, A. R., Hartshorne, T., Charles, S. M., Fail, T., Humphries, K., Aslam, M., & Khodabakhsh, P. 2009, "Joint recommendations for reporting carotid ultrasound investigations in the United Kingdom", *Eur.J.Vasc.Endovasc.Surg.*, vol. 37, no. 3, pp. 251-261.

Olin, J. W. & Sealove, B. A. 2010, "Peripheral artery disease: current insight into the disease and its diagnosis and management", *Mayo Clin.Proc.*, vol. 85, no. 7, pp. 678-692.

Pena, C. S., McCauley, T. R., Price, T. B., Sumpio, B., Gusberg, R. J., & Gore, J. C. 1996, "Quantitative blood flow measurements with cine phase-contrast MR imaging of subjects at rest and after exercise to assess peripheral vascular disease", *AJR Am.J.Roentgenol.*, vol. 167, no. 1, pp. 153-157.

Picot, P. A., Fruitman, M., Rankin, R. N., & Fenster, A. 1995, "Rapid volume flow rate estimation using transverse colour Doppler imaging", *Ultrasound Med.Biol.*, vol. 21, no. 9, pp. 1199-1209.

Poepping, T. L., Nikolov, H. N., Rankin, R. N., Lee, M., & Holdsworth, D. W. 2002, "An in vitro system for Doppler ultrasound flow studies in the stenosed carotid artery bifurcation", *Ultrasound Med.Biol.*, vol. 28, no. 4, pp. 495-506.

Poepping, T. L., Nikolov, H. N., Thorne, M. L., & Holdsworth, D. W. 2004, "A thin-walled carotid vessel phantom for Doppler ultrasound flow studies", *Ultrasound Med.Biol.*, vol. 30, no. 8, pp. 1067-1078.

Pourcelot, L. 1976, "Diagnostic ultrasound for cerebral vascular diseases," in *Present and Future of Diagnostic Ultrasound*, I. Donald & S. Levi, eds., Kooyker, Rotterdam, pp. 141-147.

Reddy, D. J., Vincent, G. S., McPharlin, M., & Ernst, C. B. 1986, "Limitations of the femoral artery pulsatility index with aortoiliac artery stenosis: an experimental study", *J.Vasc.Surg.*, vol. 4, no. 4, pp. 327-332.

Roldan-Alzate, A., Frydrychowicz, A., Niespodzany, E., Landgraf, B. R., Johnson, K. M., Wieben, O., & Reeder, S. B. 2012, "In vivo validation of 4D flow MRI for assessing the hemodynamics of portal hypertension", *J.Magn Reson.Imaging*.

Schoenberg, S. O., Knopp, M. V., Bock, M., Kallinowski, F., Just, A., Essig, M., Hawighorst, H., Schad, L., & van Kaick, G. 1997, "Renal artery stenosis: grading of hemodynamic changes with cine phase-contrast MR blood flow measurements", *Radiology*, vol. 203, no. 1, pp. 45-53.

Schoenberg, S. O., Rieger, J., Johannson, L. O., Dietrich, O., Bock, M., Prince, M. R., & Reiser, M. F. 2003, "Diagnosis of renal artery stenosis with magnetic resonance angiography: update 2003", *Nephrol.Dial.Transplant.*, vol. 18, no. 7, pp. 1252-1256.

Seitz, J., Strotzer, M., Wild, T., Nitz, W. R., Volk, M., Lenhart, M., & Feuerbach, S. 2001, "Quantification of blood flow in the carotid arteries: comparison of Doppler ultrasound and three different phase-contrast magnetic resonance imaging sequences", *Invest Radiol.*, vol. 36, no. 11, pp. 642-647.

Shakeri, A. B., Zarrintan, S., & Shakeri-Bavil, M. 2008, "The diagnostic value of the resistivity index of the common carotid arteries in severe internal carotid artery stenosis", *Folia Morphol.(Warsz.)*, vol. 67, no. 3, pp. 175-178.

SIGN 108 2008, *Management of patients with stroke or TIA: assessment, investigation, immediate management and secondary prevention*, Scottish Intercollegiate Guidelines Network, Edinburgh.

SIGN 89 2006, *Diagnosis and management of peripheral arterial disease*, Scottish Intercollegiate Guidelines Network, Edinburgh.

Slomianka, L.,2009, Blue Histology - Vascular System, University of Western Australia, Perth, accessed December 2012, http://www.lab.anhb.uwa.edu.au/mb140/corepages/vascular/vascular.htm

Smith, R. F., Rutt, B. K., & Holdsworth, D. W. 1999, "Anthropomorphic carotid bifurcation phantom for MRI applications", *J.Magn Reson.Imaging*, vol. 10, no. 4, pp. 533-544.

Sodickson, D. K. 2005, "Spatial Encoding Using Multiple rf Coils: SMASH Imaging and Parallel MRI," in *Methods in Biomedical MRI and Spectroscopy - online education exhibit*, I. R. Young, D. M. Grant, & R. K. Harris, eds., accessed December 2012 http://www.spectroscopynow.com.

Sondergaard, L., Stahlberg, F., Thomsen, C., Spraggins, T. A., Gymoese, E., Malmgren, L., Muller, E., & Henriksen, O. 1993, "Comparison between retrospective gating and ECG triggering in magnetic resonance velocity mapping", *Magn Reson.Imaging*, vol. 11, no. 4, pp. 533-537.

Soule, B., Hingorani, A., Ascher, E., Kallakuri, S., Yorkovich, W., Markevich, N., Costa, T., & Schutzer, R. 2003, "Comparison of Magnetic Resonance Angiography (MRA) and Duplex Ultrasound Arterial Mapping (DUAM) prior to infrainguinal arterial reconstruction", *Eur.J.Vasc.Endovasc.Surg.*, vol. 25, no. 2, pp. 139-146.

Stadlbauer, A., van der, R. W., Globits, S., Crelier, G., & Salomonowitz, E. 2009, "Accelerated phase-contrast MR imaging: comparison of k-t BLAST with SENSE and Doppler ultrasound for velocity and flow measurements in the aorta", *J.Magn Reson.Imaging*, vol. 29, no. 4, pp. 817-824.

Stahlberg, F., Nordell, B., Ericsson, A., Greitz, T., Persson, B., & Sperber, G. 1986, "Quantitative study of flow dependence in NMR images at low flow velocities", *J.Comput.Assist.Tomogr.*, vol. 10, no. 6, pp. 1006-1015.

Stahlberg, F., Sondergaard, L., Thomsen, C., & Henriksen, O. 1992, "Quantification of complex flow using MR phase imaging--a study of parameters influencing the phase/velocity relation", *Magn Reson.Imaging*, vol. 10, no. 1, pp. 13-23.

Stalder, A. F., Russe, M. F., Frydrychowicz, A., Bock, J., Hennig, J., & Markl, M. 2008, "Quantitative 2D and 3D phase contrast MRI: optimized analysis of blood flow and vessel wall parameters", *Magn Reson.Med.*, vol. 60, no. 5, pp. 1218-1231.

Stanisz, G. J., Odrobina, E. E., Pun, J., Escaravage, M., Graham, S. J., Bronskill, M. J., & Henkelman, R. M. 2005, "T1, T2 relaxation and magnetization transfer in tissue at 3T", *Magn Reson.Med.*, vol. 54, no. 3, pp. 507-512.

Stankovic, Z., Frydrychowicz, A., Csatari, Z., Panther, E., Deibert, P., Euringer, W., Kreisel, W., Russe, M., Bauer, S., Langer, M., & Markl, M. 2010, "MR-based visualization and quantification of three-dimensional flow characteristics in the portal venous system", *J.Magn Reson.Imaging*, vol. 32, no. 2, pp. 466-475.

Steel, R., Ramnarine, K. V., Davidson, F., Fish, P. J., & Hoskins, P. R. 2003, "Angle-independent estimation of maximum velocity through stenoses using vector Doppler ultrasound", *Ultrasound Med.Biol.*, vol. 29, no. 4, pp. 575-584.

Steffens, J. C., Link, J., Muller-Hulsbeck, S., Freund, M., Brinkmann, G., & Heller, M. 1997, "Cardiac-gated two-dimensional phase-contrast MR angiography of lower extremity occlusive disease", *AJR Am.J.Roentgenol.*, vol. 169, no. 3, pp. 749-754.

Steinman, A. H., Tavakkoli, J., Myers, J. G., Jr., Cobbold, R. S., & Johnston, K. W. 2001, "Sources of error in maximum velocity estimation using linear phased-array Doppler systems with steady flow", *Ultrasound Med.Biol.*, vol. 27, no. 5, pp. 655-664.

Sugano, S., Yamamoto, K., Sasao, K., & Watanabe, M. 1999, "Portal venous blood flow while breath-holding after inspiration or expiration and during normal respiration in controls and cirrhotics", *J.Gastroenterol.*, vol. 34, no. 5, pp. 613-618.

Summers, P. E., Holdsworth, D. W., Nikolov, H. N., Rutt, B. K., & Drangova, M. 2005, "Multisite trial of MR flow measurement: phantom and protocol design", *J.Magn Reson.Imaging*, vol. 21, no. 5, pp. 620-631.

Surry, K. J., Austin, H. J., Fenster, A., & Peters, T. M. 2004, "Poly(vinyl alcohol) cryogel phantoms for use in ultrasound and MR imaging", *Phys.Med.Biol.*, vol. 49, no. 24, pp. 5529-5546.

SVT 2001a, *Vascular Laboratory Practice: Part I* Institute of Physics and Engineering in Medicine; Society for Vascular Technology of Great Britian and Ireland, York, UK.

SVT 2001b, *Vascular Laboratory Practice: Part II* Institute of Physics and Engineering in Medicine; Society for Vascular Technology of Great Britian and Ireland, York, UK.

SVT 2001c, *Vascular Laboratory Practice: Part III* Institute of Physics and Engineering in Medicine; Society for Vascular Technology of Great Britian and Ireland, York, UK.

SVT 2004, *Vascular Laboratory Practice: Part IV Abdominal and Visceral Vascular Assessment* Institute of Physics and Engineering in Medicine; Society for Vascular Technology of Great Britian and Ireland, York, UK.

Tang, C., Blatter, D. D., & Parker, D. L. 1993, "Accuracy of phase-contrast flow measurements in the presence of partial-volume effects", *J.Magn Reson.Imaging*, vol. 3, no. 2, pp. 377-385.

Teirlinck C.J.P.M., Bezemer R.A., Kollman C., Lubbers J., Hoskins P.R., Fish P., Fredfeldt K.E., Schaarschmidt U.G., 1998, "Development of an example flow test object and comparison of five of these test objects in various laboratories", Eur J Ultrasound; vol.36:pp. 653– 660.

Thompson, R. B. & McVeigh, E. R. 2002, "High temporal resolution phase contrast MRI with multiecho acquisitions", *Magn Reson.Med.*, vol. 47, no. 3, pp. 499-512.

Thrush, A. & Hartshorne, T. 2009, *Peripheral vascular ultrasound: how, why and when.*, 3rd edn, Churchill Livingstone, Edinburgh.

Ultrasound Equipment Evaluation Project 2004a, *MHRA 04016: Technical evaluation: GE Logiq 3*, Medicine and Healthcare products Regulatory Agency, HMSO, Norwich, UK.

Ultrasound Equipment Evaluation Project 2004b, *MHRA 04032:A comparative technical evaluation of four mid-range ultrasound scanners:Philips Envisor, Toshiba Nemio, Sonosite Titan and GE LogiqBook*, Medicine and Healthcare products Regulatory Agency, HMSO, Norwich, UK.

Valiente Engelhorn, A. L., Engelhorn, C. A., Salles-Cunha, S. X., Ehlert, R., Akiyoshi, F. K., & Assad, K. W. 2012, "Ultrasound tissue characterization of the normal kidney", *Ultrasound Q.*, vol. 28, no. 4, pp. 275-280.

van Amerom, J. F., Kellenberger, C. J., Yoo, S. J., & Macgowan, C. K. 2009, "Automated measurement and classification of pulmonary blood-flow velocity patterns using phase-contrast MRI and correlation analysis", *Magn Reson.Imaging*, vol. 27, no. 1, pp. 38-47.

van der, W. R., Viergever, M. A., & Bakker, C. J. 2004, "Resolution-insensitive velocity and flow rate measurement in low-background phase-contrast MRA", *Magn Reson.Med.*, vol. 51, no. 4, pp. 785-793.

van Oostayen, J. A., Bezemer, R. A., Wasser, M. N. J. M., & Teirlinck, C. J. P. M. 1996, *"Validation of Doppler ultrasound and magnetic resonance imaging velocity measurements by means of a test object"*, European Journal of Ultrasound, vol.4, no. 2, pp.135-143

Villarreal, M. R., Wikimedia Commons, 2009, accessed December 2012, http://en.wikipedia.org/wiki/File:Arterial_System_en.svg

Visser, K. & Hunink, M. G. 2000, "Peripheral arterial disease: gadolinium-enhanced MR angiography versus color-guided duplex US--a meta-analysis", *Radiology*, vol. 216, no. 1, pp. 67-77.

Walker, A., Olsson, E., Wranne, B., Ringqvist, I., & Ask, P. 2004, "Accuracy of spectral Doppler flow and tissue velocity measurements in ultrasound systems", *Ultrasound Med Biol.*, vol. 30, no. 1, pp. 127-132.

Waters, E. A., Caruthers, S. D., & Wickline, S. A. 2005, "Correlation analysis of stenotic aortic valve flow patterns using phase contrast MRI", *Ann.Biomed.Eng*, vol. 33, no. 7, pp. 878-887.

Wentland, A. L., Korosec, F. R., Vigen, K. K., Wieben, O., Fine, J. P., & Grist, T. M. 2006, "Cine flow measurements using phase contrast with undersampled projections: in vitro validation and preliminary results in vivo", *J.Magn Reson.Imaging*, vol. 24, no. 4, pp. 945-951.

Wetzel, S., Meckel, S., Frydrychowicz, A., Bonati, L., Radue, E. W., Scheffler, K., Hennig, J., & Markl, M. 2007, "In vivo assessment and visualization of intracranial arterial hemodynamics with flow-sensitized 4D MR imaging at 3T", *AJNR Am.J.Neuroradiol.*, vol. 28, no. 3, pp. 433-438.

Wetzel, S. G., Lee, V. S., Tan, A. G., Heid, O., Cha, S., Johnson, G., & Rofsky, N. M. 2001, "Real-time interactive duplex MR measurements: application in neurovascular imaging", *AJR Am.J.Roentgenol.*, vol. 177, no. 3, pp. 703-707.

WHO 2011, *Noncommunicable diseases country profiles*, World Health Organization, Geneva.

Woo, J., 2006. "A short History of the development of Ultrasound in Obstetrics and Gynecology." accessed December 2012, http://www.ob-ultrasound.net/history1.html

World Health Organisation. Geneva. 2012. Factsheet No. 311: Obesity and overweight. Accessed December 2012, http://www.who.int/mediacentre/factsheets/fs311/en/

Yucel, E. K. 1995, *Magnetic resonance angiography : a practical approach* McGraw-Hill Inc..

Zananiri, F. V., Jackson, P. C., Halliwell, M., Harris, R. A., Hayward, J. K., Davies, E. R., & Wells, P. N. 1993, "A comparative study of velocity measurements in major blood vessels using magnetic resonance imaging and Doppler ultrasound", *Br.J.Radiol.*, vol. 66, no. 792, pp. 1128-1133.

Zhang, H. & Prince, M. R. 2004, "Renal MR angiography", *Magn Reson.Imaging Clin.N.Am.*, vol. 12, no. 3, pp. 487-503, vi.

Zhang, H. L., Sos, T. A., Winchester, P. A., Gao, J., & Prince, M. R. 2009, "Renal artery stenosis: imaging options, pitfalls, and concerns", *Prog.Cardiovasc.Dis.*, vol. 52, no. 3, pp. 209-219.